Identification and Mechanistic Elucidation of WDR23 as a Novel Regulator of Nrf2

酸化ストレス応答鍵因子 Nrf2 新規調節因子 WDR23 の同定と機構の解明

Thesis Submitted to School of Science and Technology,
Kwansei Gakuin University
for the Degree of Doctor of Science

by

Ferbian Milas Siswanto
(D67019601)

2022

Contents

Abstract

NF-E2-related factor-2 (Nrf2) is a transcription factor that regulates many cellular activities in order to maintain homeostasis and also plays a vital role in cell survival. Notwithstanding its critical role in protecting normal cells from oxidative and electrophilic stress, Nrf2 is regarded as a double-edged sword factor in cancer cells that endow resistance to chemotherapeutic drugs by inducing pro-survival genes. Kelch-like-ECH-associated protein 1 (Keap1), a substrate adaptor protein for the Cullin 3 (CUL3)-based E3 ubiquitin ligase, is currently regarded as a major regulator of Nrf2 protein stability. Since most cancers achieve the constitutive activation of Nrf2 via somatic mutations in *Keap1* or *Nrf2* that disrupt Nrf2-Keap1 interaction, there is an urgent need to identify a novel Nrf2 regulator that can be used as a therapeutic target. In Chapter I, a substrate adaptor protein for the CUL4-based E3 ubiquitin ligase called WDR23 was identified as a novel regulator of Nrf2 protein stability and transcriptional activity. In Chapter II, the crosstalk mechanism between the canonical Keap1 pathway and a newly identified WDR23 pathway was elucidated. I demonstrated that Sp1 is a novel substrate of Keap1 that mediates this crosstalk by regulating the expression of *CUL4A*. In Chapter III, I investigated the mechanism of Nrf2/SKN-1 activation by chlorogenic acid (CGA). I proved that CGA activates Nrf2/SKN-1 and increases the lifespan of *Caenorhabditis elegans* by inhibiting the activity of $CRL4A^{WDR23}$ ligase via a novel Akt-FOXO3/DAF16a-DDB1 axis. Finally, in Chapter IV, I explored the role of β-glucan to ameliorate Nrf2-dependent etoposide resistance in *Keap1*-mutant lung adenocarcinoma cell line A549. I demonstrated that in A549 cells, β-glucan enhances the $CRL4A^{WDR23}$ activity toward Nrf2 via a newly identified EphA2-RelB-CUL4A pathway. In summary, the work done in this thesis provides evidence on WDR23 as a novel regulator of Nrf2 and gives insights into the molecular mechanism of WDR23 to assist in Nrf2 regulation. The WDR23-Nrf2 system may be targeted by several compounds to improve lifespan and may be the prime target for treating diseases caused by the impaired Keap1-Nrf2 system.

General Introduction

Homeostasis maintains optimal conditions to achieve organismal health and survival. Reactive oxidants from internal metabolism and environmental toxicant exposure, however, are ubiquitous and unavoidable to all living beings and threaten to disrupt homeostasis. Excessive reactive oxidants can cause oxidative stress and are traditionally viewed as being harmful. On the other hand, controlled levels of oxidants serve a useful role as part of signaling pathways. The level of reactive oxidants is regulated by a web of intracellular antioxidant defense systems to ensure that the redox status is at hemostatic levels. NF-E2-related factor-2 (Nrf2) is the key factor at the center of the complex pathway that orchestrates cellular response to oxidative and electrophilic stress. Nrf2 is a cap'n'collar basic-region leucine zipper transcription factor that regulates approximately 250 genes encoding antioxidants, drug transporters, and various cytoprotective proteins (1).

Under the physiologic condition, Nrf2 is maintained at a low level via the proteasomal degradation pathways. Several E3 ligase systems have been identified as a regulator of Nrf2, including Kelch-like ECH-associated protein 1 (Keap1), β-transducin repeat-containing protein (β-TrCP), Seven in absentia homolog 2 (Siah2), and HMG-CoA reductase degradation 1 homolog (Hrd1) (2–5). To date, Keap1 is considered as the canonical regulator of Nrf2. Keap1 is an adaptor component of Cullin 3 (CUL3)-based E3 ubiquitin ligase complex. Upon exposure to reactive oxygen species (ROS) and electrophiles, the cysteine residue(s) of Keap1 undergo conformational changes and repress Nrf2 ubiquitination (6). This will provide time for newly synthesized Nrf2 to translocate into the nucleus, heterodimerize with the small Maf protein family, bind to antioxidant responsive elements (AREs), and activate the transcription of cytoprotective genes (7).

Due to its involvement in the stress response pathway, activation of Nrf2 is considered beneficial for health by preventing the harmful effect of ROS, electrophiles, and xenobiotics toxicity (8). For this reason, activation of Nrf2 has been implicated in the prevention of aging and lifespan extension. To link the manipulation of the Nrf2 pathway and lifespan of a whole organism, the microscopic nematode *C. elegans* with a short lifespan and evolutionary conserved molecular pathway to mammalian cells offers a powerful utilization (9). The transcription factor Skinhead-1 (SKN-1) of *C. elegans* is the homolog of the mammalian Nrf2. Furthermore, SKN-1 and Nrf2 activate many of the same gene family targets (10).

In contrast to its beneficial effects, many studies indicated that the consecutive activation of Nrf2 is detrimental in several diseases. In cancer, for instance, Nrf2 is responsible for chemoresistance by regulating factors involved in drug biotransformation and transport (11–13). Considering that most cancers

acquire the hyperactivated Nrf2 via loss-of-function mutation in *Keap1*, identification of a novel pathway that regulates Nrf2 in a condition of detrimental Keap1-Nrf2 system is essential to provide a new therapeutic strategy.

Keap1 is absent in *C. elegans*, and the level of SKN-1 is mainly regulated by WDR-23, which is a substrate recognition protein for the Cullin 4-RING ligase (CRL4) complex that consists of CUL4 as a scaffold protein, DDB1 as an adaptor protein, and RBX1 as a RING-finger protein that transfer ubiquitin from E2 to the substrate protein (14). WDR-23, or formerly known as DDB1- and CUL4-associated factor 11 (DCAF11), is a WD40-repeat protein, containing seven repeats of the tryptophan-aspartic acid (WD) containing motif (15). This structure facilitates protein-protein interactions. WDR-23 contains a conserved 16-amino-acid DWD box motif (also known as WDXR, DxR, and CDW) in which it is bind to DDB1. Interestingly, WDR-23 is evolutionary conserved from *C. elegans* to humans; thus, raises a possibility that human WDR23 also regulates Nrf2.

Chlorogenic acid (CGA), the most abundant polyphenol in coffee, is a family of esters formed between certain cinnamic acids (caffeic, ferulic, and *p*-coumaric acids) and quinic acid (16). Numerous studies have examined the various biological properties of CGA, including antibacterial, anti-inflammatory, anti-carcinogenic, and antioxidant activities (17). It has been found to possess a strong antioxidant activity by directly acting as ROS scavenger and via the activation of the Nrf2 pathway (18). A number of studies have proposed the Keap1-dependent activation of Nrf2 by GGA (19–21). However, my previous studies indicated that CGA induced accumulation of Nrf2 in a lung adenocarcinoma cell line A549 with *Keap1* loss-of-function mutation and induced SKN-1 in a *Keap1*-deficient organism *C. elegans* (Master Thesis); suggesting that CGA activates Nrf2 in a Keap1-independent manner.

β-glucan is a naturally occurring polysaccharides that abundantly present in the cell wall of plants, bacteria, and fungi. Structurally, β-glucan consists of a backbone of β(1,3)-linked-D-glucopyranosyl units with β(1,6)-linked side chains of various lengths and distributions along the backbone of the polymer. β-glucan have been widely demonstrated to have various immunomodulatory and stimulatory activities, which likely depend on the cell types involved and the receptor(s) engaged (22). Various transmembrane receptors have been identified to recognize and mediate downstream biological signaling of β-glucan, including c-type lectin receptor dectin-1, the integrin dimer consisting of $\alpha_M\beta_2$ (CD11b/CD18) receptor or complement receptor 3 (CR3), and the receptor tyrosine kinase ephrin type-A receptor 2 (EphA2) (23, 24). Due to its immunomodulatory property, β-glucan received much attention for its potential as a chemotherapeutic adjuvant. However, whether β-glucan can improve the drug sensitivity in chemo-resistant cancers, especially that of Nrf2 dependent, remain unknown.

On the basis that:

1. WDR23 locus is conserved from *C. elegans* to humans,
2. Keap1 is a known canonical regulator of Nrf2,
3. Chlorogenic acid induces SKN-1 in *C. elegans* that does not possess *Keap1,* and
4. β-glucan has been used as a chemotherapeutic adjuvant,

This thesis will therefore examine:

1. The role of WDR23 in the regulation of the Nrf2 pathway,
2. The mechanism behind signaling crosstalk between the canonical Keap1 and WDR23 pathways,
3. The mechanism of action and the biological impact of chlorogenic acid as an inducer of Nrf2/SKN-1, and
4. The role and molecular mechanism of β-glucan to modify drug resistance in cancer cells with a mutation in *Keap1*.

CHAPTER I

Identification of WDR23 as a Novel Regulator of Nrf2

[*] This chapter was modified from *Drug Metabolism and Pharmacokinetics*, Volume 35, Issue 5, Pages 441-455, (2020), Ferbian Milas Siswanto, Ami Oguro, Saki Arase, & Susumu Imaoka, WDR23 regulates the expression of Nrf2-driven drug-metabolizing enzymes.

I.1. Introduction

Exposure to drugs or xenobiotics initiates a myriad of responses at the molecular and cellular levels, which are necessary for cell survival. Members of the "cap'n'collar" (CNC) transcription factor family have been demonstrated as master regulators in response to oxidative stress and xenobiotics, which activate gene expression to promote stress resistance, detoxification, protein turnover, redox homeostasis, and longevity (25). Mammalian nuclear factor-erythroid 2 p45-related factor 2 (Nrf2) is the most well-studied CNC, functioning as a mediator to induce drug-metabolizing enzymes (DMEs) with the assistance of compounds such as antioxidants and electrophiles (26). Nrf2 is mainly regulated by Kelch-like ECH-associated protein 1 (Keap1). In physiological conditions, Keap1 and the Cullin 3 (CUL3) E3 ubiquitin ligase complex subject Nrf2 to proteasomal degradation and maintain it at a low level (4). However, with oxidative or electrophile stress, reactive cysteine residue(s) in Keap1 undergo conformational changes, disrupting its interaction with Nrf2 and preventing Nrf2 ubiquitination and degradation, thereby increasing Nrf2 levels (6). Moreover, the ubiquitin ligase adapter β-TrCP has been established to tag Nrf2 for proteasome degradation by a CUL1/Rbx1 complex (2). Previously, concomitant stabilization of Siah2 protein in hypoxic conditions was proved to provide a dominant Nrf2 degradation pathway over that of Keap1, leading to hypoxic suppression of Nrf2 by Siah2 (5).

Numerous studies have revealed that exposure to both endogenous substances and xenobiotics induces DMEs through various nuclear receptors such as aryl hydrocarbon receptor (AhR), constitutive androstane receptor (CAR), and pregnane X receptor (PXR) (27). Recently, the Keap1-Nrf2 system has been thought to play an important role to orchestrate DMEs. Nrf2 is considered to regulate cellular defense mechanisms against xenobiotic toxicity through Keap1/Nrf2-mediated induction of DMEs (28), particularly phase I and phase II DMEs such as cytochromes P450 (CYPs), heme oxygenase-1 (HO-1), NAD(P)H quinone dehydrogenase 1 (NQO1), microsomal epoxide hydrolase (mEH), and UDP glucuronosyltransferase (UGT) family (29, 30). More recently, Nrf2 was found to be a regulator of phase III drug transporters such as multidrug resistance protein 1 (MDR1) (28, 31).

Although the occasional activation of Nrf2 in response to stress was widely reported to be beneficial for the prevention of pathological conditions (8), many studies have reported contradictory effects in cancer cells. Consecutive activation of Nrf2 in cancer cells was found to be responsible for chemoresistance and the decreased therapeutic efficacy of anticancer drugs through biotransformation or increased phase III drug efflux transporters (11–13). Considering its two-way activity, tight and precise regulation of Nrf2 is essential.

The *Caenorhabditis elegans* Skinhead-1 (SKN-1) protein is an ortholog of mammalian Nrf2. Studies in *C. elegans* and other nematodes confirmed that they lack a Keap1 ortholog but possess another E3 ubiquitin ligase adapter with a homologous mechanism in modulating SKN-1 activity, WD40-repeat protein-23 (WDR-23) (14, 32). WDR-23 contains seven repeats of the tryptophan-aspartic acid (WD)-containing motif. This structure facilitates protein–protein interactions, and in particular, WD40 proteins have been reported to interact with CUL4/DDB1. WDR-23 contains a conserved 16-amino-acid DWD box motif (also known as WDXR, DxR, and CDW), which binds to DDB1 (15). Although the mechanism by which Nrf2 is regulated by Keap1 is well understood, that of SKN-1 regulation by WDR-23 is unclear.

The WDR-23 locus is highly conserved from *C. elegans* to humans (14). WDR23 functions as a substrate receptor for the DDB1-CUL4-RBX1 E3 ubiquitin-protein ligase complex, which functions in the protein ubiquitination pathway (33, 34). It possesses two isoforms produced by alternative splicing, isoform 1 and isoform 2, with isoform 2 being deficient in 45–70th amino acid of isoform 1. In mammalian cells, WDR23 has been reported to subject several proteins to degradation via ubiquitination, including p21 (35) and stem-loop binding protein (SLBP) (36). However, the role and effect of WDR23 on Nrf2 pathway has not been widely studied.

Considering the conservation of WDR23, in this study the role of WDR23 in Nrf2 regulation and the expression of DMEs were investigated. Human hepatocellular carcinoma cells (Hep3B) were used because the liver is the main organ for the metabolism of drugs and xenobiotics, whereas human cervical carcinoma cells (HeLa) were used to determine whether the effect of WDR23 on DMEs was cell-specific or not. Then, the role of WDR23 in the canonical Keap1-regulated Nrf2 pathway was examined to clarify which regulator is more important regarding Nrf2 stability and activity.

I.2. Materials and methods

Materials

Dulbecco's modified Eagle's medium (DMEM), tert-butylhydroquinone (tBHQ), and 3,3'-diaminobenzidine (DAB) were purchased from Wako Pure Chemical (Osaka, Japan). MG132 (Z-Leu-Leu-Leu-H) was purchased from Peptide Institute (Osaka, Japan). Penicillin-streptomycin solution and geneticin (G418) were from Sigma Chemical Co. (St. Louis, MO). Fetal bovine serum was from Biological Industries (Kibbutz, Israel). Nitrocellulose membrane, horseradish-peroxidase-conjugated goat anti-rabbit IgG, and 4-chloro-1-naphthol were

purchased from Bio-Rad Laboratories (Hercules, CA). Isogen was from Nippon Gene (Toyama, Japan), and Revert Aid™ M-MuLV Reverse Transcriptase was from MBI Fermentas (Vilnius, Lithuania). KOD Fx Neo and KOD Plus Neo DNA polymerase were from Toyobo (Tokyo, Japan). DAPI (4′,6-diamidino-2-phenylindole) was from Dojindo (Kumamoto, Japan). Alexa Fluor® 488- and Alexa Fluor® 594-conjugated goat anti-rabbit IgG were purchased from Invitrogen (Carlsbad, CA). Anti-DYKDDDDK (FLAG) tag monoclonal antibodies were purchased from Wako Pure Chemical (Osaka, Japan). The anti-Nrf2, anti-Keap1, and anti-β-actin antibodies were prepared as described previously (5).

Cell culture

The human hepatoma cell line Hep3B was obtained from the Cell Resource Center for Biomedical Research at the Institute of Development, Aging, and Cancer of Tohoku University (Sendai, Japan). The human non-small cell lung adenocarcinoma A549 was obtained from the RIKEN BRC Cell Bank (Tsukuba, Japan). All cells were cultured in DMEM containing 10% FBS, penicillin (100 units/mL), and streptomycin (100 μg/mL), and maintained at 37°C in 5% CO_2 and 95% air. The chemical inhibition of Keap1 was induced by tBHQ treatment (dissolved in DMSO, added to the cells at a final concentration of 60 μM for 4 or 8 hours). Cells were treated with H_2O_2 (100 μM; 8 h), BPA (50 μM, 8 h), CGA (50 μM, 8 h), or sulforaphane (10 μM; 8 h).

Preparation of constructs

For overexpression of FLAG-fused WDR23 in HeLa and Hep3B cells, cDNA of human WDR23 isoform 1 (GenBank™ accession number NM_025230.4) was amplified by PCR using primer set 1 and 2 as shown in Table 1. Thirty cycles of PCR (98°C for 10 s, 55°C for 30 s, and 68°C for 2 min) were performed using the cDNA obtained from reverse transcription of total RNA from Hep3B cells as the template with KOD Fx Neo DNA polymerase and corresponding primer pairs. Primers were accompanied by a restriction site (underline). The endogenous expression of isoform 2 mRNA was too low to be used in the preparation of the construct. Therefore, the cDNA of human WDR23 isoform 2 which is the splicing variant (NM_181357.2) with a deletion in 133–210th nucleotide (45–70th amino acid) of isoform 1, was obtained by PCR with two steps using WDR23 isoform 1 cDNA as a template. In the first PCR, nucleotide fragment 1 was amplified with primer set 1 and 3 (94°C for 30 s, 55°C for 30 s, and 68°C for 30 s; thirty cycles). Nucleotide fragment 2 was amplified with primers 2 and 4 (98°C for 10 s, 53°C for 30 s, and 68°C for 90 s; thirty cycles). The full-length WDR23 isoform 2 was amplified in the second round of PCR from the fragments 1 and 2 with primers 1 and 2. The amplified WDR23 isoform 1 and 2 were digested by the restriction enzymes *Not*I and *Xba*I, and then ligated into pcDNA4 TO-3×FLAG (Invitrogen, Carlsbad, CA). For expression and purification of WDR23 in *E. coli* DH5α

(TOYOBO, Tokyo, Japan), cDNAs of human WDR23 isoform 1 (574–1641th nucleotide) (NM_025230.4) was amplified by thirty cycles of PCR (94°C for 30 s, 55°C for 30 s, and 68°C for 1 min) with KOD Plus Neo DNA polymerase and primer set 5 and 6. The amplified cDNA was digested by the restriction enzymes *Kpn*I and *Sal*I, and ligated into pQE-80L vectors (Qiagen, Hilden, Germany) with DNA Ligation Kit ver.1 (Takara Bio Inc., Shiga, Japan). In the BiFC assay, both isoforms of human WDR23 were amplified by PCR with primer sets 7 and 8 using pcDNA4/WDR23 isoforms 1 and 2 as templates, digested with *SalI* and *NotI*, and inserted into the pBiFC-VN155 vector. Human Keap1 cDNA (NM_203500.2) was amplified by PCR with primers 9 and 10 and then inserted into the pcDNA3.1(+) vector with the *BamH*I and *Xho*I sites. The cDNA of human WT Nrf2 (NM_006164.5) was isolated with primers 11 and 12. For the ΔETGE Nrf2 construct, nucleotide fragment 1 was amplified with primer set 11 and 13, while the nucleotide fragment 2 was amplified with primers 12 and 14. The ΔETGE Nrf2 cDNA was amplified in the second round of PCR from the fragments 1 and 2 with primers 11 and 12. Both WT and ΔETGE Nrf2 cDNA were digested by *BamH*I and *Xba*I, and then inserted into the pcDNA4 TO-3×FLAG vector. For the BiFC assay, human Nrf2 cDNA was amplified by PCR with primers 15 and 16 and then inserted into the pBiFC-VC155 vector with *Sal*I and *Kpn*I.

Table 1. Primers used for human WDR23 cDNA isolation

No.	Sequences	Descriptions
1	5'- ATAAGAATGCGGCCGCATGGGATCGCGGAACAGCAG -3'	Fw; underline, *Not*I site; double underline, start codon
2	5'- TATCTAGACTACTGGGGTGAGGAAAAGG-3'	Rv; underline, *Xba*I site; double underline, stop codon
3	5'- GTCCAAGAGGGCCTGGGCCAGATCCACATC -3'	Rv; 115–144th nucleotide of *WDR23* isoform 2; dotted underline, complementary to the primer 4
4	5'- CAGGCCCTCTTGGACTCAGA -3'	Fw; 129–149th nucleotide of *WDR23* isoform 2; dotted underline, complementary to the primer 3
5	5'- AAGGTACCCAAGACCAGACAATCCGACT -3'	Fw; 574–593rd nucleotide of *WDR23* Isoform 1 for pQE80L; underline, *Kpn*I site
6	5'- ATTTGTCGACCTACTGGGGTGAGGAAAAGG -3'	Rv; *WDR23* Isoform 1 for pQE80L underline, SalI site; double underline, stop codon
7	5'- ATTAGTCGACTATGGATTACAAGGATGACGATGACAAG -3'	Fw; 1014–1037 of pcDNA4 TO-3×FLAG vector; underline, *Sal*I site; double underline, start codon
8	5'- AATGGTACCCTGGGGTGAGGAAAAGGGTG -3'	Rv; 1618–1638 of human *WDR23* isoform 1 cDNA; underline, *Kpn*I site.
9	5'- AATGGATCCATGCAGCCAGATCCCAGGCC -3'	Fw; 1–20 of human *Keap1* cDNA; underline, *BamH*I site; double underline, start codon
10	5'- CCGCTCGAGTCAACAGGTACAGTTCTGCT -3'	Rv; 1856–1875 of human *Keap1* cDNA; underline, *Xho*I site; double underline, stop codon
11	5'- AAGGATCCATCATGATGGACTTGGAGCT -3'	Fw; 1–17 of human *Nrf2* cDNA; underlined, *BamH*I site; double underline, start codon
12	5'- TTCTAGACTAGTTTTTCTTAACATC -3'	Rv; 1801–1818 of human *Nrf2* cDNA; underlined, *Xba*I site; double underlined, stop codon
13	5'- CTGAATTGGGAGAAATTCATCTAGTTGTAA -3'	Rv; 219–234th followed by 247–266th nucleotide of *Nrf2*; dotted underline, complementary to the primer 14
14	5'- TTTCTCCCAATTCAGCCAGC -3'	Fw; 247–266th nucleotide of *Nrf2*; dotted underline, complementary to the primer 13
15	5'- ATTAGTCGACTATGATGGACTTGGAGCTGCC -3'	Fw; 1–20th nucleotide of human *Nrf2* cDNA; underline, *Sal*I site; double underline, start codon
16	5'- CCGGGTACCGTTTTTCTTAACATCTGGCT -3'	Rv; 1796–1815th nucleotide of human *Nrf2* cDNA; underline, *Kpn*I site

Preparation of WDR23 antibody

The anti-WDR23 antibody was prepared as follows: pQE-80L vector containing WDR23 isoform 1 cDNA (574–1641st nucleotide, which is the common region in isoforms 1 and 2), was transfected into *E. coli* DH5α (TOYOBO, Tokyo, Japan) and expressed by the addition of isopropyl β-d-1-thiogalactopyranoside (IPTG). The bacterial lysate was solubilized with 1% *n*-octyl-β-D-glucoside, then the solution was centrifuged. The resulting pellet and the supernatant were separated. The supernatant was applied onto a Ni-NTA Agarose (QIAGEN) to purify the 6xHis-tagged WDR23 peptide (192-546th amino acid). The absorbed WDR23 protein was eluted from an Ni-NTA Agarose with 100 mM sodium phosphate buffer (pH 7.2) containing 250 mM imidazole. The concentration of eluted protein was low; therefore, the pellet from centrifugation was solubilized by sodium dodecyl sulfate (SDS: final concentration of 0.5%) and analyzed by SDS-polyacrylamide gel electrophoresis (SDS-PAGE). Almost a single band appeared on the same mobility with the newly appeared band by the addition of IPTG in DH5α cells on SDS-PAGE. I tried several kinds of detergent and only SDS was effective. The solubilized protein (60 μg each) was injected into a rabbit with Freund's complete adjuvant for immunization and incomplete adjuvant as a booster (3 times every two weeks), and the antibody was raised against WDR23 as described previously (37). The cross-reactivity of the antibody was confirmed using purified WDR23 protein from *E. coli* and WDR23 overexpressed in HeLa cells.

Transfection, shRNA, and siRNA experiment

Transient transfection of the constructs into cells was performed using the calcium phosphate method. For the knockdown of Keap1 using shRNA, specific target regions of Keap1 were designated and inserted into a pBAsi-hU6 Neo Vector (Takara Bio Inc.) in accordance with a previously described procedure (5). The target sequence for Keap1-knockdown was 5'-GCAGGCCUUUGGCAUCAUGAACG-3', and the target sequence for control shRNA against GFP was 5'-CUCGAGUACAACUAUAACUCA-3'. For the knockdown of WDR23, siRNA-WDR23 (Cat. No. SI05029899) and siRNA-control (Cat. No. SI03650318) were purchased from QIAGEN (Hilden, Germany). The target sequence for human WDR23-knockdown was 5'-CUGGGUCUUUAGGGUAGGACA -3'. Both Keap1 shRNA and WDR23 RNAi were transfected into cells using ScreenFect™ A (Wako Pure Chemical Industries, Ltd.) in accordance with the manufacturer's instructions. Transfectants of shRNA-GFP or shRNA-Keap1 were selected using G418 for 4 days.

Subcellular fractionation

WDR23-overexpressing cells were washed with cold PBS and collected prior to 5,000 × g, 3 min centrifugation. One milliliter of Buffer A (10 mM HEPES pH

7.9, 1.5 mM $MgCl_2$, 10 mM KCl, 0.5 mM DTT, 0.05% protease inhibitor cocktail, and 0.1% Triton X-100) was added to the precipitate. The mixture was kept on ice for 10 minutes. The solution was vortexed for 10 seconds, centrifuged at 12,000 × g for 2 minutes, and the supernatant was transferred as the cytosolic fraction. The precipitate was then mixed with 30 μL of Buffer B (20 mM HEPES pH 7.9, 420 mM NaCl, 1.5 mM $MgCl_2$, 0.2 mM EDTA, 25% Glycerol, 0.5 mM DTT, and 0.05% protease inhibitor cocktail). After being incubated on ice for 2 hours, the mixture was centrifuged at 14,000 × g for 15 min and the supernatant was transferred as the nuclear fraction.

Immunoprecipitation and immunoblotting

WDR23-overexpressing HeLa cells were treated with MG132 (4 h, 5 μM) and tBHQ (4 h, 60 μM). Then, they were washed with ice-cold PBS, and collected. The cells were lysed in immunoprecipitation buffer (50 mM Tris-HCl, pH 7.5 and 150 mM NaCl, 0.5% Nonidet P-40, and 0.1% protease inhibitor mixture) and were centrifuged at 14,000 × g for 15 min and 1000 μg/μL of the protein-containing supernatant was incubated with 2 μL of anti-Nrf2 antibody, anti-FLAG antibody, or unimmunized rabbit serum for 2 h at 4°C. Then, 20 μL of Protein A- or protein G-Sepharose (50% (w/v); GE Healthcare, Chicago, IL) was added to the solution and incubated for 1 h at 4°C. The samples were washed with immunoprecipitation buffer containing 0.05% Nonidet P-40. For immunoblotting, anti-Nrf2, anti-WDR23, anti-FLAG, anti-Keap1, anti-ubiquitin, anti-HSP90α, anti-β-actin, or anti-histone H3 were used. The band intensity was quantified using NIH Image software ImageJ.

Immunofluorescence

HeLa or Hep3B cells were cultured in 3.5-cm glass-bottomed dishes (Thermo Fisher Scientific, Waltham, MA). Cells were transfected with FLAG-tagged WDR23 isoform 1 or isoform 2, FLAG-$Nrf2^{WT}$ or FLAG-$Nrf2^{\Delta ETGE}$ (3 μg of DNA) using the calcium phosphate method. Cells were washed with PBS and fixed with 4% paraformaldehyde (PFA) for 20 minutes at 4°C, followed by washing 5 min × 3 times with TPBS (PBS + 0.2% Tween 20 (Bio-Rad, Hercules, CA)). Permeabilization and blocking treatment were carried out using blocking buffer (0.1% bovine serum albumin (Wako) in TPBS for 1 h at 4°C). Cells were subsequently incubated either with anti-Nrf2, anti-FLAG, anti-CUL4 or anti-DDB1 antibodies for 1 h at 4°C and washed twice with TPBS. Next, cells were incubated with Alexa Fluor® 488- and Alexa Fluor® 594-conjugated goat anti-rabbit IgG (1:1000 dilution, Invitrogen) for Nrf2 and FLAG, CUL4 or DDB1 staining, respectively, for 1 h at 4°C. Cells were washed twice with TPBS and immunofluorescence was detected by confocal microscopy (Nikon A1, Tokyo, Japan or TCS SP8, Leica Microsystems, Wetzlar, Germany). The nucleus was counterstained using DAPI (1:1000 dilution, Dojindo, Kumamoto, Japan). To

investigate WDR23 isoform 1 localization, leptomycin B (Wako Pure Chemical Industries, Ltd.) was dissolved in 99% ethanol, added to cells at a final concentration of 5 nM, and cultured for 6 hours before the immunofluorescence assay.

Bimolecular fluorescence complementation (BiFC) assay

VN155 (N-terminal half of Venus) fused to the C-terminal of FLAG-WDR23 isoform 1 or isoform 2 was co-expressed with VC155 (the C-terminal half of Venus) fused to the C-terminal of Nrf2 in Hep3B cells. Twenty-four hours after transfection, cells were rinsed with PBS solution and fixed for 20 minutes with 4% paraformaldehyde (PFA) in PBS, then rinsed with TPBS (PBS + 0.2% Tween 20 (Bio-Rad, Hercules, CA)), followed by blocking with 0.1% bovine serum albumin (Wako, Osaka, Japan) in TPBS. Cells were subsequently incubated with anti-FLAG and anti-Nrf2 antibodies, followed by an incubation with Alexa Fluor® 594-conjugated goat anti-mouse IgG and Alexa Fluor® 647-conjugated goat anti-rabbit IgG. The nucleus was counterstained using DAPI. Images were obtained by confocal microscopy TCS SP8 (Leica Microsystems, Wetzlar, Germany). Venus fluorescence was detected as a BiFC signal.

Isolation of RNA and reverse transcription-PCR

Total RNA was extracted from cells using Isogen in accordance with the manufacturer's instructions and converted to cDNA by reverse transcription as described previously (38). PCR was performed at 94°C for 2 min, and then for a particular number of cycles of 94°C for 30 s, 55°C for 30 s, and 72°C for 30 s in a reaction mixture containing 10 pmol of each primer (Table 2), Go Taq polymerase (Promega, WI), and cDNA (100 ng). The PCR products were separated by electrophoresis on a 1% agarose gel, visualized with ethidium bromide staining, and quantified using ImageJ (Version 1.36b; National Institutes of Health, Bethesda, MD). The relative mRNA level was normalized to β-actin.

Table 2. Primers used for gene expression assessment

Primers			Sequences
WDR23	NM_181357.2	Forward	5'- CACAGGATTGGAGAAGGAGG -3'
		Reverse	5'- TCGGCAGTCATAGAGTCGGA -3'
Keap1	NM_203500.2	Forward	5'- TCTTCAAGGCCATGTTCACC -3'
		Reverse	5'- GGCACGCTGGTGCAACTCCA -3'
HO-1	NM_002133	Forward	5'- CCAGCCATGCAGCACTATGT -3'
		Reverse	5'- AGCCCTACAGCAACTGTCGC -3'
NQO1	NM_000903	Forward	5'- TGATCGTACTGGCTCACTCA -3'
		Reverse	5'- GTCAGTTGAGGTTCTAAGAC -3'
mEH	NM_001136018.3	Forward	5'- AAGAACCATGGCCTGAGCGA -3'
		Reverse	5'- AGAATACCTTCTCCTGCACG -3'
MDR1	NM_000927	Forward	5'- GGAGGATTATGAAGCTAAAT -3'
		Reverse	5'- GTAATTACAGCAAGCCTGGA -3'

CYP1A1	NM_000499.5	Forward	5'- GGAGACCTTCCGACACTCTT -3'
		Reverse	5'- CCTTGTCGATAGCACCATCA -3'
CYP2C9	NM_000771.4	Forward	5'- TGTGATTGGCAGAAACCGGA -3'
		Reverse	5'- CACAGTGAAACATAGGAAAC -3'
CYP2D6	NM_000106.6	Forward	5'- CAACCTGCTGCATGTGGACT -3'
		Reverse	5'- AAGTTGCGCAAGGTGGAGAC -3'
CYP2E1	NM_000773.4	Forward	5'- TGACCACCCTCCGGAACTAT -3'
		Reverse	5'- TGGCTTCCAGGCAAGTAGTG -3'
CYP3A4	NM_001202855.3	Forward	5'- TCACCAACACATCTCCATAC-3'
		Reverse	5'- AACCACGAGCAGTGTTCTCT -3'
CYP3A5	NM_000777.5	Forward	5'- GCTCCTCTATCTATATGGGA -3'
		Reverse	5'- CTGCTTCCCGCCTCAAGTTT -3'
CYP4B1	NM_001099772.2	Forward	5'- TTGCAGCACCGCAAGCTGCT -3'
		Reverse	5'- CCTGCAGGATGAGAAGGTGC -3'
UGT1A1	NM_000463.2	Forward	5'- CTCATTCAGATCACATGACC -3'
		Reverse	5'- AGCATCAGCAATTGCCATAG -3'
UGT1A9	NM_021027.3	Forward	5'- CTCTCAGCTGCAGTTCTCTG -3'
		Reverse	5'- CATGGGCAAAAGCCTTGAAC -3'
β-actin	NM_001101	Forward	5′- CAAGAGATGGCCACGGCTGCT -3′
		Reverse	5′- TCCTTCTGCATCCTGTCGGCA -3′

Statistical analysis

All data are given as the mean ± standard deviation (SD) and analyzed *p*-values were determined by Student's *t*-test or one-way ANOVA followed by Bonferroni's multiple comparison test. The differences were considered as significant when p was <0.05 (*) or p was <0.01 (**).

I.3. Results

Effects of WDR23 overexpression on Nrf2 levels and activities

In *C. elegans,* WDR23 is known to regulate SKN-1 (functional homolog of Nrf2) (14). In order to examine the effects of human WDR23 on the Nrf2 protein level, both FLAG-tagged WDR23 isoform 1 and isoform 2 were overexpressed in HeLa (Fig. 1*A*) and Hep3B (Fig. 1*B*) cells. Overexpression of WDR23 isoforms 1 and 2 was detected by antibodies against FLAG and WDR23 itself. FLAG-fused WDR23 were strongly expressed and the native WDR23 seemed to be detected slightly. There were no changes in total Nrf2 protein levels following WDR23 overexpression in both HeLa (Fig. 1*C*) and Hep3B (Fig. 1*D*) cells. As the Keap1-dependent Nrf2 regulation pathway is a canonical and evolutionarily conserved mechanism in mammalian cells (39), I hypothesized that WDR23 regulates Nrf2 to support Keap1. Because WDR23 is a substrate receptor for the DDB1-CUL4-RBX1 E3 ubiquitin-protein ligase complex, it may regulate Nrf2 by binding and subjecting Nrf2 to proteasomal degradation when Keap1 function is impaired. Therefore, the effects of WDR23 under chemical and genetic inhibition of Keap1 were examined.

tBHQ has been extensively proven to strongly inhibit the Keap1-dependent Nrf2 ubiquitination (40, 41). However, there were no changes observed in total Nrf2 levels after WDR23 overexpression in tBHQ-treated HeLa cells (Fig. 1*C*) and Hep3B cells (Fig. 1*D*). Because Nrf2 is a transcription factor that regulates the gene expression by binding to ARE sequences of DNA in the nucleus, the effect of WDR23 overexpression on nuclear Nrf2 levels in tBHQ-treated cells were investigated. The levels of nuclear Nrf2 did not appear to be reduced by WDR23 overexpression in HeLa cells (Fig. 1*E*), whereas the isoform 2 of WDR23 reduced the nuclear Nrf2 in Hep3B cells (Fig. 1*F*).

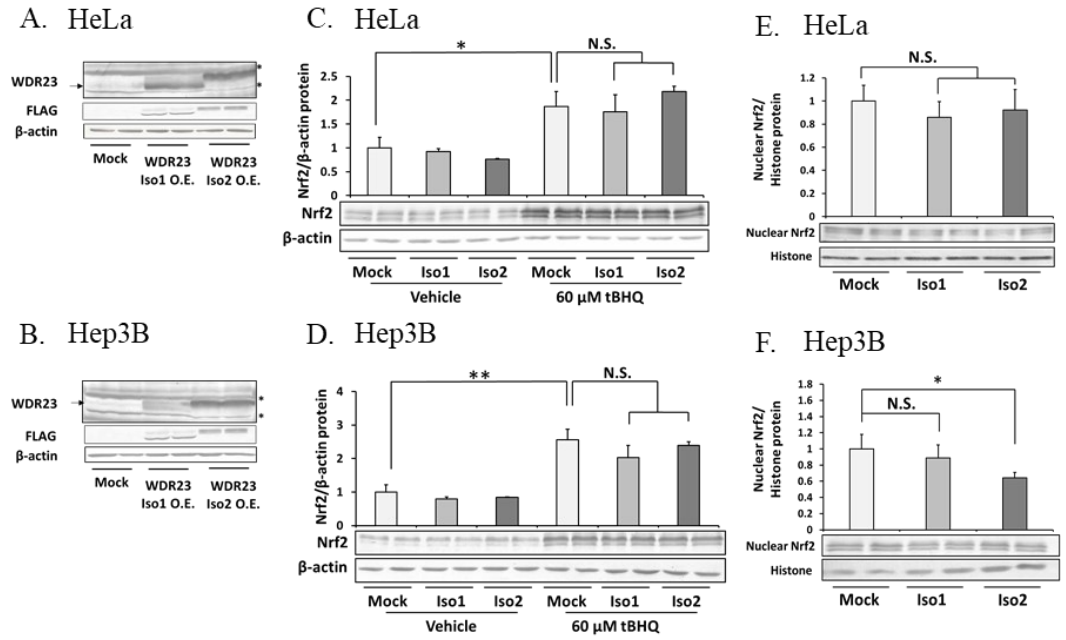

Figure 1. Effects of WDR23 isoforms 1 and 2 overexpression on Nrf2 protein levels. (A and B) Representative immunoblotting using anti-WDR23 and anti-FLAG antibodies with 30 μg protein from total cell lysate showed the efficiency of WDR23 overexpression in HeLa (A) and Hep3B (B) cells. Protein loading was normalized using β-actin (5 μg). The asterisks indicate nonspecific bands, and the arrow indicates WDR23. (C and D) WDR23-overexpressing HeLa cells (C) and Hep3B cells (D) were grown in the presence or absence of tBHQ (60 μM; 4 h). Immunoblotting analysis of Nrf2 levels with 15 μg of total cell lysate was performed, and β-actin was used as the loading control (n=3). (E and F) WDR23-overexpressing HeLa cells (C) and Hep3B cells (D) were grown in the presence of tBHQ (60 μM; 4 h). Immunoblotting analysis of Nrf2 levels with 15 μg of nuclear fraction was performed, and histone was used as the loading control (n=3). The band intensity was calculated using Image J. The value of the mock-transfected cells in vehicle was set at 1.0. The values are given as the mean ± S.D. of three different samples relative to the loading control (*p<0.05, N.S. not significant).

The overexpression of WDR23 isoform 1 or isoform 2 did not alter the expression of *HO-1* in HeLa cells (Fig. 2*A*) and Hep3B cells (Fig. 2*B*) in the absence of tBHQ, which were in line with the total levels of Nrf2 protein. In the presence of tBHQ, the expression of *HO-1* in HeLa cells (Fig. 2*A*) was not changed; however, the expression levels of *HO-1* in tBHQ-treated Hep3B cells were decreased by WDR23 isoform 1 and isoform 2 overexpression (Fig. 2*B*) even though the total Nrf2 protein was not changed.

The expression levels of *NQO1* in HeLa cells (Fig. 2*C*) and Hep3B cells (Fig. 2*D*) in the absence of tBHQ were not altered by the overexpression of WDR23, supporting the Nrf2 protein level assessment. In the presence of tBHQ, *NQO1* levels in HeLa cells were not affected by WDR23 (Fig. 2*C*). On the other hand, WDR23 isoform 2, but not WDR23 isoform 1, decreased the expression of *NQO1* in tBHQ-treated Hep3B cells (Fig. 2*D*).

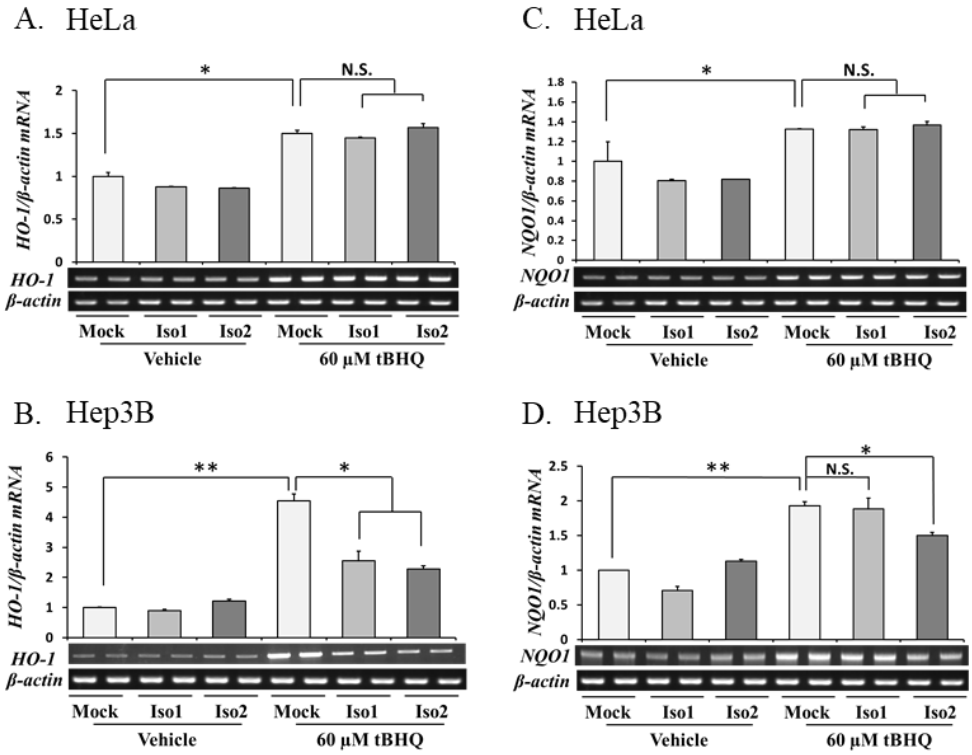

Figure 2. Effects of WDR23 overexpression on the Nrf2-regulated gene expression. (A and B) The expression levels of *HO-1* mRNA in HeLa (A) and Hep3B (B) cells transfected with WDR23 isoforms 1 and 2 in the presence or absence of tBHQ (60 μM; 8 h) were examined using RT-PCR. (C and D) The expression levels of *NQO1* mRNA in HeLa (C) and Hep3B (D) cells transfected with WDR23 isoforms 1 and 2 in the presence or absence of tBHQ (60 μM; 8 h) were examined using RT-PCR. β-actin mRNA was used as the loading control (n=3). The band intensity was calculated using Image J. The value of the mock-transfected cells in vehicle was set at 1.0. The values are given as the mean ± S.D. of three different samples relative to the loading control (**p<0.01).

Next, with genetic inhibition of Keap1 by shRNA in HeLa (Fig. 3*A*) and Hep3B (Fig. 3*B*) cells, and the overexpression of WDR23 in HeLa (Fig. 3*C*) and Hep3B (Fig. 3*D*) cells significantly reduced Nrf2 levels (Fig. 3*E* for HeLa and Fig. 3*F* for Hep3B). This was supported by changes in Nrf2 downstream gene expression after FLAG-WDR23 and shRNA-Keap1 co-transfection, including *HO-1* (Fig. 4*A* for HeLa and Fig. 4*B* for Hep3B) and *NQO1* (Fig. 4*C* for HeLa and Fig. 4*D* for Hep3B). These results support the hypothesis that WDR23 regulates Nrf2 under the condition where canonical Keap1 pathway is disturbed.

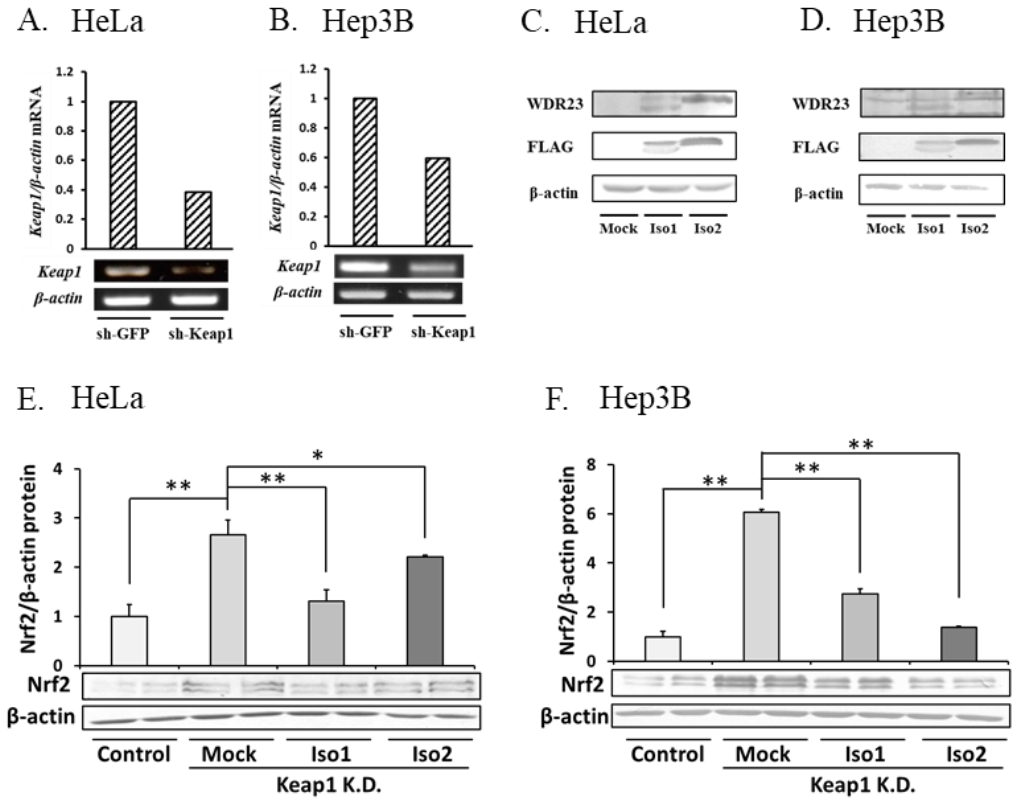

Figure 3. Effects of WDR23 overexpression and shRNA-induced Keap1 knockdown on Nrf2 protein levels. (A and B) The Keap1 knockdown efficiency in HeLa (A) and Hep3B (B) cells was confirmed using RT-PCR. (C and D) Representative immunoblotting using anti-WDR23 and anti-FLAG antibodies with 30 μg protein from total cell lysate showed the efficiency of WDR23 overexpression in HeLa (C) and Hep3B (D) cells. Protein loading was indicated using β-actin. (E and F) Immunoblotting analysis of Nrf2 levels using 15 μg of total cell lysate from HeLa (E) and Hep3B (F) cells co-transfected with FLAG-WDR23 and shRNA-Keap1. Control cells were transfected with shRNA-GFP, and the mock cells were co-transfected with pcDNA- and shRNA-Keap1. The ratio of Nrf2 to β-actin protein in the control cells was set at 1.0. All graphs present the mean ± S.D. (n= 3). *p<0.05, **p<0.01 *versus* indicated cells.

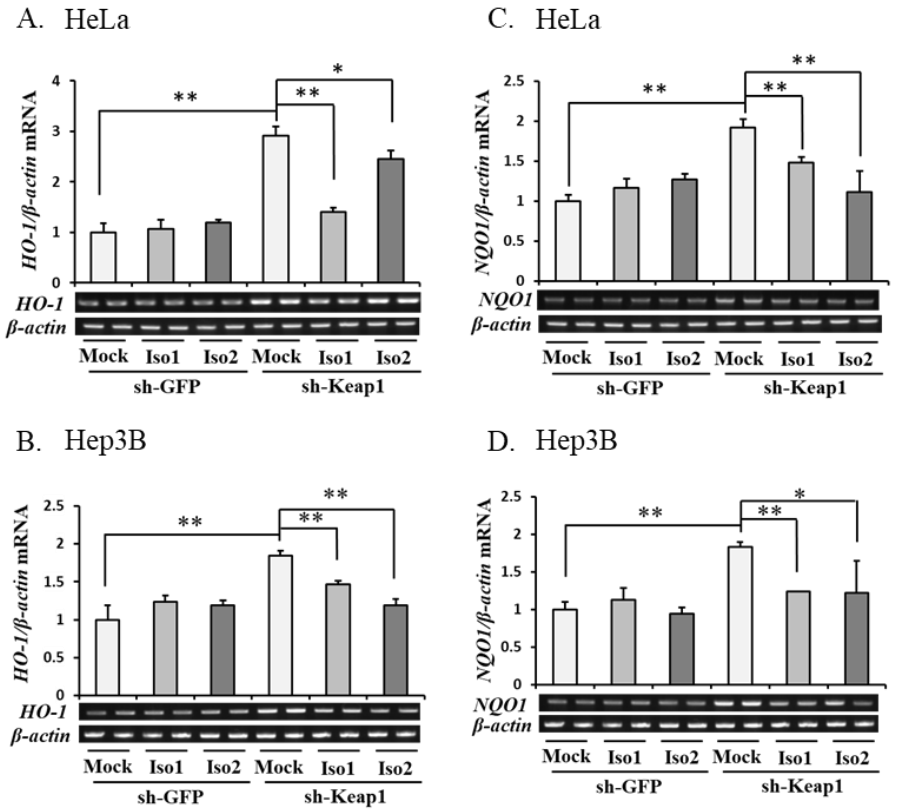

Figure 4. Effects of WDR23 overexpression and shRNA-induced Keap1 knockdown on Nrf2-driven gene expression. (A and B) The mRNA levels of *HO-1* in HeLa (A) and Hep3B (B) cells after co-transfection of pcDNA-mock or FLAG-WDR23 and shRNA-GFP or shRNA-Keap1 using RT-PCR. (C and D) The mRNA levels of *NQO1* in HeLa (C) and Hep3B (D) cells after co-transfection of FLAG-WDR23 and shRNA-Keap1 using RT-PCR. The values represent a ratio relative to β-actin mRNA levels. The value of the pcDNA-mock- and shRNA-GFP- transfected cells was set at 1.0. All graphs present the mean ± S.D. (n= 3). *p<0.05, **p<0.01 *versus* indicated cells.

Because the WDR23 effects on Nrf2 were limited when Keap1 activity was impaired, it is expected that reduced WDR23 activity in normal conditions has no effect either on Nrf2 levels or activity. To examine this, the effects of WDR23 overexpression in HeLa (Fig. 5*A*) and Hep3B (Fig. 5*B*) cells to Keap1 overexpression in HeLa (Fig. 5*C*) and Hep3B (Fig. 5*D*) cells were compared. As expected, Keap1 overexpression resulted in lower Nrf2 protein levels than WDR23 overexpression both in HeLa (Fig. 5*E*) and Hep3B (Fig. 5*F*) cells, although they were not significant. Next, the effects of WDR23 knockdown (Fig. 5*G* for HeLa and Fig. 5*H* for Hep3B) and Keap1 knockdown (Fig. 5*I* for HeLa and Fig. 5*J* for Hep3B) were compared. In support of the overexpression data, Keap1 knockdown in both HeLa cells (Fig. 5*K*) and Hep3B cells (Fig. 5*L*) caused higher Nrf2 protein levels than WDR23 knockdown.

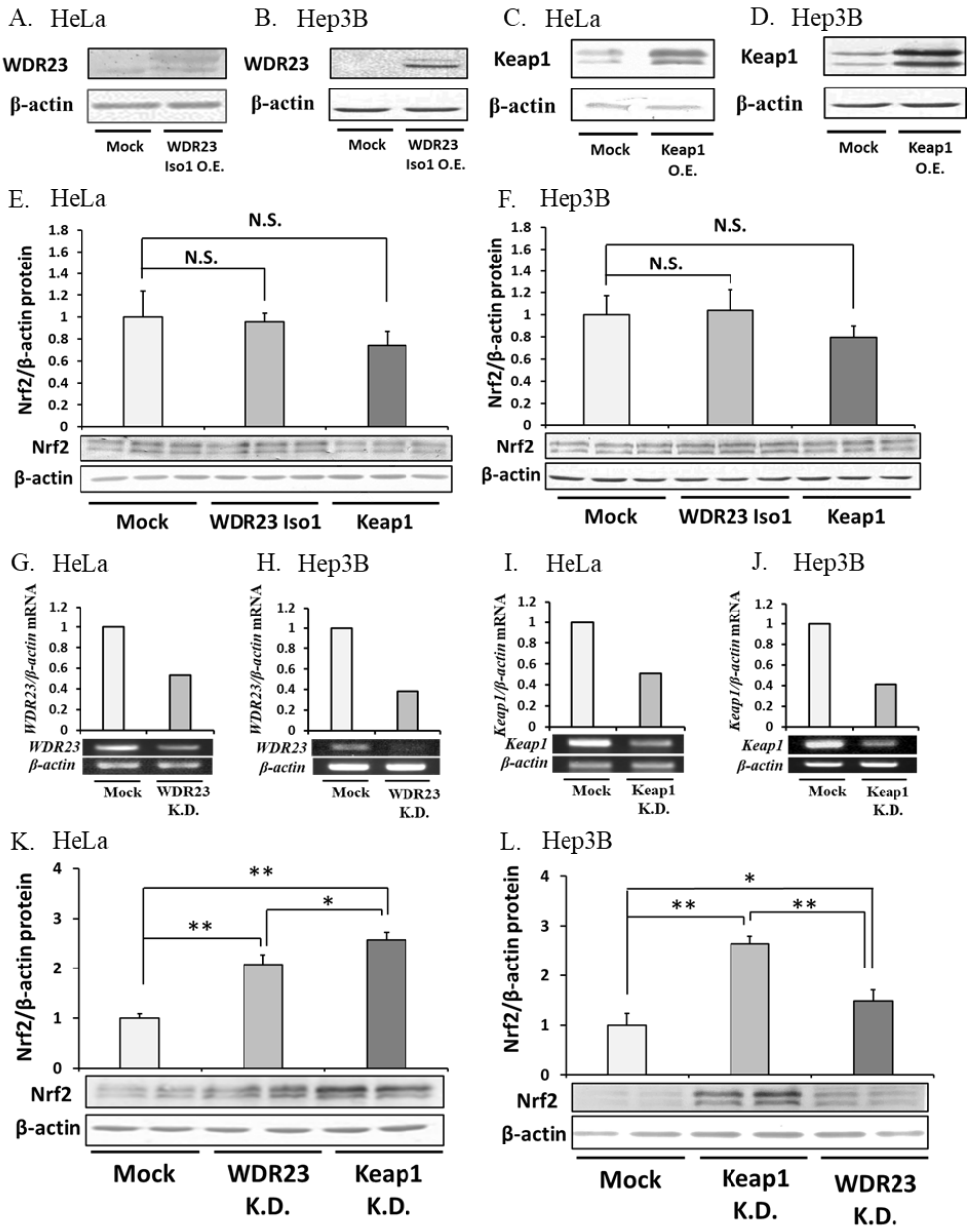

Figure 5. Effects of WDR23 and Keap1 overexpression and knockdown on Nrf2 protein levels in HeLa cells. (A and B) Representative immunoblotting with 30 μg of total cell lysate using anti-WDR23 and anti-β-actin antibodies showing the efficiency of WDR23 isoform 1 overexpression in HeLa (A) and Hep3B (B) cells. (C and D) Representative immunoblotting with 30 μg of total cell lysate using anti-Keap1 and anti-β-actin antibodies showing the efficiency of Keap1 overexpression in HeLa (C) and Hep3B (D) cells. (E and F) Changes in protein levels of Nrf2 by overexpression of WDR23 isoform 1 and Keap1 were assessed by immunoblotting with 15 μg of total cell lysate from HeLa (E) and Hep3B (F) cells (n=3). (G-J) The efficiency of Keap1 knockdown (shRNA-Keap1) in HeLa (G) and Hep3B (H) cells, as well as the WDR23 knockdown (siRNA-WDR23) in HeLa (I) and Hep3B (J) cells was confirmed using RT-PCR. (K and L) Twenty-four hours after transfection, total cell lysates from HeLa (K) and Hep3B (L) cells were immunoblotted using anti-Nrf2 and anti-β-actin antibodies. Mock cells were transfected with both shRNA-GFP and siRNA-control. All graphs are the mean ± S.D. The mock value was set as 1.0. *p<0.05, **p<0.01, N.S. not significant *versus* indicated cells.

Cellular localization of WDR23 isoform 1 and isoform 2

To gain insight into the mechanism by which WDR23 regulates Nrf2, the cellular localization of both isoforms of WDR23 was assessed. Based on immunofluorescence staining of FLAG-tagged WDR23-overexpressed HeLa cells, WDR23 isoform 1 was primarily localized in the cytoplasm (Fig. 6*A*), whereas isoform 2 predominantly resided in the nucleus but was also in the cytoplasm (Fig. 6*B*). To assess whether these isoforms of WDR23 are regulated by the nuclear export mechanism, the cells were treated with the nuclear export inhibitor leptomycin B. Nuclear export inhibition resulted in nuclear accumulation of isoform 1 (Fig. 6*A*), but no change in isoform 2 localization was observed (Fig. 6*B*). These results suggested that both isoforms of WDR23 contain a nuclear localization signal causing both to be nuclear, but only isoform 1 was transported back into the cytoplasm due to its nuclear export signal (NES). The 45–70th amino acids of isoform 1 are absent from isoform 2; therefore, it is highly possible that the NES is located within this region.

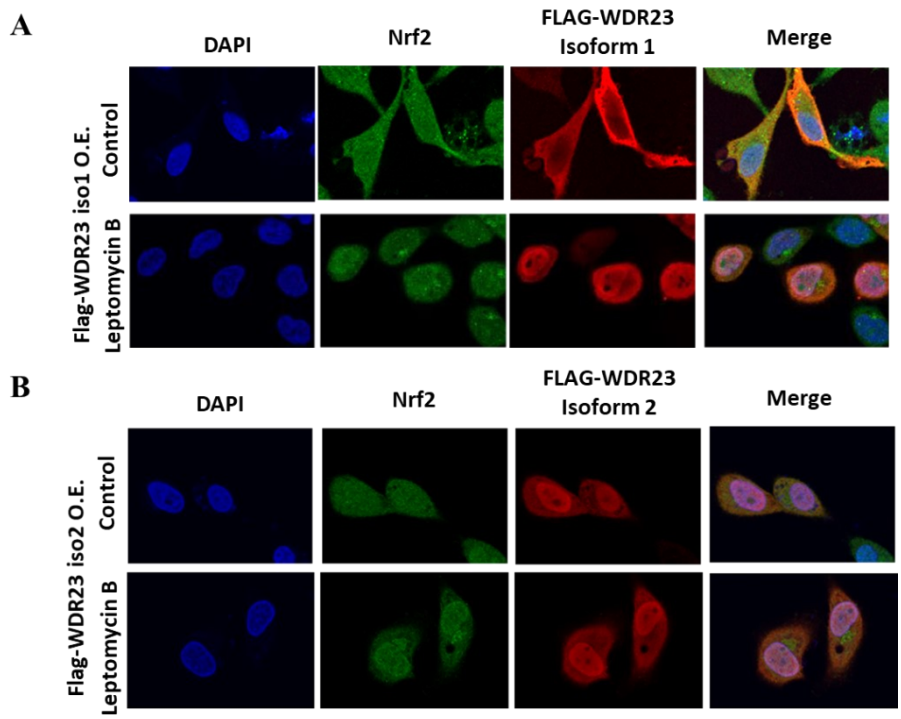

Figure 6. Subcellular localization of WDR23 isoform 1 and isoform 2. Representative images of immunofluorescence with DAPI staining to indicate the location of the nucleus, FLAG-WDR23 (red), and Nrf2 (green). (A) In HeLa cells transfected with isoform 1 of FLAG-WDR23, most isoform 1 was located in the cytoplasm, whereas (B) in HeLa cells transfected with isoform 2 of FLAG-WDR23, most isoform 2 was in the nucleus. Leptomycin B (nuclear export inhibitor) was added to cells at final concentration of 5 nM 6 h before the immunofluorescence assay was performed.

Interaction between WDR23 and Nrf2

In order to clarify whether WDR23 regulates Nrf2 directly, the physical interaction between WDR23 and Nrf2 was tested. FLAG-tagged WDR23 cDNA was transfected into HeLa cells. Immunoprecipitation was performed with an anti-FLAG antibody. The WDR23 was found to interact with Nrf2 in accordance with immunoblotting using an anti-Nrf2 antibody and anti-FLAG antibody on lysate obtained from pulldown with FLAG antibodies (Fig. 7*A* and *B*).

This study and others have demonstrated that WDR23 isoforms 1 and 2 primarily localized to the cytosol and nucleus, respectively, of cells in both humans (42, 43) and the nematode *Caenorhabditis elegans* (14). However, the subcellular localization pattern of the WDR23-Nrf2 complex, which may impact the biological importance of the WDR23-dependent Nrf2 regulation, remains unknown. In the present study, using the BiFC assay, I confirmed that the WDR23 isoform 1-Nrf2 complex was present in the cytosol, whereas the WDR23 isoform 2-Nrf2 complex was observed in the nucleus (Fig. 7*C* and *D*). These results indicated that isoforms 1 and 2 of WDR23 regulate cytosolic and nuclear Nrf2, respectively.

Since WDR23 is an adaptor for CUL4-based E3 ubiquitin ligase and that WDR23 physically interacts with Nrf2, next I examined the effects of WDR23 on the ubiquitination of Nrf2. The overexpression of both isoforms of WDR23 increased the ubiquitinated Nrf2 levels (Fig. 7*E*). These findings indicated that WDR23 regulates the turnover of Nrf2 via the ubiquitin proteasome system, as it is observed for the Keap1-dependent Nrf2 pathway.

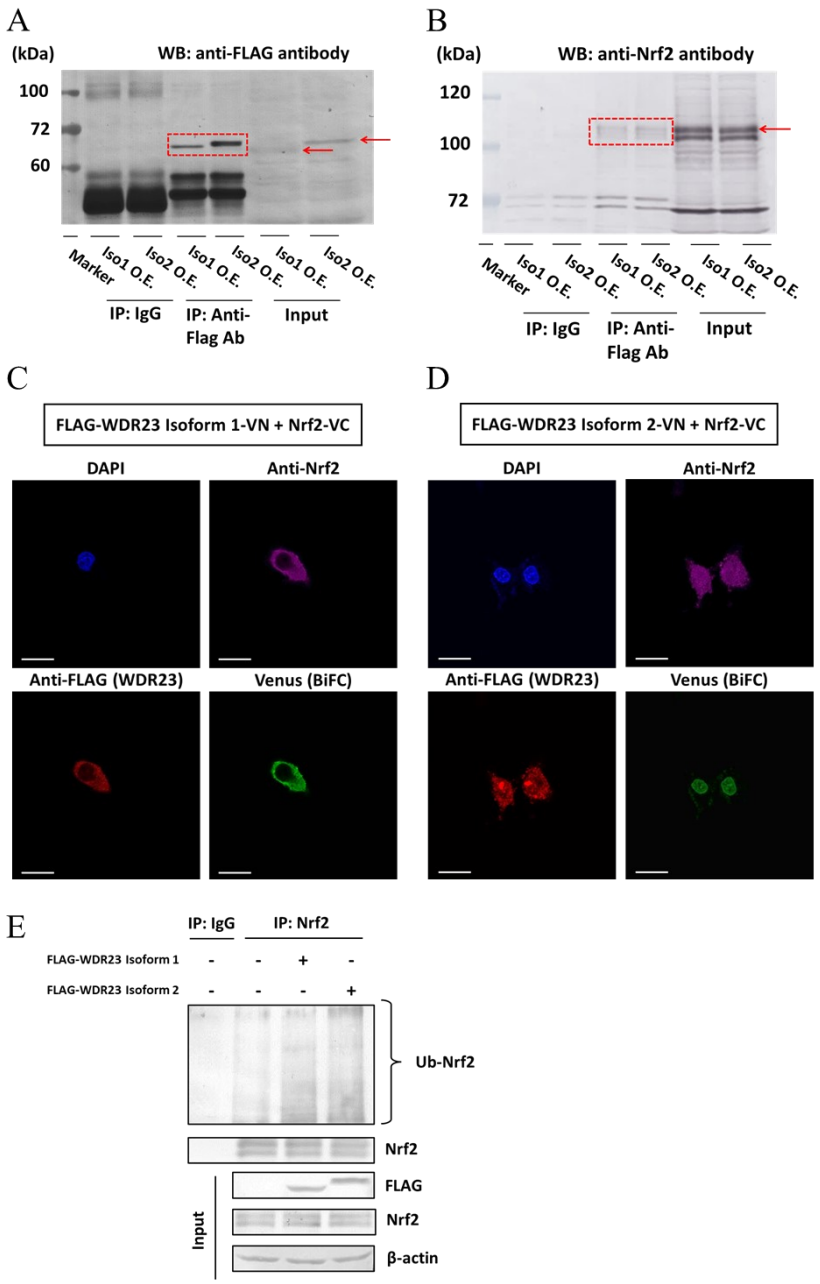

Figure 7. Interaction of WDR23 with Nrf2. HeLa cells were transfected with FLAG-WDR23 isoform 1 and FLAG-WDR23 isoform 2. Transfected cells were immunoprecipitated with an anti-FLAG antibody, and the immunoprecipitated proteins were subjected to immunoblotting analysis with anti-FLAG (A) and anti-Nrf2 (B) antibodies. (C-D) N- and C-terminal fragments of Venus fluorescent proteins were fused to the C-terminal of FLAG-WDR23 isoform 1 or FLAG-WDR23 isoform 2 and Nrf2, respectively. The interaction between each isoform of WDR23 and Nrf2 brings the N- and C-terminal fragments in proximity to reconstitute an intact fluorescent protein. (C) FLAG-WDR23 isoform 1-VN was co-expressed with Nrf2-VC in Hep3B. (D) FLAG-WDR23 isoform 2-VN was co-expressed with Nrf2-VC in Hep3B cells. Overexpression was confirmed with anti-Nrf2 or anti-FLAG antibodies. Venus fluorescence as the BiFC signal indicates the interaction. Scale bar: 20 μm. (E) Keap1-knockdown Hep3B cells were transfected with either FLAG-WDR23 isoform 1 or FLAG-WDR23 isoform 2 and were treated with MG132 (5 μM, 8 h), cell lysates were immunoprecipitated with the anti-Nrf2 antibody, subjected to immunoblotting using anti-Nrf2, anti-ubiquitin, anti-FLAG, and anti-β-actin antibodies.

The role of WDR23 isoform 2 on the regulation of nuclear Nrf2

To date, the regulation of Nrf2 protein stability is thought to occur strictly in the cytosol by Keap1. The identification of WDR23 isoform 2 that mainly localizes in nucleus as a regulator of Nrf2, raises a question of whether this isoform regulates nuclear Nrf2. In order to address this question, the effects of WDR23 isoform 2 on the nuclear Nrf2 were examined. WDR23 isoform 2 overexpression did not alter the cytosolic Nrf2 but significantly reduced nuclear Nrf2 (Fig. 8*A*).

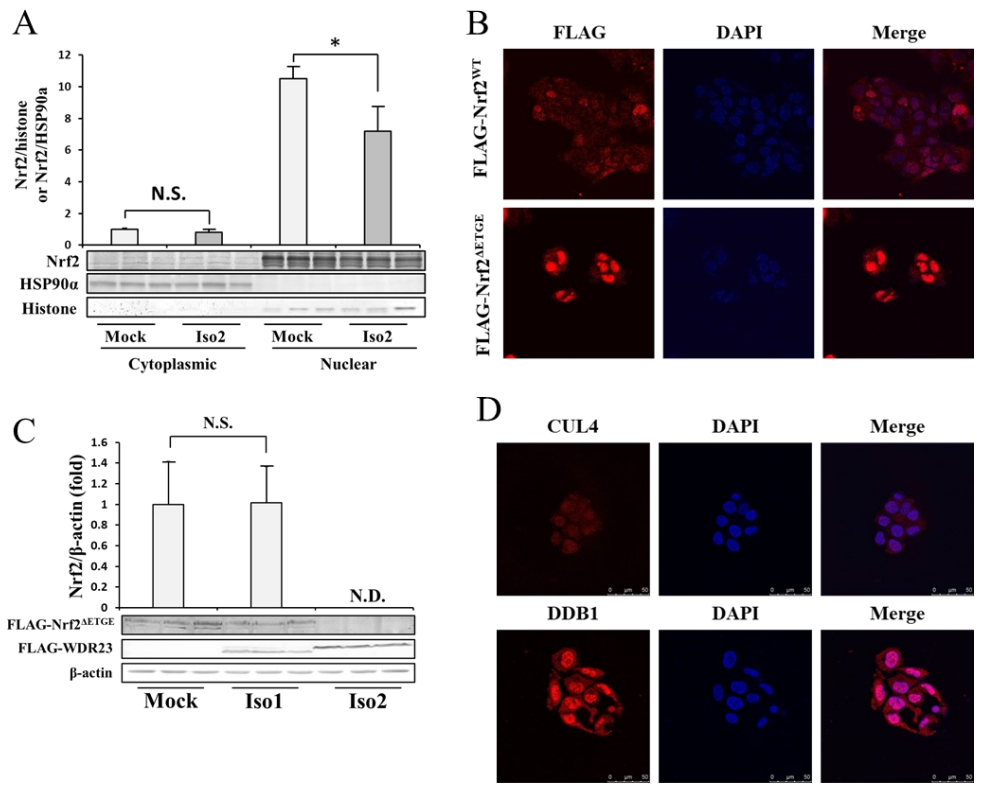

Figure 8. The role of WDR23 isoform 2 on the nuclear Nrf2 levels. (A) Keap1-knockdown Hep3B cells were transfected with FLAG-WDR23 isoform 2, and the changes of Nrf2 protein levels from the cytoplasmic or nuclear fraction were assessed by immunoblotting. (B) Representative images of immunofluorescence with DAPI staining to indicate the location of the nucleus (blue), FLAG-Nrf2^{WT} or FLAG-Nrf2$^{\Delta ETGE}$ (red). (C) Keap1-knockdown Hep3B cells were transfected with FLAG-Nrf2$^{\Delta ETGE}$ and either FLAG-WDR23 isoform 1 or isoform 2, and whole cell lysate was analyzed by immunoblotting against anti-FLAG and anti-β-actin antibodies. Graphs represent mean ± S.D. The value of the mock was set as 1.0. N.S. not significant, *$p<0.05$, N.D. not detected. (D) Representative images of immunofluorescence with DAPI staining to indicate the location of the nucleus (blue), CUL4 or DDB1 (red).

To further support this data, I constructed FLAG-tagged Nrf2$^{\Delta ETGE}$ mutant that localizes strictly in the nucleus (Fig. 8*B*) due to its inability to bind to Keap1 (44). The overexpression of WDR23 isoform 1 did not change the abundance of

Nrf2$^{\Delta ETGE}$, but the isoform 2 did (Fig. 8*C*) supporting the notion of spatial specificity of WDR23 isoforms in respect to their activity on Nrf2. Since the WDR23 is a substrate recognition protein for CRL4 E3 ligase, it requires the component of the CRL4 ligase including CUL4 and DDB1 for its activity. Because both isoforms of WDR23 are physiologically active in a distinct compartment of the cells, both CUL4 and DDB1 have to be present in cytosol and nucleus. In the present study, I proved that CUL4 was distributed evenly in cytosol and nucleus, while DDB1 was present in both compartment with the major distribution in the nucleus (Fig. 8*D*).

Identification of Nrf2 activators that modulate WDR23-Nrf2 system

A multitude of Nrf2 activators have been reported, most of which were identified to regulate Nrf2 via Keap1-dependent pathway. Hydrogen peroxide (H_2O_2) was reported to prevent Nrf2 ubiquitination by modifying Cys226, Cys613, Cys622, and Cys624 residues of the Keap1 (45). In response to tBHQ and sulforaphane (SFN), Cys151 has been found to be critical for the Keap1 sensor activity (40, 46). Bisphenol A (BPA) increases nitric oxide (NO) levels and activates Nrf2 via nitrosylation and subsequent inactivation of Keap1 (31). Chlorogenic acid also activates Nrf2 via a currently unknown mechanism (47). Because in the present study I speculated that WDR23-Nrf2 system supports the Keap1-Nrf2, studying whether WDR23 could completely replace Keap1, and whether WDR23 could act as a sensor of electrophiles and ROS, are necessary. To this end, I treated both Hep3B and lung adenocarcinoma cell line A549 with various Nrf2 activators. A549 cells harbor a G333C loss-of-function mutation of Kelch-like ECH associated protein 1 (Keap1) which results in the hyperactivation of the Nrf2 pathway (48), and A549 cells do not show any mutation in WDR23 based on the publicly available database DBKERO (Database of Kashiwa Encyclopedia for human genome mutations in Regulatory regions and their Omics contexts, https://kero.hgc.jp/) (49).

The treatment of Hep3B cells with all Nrf2 activators used in the present study significantly increased the total protein abundance of Nrf2 (Fig. 9*A*). However, the treatment of A549 cells with H_2O_2, tBHQ and BPA did not change Nrf2 levels. Interestingly, both CGA and SFN significantly increased Nrf2 levels in A549 cells (Fig. 9*B*). To further confirm these results, I overexpressed A549 cells with Keap1-WT construct, and the effects of those chemicals on Nrf2 were examined. As expected, the Nrf2 protein levels were elevated in Keap1-WT overexpressed A549 cells treated with H_2O_2, tBHQ, BPA, CGA and SFN (Fig. 9*C*). These results suggest that: (1) WDR23 does not act as a sensor for H_2O_2, tBHQ and BPA; and (2) CGA and SFN might regulate Nrf2 in a Keap1-independent and WDR23-dependent pathway.

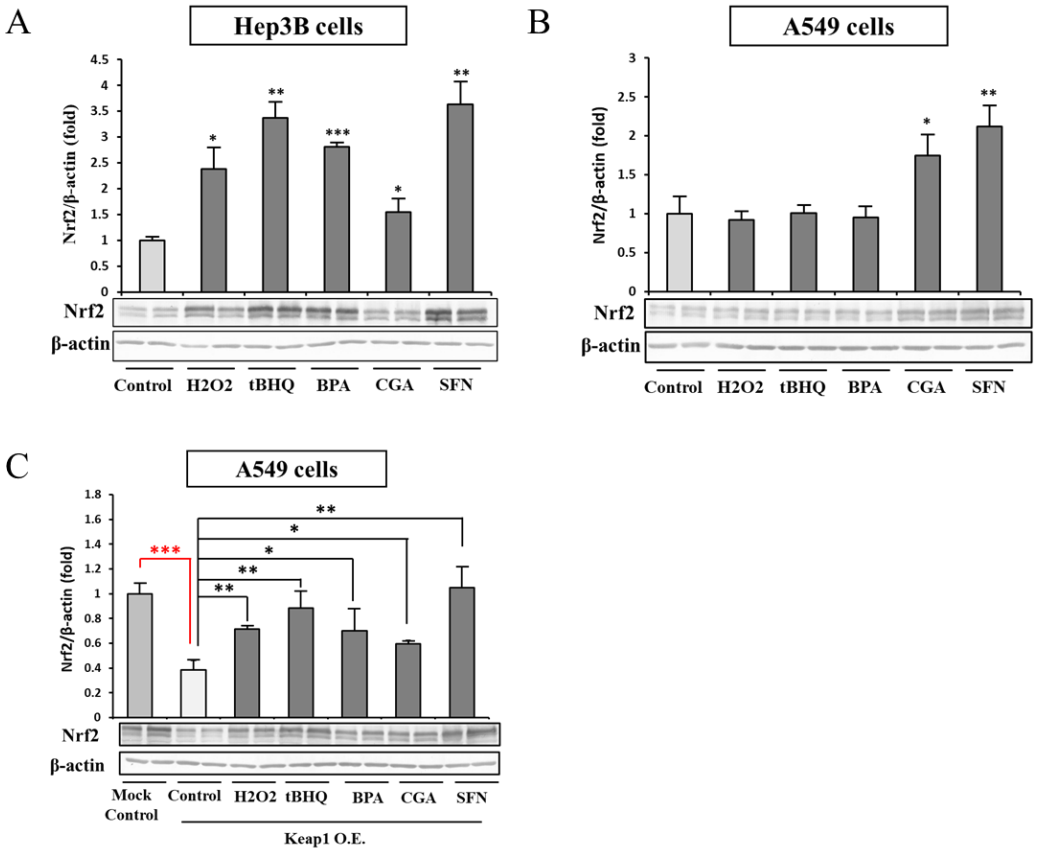

Figure 9. Effects of Nrf2 activators on WDR23-Nrf2 system. (A-B) Hep3B cells (A) and A549 cells (B) were treated with vehicle, H_2O_2 (100 μM; 8 h), tBHQ (60 μM; 8 h), BPA (50 μM, 8 h), CGA (50 μM, 8 h), or sulforaphane (10 μM; 8 h) and whole cell lysate was analyzed by immunoblotting against anti-Nrf2 and anti-β-actin antibodies. (C) A549 cells were transfected with Keap1-WT and after 24 hours were treated with vehicle, H_2O_2 (100 μM; 8 h), tBHQ (60 μM; 8 h), BPA (50 μM, 8 h), CGA (50 μM, 8 h), or sulforaphane (50 μM; 8 h). Total protein levels of Nrf2 were then assessed by immunoblotting. Graphs represent mean ± S.D. The value of the mock was set as 1.0. N.S. not significant, *p<0.05, **p<0.01 *versus* indicated cells.

Changes in DME mRNA levels by WDR23 knockdown

The knockdown of WDR23 in HeLa (Fig. 10*A*, *B*) and Hep3B (Fig. 11*A*, *B*) cells did not change the level of *Keap1* mRNA and vice versa. In order to examine the effect of Keap1 and WDR23 knockdown on the DME expression, Hep3B cells were mainly used, because HeLa cells only express 7 out of 13 genes tested (Fig. 10*C*-*O*). Almost all DME mRNA levels tested increased due to Keap1 knockdown in Hep3B cells, except for *mEH*, which was unaffected, and *CYP2E1* and *UGT1A9*, which were reduced. Of note, WDR23 knockdown increased Nrf2 levels and the expression of some Nrf2-driven DMEs, namely *CYP1A1*, *CYP3A4*, *CYP4B1*, *HO-1*, *NQO1*, and *UGT1A9*, whereas the expression of *CYP2C9*, *CYP2E1*, *CYP3A5*, *mEH*, and *MDR1* were not affected by WDR23 knockdown.

In contrast, the expression of *CYP2D6* and *UGT1A1*, which was increased by Keap1 knockdown, was reduced by WDR23 knockdown (Fig. 11*C-O*). The effects of Keap1 and WDR23 knockdown on DME expression of Hep3B cells are summarized in Table 3. These results suggested that either WDR23 regulates factors other than Nrf2 or that WDR23 regulates Nrf2 transcriptional activity in addition to protein levels.

Table 3. Summary of the effects of Keap1 and WDR23 knockdown on DMEs expression of Hep3B cells

Class	**Genes**	**Treatment**	
		Keap1 K.D.	**WDR23 K.D.**
Phase I Oxidation	CYP1A1	↑↑	↑↑
	CYP2C9	↑↑	=
	CYP2D6	↑↑	↓↓
	CYP2E1	↓	=
	CYP3A4	↑↑	↑↑
	CYP3A5	↑↑	=
	CYP4B1	↑↑	↑↑
	HO-1	↑↑	↑
Phase I Reduction	NQO1	↑↑	↑↑
Phase I Hydrolysis	mEH	=	=
Phase II Conjugation	UGT1A1	↑↑	↓
	UGT1A9	↓↓	↑
Phase III Transporter	MDR1	↑↑	=

'=' not changed, '↑' increased modestly, '↑↑' increased strongly, '↓' decreased modestly, '↓↓' decreased strongly

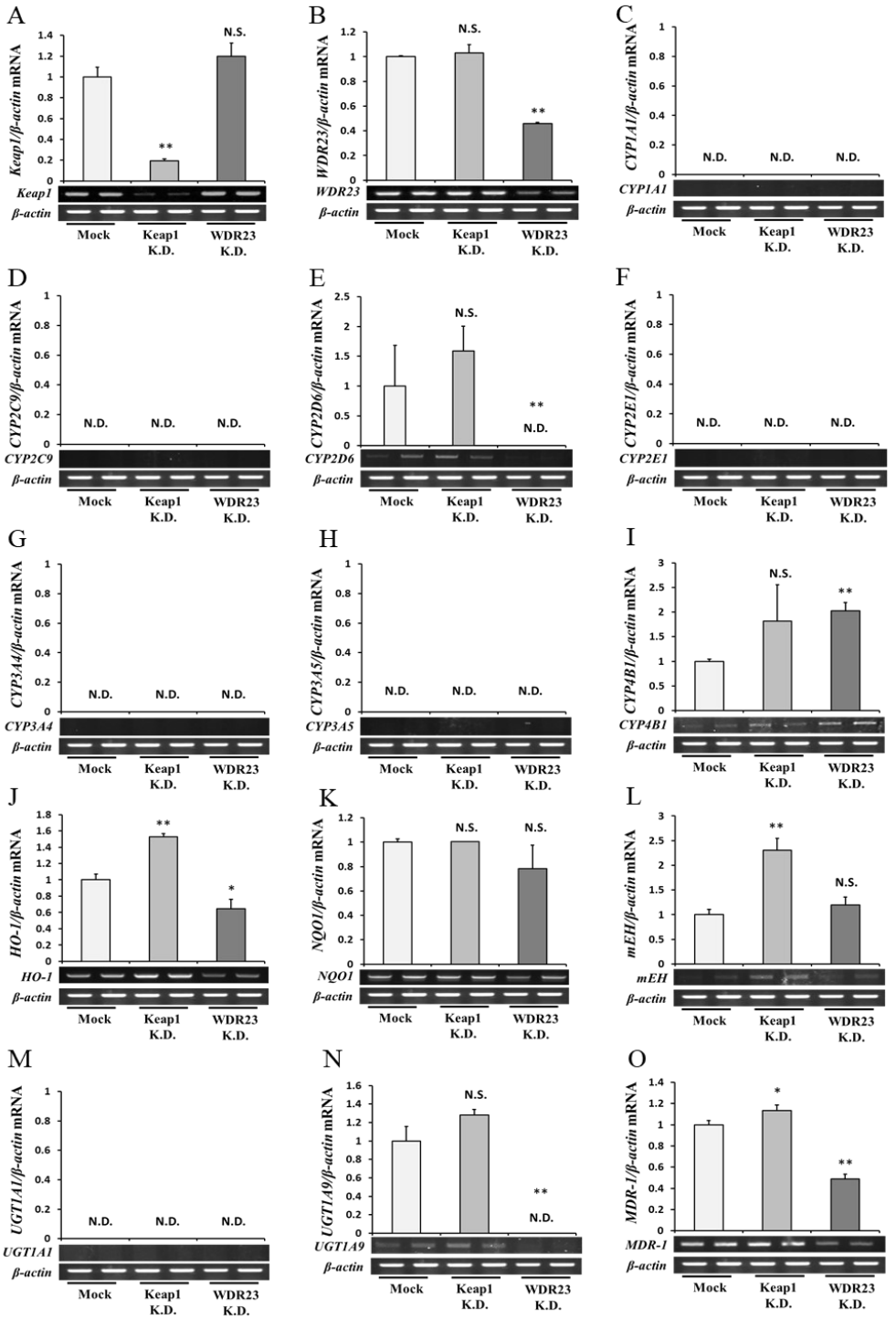

Figure 10. Changes in expression of Nrf2-regulated DMEs in Keap1- and WDR-23-knockdown HeLa cells. Keap1 knockdown (A) and WDR23 knockdown (B) efficiency was confirmed using RT-PCR. The mRNA expression levels of phase I oxidizing enzymes including *CYP1A1* (C), *CYP2C9* (D), *CYP2D6* (E), *CYP2E1* (F), *CYP3A4* (G), *CYP3A5* (H), *CYP4B1* (I), and *HO-1* (J), phase I reducing enzyme *NQO1* (K), phase I hydrolysis enzyme *mEH* (L), phase II conjugating enzymes including *UGT1A1* (M) and *UGT1A9* (N), and phase III transporter protein *MDR1* (O) were quantified using ImageJ, and presented as relative values to β-actin. All graphs are the mean ± S.D. The value of the mock (shRNA-GFP control cells transfected with siRNA-control) was set as 1.0. N.S. not significant, *p<0.05, **p<0.01 significantly different from the mock cells, N.D. not detected.

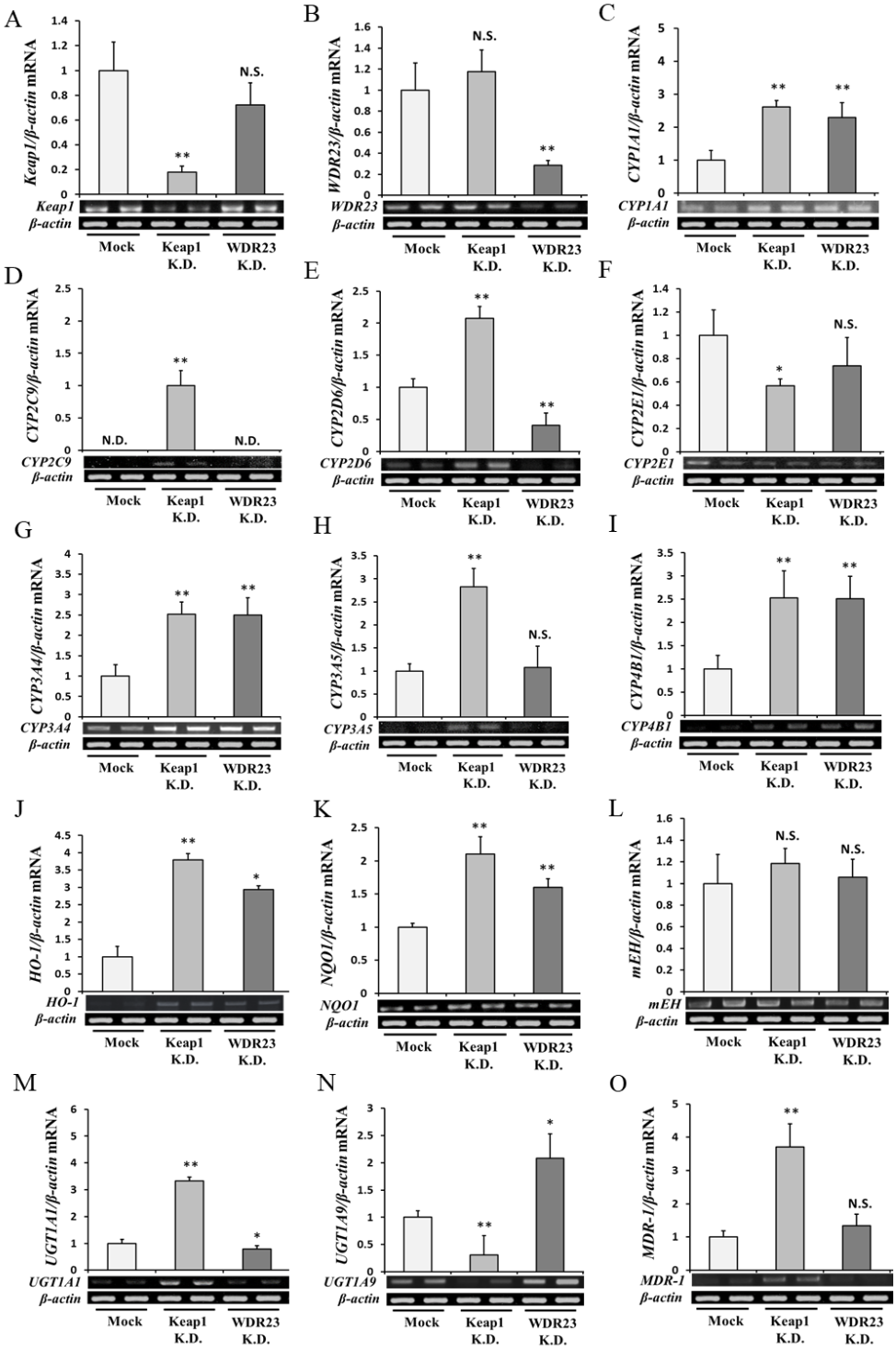

Figure 11. Changes in expression of Nrf2-regulated DMEs in Keap1- and WDR-23-knockdown Hep3B cells. Keap1 knockdown (A) and WDR23 knockdown (B) efficiency was confirmed using RT-PCR. The mRNA expression levels of *CYP1A1* (C), *CYP2C9* (D), *CYP2D6* (E), *CYP2E1* (F), *CYP3A4* (G), *CYP3A5* (H), *CYP4B1* (I), *HO-1* (J), *NQO1* (K), *mEH* (L), *UGT1A1* (M), *UGT1A9* (N), and *MDR1* (O) were quantified using ImageJ, and presented as relative values to β-actin (mean ± S.D). The value of the mock (shRNA-GFP control cells transfected with siRNA-control) was set as 1.0. N.S. not significant, *p<0.05, **p<0.01 significantly different from the mock cells, N.D. not detected.

I.4. Discussion

In this study, I demonstrated that overexpression of both WDR23 isoforms changed neither the level of Nrf2 nor the expression of DMEs. Results from this study were in contrast to the results of a previous study by Lo et al. (42), who reported that WDR23 overexpression alone in HEK-293T cells decreased the abundance of co-transfected Nrf2. This difference is likely due to the different cell types used in this study, for instance, Lo et al. used normal human embryonic kidney cells while in this study, cells derived from cancer were used instead, which may have different physiology from normal cells (50, 51). Additionally, the endogenous Nrf2 levels were investigated in this study instead of ectopically overexpressed Nrf2. Conversely, knockdown of WDR23 resulted in higher Nrf2 protein levels and diverse expression of many DMEs. These results suggested that both Keap1 and WDR23 simultaneously regulate Nrf2 protein levels in normal conditions. However, the effects of Keap1 knockdown more strongly increased Nrf2 and DME expression compared with WDR23 knockdown, indicating that Keap1 is a dominant regulator of Nrf2.

In addition, the study presented herein showed the physical interaction between both isoforms of WDR23 and Nrf2, demonstrating that WDR23 regulates the expression of Nrf2-regulated DME directly. WDR23 was reported previously to act as an adapter for CUL4-DDB1-RBX1 E3 ubiquitin ligase and subject several proteins to proteasomal degradation (33, 34). To gain insight into the role of WDR23 in the regulation of Nrf2 and Nrf2-dependent DMEs, the cellular localization of WDR23 in mammalian cells was investigated. Consistent with previous reports using *C. elegans* (14), human WDR23 isoform 1 localizes mainly in the cytoplasm, whereas isoform 2 resides in the nucleus. In addition, other components of CRL4 E3 ligase, including CUL4 and DDB1, were detected in both compartments, suggesting that both isoforms of WDR23 are biologically active. Distinct localization of WDR23 isoforms may impact their physiological roles. Recently, a study in *C. elegans* suggested that the distinct localization of WDR23 differentiates the functions, i.e., the proteasome and the proteasome-independent functions for isoform 2 and isoform 1, respectively (52). In this present study, there were differential effects of each isoform on Nrf2 and the expression of DMEs. WDR23 isoform 2 was found to regulate the abundance of nuclear Nrf2. The nuclear Nrf2 was thought to be regulated via nuclear export mechanism mediated by Fyn kinase, which phosphorylates tyrosine 568 of Nrf2 and subsequently degraded by cytosolic Keap1 (53). Thus, current findings expand our knowledge on the proteasome-dependent regulation of nuclear Nrf2. On the other hand, WDR23 isoform 1, which is exclusively located in the cytoplasm, may regulate the cytosolic Nrf2 levels together with Keap1 and prevent nuclear translocation of Nrf2.

The isoform 2 lacks 45–70th amino acid in isoform 1. Therefore, this sequence is hypothesized to be an NES. As expected, pretreatment of cells with the nuclear export inhibitor, leptomycin B, caused the nuclear accumulation of isoform 1, but no change in isoform 2 localization was observed. Thus, the 45–70th amino acid of isoform 1 may function as an NES. NES is a short leucine-rich peptide in a protein recognized by exportin/CRM1 that targets it for export from the nucleus to the cytoplasm (54). A study revealed that the most conserved pattern of NES is LxxLxL and a less common motifs to be LxxxLxL and LxxxLxxL, where "L" is a hydrophobic residue (often leucine) and "x" is any amino acids (55). Indeed, the sequence of LAQVLAYL is present within 45–70th amino acid of isoform 1 which is consistent with the LxxxLxxL NES motif.

Since CUL4, DDB1, and RBX1 are critical for the biological activities of the WDR23 system, all of these factors are required in both cytoplasm and nucleus for the WDR23 isoform 1 and 2, respectively. In the present study, I proposed the mechanism by which two isoforms of WDR23 are spatially regulated. The regulation of cellular localization of other components of this system, however, was not examined. Regardless, previous studies have proposed the mechanism by which the localization of CUL4, DDB1, and RBX1 is regulated. Guerrero-Santoro et al. (56) and Zou et al. (57) identified that the N-terminal of CUL4A contains the NLS, specifically between the 729 and 735 amino acid residues. The NLS scores by the PSORTII program showed that CUL4A has a low nuclear localization potential (−0.22), which was responsible for moderate CUL4A's nuclear localization and caused even distribution between cytosol and nucleus (56). In contrast to WDR23 and CUL4, DDB1 lacks NLS and is known to have the capability to enter the nucleus by forming a complex with either p48 (58) or CUL4 (56), which contain the NLS. As for the RBX1, there is currently no evidence of the mechanism by which its cellular distribution is regulated. Since RBX1 is a component of all members of the cullin protein family, its presence in all compartments of cells in which cullin E3 ligases are active is crucial. In the present study, I did not examine the localization of RBX1 due to its relationship with other cullins. Of note, other regulators of Nrf2, namely β-TrCP/CUL1 and Keap1/CUL3, also require RBX1 as its components, suggesting its low specificity. Regardless, study showed that RBX1 was detected in all compartment of the cells (58). Those study also showed that RBX1-CUL1 interaction was crucial for CUL1 translocation across the nuclear membrane, which may suggest that RBX1 nuclear translocation is mediated by the NLS present in CUL1 (59). This mechanism may also apply for other cullins, since all cullins bind to RBX1 (60).

Additionally, it is worth noting that the shape of FLAG-WDR23 isoform 1-overexpressing cells were different from other cell groups. This was probably because WDR23 regulates factors that play a role in the cell shape. FLAG-WDR23

isoform 1 exclusively localizes in the cytoplasm, whereas treatment with leptomycin B in FLAG-WDR23 isoform 1-overexpressing cells caused nuclear accumulation of WDR23 isoform 1. Isoform 2 localized mainly in nucleus, with or without leptomycin treatment. Hence, suggesting that WDR23 regulates nuclear factors that determine the shape of the cells. Nevertheless, further study is required to identify what nuclear factors regulated by WDR23 are responsible for the change in the shape of the cells.

Almost all phase I enzymes in this study were induced by Keap1 knockdown, except for *mEH*, which was unaffected, and *CYP2E1* which were reduced. Little has been reported regarding the regulation of phase I oxidative DMEs by Nrf2. Previously, the induction of *Cyp2a5* by Nrf2 in mouse primary hepatocytes was reported (61). BPA induced *Cyp1a1*, but not *Cyp3a2*, expression in the livers of rats, and this was found to be mediated by the nitrosylation of Keap1 (31). Another study reported that Keap1-hepatocyte knockout mice exhibit higher expression levels of *Cyp2a5*, *Cyp2c50*, *Cyp2c54*, and *Cyp2g1* (62). In contrast to this study, previous studies reported that Nrf2 drives *mEH* transcription in mouse hepatocytes (29, 63) and mouse embryonic fibroblasts (64). In this study, the hepatoma cell line Hep3B was used, which may have caused the differing results from previous *in vivo* investigations (65). Keap1 knockdown in this study also induced increased expression of the phase II enzyme *UGT1A1* and phase III transporter *MDR1*. Similar results have been reported and reviewed (30). Although the induction of *UGT1A1* by a Keap1/Nrf2-dependent mechanism was reported previously (66), there are few studies on Keap1/Nrf2-dependent regulation of *UGT1A9*. Results reported herein showed that Keap1 knockdown reduced *UGT1A9* expression. Consistent with this result, Kalthoff et al. (67) reported that *UGT1A9* lacks tBHQ (Nrf2)-mediated induction due to its different ARE motif with a single base pair located in the binding element.

The knockdown of WDR23 led to a similar but weaker increase in DMEs, including *CYP1A1*, *CYP3A4*, *CYP4B1*, *HO-1*, and *NQO1*. The knockdown of WDR23 did not affect the expression of *CYP2C9*, *CYP2E1*, *CYP3A5*, *mEH*, or *MDR1*. The opposite effect of Keap1 and WDR23 knockdown was observed in the expression of *CYP2D6*, *UGT1A1*, and *UGT1A9*. Although *CYP2D6* was expressed at a low level in the human liver (68), it is a highly polymorphic enzyme that catalyzes the metabolism of many types of drugs (69). Thus, only a small number of studies have investigated the transcriptional regulation of *CYP2D6*, including the role of hepatocyte nuclear factor 4*α* (70) and CCAAT/enhancer-binding protein (C/EBP) α (71). To the best of my knowledge, this study is the first to report the potential involvement of Keap1-Nrf2 and WDR23-Nrf2 in the transcriptional regulation of *CYP2D6*. However, the opposite effect of Keap1 and WDR23 knockdown on the expression of *CYP2D6* remains unclear. WDR23 also had an

opposite effect to Keap1 knockdown regarding *UGT1A1* and *UGT1A9*. Keap1 knockdown increased *UGT1A1* expression mediated by Nrf2 binding to the ARE in the phenobarbital-response enhancer module region of the *UGT1A1* gene (66). In contrast, WDR23 knockdown inhibited *UGT1A1* expression. The expression of *UGT1A1* was inhibited by the CDK2 signaling pathway (72), and CDK2 was recently reported to be regulated by WDR23 (73). Therefore, the differential effects of Keap1 and WDR23 knockdown may involve Nrf2 and many other signaling pathways. It is also possible that Keap1 and WDR23 regulate Nrf2 transcriptional activity through a mechanism other than proteasomal degradation. However, further studies are necessary to elucidate the mechanism of differential DME responses to Keap1 and WDR23.

The *Keap1* gene is frequently mutated in cancer cells, leading to concomitant activation of Nrf2 (74). Because Nrf2 activates cytoprotective genes and improves phase III drug efflux transport, mutations in *Keap1* correlate with chemoresistance and result in poorer clinical outcomes (75). Previous studies revealed that patient survival is significantly lower in those with tumors with *Keap1* mutation (76–78). Therefore, interventions that activate WDR23 in cancer cells bearing *Keap1* mutation may be useful.

Taken together, this study provides evidence of WDR23 as a novel regulator of DMEs. These data support a long-standing theory that Keap1 is a canonical regulator of Nrf2 in mammalian cells and that WDR23 assists in Nrf2 regulation when Keap1 function is impaired (Fig. 12). Many factors can induce the activation of Nrf2 pathway such as oxidants, electrophiles, and kinases. Mammalian cells evolutionary developed Keap1 signaling in order to adapt and respond to more complex insults. However, the preservation of WDR23 is important to support the impairment of Keap1. Therefore, this study demonstrated WDR23 to be an important supporter of Keap1 that regulates Nrf2-dependent DMEs. Further studies are required to clarify in which conditions and the mechanism by which WDR23 supports Keap1 signaling.

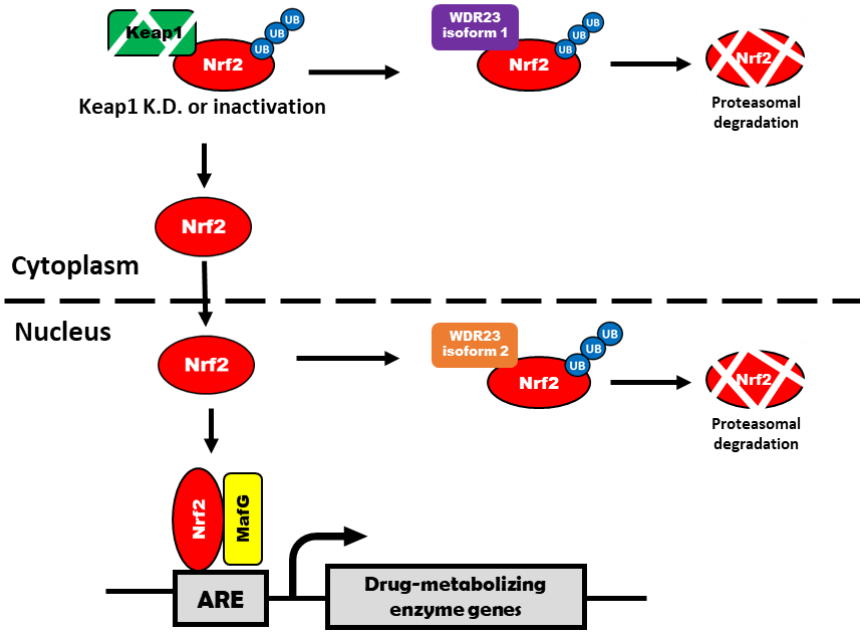

Figure 12. Proposed model of Nrf2 regulation by Keap1 and WDR23. Under basal conditions, Nrf2 interacts with both Keap1 and WDR23 isoform 1 in the cytosol, and with WDR23 isoform 2 in the nucleus. These interactions lead to the ubiquitination and proteasomal degradation of Nrf2. Under Keap1 down-regulation or inactivation by oxidative stress or somatic mutations, Nrf2 regulation is shifted to the WDR23 system.

CHAPTER II

The Mechanism Behind Signaling Crosstalk between Keap1 and WDR23 Pathways

[*] This chapter was adapted from the *Journal of Biological Chemistry*, Volume 296, doi: 10.1016/j.jbc.2021.100704, (2021), Ferbian Milas Siswanto, Ami Oguro, & Susumu Imaoka, Sp1 is a substrate of Keap1 and regulates the activity of $CRL4A^{WDR23}$ ubiquitin ligase toward Nrf2.

II.1. Introduction

The transcription factor nuclear factor erythroid 2 (NFE2)-related factor 2 (Nrf2) is a central regulator of cellular redox homeostasis. It is beneficial for cytoprotection against harmful extrinsic and intrinsic insults, such as xenobiotics and oxidative stress. Under basal conditions, Nrf2 mRNA is constitutively expressed (79), and the abundance of Nrf2 protein is regulated at the protein level by Kelch-like-ECH-associated protein 1 (Keap1), a substrate adaptor protein for the Cullin 3 (CUL3)-containing E3 ubiquitin ligase complex (80). Keap1 is a cysteine-rich protein, and human Keap1 has 27 cysteine residues that function as sensors of various oxidants and electrophiles (81). Homodimeric Keap1 binding to monomeric Nrf2 through the ETGE and DLG motifs promotes Nrf2 degradation by the ubiquitin-proteasome pathway, thereby maintaining low cellular levels of Nrf2. The cysteine residues in Keap1 are modified by oxidative stress, which results in conformational changes in Keap1 and releases the weaker interaction with the DLG motif (6, 44). Although Keap1-ETGE binding is preserved, the ubiquitination of Nrf2 does not occur, providing time for newly synthesized Nrf2 to accumulate and translocate into the nucleus. In the nucleus, Nrf2 heterodimerizes with small Maf (sMaf) protein family members and binds to antioxidant response elements (AREs) or electrophile responsive elements (EpREs) located in the regulatory regions of antioxidative and phase II cytoprotective genes, such as heme oxygenase-1 (HO-1) and NAD(P)H quinone dehydrogenase 1 (NQO1) (82, 83).

In addition to the canonical Keap1 pathway, β-transducin repeat-containing protein (β-TrCP) and HMG-CoA reductase degradation 1 homolog (Hrd1) have been reported to induce proteasome-dependent Nrf2 degradation in a Keap1-independent manner (2, 3). WD40 Repeat Protein 23 **(**WDR23) was recently shown to function as a regulator of Nrf2 levels and activity independently of Keap1 (42, 84). Additionally, WDR23 was recently found to regulate the expression of Nrf2-driven drug-metabolizing enzymes (43). WDR23, also known as DDB1 and Cullin4 associated factor 11 (DCAF11) in mammalian cells, is a substrate recognition protein for the Cullin 4-RING ligase (CRL4) complex that consists of CUL4 as a scaffold protein, DDB1 as an adaptor protein, and RBX1 as a RING-finger protein (85). Mammalian WDR23 possesses two isoforms produced by alternative splicing, isoforms 1 and 2, with isoform 2 being deficient in the 45–70th amino acids of isoform 1. WDR23 isoform 1, which primarily localizes in the cytoplasm, regulates cytoplasmic proteins, whereas isoform 2 predominantly resides in the nucleus to inhibit the activity of nuclear factors by promoting protein turnover (52). WDR23 targets various proteins involve in diverse pathways for degradation via ubiquitination, including Holliday junction resolvase GEN-1 (52), p21 (35), stem-loop binding protein (SLBP) (36), KRAB-associated protein 1 (Kap1) (86), centromeric protein A (CENP-A) (87) and Nrf2 (42).

The transient activation of Nrf2 in normal cells is beneficial for cytoprotection and the prevention of pathological conditions; however, its consecutive activation in cancer cells is responsible for chemoresistance and is associated with a poor prognosis (88). Therefore, the precise regulation of Nrf2 levels is crucial. A somatic mutation in highly conserved Kelch or the intervening region domain of the *Keap1* protein that results in the constitutive activation of Nrf2 often occurs in cancer cells (48, 89). Therefore, the second layer of Nrf2 regulation is important for preventing carcinogenesis and chemoresistance. In CHAPTER I, it was found that the knockdown of WDR23 was sufficient to increase the level and transactivity of Nrf2, whereas its overexpression only affected Nrf2 under Keap1 knockdown (43). These findings indicate that WDR23 regulates Nrf2 under basal conditions, while the further induction of WDR23 activity toward Nrf2 requires the inhibition of Keap1. Therefore, WDR23 might play a major role in the regulation of Nrf2 in cancer cells bearing *Keap1* mutation. However, the molecular mechanisms underlying crosstalk between these two independent and parallel regulators of Nrf2, particularly that by which WDR23 senses the function of Keap1, have not yet been elucidated.

Specificity protein 1 (Sp1) is a ubiquitously expressed nuclear transcription factor belonging to the C_2H_2-type zinc-finger protein family. Sp1 regulates gene expression via protein-protein interactions, such as with vascular endothelial growth factor receptor-2 (VEGFR-2) (90), or acts in concert with other transcription factors, including Stat1 (91), nuclear factor-κB (NF-κB) (92), and EGR-1 (93), in the absence of the TATA box. It binds to the sequence known as the GC box (GGGCGG or CCGCCC) in the promoters of numerous genes with high affinity (94, 95). Sp1 was initially regarded as a coordinator of the constitutive expression of housekeeping genes; however, recent studies showed that Sp1 responded to physiological and pathological stimuli (96, 97). Previous findings clearly demonstrated that Sp1 protein levels and transcriptional activity were induced by oxidative stress (98–100). For example, study reported that high glucose-induced oxidative stress increased nuclear Sp1 levels, which inhibited the expression of *sEH* (97). Increases in the level and activity of Sp1 have been widely proven to be responsible for oxidative stress-related carcinogenesis, including proliferation, the cell cycle, invasion, metastasis, angiogenesis, and the inhibition of apoptosis in hepatocellular carcinoma (101). Although Sp1 plays a role in the oxidative stress response pathway, the underlying molecular mechanisms have not yet been elucidated in detail.

In the present study, I demonstrated the role of Sp1 as a mediator of Keap1-WDR23 crosstalk for the regulation of Nrf2. The results obtained herein revealed that Keap1 directly regulates Sp1. The stabilization of Sp1 during the Keap1 knockdown resulted in the transcriptional activation of *CUL4A* and induced the WDR23-dependent regulation of Nrf2.

II.2. Materials and methods

Materials

Dulbecco's modified Eagle's medium (DMEM), tert-butylhydroquinone (tBHQ), hydrogen peroxide, an anti-DYKDDDDK (FLAG) antibody, anti-Myc tag monoclonal antibody, anti-GFP(VC) antibody (mFX75), and horseradish-peroxidase-conjugated goat anti-mouse IgG were purchased from Wako Pure Chemical Industries (Osaka, Japan). MG132 (Z-Leu-Leu-Leu-H) was purchased from the Peptide Institute (Osaka, Japan). Mithramycin A was from Cayman Chemicals (Ann Arbor, MI). Penicillin-streptomycin solution, fetal bovine serum (FBS), and geneticin (G418) were from Sigma Chemical Co. (St. Louis, MO). Nitrocellulose membrane, horseradish-peroxidase-conjugated goat anti-rabbit IgG, and 4-chloro-1-naphthol were purchased from Bio-Rad Laboratories (Hercules, CA). Isogen was from Nippon Gene (Toyama, Japan), and Revert Aid^{TM} M-MuLV Reverse Transcriptase was from MBI Fermentas (Vilnius, Lithuania). KOD Plus Neo and Fx Neo DNA polymerase were from Toyobo (Tokyo, Japan). DAPI (4′,6-diamidino-2-phenylindole) was from Dojindo (Kumamoto, Japan). Alexa Fluor® 594-conjugated goat anti-mouse IgG and Alexa Fluor® 647-conjugated goat anti-rabbit IgG were from Abcam (Carlsbad, CA). Anti-CUL4, anti-KLF15, and anti-AP2α antibodies were from Santa Cruz Biotechnology (Santa Cruz, CA). An anti-Sp1 antibody was purchased from Cell Signaling Technology. An anti-ubiquitin antibody (clone FK2) was from StressMarq Bioscience. The anti-Nrf2, anti-Keap1, anti-WDR23, anti-β-actin, and anti-histone H3 antibodies were prepared as described previously (5, 43, 102).

Plasmid constructs

The entire coding region of human Sp1 (NM_138473.2) was amplified by PCR with primer sets 1 and 2 (Table 1). Primers were accompanied by a restriction site (underline). Amplified DNA was then digested by the restriction enzymes *EcoR*I and *Xho*I and ligated into the pCMV-Myc vector (Clontech Laboratories). In the BiFC assay, Sp1 cDNA was amplified with primers 2 and 3, VN155 without the stop codon was amplified using pBiFC-VN155 (Addgene, Watertown, MA) as a template with primer sets 4 and 5, and oligonucleotide sets 6 and 7 for the linker $(GGGS)_2$ were annealed and then subsequently inserted into the pcDNA3.1(+) vector (Invitrogen, Carlsbad, CA) with *EcoR*I and *Xho*I, *Hind*III and *BamH*I, and *EcoR*I respectively. Mouse Sp1 (AF022363.1) was amplified by PCR with primer sets 8 and 9, digested by the restriction enzymes *Sal*I and *Not*I and ligated into the pCMV-Myc vector. The cDNA of human CUL4A (NM_001008895.4) and mouse CUL4A (NM_146207.3) were amplified by PCR with primers 10 and 11; and 12 and 13, respectively and then inserted into the pCMV-Myc vector with the *Sal*I and *Not*I sites.

Table 1. Primers used for plasmid constructs

No.	Sequences	Descriptions
1	5'- CTGAATTCCCATGAGCGACCAAGATCACTCCAT -3'	Fw; 1–23 of human *Sp1* cDNA; underline, *Eco*RI site; double underline, start codon
2	5'- TAACTCGAGGTATGGCCCATATGTCTCTGGCC -3'	Rv; downstream of human *Sp1* cDNA; underline, *Xho*I site; stop codon is upstream of this primer
3	5'- GGAATTCATGAGCGACCAAGATCACTC -3'	Fw; 1–20 of human *Sp1* cDNA; underline, *Eco*RI site; double underline, start codon
4	5'- TATAAGCTTACCATGGTGAGCAAGGGCGAGGAGC -3'	Fw; 1–22 of VN155; underline, *Hind*III site; double underline, start codon
5	5'- TTGGATCCGGCGGTGAGATAGACGTTGTGGCTG -3'	Rv; 441-465 of VN155; underline, *BamH*I site
6	5'- AATTCTGGAGGTGGCGGGAGCGGAGGTGGCGGGAGTG -3'	$(GGGS)_2$ linker sequence; sense
7	5'- AATTCACTCCCGCCACCTCCGCTCCCGCCACCTCCAG -3'	$(GGGS)_2$ linker sequence; antisense
8	5'- ATAAGTCGACCATGAGCGACCAAGATCACTCCAT-3'	Fw; 1–23 of mouse *Sp1* cDNA; underline, *Sal*I site; double underline, start codon
9	5'- TAGCATTTATGCGGCCGCTTAGAAACCATTGCCACTGA -3'	Rv; 2336–2355 of mouse *Sp1* cDNA; underline, *Not*I site; double underline, start codon
10	5'- ATAAGTCGACCGCGGACGAGGCCCCGCGGAA -3'	Fw; 3–23 of human *CUL4A* cDNA; underline, *Sal*I site
11	5'- TAGCATTTATGCGGCCGCTCAGGCCACGTAGTGGTACT -3'	Rv; 2261–2280 of human *CUL4A* cDNA; underline, *Not*I site; double underline, stop codon
12	5'- ATAAGTCGACCATGGCGGACGAGGGCCCTCG -3'	Fw; 1–20 of mouse *CUL4A* cDNA; underline, *Sal*I site; double underline, start codon
13	5'- TAGCATTTATGCGGCCGCTCATGCCACGTAGTGGTACT -3'	Rv; 2261–2280 of mouse *CUL4A* cDNA; underline, *Not*I site; double underline, stop codon
14	5'- ATAAGAATGCGGCCGCATGGGATCGCGGAACAGCAG -3'	Fw; 1–20 of human *WDR23* isoform 1 cDNA; underline, *Not*I site; double underline, start codon
15	5'- TATCTAGACTACTGGGGTGAGGAAAAGG -3'	Rv; 1621–1641 of human *WDR23* isoform 1 cDNA; underline, *Xba*I site; double underline, stop codon
16	5'- GTCCAAGAGGGCCTGGGCCAGATCCACATC -3'	Rv; 115–144 of human *WDR23* isoform 2 cDNA; dotted underline, complementary to the primer 17
17	5'- CAGGCCCTCTTGGACTCAGA -3'	Fw; 129–149 of human *WDR23* isoform 2 cDNA; dotted underline, complementary to the primer 16
18	5'- CTGAATTCTATGGGATCACGGAACAGCAG -3'	Fw; 1–20 of mouse *WDR23* isoform 1 cDNA; underline, *Eco*RI site; double underline, start codon
19	5'- CTGAATTCTATGAAGATGTGGATCTGGCCCAGAGGCCAAGTGAGACTGG -3'	Fw; 1–40 of mouse *WDR23* isoform 2 cDNA; underline, *Eco*RI site; double underline, start codon
20	5'- TAGCATTTATGCGGCCGCCTACTGAGGTGAGGAAAAGG -3'	Rv; 1631–1650 of mouse *WDR23* isoform 1 cDNA; underline, *Not*I site; double underline, stop codon
21	5'- AATGGATCCATGCAGCCAGATCCCAGGCC -3'	Fw; 1–20 of human *Keap1* cDNA; underline, *BamH*I site; double underline, start codon
22	5'- CCGCTCGAGTCAACAGGTACAGTTCTGCT -3'	Rv; 1856–1875 of human *Keap1* cDNA; underline, *Xho*I site; double underline, stop codon
23	5'- ATTAGTCGACTATGCAGCCAGATCCCAGGCC -3'	Fw; 1–20 of human *Keap1* cDNA; underline, *Sal*I site; double underline, start codon
24	5'- CCGGGTACCACAGGTACAGTTCTGCTGGT -3'	Rv; 1853–1872 of human *Keap1* cDNA; underline, *Kpn*I site

The cDNA of human WDR23 isoform 1 (NM_025230.4) was amplified using primer sets 14 and 15. The cDNA of human WDR23 isoform 2 (NM_181357.2) was obtained by PCR with two steps using human WDR23 isoform 1 cDNA as a template, as previously described (43). In brief, nucleotide fragment 1 was amplified with primer sets 14 and 16. Nucleotide fragment 2 was amplified with primers 15 and 17. Full-length human WDR23 isoform 2 was amplified in the second round of PCR from fragments 1 and 2 with primers 14 and 15. Amplified human WDR23 isoforms 1 and 2 were digested by the restriction enzymes *Not*I and *Xba*I and then ligated into the 3×FLAG-pcDNA4 vector (Invitrogen). Mouse WDR23 isoform 1 (NM_001199009.1) and isoform 2 (XM_006519087.5) were amplified by PCR with primers 18 and 20; and 19 and

20, respectively and then inserted the 3×FLAG-pcDNA4 vector with the *EcoR*I and *Not*I sites. Human Keap1 cDNA (NM_203500.2) was amplified by PCR with primers 21 and 22 and then inserted into the 3×FLAG-pcDNA4 vector with the *BamH*I and *Xho*I sites. In the BiFC assay, human Keap1 cDNA without a stop codon was amplified using primers 23 and 24 and then inserted into the pBiFC-VC155 vector (Addgene) with the *Sal*I and *Kpn*I sites.

RNA interference

Regarding the knockdown of Keap1 and Sp1 using shRNA, specific target regions of Keap1 and Sp1 were designated and inserted into the pBAsi-hU6 Neo Vector (Takara Bio Inc.) according to a previously described procedure (5, 97). The target sequence for Keap1 was 5'-GCAGGCCTTTGGCATCATGAACG-3' and the target for Sp1 was 5'-AATGCCAATAGCTACTCAACT-3'. The nucleotide sequence for control shRNA against GFP was 5'-CTCGAGTACAACTATAACTCA-3'. In the WDR23 knockdown, siRNA against WDR23 (Cat. No. SI05029899) with the target sequence of 5'-CUGGGUCUUUAGGGUAGGACA -3' was purchased from Qiagen (Hilden, Germany). AllStars Negative Control (SI03650318, Qiagen) was used as control siRNA. shRNA and siRNA were transfected into cells using ScreenFect™ A (Wako, Osaka, Japan) according to the manufacturer's instructions. Transfectants of shRNA-Mock, shRNA-Keap1, or shRNA-Sp1 were selected using G418.

Cell culture, transfection, and treatment

The human hepatoma cell line Hep3B was obtained from the Cell Resource Center for Biomedical Research at the Institute of Development, Aging, and Cancer of Tohoku University (Sendai, Japan). The mouse hepatoma cell line Hepa1-6 (RCB1638) was from RIKEN BRC Cell Bank (Tsukuba, Japan). Primary mouse hepatocyte was isolated from male C57BL/6JJc1 mice (5 weeks old, CLEA Japan) by the two-step collagenase perfusion technique according to previously described method with minor modifications (103). Experiments that included animals were conducted in accordance with guidelines on the welfare of the experimental animals and with approval of the Ethics Committee on the use of animals of Kwansei Gakuin University. Cells were cultured in DMEM containing 10% (v/v) FBS, penicillin (100 units/mL), and streptomycin (100 μg/mL), and maintained at 37°C in 5% CO_2 and 95% air. The transfection of the indicated constructs was performed using the calcium phosphate method or Effectene® (Qiagen, Hilden, Germany). Cells were cultured in the presence or absence of mithramycin A (100 nM, 8 h), tBHQ (60 μM, 8 h), H_2O_2 (100 μM; 8 h), or MG132 (5 μM, 8 h).

Immunoprecipitation and immunoblotting

Cells were washed with ice-cold PBS, collected, lysed in immunoprecipitation buffer (50 mM Tris-HCl, pH 8.0 and 150 mM NaCl, 1% Triton X-100, and 1 mM phenylmethylsulfonyl fluoride), and centrifuged at 14,000 × *g* for 15 min. The protein-containing supernatant was incubated with 2 μL of the anti-Myc antibody, anti-FLAG antibody, or unimmunized mouse serum at 4°C for 2 h. Twenty microliters of protein G-Sepharose (50% (w/v); GE Healthcare, Chicago, IL) was then added to the solution and incubated at 4°C for 1 h. Samples were washed with immunoprecipitation buffer containing 0.1% Triton X-100. Anti-Nrf2, anti-CUL4, anti-Sp1, anti-Keap1, anti-WDR23, anti-ubiquitin, anti-Myc, anti-FLAG, or anti-β-actin was used for immunoblotting. In the present study, β-actin was used as a loading control. Band intensity was quantified using NIH Image software ImageJ.

BiFC assay

VN155 (N-terminal half of Venus) fused to the N-terminal of Sp1 was co-expressed with VC155 (C-terminal half of Venus) fused to the C-terminal of Keap1. Twenty-four hours after transfection, cells were rinsed with PBS and fixed for 20 minutes with 4% paraformaldehyde (PFA) in PBS, then rinsed with TPBS (PBS + 0.2% Tween 20 (Bio-Rad, Hercules, CA)), followed by blocking with 0.1% bovine serum albumin (Wako, Osaka, Japan) in TPBS. Cells were subsequently incubated either with the anti-Keap1 and anti-VC antibody followed by an incubation with Alexa Fluor® 594-conjugated goat anti-mouse IgG and Alexa Fluor® 647-conjugated goat anti-rabbit IgG. The nucleus was counterstained using DAPI. Images were obtained by confocal microscopy TCS SP8 (Leica Microsystems, Wetzlar, Germany). Venus fluorescence was detected as a BiFC signal.

Luciferase reporter gene assay

Hep3B cells were transiently transfected with 0.25 μg of the pGL3-containing *CUL4A* promoter or NQO1-ARE and pRL-null vector (12.5 ng) as an internal control with GenePORTER TM2 transfection reagent (Gene Therapy Systems). Cells were co-transfected with 0.25 μg of shGFP, shKeap1, or shSp1 in pBAsi-hU6, pCMV-Mock, or pCMV-Sp1. Forty-eight hours post-transfection, luciferase activity was assayed with a luminometer (Lumat LB9507; Berthold) using the Dual-Luciferase Reporter Assay System (Promega) according to the manufacturer's protocol. Firefly luciferase activity was normalized to Renilla luciferase activity.

ChIP assay

The ChIP assay was performed as described previously (97). In brief, Hep3B cells were crosslinked with 1.5% (w/v) formaldehyde for 10 min. The crosslinking reaction was quenched by the addition of glycine to a final concentration of 0.125

M. Cells were then washed three times with ice-cold PBS and lysed in ChIP buffer containing 0.5% NP-40, 1% Triton X-100, 150 mM NaCl, 50 mM Tris-HCl (pH 7.5), 0.5 mM DTT, 5 mM EDTA, 0.5 mM PMSF, and 10 mM NaF, sonicated on ice, and centrifuged (14,000 × *g* at 4°C for 10 min). Fifty microliters of the supernatant was collected as the input, and the remnant was incubated with control IgG or the anti-Sp1 antibody at room temperature for 30 min. Protein A-Sepharose beads were added and incubated at 4°C for 45 min. Beads were washed five times with ChIP buffer. After an extensive wash step, complexes were eluted with buffer containing 0.1 M $NaHCO_3$ and 1% SDS followed by an incubation at room temperature for 15 min. Reverse crosslinking was performed with the addition of 0.4 M NaCl at 65°C overnight. The mixture was then treated with proteinase K at 50°C for 30 min and DNA was purified. The *CUL4A* promoter fragments, −55 to +155, −265 to −56 and −825 to −626, were detected with primer sets 1 and 2, 3 and 4, and 5 and 6 respectively (Table 2).

Table 2. Primers used for ChIP assay

No.	Sequences	Descriptions
1	5'- CGGAGCTCGGCGGGCGGCGG -3'	Fw; upstream of *CUL4A* −55 to −36
2	5'- GGTCTGTCTCGGAAGTTCTT -3'	Rv; upstream of *CUL4A* +136 to +155
3	5'- CGGGAGTCCCGGCGCGCGCC -3'	Fw; upstream of *CUL4A* −265 to −246
4	5'- CTCCGCCCGCCCCGGTCCGC -3'	Rv; upstream of *CUL4A* −75 to −56
5	5'- TGAGGGGGCCCGGGGTCTTT -3'	Fw; upstream of *CUL4A* −825 to −806
6	5'- GCGCGGAGGGTCCTCCGCGG -3'	Rv; upstream of *CUL4A* −645 to −626

Isolation of RNA and RT-PCR

Total RNA was extracted using Isogen according to the manufacturer's instructions and converted to cDNA by reverse transcription. PCR was performed with 10 pmol of each primer (Table 3), Go Taq polymerase (Promega, Madison, WI), and cDNA (100 ng) under the following conditions: 2 min at 94˚C and then a number of cycles at 94˚C for 30 s, 55˚C for 30 s, and 72˚C for 30 s. PCR products were separated by electrophoresis on a 1% agarose gel, visualized with ethidium bromide staining, and quantified by scanning densitometry using ImageJ software (Version 1.36b; National Institutes of Health, Bethesda, MD).

Table 3. Primers used for gene expression assessment

Primers	GenBank Accession No.		Sequences
Keap1	NM_203500.2	Forward	5'- TCTTCAAGGCCATGTTCACC -3'
		Reverse	5'- GGCACGCTGGTGCAACTCCA -3'
WDR23	NM_181357.2	Forward	5'- CACAGGATTGGAGAAGGAGG -3'
		Reverse	5'- TCGGCAGTCATAGAGTCGGA -3'

CUL4A	NM_001008895.4	Forward	5'- CAGGCACAGATCCTTCCGTT -3'
		Reverse	5'- TGGTTTCTGTGTGCTGTGGT -3'
DDB1	NM_001923.5	Forward	5'- CAGTGTTTCGGGGTCCTCTC -3'
		Reverse	5'- AAGTCGCCCTTGGTCTTCAG -3'
RBX1	NM_014248.4	Forward	5'- ACTTCCACTGCATCTCTCGC -3'
		Reverse	5'- AAGTGATGCGCTCAGAGGAC -3'
HO-1	NM_002133	Forward	5'- CCAGCCATGCAGCACTATGT -3'
		Reverse	5'- AGCCCTACAGCAACTGTCGC -3'
NQO1	NM_000903	Forward	5'- TGATCGTACTGGCTCACTCA -3'
		Reverse	5'- GTCAGTTGAGGTTCTAAGAC -3'
Sp1	NM_138473.3	Forward	5'- ACAGTTCCAGACCGTTGATG -3'
		Reverse	5'- TGGTAGTAAAGTTCATAATT -3'
Nrf2	NM_001145412	Forward	5'-GCCATTCACTCTCTGAACTT-3'
		Reverse	5'-GGTGACAAGGGTTGTACCAT-3'
β-actin	NM_001101	Forward	5′- CAAGAGATGGCCACGGCTGCT -3′
		Reverse	5′- TCCTTCTGCATCCTGTCGGCA -3′

Bioinformatics analysis of the promoter region

The sequence of the human *CUL4A* promoter and human *CUL4A* mRNA (GenBank™ accession number NM_001008895.4) were obtained from the National Center for Biotechnology Information (NCBI). The prediction of putative transcription factor-binding sites on the *CUL4A* promoter was performed with the JASPAR database (http://jaspar.genereg.net/) (104). The mammalian conservation of Sp1-binding sites based on multiple alignments of 100 vertebrate species was mapped onto the human *CUL4A* promoter built on the UCSC genome browser (https://genome.ucsc.edu/) (105).

Statistical analysis

Data are shown as the mean ± standard deviation (SD). The significance of differences was examined using the Student's *t*-test when two means were compared, and a one-way ANOVA followed by the Bonferroni *post hoc* test when multiple comparisons were performed. $P < 0.05$ was considered to be significant (*$p < 0.05$, **$p < 0.01$, ***$p < 0.001$).

II.3. Results

Effects of Keap1 knockdown on the expression of CRL4A^{WDR23} components

The identification of WDR23 as a novel regulator of Nrf2 in addition to the well-established Keap1 pathway has attracted interest due to its potential to enhance the stress response, refine the type of stress response induced, or control tissue specificity (42). However, the mechanisms by which Keap1 and WDR23 signaling interact with each other remain unclear. Since data presented in CHAPTER I suggested that WDR23 activity was limited to Keap1 (43), I initially examined the

effects of the Keap1 knockdown on the expression of $CRL4A^{WDR23}$ components, including *WDR23*, *CUL4A*, *DDB1*, and *RBX1*.

The short hairpin RNA (shRNA)-mediated knockdown of Keap1 significantly decreased (~60%) Keap1 mRNA levels, suggesting successful knockdown (Fig. 1*A*). The present results showed that the Keap1 knockdown up-regulated the expression of *CUL4A*, but not *WDR23*, *DDB1*, or *RBX1* (Fig. 1, *B-E*). Similarly, the chemical inhibition of Keap1 by tert-butylhydroquinone (tBHQ) increased *CUL4A* mRNA levels, whereas those of *WDR23*, *DDB1*, and *RBX1* remained unchanged (Fig. 1, *F-I*). Since Keap1 is an intracellular sensor of oxidative and electrophilic insults, it is likely that the effects of Keap1 knockdown on the expression of $CRL4A^{WDR23}$ components may be mimicked by hydrogen peroxide, which is an oxidizing agent that disrupts the Keap1-Nrf2 interaction. I found that the expression of *CUL4A* was also increased by the H_2O_2 treatment (Fig. 1, *J-M*). The effects of Keap1 knockdown on the protein levels of CUL4A were then examined and found that they were elevated (Fig. 1*N*).

To elucidate the mechanisms underlying the regulation of *CUL4A* expression by Keap1, *CUL4A* promoter activity under Keap1 knockdown conditions was investigated using a luciferase reporter assay. Luciferase reporter plasmids (pGL3-basic) containing −1920/+50 bp of the *CUL4A* genomic region were constructed and transfected into Hep3B cells. Keap1 knockdown induced a 2.5-fold increase in promoter activity (Fig. 1*O*). To identify the promoter region required for the transcriptional activation of *CUL4A*, a deletion analysis of the promoter was performed. Basal promoter activity was gradually decreased by the consecutive 5′-end deletion of the upstream region of *CUL4A.* However, Keap1 knockdown still enhanced the promoter activity of the −230/+50 construct, suggesting that the regulatory region of *CUL4A* by Keap1 is present within this segment.

The role of Sp1 on the Keap1 KD-mediated induction of CUL4A

To elucidate the transcriptional regulation of *CUL4A*, particularly with the Keap1 knockdown, I attempted to identify the relevant transcription factor(s) responsible for the regulation of *CUL4A* transcription. Nrf2 protein levels were significantly increased by Keap1 knockdown due to the depletion of Nrf2 ubiquitination, indicating that the WDR23 pathway might be activated by Nrf2 as a self-regulatory feedback mechanism. However, I found that the overexpression of WDR23 did not affect Nrf2 protein levels in Nrf2-overexpressing cells with intact Keap1 function (Fig. 2*A*). Furthermore, the overexpression of Nrf2 alone did not change the mRNA expression of *CUL4A* (Fig. 2*B*). These results support the idea that activity of the WDR23 pathway being limited to the function of Keap1.

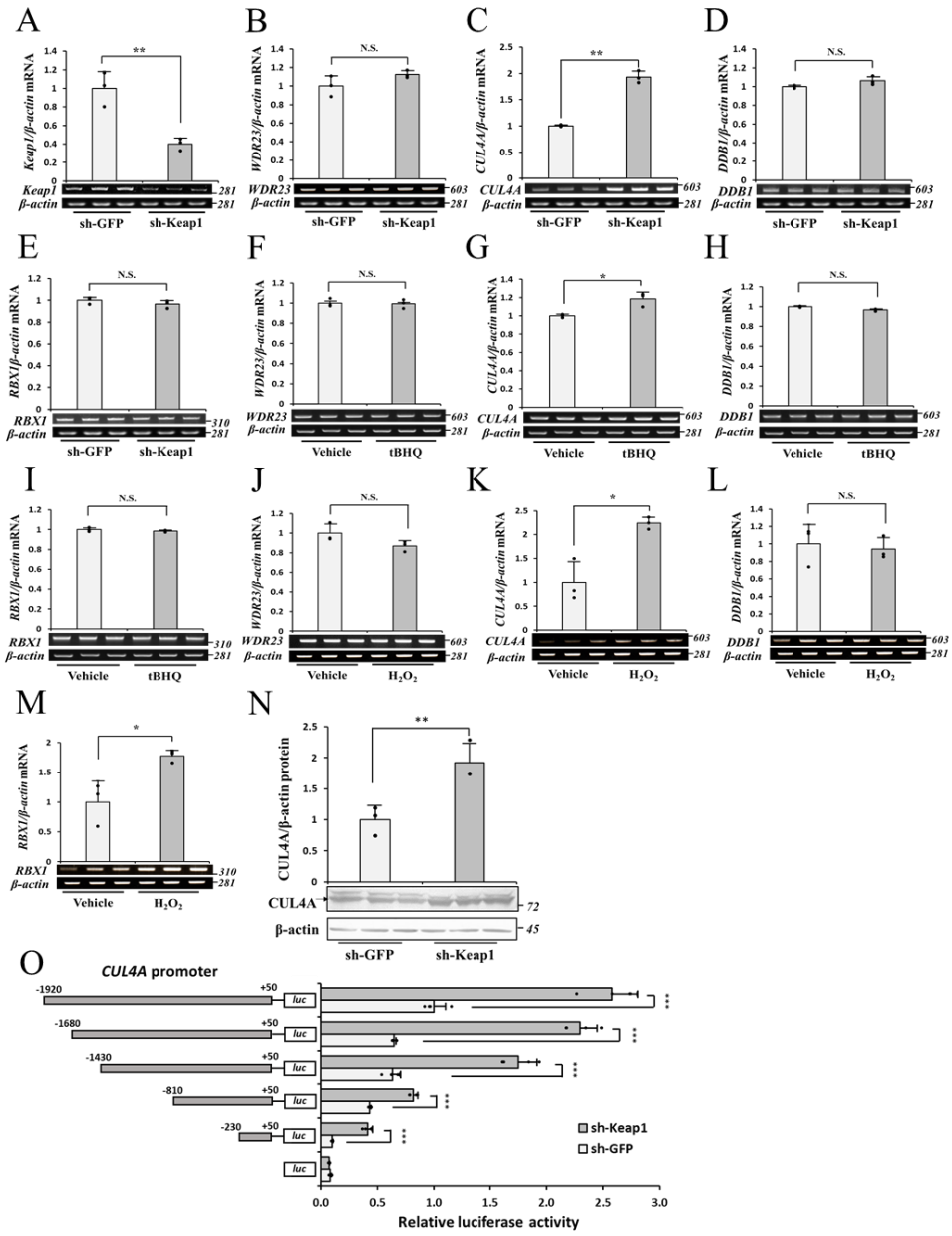

Figure 1. The knockdown of Keap1 increases transcript and protein levels of CUL4A. (A-E) Keap1 knockdown cells were generated using sh-RNA in Hep3B cells and the mRNA expression levels of *Keap1, WDR23*, *CUL4A*, *DDB1*, and *RBX1* were measured by RT-PCR. The β-actin was used as a loading control, and the same panel was used for Fig. 1 *A-E.* (F-I) Hep3B cells were grown in the presence or absence of tBHQ (60 μM; 8 h) and the abundance of mRNA was examined by RT-PCR with the same β-actin panel as a loading control. (J-M) Hep3B cells were treated with H_2O_2 (100 μM; 8 h) and mRNA expression levels were assessed by RT-PCR with the same β-actin panel as a loading control. (N) Total cell lysates from control (sh-GFP) and Keap1 knockdown (sh-Keap1) cells were subjected to immunoblotting against the anti-CUL4 antibody. (O) The upstream region −1920/+50 of *CUL4A* in pGL3 or its 5′-endo deletion construct was co-transfected with pRL-null as an internal control plasmid into control and Keap1 knockdown Hep3B cells. Luciferase activity was assessed 48 h after transfection using the Dual-Luciferase Reporter Assay system relative to the promoter-less construct pGL3-Basic. Results are shown as a ratio relative to the activity of *CUL4A* promoter −1920/+50 in control cells. All values are means ± S.D. from three independent experiments. N.S. not significant, *p<0.05, **p<0.01, ***p<0.001.

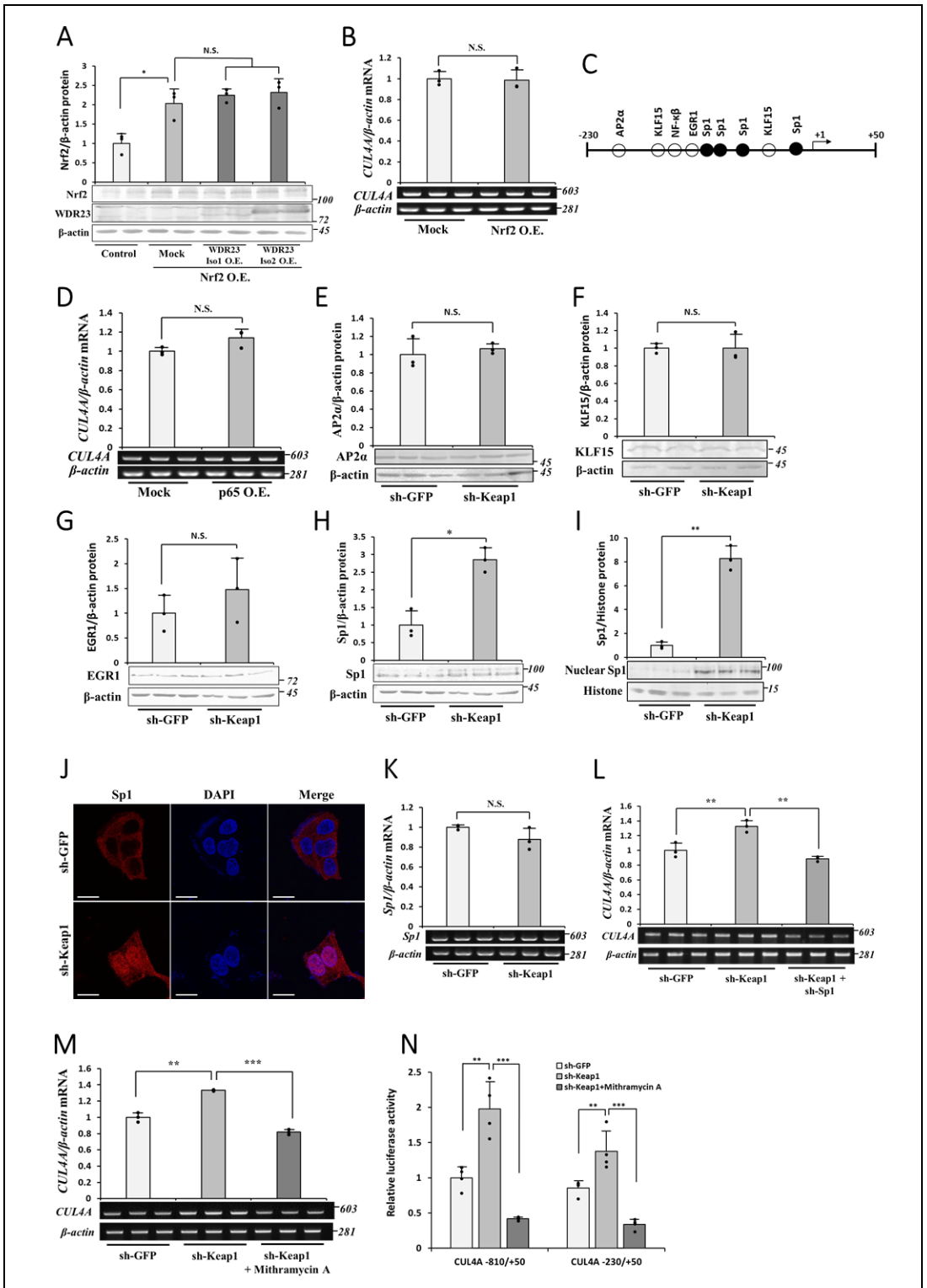

Figure 2. The requirement of Sp1 in Keap1 KD-induced *CUL4A* expression. (A) Nrf2 and WDR23 protein levels were assessed by immunoblotting using the cell lysates from Control (pcDNA-Mock only), Mock (pcDNA-Mock and pcDNA-Nrf2), and WDR23-overexpressed (pcDNA-WDR23 isoform 1 or 2 and pcDNA-Nrf2) cells. (B) The abundance of mRNA encoding CUL4A was assessed from Mock and Nrf2-overexpressing cells by RT-PCR. (C) Schematic representation of the −230/+50 of human *CUL4A*, with +1 representing the transcription start site.

The position of transcription factor-binding sites was predicted by the JASPAR database. (D) p65 in pcDNA3.1(-) was transfected in Hep3B cells and the mRNA level of *CUL4A* was evaluated by RT-PCR. (E-H) The abundance of the AP2α, KLF15, EGR1, and Sp1 proteins was examined in whole cell lysates from control (sh-GFP) and Keap1 knockdown (sh-Keap1) Hep3B cells by immunoblotting. Fig. *G* and *H* were from same lysates with same β-actin as a loading control. (I) The abundance of the nuclear Sp1 from control and Keap1 knockdown Hep3B cells was examined by immunoblotting. (J) Cellular localization of Sp1 (red) was examined by immunofluorescence counterstained with DAPI staining (blue) to indicate the location of the nucleus in the control and Keap1 knockdown Hep3B cells, scale bar: 20 μm. (K) Sp1 mRNA abundance was measured by RT-PCR. (L-M) The effects of Sp1 knockdown or mithramycin A (100 nM, 6 h) on the *CUL4A* mRNA levels of Keap1 knockdown cells were investigated by RT-PCR. (N) Control and Keap1 knockdown Hep3B cells in the presence or absence of mithramycin A (100 nM, 6 h) were transfected with pGL3-containing *CUL4A* promoter −810/+50 or −230/+50. Luciferase activity was measured 48-h post-transfection. Graphs are means ± S.D. from three independent experiments. N.S. not significant, *p<0.05, **p<0.01, ***p<0.001 *versus* the indicated cells.

I then predicted several putative transcription factor-binding sites using the JASPAR database. The putative binding sites of AP2α, KLF15, EGR1, NF-κβ, and Sp1 were found within −230/+50 bp of *CUL4A* (Fig. 2*C*). Among all possible transcription factors, only NF-κβ has been reported as a downstream target of Keap1. Since Keap1 directly interacts with and induces the autophagic degradation of IKKβ, its depletion results in the up-regulation of NF-κB (106, 107). However, the overexpression of p65 did not change the expression of *CUL4A* (Fig. 2*D*), suggesting that the effects of Keap1 knockdown on *CUL4A* were independent of NF-κβ. The protein levels of other potential transcription factors under Keap1 knockdown were then examined. AP2α, KLF15, and EGR1 protein levels were unaffected by Keap1 knockdown (Fig. 2, *E*-*G*, respectively). In contrast, total and nuclear Sp1 protein levels were elevated (Fig. 2, *H* and *I*). In Keap1 knockdown cells, Sp1 accumulated in the nucleus (Fig. 2*J*). The mRNA levels of Sp1 were unaltered by Keap1 knockdown (Fig. 2*K*), suggesting that the Sp1 elevation induced by Keap1 knockdown occurred at the post-transcriptional level.

To confirm the involvement of Sp1 on Keap1 KD-induced *CUL4A* expression, the activity of Sp1 was inhibited using a genetic and chemical approach. The shRNA-mediated genetic inhibition of Sp1 in Keap1 knockdown Hep3B cells attenuated the up-regulated expression of *CUL4A* (Fig. 2*L*). Similarly, the treatment of Keap1 knockdown cells with mithramycin A (100 nM, 6 h), a potent chemical inhibitor of Sp1, reduced the expression of *CUL4A* (Fig. 2*M*). This is consistent with the results showing that mithramycin A abolished Keap1 KD-induced increases in *CUL4A* promoter activity (Fig. 2*N*). Collectively, these results support the role of Sp1 in the regulation of *CUL4A* expression under Keap1 knockdown conditions.

Transcriptional regulation of the CUL4A promoter by Sp1

Sp1 is a ubiquitously expressed transcription factor that regulates the expression of numerous genes. To further investigate the role of Sp1 on *CUL4A* gene expression, the expression of CUL4A at the transcript and protein levels after the knockdown or ectopic overexpression of Sp1 were investigated (Fig. 3, *A* and *B*). The results showed that Sp1 knockdown significantly decreased *CUL4A* mRNA levels, which slightly reduced CUL4A protein levels. In contrast, the overexpression of Sp1 elevated *CUL4A* mRNA levels and induced an approximately 7-fold increase in the accumulation of the CUL4A protein (Fig. 3, *C* and *D*), suggesting that Sp1 contributes to the expression of *CUL4A*. These results indicate that Sp1 regulates the basal and inducible expression of *CUL4A.* Next, a luciferase reporter assay to further confirm the results outlined above was performed. Similar to the phenomena observed under Keap1 knockdown conditions, the overexpression of Sp1 significantly enhanced the luciferase activity of the pGL3-containing −1920/+50 bp of the *CUL4A* genomic region. Constructs containing a series of 5′ end deletions were all responsive to the overexpression of Sp1 (Fig. 3*E*). In contrast, Sp1 knockdown markedly decreased the promoter activity of pGL3-containing −810/+50 bp and −230/+50 bp of the *CUL4A* genomic region construct by approximately 50% (Fig. 3*F*).

Within the *CUL4A* promoter −230/+50 region, four Sp1-binding sites were identified using the JASPAR database. To verify the contribution of Sp1-binding sites to the functional activity of the proximal *CUL4A* promoter, each Sp1 putative site within the −230/+50 construct was individually mutated (Fig. 3*G*). Since Sp1 is known to bind to various consensus sequences, the core GG sequences were replaced with TT. The mutant constructs Sp1_M1, Sp1_M2, and Sp1_M3 exhibited similar basal promoter activities to the wild-type construct, whereas Sp1_M4 basal promoter activity was weaker than that of the wild-type. The mutation in the fourth site (Sp1_M4) suppressed the activation of promoter activity by the overexpression of Sp1, suggesting its crucial role for the Sp1-activated *CUL4A* promoter (Fig. 3*H*). The mutation in the fourth site also abrogated the response of the *CUL4A* promoter to the knockdown of Keap1 (Fig. 3*I*), which is consistent with the results described above, suggesting that Sp1 binding to the fourth putative site plays an important role in Keap1 KD-induced *CUL4A* expression. Consistently, I found that the fourth Sp1-binding site was highly conserved in mammals and based on multiple species alignment phylogenetic P-values (PhyloP), the conservation of the fourth site was significantly greater than that of the other sites (Fig. 3*J*).

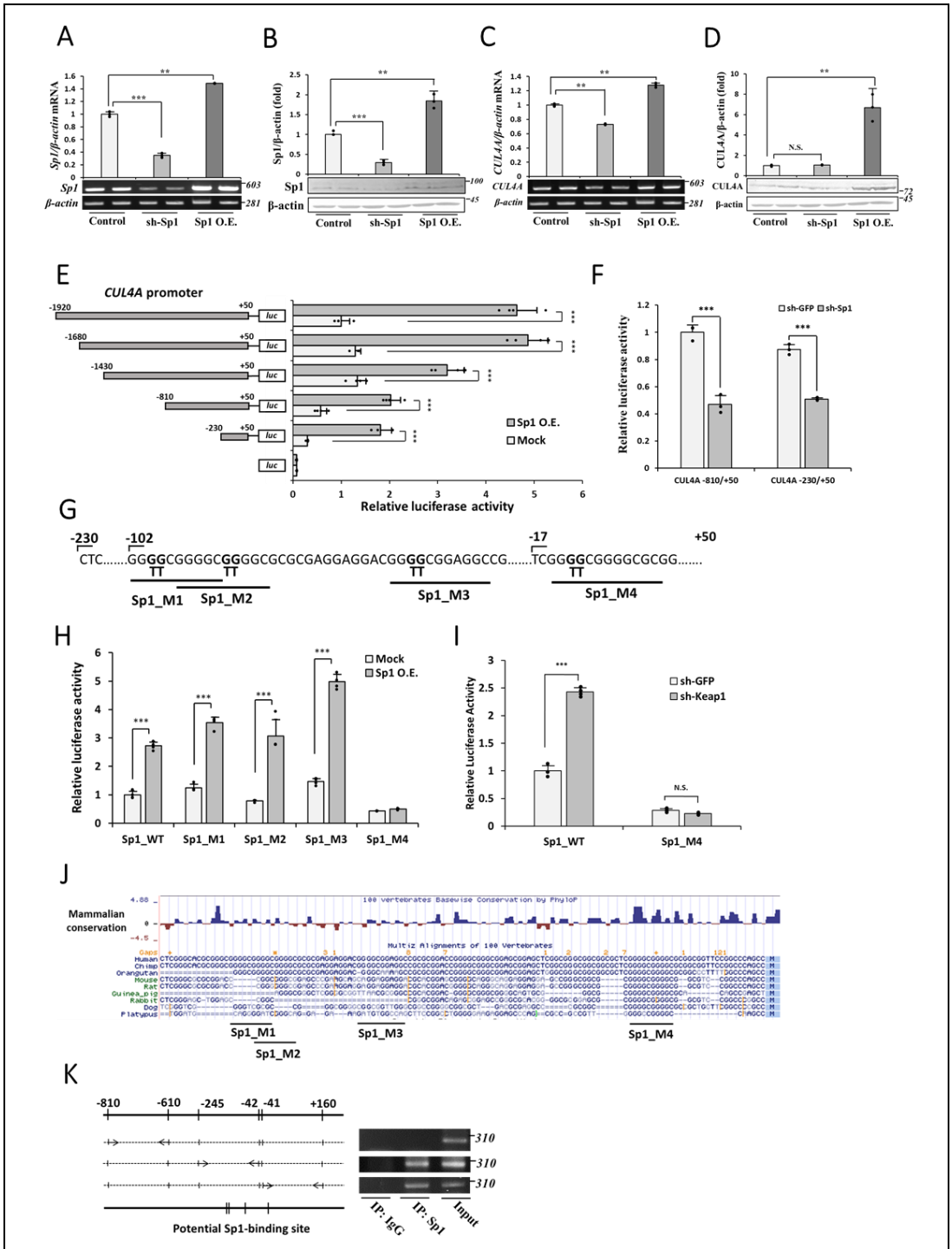

Figure 3. Sp1 regulates *CUL4A* expression and promoter activity. (A-B) Sp1 knockdown cells were generated using sh-RNA in Hep3B cells and overexpression was achieved by the transfection of Sp1 in pCMV-Myc. The abundance of mRNA and the protein levels of Sp1 from control, Sp1 KD, and Sp1 overexpressed cells were evaluated by RT-PCR and immunoblotting, respectively, to confirm the efficiency of knockdown and overexpression. (C-D) The mRNA and protein levels of CUL4A from Sp1 knockdown and overexpressing cells were examined by RT-PCR and immunoblotting, respectively. Fig. *A* and *C*, as well as *B* and *D,* were from same lysates with the same β-actin panel as a loading control. (E) The upstream region −1920/+50 of *CUL4A* in pGL3 or its consecutive 5′-end deletion construct was co-transfected with pRL-null and pCMV-Mock or

pCMV-Sp1 in Hep3B cells. Luciferase activity was assessed 48-h post-transfection. (F) Control (sh-GFP) and Sp1 knockdown (sh-Sp1) Hep3B cells were transfected with pGL3-containing *CUL4A* promoter −810/+50 or −230/+50. Luciferase activity was assessed 48-h post-transfection. (G) Sp1-binding sites and its mutated construct (Sp1_M1–Sp1_M4) within the *CUL4A* promoter −230/+50. (H) Wild-type *CUL4A* promoter −230/+50 or the mutant construct, in which each Sp1-binding motif was mutated, was co-transfected with pRL-null and pCMV-Mock or pCMV-Sp1 in Hep3B cells, and luciferase activity was measured. (I) Wild-type *CUL4A* promoter −230/+50 or the Sp1_M4 mutant construct was co-transfected with pRL-null in control (sh-GFP) or Keap knockdown (sh-Keap1) Hep3B cells, and luciferase activity was measured. Graphs are means ± S.D. from three independent experiments. *p<0.05, **p<0.01, ***p<0.001 *versus* the indicated cells. (J) The sequences of the *CUL4A* promoter from 100 vertebrate species were mapped onto the human *CUL4A* promoter built on the UCSC genome browser. Phylogenetic P-values (PhyloP) indicate conservation. (K) Left panel: Genomic positions of regions that were selected for a PCR-based analysis in the ChIP assay. The indicated Sp1-binding sites within the *CUL4A* promoter were predicted by the JASPAR database. Right panel: ChIP assay with an Sp1 antibody or control mouse IgG, with input chromatin as the positive control. After reverse cross-linking, DNA was amplified using the indicated primer sets.

Based on the result showing that Sp1 plays an important role in the regulation of *CUL4A* promoter activity, I was prompted to investigate whether this transcription factor regulates the expression of *CUL4A* at the transcriptional level by directly binding to its promoter. The ChIP assay was conducted using the Sp1 antibody in Hep3B cells and detected *CUL4A* promoter-bound DNA fragments using specific primers. ChIP PCR products were identified using primers that amplified regions −230 to −42 and −41 to +160 of the *CUL4A* gene, but not with primers that amplified regions −810 to −610 with no potential Sp1-binding sites (Fig. 3*K*). The input was unfragmented chromatin as a positive control in PCR for each segment of interest.

Direct interaction of Keap1 with Sp1

Since Sp1 protein levels were increased by Keap1 knockdown and that Sp1 mediates the activation of Keap1 KD-induced *CUL4A* expression, I postulated that Sp1 is directly bound to and regulated by Keap1. To test this hypothesis, the intracellular interaction of Sp1 with Keap1 was investigated using bimolecular fluorescence complementation (BiFC) assay. BiFC relies on the principle that interacting proteins tagged with the non-fluorescent N- or C-terminal fragments of a β-barrel fluorescent protein enable the fragments of the fluorescent protein to fuse and refold, leading to the acquisition of a fluorescent complex (108). When the N-terminal fragment of Venus (VN155, I152L) fused to the N-terminal of Sp1 was co-expressed with Keap1 fused to the C-terminal fragment of Venus (VC155) in Hep3B cells, Venus fluorescent was mainly detected in the cytosol as a BiFC signal, suggesting the direct interaction of Sp1 with Keap1 (Fig. 4*A*). To clarify which domain of Sp1 and Keap1 contribute to this interaction, the interaction of full-length and several truncated Sp1 and Keap1 mutants were assessed using an

immunoprecipitation assay. Keap1 was present in the lysate pulled down with the Myc antibody in full-length Sp1-overexpressing cells. Keap1 binding with all Sp1 truncated mutants were detected, except for Sp1 ΔNTR, indicating that it interacts with the N-Terminal Region (NTR) domain of Sp1 (Fig. 4*B*). Further studies revealed that Sp1 bound to full-length Keap1, but not Keap1 ΔDGR (Fig. 4*C*), which is the Nrf2-binding domain.

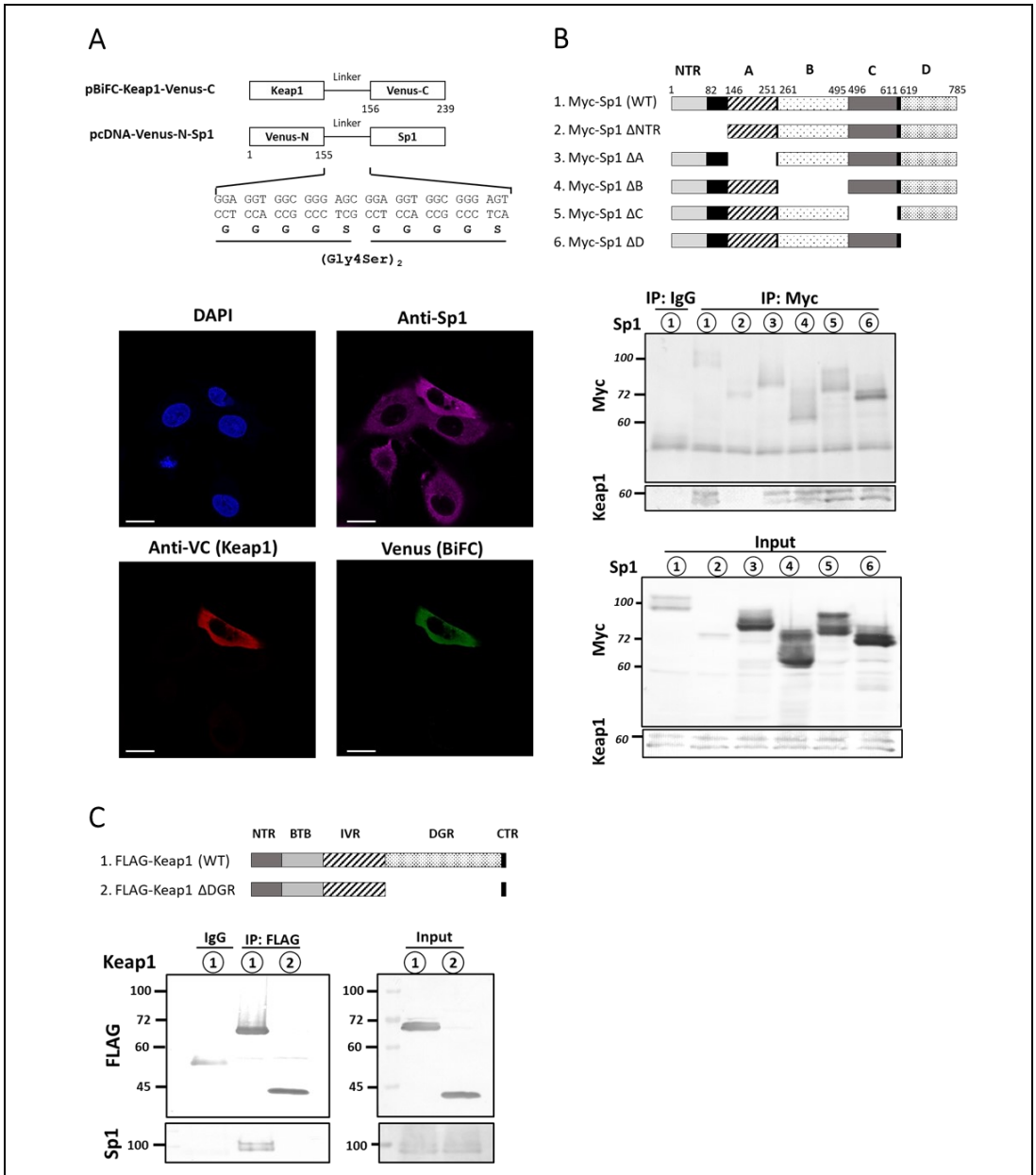

Figure 4. Direct interaction of Keap1 with Sp1. (A) N- and C-terminal fragments of Venus fluorescent proteins were fused to the N-terminal of Sp1 and C-terminal of Keap1, respectively (upper panel). The interaction between Sp1 and Keap1 brings the N- and C-terminal fragments in proximity to reconstitute an intact fluorescent protein. VN-Sp1 was co-expressed with Keap1-VC in Hep3B cells and overexpression was confirmed with an anti-Sp1 or anti-VC antibody. Venus

fluorescence as the BiFC signal indicates the interaction (below panel). Scale bar: 20 μm. (B) The immunoprecipitation assay was performed to evaluate the domain responsible for the binding of Sp1 with Keap1. Hep3B cells were transfected with Myc-Sp1 full-length, or domain-truncated mutants as indicated in the diagram (upper panel). Transfected cells were immunoprecipitated with an anti-Myc antibody, and immunoprecipitated proteins were subjected to an immunoblotting analysis with anti-Myc and anti-Keap1 antibodies. NTR, N-terminal region; A, Transactivation domain A; B, Transactivation domain B; C, Transactivation domain C; D, Transactivation domain D. (C) Hep3B cells were transfected with the FLAG-Keap1 full-length or ΔDGR mutant as indicated in the diagram (upper panel). Transfected cells were immunoprecipitated with an anti-FLAG antibody, and immunoprecipitated proteins were subjected to an immunoblotting analysis with an anti-FLAG and anti-Sp1 antibody. NTR, N-terminal region; BTB, Bric-a-Brac; IVR, intervening region; DGR, double glycine repeat, CTR, C-terminal region.

Ubiquitination of Sp1 by Keap1

The direct interaction of Sp1 and Keap1 might imply that Keap1 subjects Sp1 to ubiquitination because Keap1 is a substrate adaptor protein for the CUL3-containing E3 ubiquitin ligase complex (80). I then investigated whether Sp1 is regulated by ubiquitin-dependent proteasome degradation. Sp1 protein levels were elevated by the treatment with the proteasome inhibitor MG132 (5 μM, 8 h), confirming that Sp1 is subjected to proteasomal degradation (Fig. 5*A*). The ubiquitination of Sp1 by Keap1 in the presence of MG132 was then examined. Sp1 incorporated approximately 1.5-fold more ubiquitin in Keap1-overexpressing cells than in control cells, and Keap1 knockdown significantly decreased (~70%) the ubiquitination of Sp1 (Fig. 5*B*). Collectively, these results showed that Keap1 directly regulated the protein stability of Sp1 via the ubiquitin-dependent proteasome pathway.

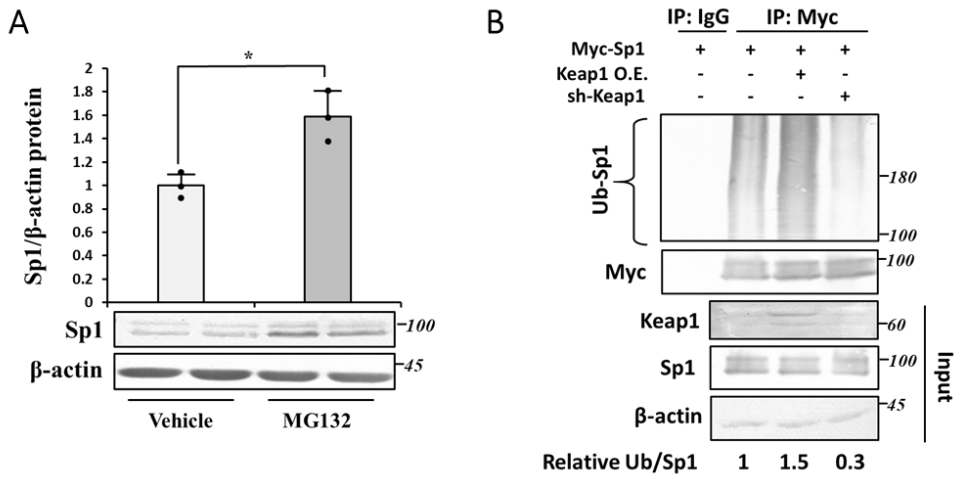

Figure 5. Effects of Keap1 overexpression and knockdown on Sp1 ubiquitination. (A) Hep3B cells were treated with the proteasome inhibitor MG132 (5 μM, 8 h) and Sp1 protein levels were

measured by immunoblotting against an anti-Sp1 antibody. Protein loading was normalized by β-actin. The vehicle-treated cell value was set as 1.0. Graphs are means ± S.D. from three independent experiments. *p<0.05. (B) Control (sh-GFP) or Keap1 knockdown (sh-Keap1) cells were transfected with pCMV-Sp1, pcDNA-Keap1, or both. Cells were grown in the presence of MG132 (5 μM, 8 h), cell lysates were immunoprecipitated using an anti-Myc antibody, and immunoblotting using anti-Myc, anti-ubiquitin, anti-Keap1, anti-Sp1 and anti-β-actin antibodies was then performed. The quantification of ubiquitinated Sp1 relative to immunoprecipitated Sp1 was performed using ImageJ.

The role of Sp1 on Nrf2 protein levels

The relationship between Sp1 and Keap1, in addition to the role of Sp1 in the regulation of *CUL4A* expression, led to the question whether Sp1 correlates with the intracellular level of Nrf2. Previous studies suggested that the protein level and transcriptional activity of Sp1 are induced by oxidative stress; however, their relationship with Nrf2 remains unclear (98–100). The overexpression and knockdown of Sp1 (Fig. 6*A*) decreased and increased Nrf2 protein levels, respectively (Fig. 6*B*). These effects of Sp1 on Nrf2 appeared to occur at the post-transcriptional level because the mRNA levels of Nrf2 were unaltered by the overexpression or knockdown of Sp1 (Fig. 6*C*). This is consistent with Sp1 being a mediator of the activation of the WDR23 pathway when the function of Keap1 is disabled. Next, the overexpression and knockdown of Sp1 decreased and increased Nrf2 transcriptional activity as shown by the assessment of Nrf2 target genes expression, the *HO-1* (Fig. 6*D*) and *NQO1* (Fig. 6*E*). These results were further supported by the evaluation of ARE luciferase reporter which showed that Nrf2 activity was inhibited and enhanced by overexpression and knockdown of Sp1, respectively (Fig. 6*F*).

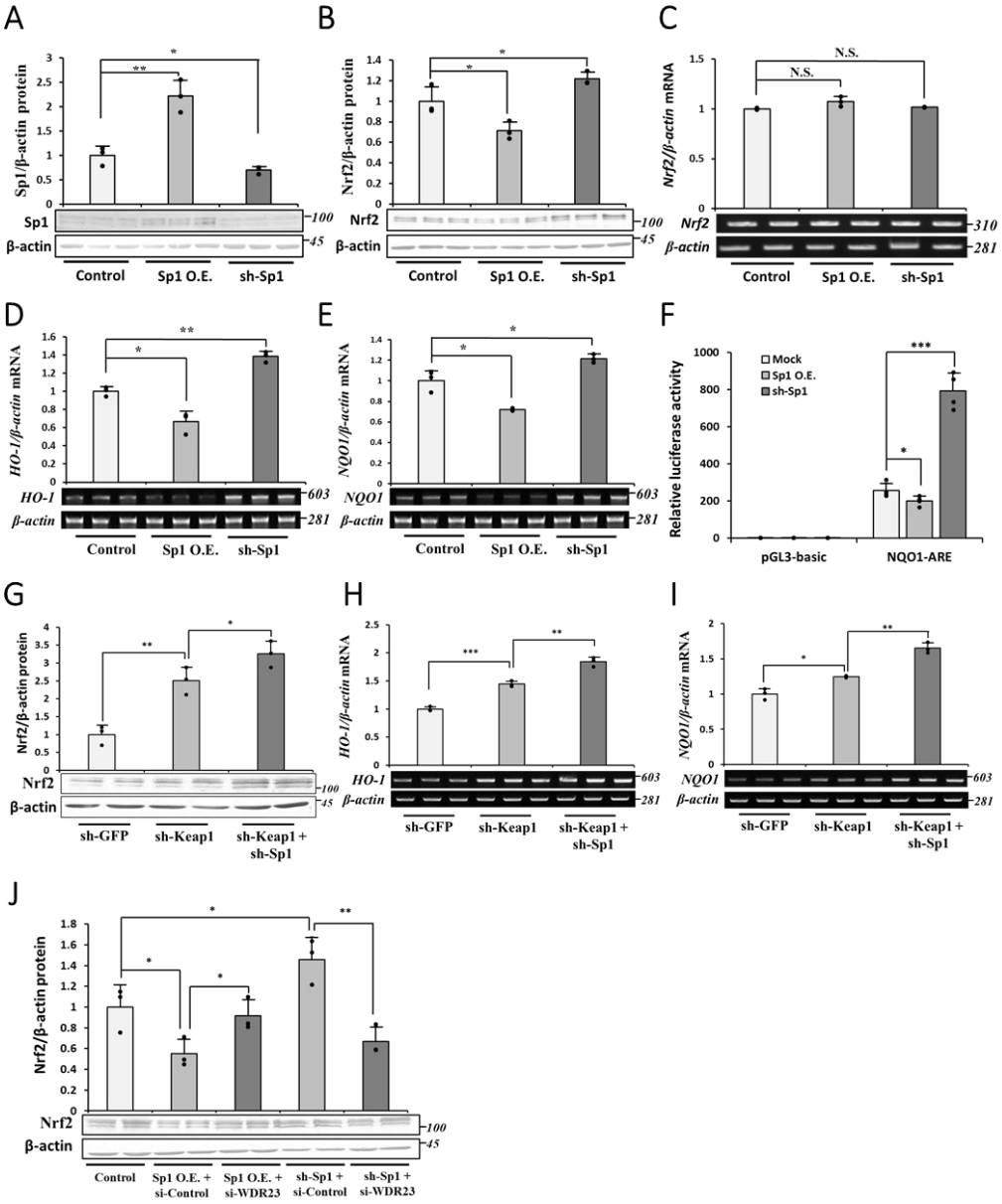

Figure 6. Effects of Sp1 on Nrf2 protein levels. (A-F) Sp1 knockdown cells were generated using sh-RNA and overexpression was performed by the transfection of Sp1 in pCMV-Myc. Control cells were sh-GFP + pCMV-Mock. (A) Knockdown and overexpression were confirmed by immunoblotting against an anti-Sp1 antibody. (B-C) The abundance of intracellular Nrf2 protein and mRNA was measured with immunoblotting and RT-PCR, respectively. (D-E) *HO-1* and *NQO1* mRNA levels were assessed in cell lysates by RT-PCR with the same β-actin panel as a loading control. (F) Nrf2 activity was measured in cells expressing an NQO1-ARE luciferase reporter. Luciferase activity was measured 48-h post-transfection. Graphs are means ± S.D. from three independent experiments. (G) The effects of Keap1 and Sp1 knockdown on Nrf2 protein abundance were observed by immunoblotting. (H-I) The effects of Keap1 and Sp1 knockdown on the expression of *HO-1* and *NQO1* levels were assessed in cell lysates by RT-PCR with the same β-actin panel as a loading control. (J) Control (sh-GFP) or Keap1 knockdown (sh-Keap1) was co-transfected with pCMV-Mock or pCMV-Sp1 and si-Control or si-WDR23. The protein level of Nrf2 was then observed with immunoblotting. All graphs present means ± S.D. from three independent experiments. N.S. not significant, *p<0.05, **p<0.01, ***p<0.001 *versus* the indicated cells.

Furthermore, Sp1 knockdown further increased Nrf2 protein levels and transactivity in Keap1 knockdown cells (Fig. 6*, G-I*) which may be attributed to the inability of these cells to up-regulate the expression of *CUL4A* and activate the WDR23 pathway (consistent with Fig. 2*L*). Nevertheless, this raises the critical question of whether Sp1 is really an upstream of WDR23 activity or functions as an independent pathway for Nrf2 stability. Therefore, I treated Sp1-overexpressing and knockdown cells with siRNA against both isoforms of WDR23. The result obtained demonstrated that WDR23 knockdown attenuated the effects of Sp1 on Nrf2 (Fig. 6*J*), supporting my proposal that Sp1 requires and acts as an upstream regulator of WDR23. Collectively, these results highlight the relevance of Sp1 and the activity of the WDR23-dependent Nrf2 regulatory pathway.

Sp1 or CUL4A overexpression recapitulates Keap1 knockdown required for WDR23 activity

If Sp1-regulated *CUL4A* expression mediates crosstalk between Keap1 and WDR23, the direct overexpression of Sp1 or CUL4A is expected to bypass the requirement of the Keap1 knockdown in cells to respond to the overexpression of WDR23. I used this strategy to further confirm whether Sp1 and CUL4A play critical roles in the crosstalk between the two independent and parallel regulators of Nrf2. The overexpression of both isoforms of WDR23, Sp1, and CUL4A in Hep3B cells was confirmed by immunoblotting (Fig. 7*A*). Consistent with earlier results, no changes were observed in total Nrf2 protein levels after the overexpression of WDR23 in control Hep3B cells. However, the co-expression of WDR23 with Sp1 markedly decreased Nrf2 protein levels by ~80 and ~50% for the overexpression of WDR23 isoforms 1 and 2, respectively (Fig. 7*B*). Furthermore, the co-expression of WDR23 with CUL4A also reduced Nrf2 protein levels (Fig. 7*C*). These results demonstrated that Sp1 and CUL4A play roles in and mediate the activation of the WDR23 pathway, particularly under Keap1 knockdown conditions. To study whether this phenomenon also occurs in normal cells, human embryonic kidney (HEK293) cells were used. Similar results were obtained by using these cells (Fig. 7, *D-F*) suggesting that Sp1-CUL4A axis also plays a role to mediate crosstalk between Keap1 and WDR23 pathways in normal cells and independent of the cell type. Next, these phenomena were studied in the murine hepatoma cell line, Hepa1-6 (Fig. 7, *G-I*). The results showed a similar trend indicating that this mechanism is conserved among mammalians. In addition, I validated these findings by using primary mouse hepatocyte cells (Fig. 7, *J* and *K*) that provide more relevant and reflective results to that of the *in vivo* environment.

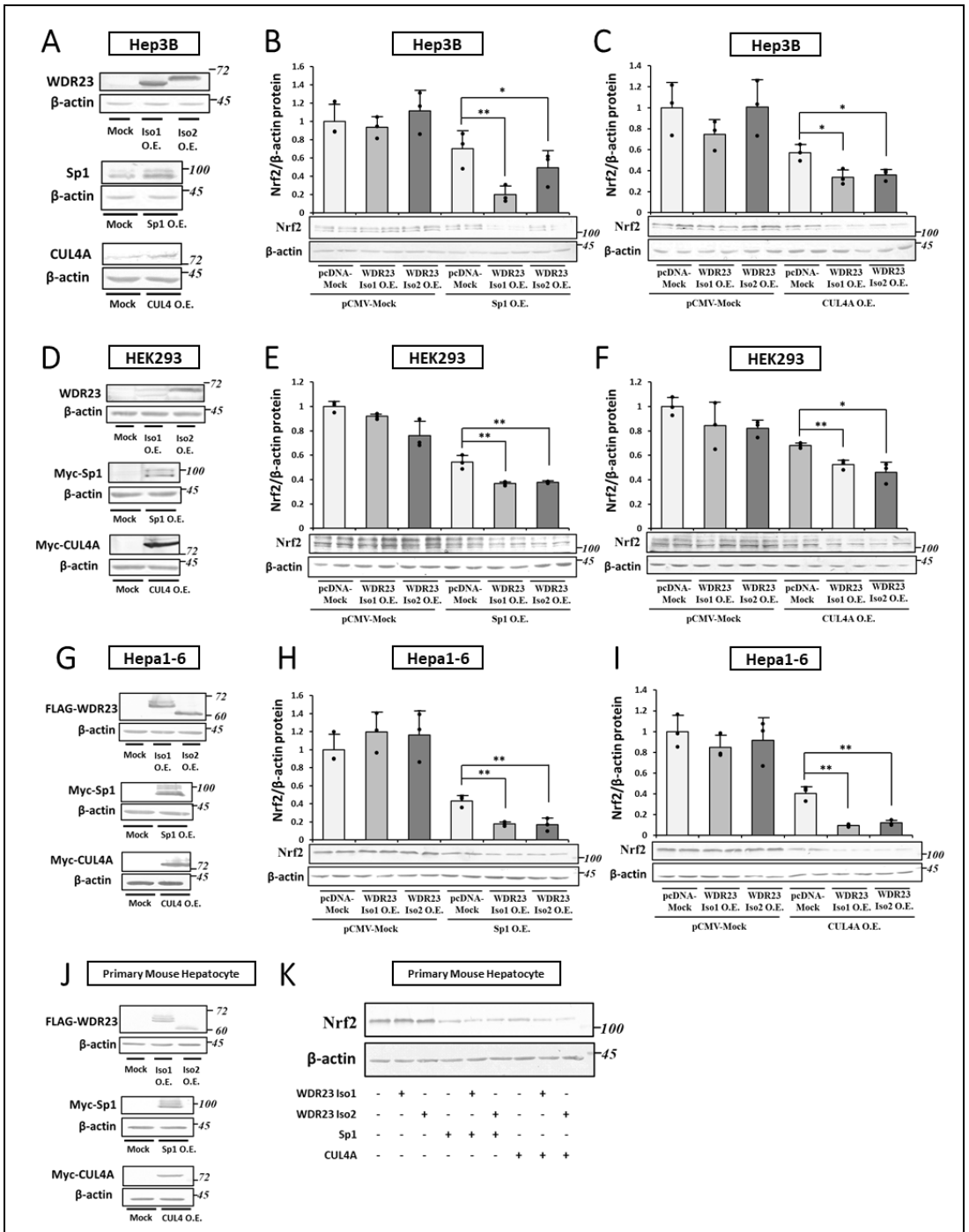

Figure 7. Effects of Sp1 and CUL4A overexpression on the activity of ectopic WDR23. (A-C) WDR23 isoform 1 or 2 in 3×FLAG-pcDNA4 and Sp1 or CUL4A in pCMV-Myc were transfected into Hep3B cells. (A) Overexpression was confirmed by immunoblotting with an anti-WDR23, anti-Sp1, or anti-CUL4A antibody. (B-C) Immunoblotting analysis of Nrf2 levels with 15 μg of the total cell lysate from cells co-transfected with pcDNA-Mock, pcDNA-WDR23 isoform 1 or 2, and pCMV-Mock, pCMV-Sp1 or pCMV-CUL4A. (D-F) The 3×FLAG-pcDNA4 vector containing WDR23 isoform 1 or 2 and pCMV-Myc containing Sp1 or CUL4A were transfected into HEK293 cells. (D) Overexpression was confirmed by immunoblotting. (E-F) Immunoblotting analysis of Nrf2 levels with 15 μg of the total cell lysate from cells co-transfected with pcDNA-Mock, pcDNA-WDR23 isoform 1 or 2, and pCMV-Mock, pCMV-Sp1 or pCMV-CUL4A. (G-I) WDR23 isoform 1 or 2 in 3×FLAG-pcDNA4 and Sp1 or CUL4A in pCMV-Myc were transfected into HEPA1-6

cells. The abundance of WDR23, Sp1, CUL4A and Nrf2 was measured with immunoblotting. (J-K) WDR23 isoform 1 or 2 in 3×FLAG-pcDNA4 and Sp1 or CUL4A in pCMV-Myc were transfected into primary mouse hepatocyte cells. The abundance of WDR23, Sp1, CUL4A and Nrf2 was assessed with immunoblotting. All graphs present means ± S.D. from three independent experiments. *p<0.05, **p<0.01 *versus* the indicated cells.

Effects of the overexpression of $CRL4A^{WDR23}$ on Nrf2 levels and activity

The contribution of *CUL4A* gene expression on the regulation of $CRL4A^{WDR23}$ activity toward Nrf2 suggests that the CUL4A is the rate-limiting factor of this E3 ligase complex. To test this, individual component of $CRL4A^{WDR23}$ complex were overexpressed. I found that the overexpression of CUL4A alone was sufficient to decrease Nrf2 protein levels (Fig. 8*A*) and down-regulate the expression of Nrf2 target genes (Fig. 8*, B* and *C*). In contrast, the overexpression of WDR23 (Fig. 8, *D*-*F*) or DDB1 (Fig. 8, *G*-*I*) had no effects on both protein levels and activity of Nrf2. These results revealed that CUL4A is indeed the rate-limiting factor of $CRL4A^{WDR23}$. I herein established that the Sp1-mediated up-regulated expression of *CUL4A* during the Keap1 knockdown is the mechanism underlying crosstalk between the Keap1 and WDR23 pathways for the regulation of Nrf2.

II.4. Discussion

The aberrant activation of Nrf2 is frequently observed in many cancers, and promotes cancer growth and metastasis and also confers chemo- and radio-resistance (109–111). Somatic mutations within *Keap1* or *Nrf2* (exclusively found in the DLG and ETGE motifs) are the most frequent causes of hyperactive Nrf2 in cancer (110). Therefore, determining other regulatory mechanisms of Nrf2 that may be used as a therapeutic target to improve cancer responses to chemotherapy are important. WDR23 was recently identified as a novel regulator of Nrf2 and Nrf2-dependent drug-metabolizing enzymes (42, 43). In CHATER I, the WDR23 pathway was found to be activated when the function of Keap1 was impaired; however, the underlying mechanisms remain unclear. In the present study, the mechanism underlying the activation of WDR23 during the inhibition of Keap1 was elucidated and found to be mediated by the Sp1-regulated expression of *CUL4A* (Fig. 9).

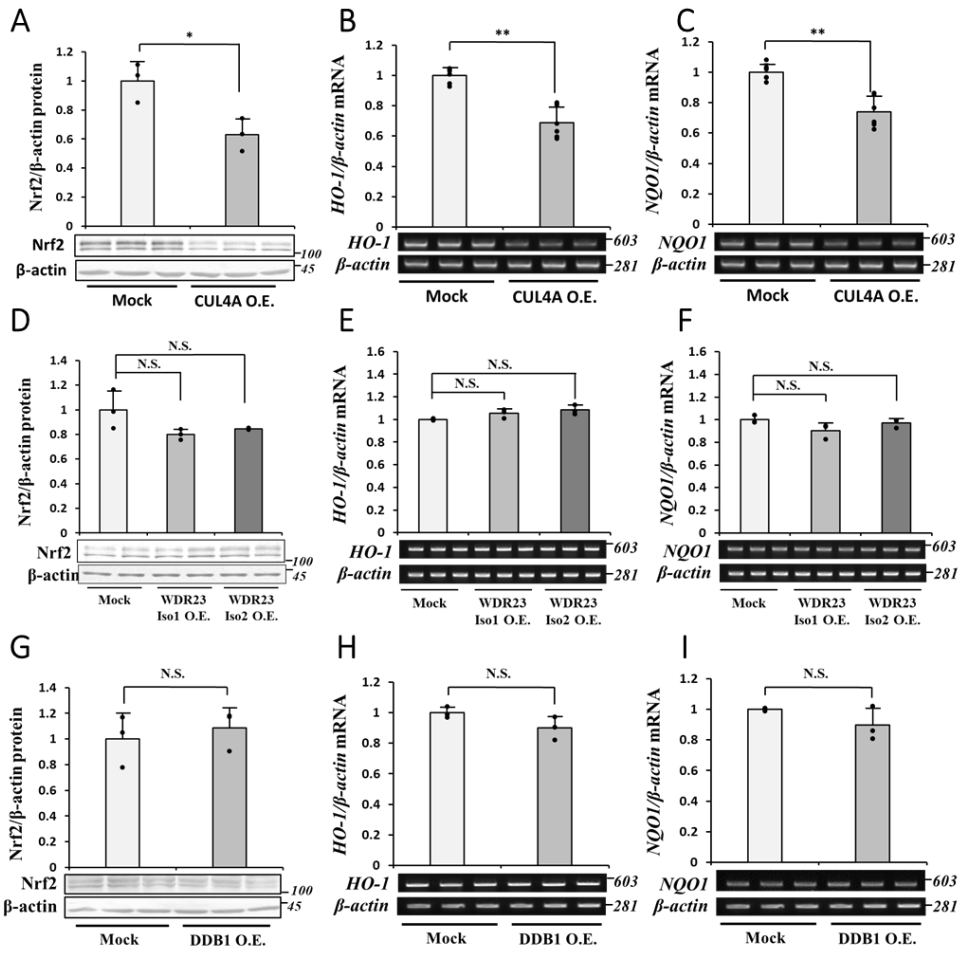

Figure 8. Effects of CUL4A, WDR23 and DDB1 overexpression on Nrf2 levels and activity. (A-C) CUL4A in the pCMV-Myc vector was transfected into Hep3B cells. (A) Nrf2 protein levels were analyzed by immunoblotting. (B-C) The abundance of mRNA encoding *HO-1* and *NQO1* was assessed from Mock and CUL4A-overexpressing cells by RT-PCR with the same β-actin panel as a loading control. (D) The abundance of Nrf2 in WDR23 isoforms 1 and 2 overexpressing Hep3B cells was examined by immunoblotting. (E-F) The abundance of *HO-1* and *NQO1* mRNA in WDR23 isoforms 1 and 2 overexpressing Hep3B cells was examined by RT-PCR with the same β-actin panel as a loading control. (G) Nrf2 protein levels were assessed in cell lysates obtained from DDB1-overexpressed Hep3B cells. (H-I) The abundance of mRNA encoding *HO-1* and *NQO1* was examined from Mock and DDB1-overexpressed cells by RT-PCR with the same β-actin panel as a loading control. All graphs present means ± S.D. from three independent experiments. *p<0.05, **p<0.01 *versus* the indicated cells.

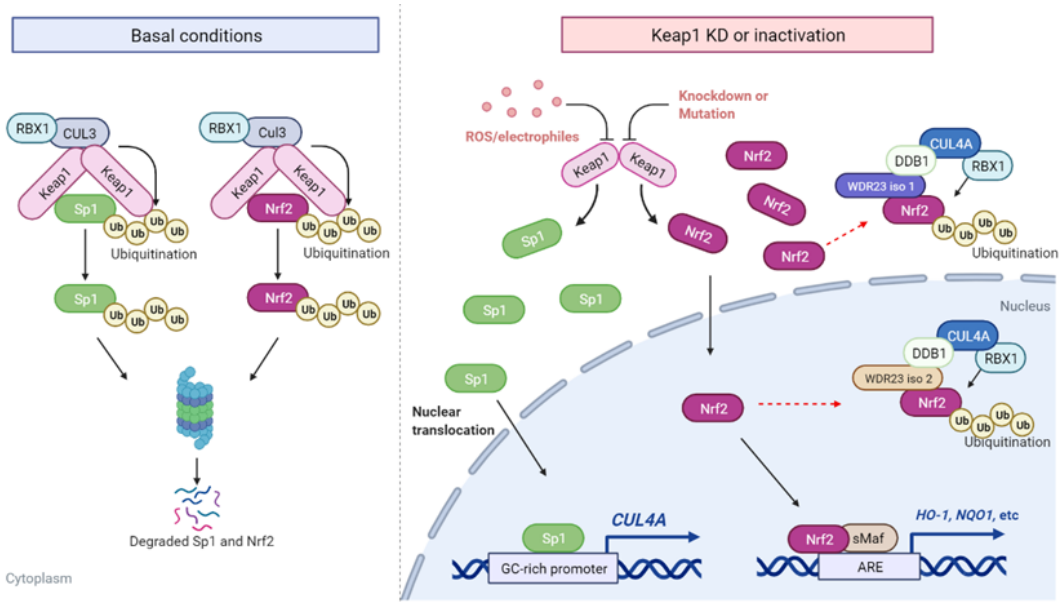

Figure 9. Proposed model of crosstalk between Keap1 and WDR23 pathways in Nrf2 regulation. Under basal conditions, Keap1 interacts with both Nrf2 and Sp1. These interactions lead to the ubiquitination and sequential degradation of Nrf2 and Sp1, maintaining their low basal protein levels. The down-regulation or inactivation of Keap1 by oxidative stress or somatic mutations leads to the stabilization and transactivation of Nrf2 and Sp1. In this regard, accumulated Sp1 induces the transcription of *CUL4A*. Overexpressed CUL4A acts as a scaffold that associates with WDR23, DDB1, and RBX1 to form a functional $CRL4A^{WDR23}$ E3 ligase that promotes the ubiquitination of Nrf2.

In the present study, the expression of *CUL4A,* but not that of other components of $CRL4A^{WDR23}$, was up-regulated by the knockdown of Keap1. In an examination of the promoter region of *CUL4A*, I identified multiple Sp1 putative binding sites. The effects of Keap1 knockdown appear to require Sp1 because the mithramycin A and knockdown of Sp1 prevented the expression of *CUL4A* being up-regulated by Keap1 knockdown. Based on the critical role of Sp1 in this context, I investigated the ability of Sp1 to regulate the expression of *CUL4A*. The knockdown of Keap1 and overexpression of Sp1 both induced the promoter activity of a 1,920-bp fragment of the 5′-flanking sequence and its consecutive 5′-end deletion toward the −230 bp of *CUL4A*. There are four possible Sp1-binding sites within the −230/+50 region of *CUL4A*, and by using site-directed mutagenesis, the fourth site (−30/−21 bp from TSS; Sp1_M4) was shown to be the critical region for the regulation of *CUL4A* promoter activity by Sp1. Additionally, the ChIP assay revealed that Sp1 was associated with this binding site. The present study is the first to reveal a relationship between the transcription factor Sp1 and the regulation of *CUL4A* gene expression.

Despite its crucial role in malignancy, the regulation of CUL4A at the transcriptional level has not yet been examined in detail. For example, a study on the Wnt-dependent regulation of $p27^{KIP1}$ unexpectedly showed that the TCF/LEF1 complex bound to and activated the promoter of mouse *Cul4a* (112). A recent study reported that cyclic adenosine monophosphate (cAMP) response element-binding protein (CREB) bound to the cAMP-responsive element located in the −926/−764 of *CUL4A* and activated its transcription (113). The present results revealed that the −230 bp fragment of the 5′-flanking sequence of *CUL4A* did not contain TCF/LEF1 or CREB-binding motifs, but was still responsive to the knockdown of Keap1, indicating that neither the Wnt pathway nor CREB is involved in this context.

Sp1 is a crucial transcriptional factor that regulates the basal transcription of genes with a TATA-less promoter. Deniaud *et al.* (114) identified a set of genes that are regulated by Sp1 using genome-wide expression profiling, including those involved in metabolism, the transcriptional machinery, adhesion, apoptosis, cell growth, exocytosis, inflammation, signal transduction, ubiquitination, and many genes with unknown functions (114). Regarding the role of Sp1 in the expression of ubiquitination-related factors, they found that the overexpression of Sp1 up-regulated the expression of ariadne E2-binding protein homolog 1 (Arih1) and F-box and WD-40 domain protein 2 (Fbxw2) and down-regulated the expression of praja 2 (Pja2) E3 ligase. Burger *et al*. (115) indicated that Sp1 regulated the basal transcriptional activity of Breast Cancer-Associated gene 2 (BCA2) E3 ligase (115). In the present study, the result showing that Sp1 regulated the basal and inducible expression of *CUL4A* expands our knowledge on the involvement of Sp1 as a regulator of the ubiquitination pathway.

The present results demonstrated that the increase observed in Sp1 following the Keap1 knockdown was due to the direct regulation of Sp1 by Keap1. The DGR domain of Keap1 physically interacted with the NTR domain of Sp1 and subjected Sp1 to ubiquitination. Therefore, Keap1 knockdown was directly responsible for the stabilization of Sp1 and its transcriptional activity. Keap1 binds to conserved DLG and ETGE in Nrf2; however, the NTR domain of Sp1 does not contain these motifs. Instead, I identified the DLT motif within the NTR domain of Sp1, which resembled the DLG domain of Nrf2. Similar to this result, iASPP was previously shown to interact with Keap1 through its DLT motif (116) suggesting that Sp1 binds with Keap1 via this DLT motif.

The regulation of Sp1 by ubiquitination has not yet been examined in detail. To the best of my knowledge, only two proteasome-mediated degradation pathways have been shown to regulate Sp1. β-TrCP subjects Sp1 to proteasomal degradation in response to glucose starvation (117) and Ring finger protein 4 (RNF4) targets sumoylated Sp1 for degradation under basal conditions (118, 119). In the present study, the role of Keap1 as a novel regulator of Sp1 ubiquitination and proteasomal

degradation was revealed, which provides additional insights into alternative mechanisms of Sp1 regulation by proteasome degradation machinery.

The direct Keap1-Sp1 interaction implies that structural changes in Keap1 by reactive oxygen species (ROS) and electrophiles may also induce the stabilization of Sp1, similar to Nrf2. For example, hydrogen peroxide has been shown to modify 4 cysteine residues (Cys226, Cys613, Cys622, and Cys624) in Keap1, thereby inducing structural modifications (45). Consistent with these findings, Ryu *et al*. (98) were the first to report that oxidative stress increases Sp1 protein levels and transactivity in neurons. Previously, study demonstrated that high glucose-induced oxidative stress increased nuclear Sp1 levels (97). However, Yeh *et al*. (120) showed that H_2O_2-induced Sp1 protein levels were mediated by the activation of the internal ribosomal entry site (IRES) pathway and increased the translation of Sp1, suggesting the Keap1-independent regulation of Sp1 by oxidative stress (120). Collectively, the present results and previous findings imply the multilayered, involving translational and posttranslational, regulation of Sp1 by oxidative stress.

A previous study reported that Sp1 regulated the expression of *Keap1* by directly binding to its binding sites in the −160/−153 region of the *Keap1* promoter (121). These findings combined with the present results suggest that the regulation of Sp1 by Keap1 provides an autoregulatory feedback loop that compensates for reduced Keap1 activity. This positive feedback of *Keap1* gene expression and the additional induction of the $CRL4A^{WDR23}$ pathway may ensure a robust and efficient response towards insults on the Keap1-dependent Nrf2 regulation pathway.

Growing evidence has shown that Sp1 and CUL4A are both overexpressed in many cancers and are associated with a poor prognosis (122–125). The mechanisms contributing to high Sp1 protein levels in tumors remain unclear (123); therefore, the present results indicate that the somatic mutations in *Keap1* frequently observed in various tumors are the reason for elevated Sp1 protein levels. Additionally, the targeting of Sp1 as a cancer treatment has been suggested (122); however, the role of Sp1 in malignancy is complex. Sp1 activates and suppresses the expression of oncogenes and tumor suppressor genes as well as genes involved in essential cellular functions (126). In the present study, the activation of Sp1 under Keap1 knockdown conditions was important for the activation of the $CRL4A^{WDR23}$ machinery and prevented the constitutive activation of Nrf2, which may enhance the expression of drug-metabolizing enzymes. Based on the results of the present study, I added a role for Sp1 as a tumor suppressor factor. A more comprehensive understanding of the function of Sp1 in cancer is needed to verify its potential as a therapeutic target.

In the present study, the overexpression of both Sp1 and CUL4A recapitulate the necessity of Keap1 knockdown for the activity of ectopically expressed WDR23 on Nrf2, which further supports the concept that Sp1 and CUL4A mediate the

interplay between Keap1 and WDR23. It is important to note that the overexpression of CUL4A alone was sufficient to decrease Nrf2 protein levels, indicating that CUL4A is the rate-limiting factor of $CRL4A^{WDR23}$ under basal conditions. Therefore, the up-regulated expression of CUL4A during the Keap1 knockdown is the mechanism underlying the crosstalk between the Keap1 and WDR23 pathways for the regulation of Nrf2. Research has so far focused on the role of CUL4A in the regulation of the cell cycle and maintenance of genomic integrity. Hence, the present results provide a novel insight into the contribution of inducible CUL4A expression in the oxidative stress response and Nrf2-dependent drug metabolism.

In conclusion, the present study identified a novel role for Keap1 as a regulator of Sp1 stability. I established that Sp1 is a transcriptional activator of *CUL4A*. Furthermore, *CUL4A* appears to be the rate-limiting factor of $CRL4A^{WDR23}$. Collectively, the present results revealed that during the knockdown or inactivation of Keap1, Sp1 evades proteasomal degradation and activates the transcription of *CUL4A*, which ultimately leads to the activation of the $CRL4A^{WDR23}$ machinery regulating the protein levels of Nrf2. The present study elucidated the molecular mechanism underlying the crosstalk between two independent and parallel regulators of Nrf2, which may be useful for the development of a therapeutic strategy for Nrf2-dependent cancer chemoresistance.

CHAPTER III

Chlorogenic Acid Activates Nrf2/SKN-1 via WDR23 Pathway

III.1. Introduction

Oxidative and electrophilic stresses are major contributing factors to the pathological pathways driving the development of multiple diseases, including cancer and other age-related diseases. These stressors induce cell damage and promote "Warburg-like" metabolic changes (50). The intracellular detoxification system plays a crucial role in maintaining cellular health and homeostasis in the face of oxidative insults. Nuclear factor-erythroid 2-related factor 2 (Nrf2) is a cap'n'collar basic-region leucine zipper transcription factor that orchestrates a cellular response to oxidative stress by regulating approximately 250 genes encoding antioxidants, drug transporters and various cytoprotective proteins (1). In the absence of oxidants or electrophiles, Nrf2 interacts with Kelch-like-ECH-associated protein 1 (Keap1), which promotes Nrf2 ubiquitination and proteasomal degradation (4). Under oxidative stress, Nrf2 dissociates from Keap1, evades proteasomal degradation, and translocates to the nucleus. In the nucleus, Nrf2 forms a complex with small Maf (sMaf) protein family members and binds to antioxidant response elements (AREs) located in the promoters of antioxidant and phase II cytoprotective genes, such as heme oxygenase-1 (HO-1) and NAD(P)H quinone dehydrogenase 1 (NQO1) (83). β-transducin repeat-containing protein (β-TrCP) (2), seven in absentia homolog 2 (Siah2) (5), and HMG-CoA reductase degradation 1 homolog (Hrd1) (3) were recently reported to regulate the abundance of the Nrf2 protein in a similar manner but independent of Keap1. In CHAPTER I and II, WD40 repeat protein 23 (WDR23) was found to regulate Nrf2 via ubiquitination-dependent proteasomal degradation.

WDR23 functions as a substrate recognition protein for the Cullin 4-RING ligase (CRL4) complex comprising CUL4, DDB1, and RBX1 (85), and this complex is known as $CRL4^{WDR23}$. Two isoforms of WDR23 produced by alternative splicing have biologically different roles due to their distinct cellular localization. WDR23 isoform 1 localizes to the cytoplasm and regulates cytoplasmic Nrf2, and isoform 2 to the nucleus for the regulation of nuclear Nrf2 protein turnover (43, 127).

Epidemiological and experimental studies reported that the occasional activation of Nrf2 is beneficial for longevity and the determination of healthspan due to its pivotal role in maintaining redox homeostasis. A previous study on long-lived rodents showed that constitutive elevations in both GSH and GST regulated by Nrf2 were responsible for extended longevity (128, 129). Another study detected constitutively activated Nrf2 in long-lived humans, centenarians, which allowed them to respond better to age-related cellular stresses (130). Therefore, Nrf2 is regarded as a potential target for drug therapy to enhance not only lifespan, but also healthspan. Naturally occurring small molecules that are capable of enhancing Nrf2-regulated cellular stress resistance are being extensively examined.

Polyphenols, a secondary metabolite of plants that are naturally found in fruits, vegetables, and beverages, have been shown to exert their beneficial effects through the activation of the Nrf2 (131).

Chlorogenic acid (CGA; 3-*O*-caffeoylquinic acid), an abundant polyphenol in coffee, is an ester of caffeic acid and quinic acid with potent antioxidant activity (132). Study on the effects of coffee consumption in longevity was pioneered by Sperling and colleagues that led to numerous laboratory and epidemiology studies (133). The various biological properties of coffee and CGA that lead to longevity, including antibacterial, anti-inflammatory, anti-carcinogenic, and antioxidant activities, have been extensively examined. The antioxidant and other health-promoting properties of CGA were found to be mediated by the activation of Nrf2 (134, 135). Although CGA has consistently been shown to exhibit antioxidant activity by activating the Nrf2 pathway, the underlying mechanisms remain unclear.

A number of studies have proposed the mechanism of Nrf2 activation by GGA. Using molecular docking experiment, Wei *et al.* (19) initially predicted a direct interaction between CGA and the Nrf2 binding site in Keap1 that resulted in the dissociation of Nrf2 from Keap1. Liang *et al*. (20) then simulated the binding of several CGA isomers with Keap1 using a computational molecular dynamic method and found that these interactions were restricted to the hydrophobic core of the Keap1 β-propeller. Another study suggested that the activation of Nrf2 by CGA requires $p21^{Cip1}$ (21), a cell cycle regulatory factor that binds to Nrf2 and, thus, competes with Keap1 for Nrf2 binding, thereby compromising the ubiquitination of Nrf2. Although accumulated evidence supports the beneficial effects of CGA through the activation of Nrf2, the exact mechanism of action of CGA remains elusive.

In the present study, I demonstrated that CGA increased Nrf2 protein levels and activity in Keap1 and β-TrCP knockdown cells, but not in WDR23 knockdown cells, suggesting that CGA requires WDR23 for its activity towards Nrf2. I found that CGA regulated a newly identified Akt-FOXO3-DDB1 axis that was responsible for the inhibition of $CRL4^{WDR23}$ activity toward Nrf2. Based on the present results, I established a novel axis that links nutrient sensing and oxidative stress response pathways and accounts for CGA-mediated Nrf2 activation.

III.2. Materials and methods

Materials

Chlorogenic acid (CGA), a PI3K inhibitor (LY294002), leptomycin B, Dulbecco's modified Eagle's medium (DMEM), bovine serum albumin, hydrogen peroxide, ScreenFect™ A, an anti-DYKDDDDK (FLAG) antibody, anti-Myc tag

monoclonal antibody, and horseradish peroxidase-conjugated goat anti-mouse IgG were purchased from Wako Pure Chemical Industries (Osaka, Japan). Akt inhibitor XI was from Cayman Chemicals (Ann Arbor, MI). MG132 (Z-Leu-Leu-Leu-H) was purchased from the Peptide Institute (Osaka, Japan). Penicillin-streptomycin solution, fetal bovine serum (FBS), protease inhibitor cocktail (PIC), and geneticin (G418) were from Sigma Chemical Co. (St. Louis, MO). Nitrocellulose membranes, horseradish peroxidase-conjugated goat anti-rabbit IgG, 4-chloro-1-naphthol, and Tween20 were purchased from Bio-Rad Laboratories (Hercules, CA). Isogen was from Nippon Gene (Toyama, Japan), and Revert Aid^{TM} M-MuLV Reverse Transcriptase was from MBI Fermentas (Vilnius, Lithuania). Go Taq polymerase was from Promega, Madison, WI. KOD Plus Neo and Fx Neo DNA polymerase were from Toyobo (Tokyo, Japan). DNA Ligation Kit ver.1 was from Takara Bio Inc. (Shiga, Japan). DAPI (4′,6-diamidino-2-phenylindole) was from Dojindo (Kumamoto, Japan). Protein G-Sepharose was purchased from GE Healthcare, Chicago, IL. Alexa Fluor® 488-conjugated goat anti-rabbit IgG and Alexa Fluor® 594-conjugated goat anti-mouse IgG were from Abcam (Carlsbad, CA). Anti-DDB1 and anti-IPO7 antibodies were from Santa Cruz Biotechnology (Santa Cruz, CA); an anti-phosphoserine/threonine/tyrosine antibody was from GeneTex (Irvine, CA, USA); and an anti-ubiquitin antibody (clone FK2) was from StressMarq Bioscience.

Cell culture, treatments, and reagents

Hep3B and HeLa cells were cultured in DMEM high glucose containing 10% (v/v) FBS, penicillin (100 units/mL), and streptomycin (100 μg/mL). A549 cells were cultured in DMEM low glucose with 10% FBS and penicillin-streptomycin. HEK293 cells were cultured in DMEM/Ham'sF-12 with 10% FBS and penicillin streptomycin. Cells were maintained at 37°C in 5% CO_2 and 95% air in the presence or absence of CGA (50 or 100 μM, 8 h), LY294002 (50 μM, 8 h), Akt inhibitor XI (1 μM; 8 h), or H_2O_2 (250 or 500 μM; 48 h).

Preparation of constructs

The cDNA of human *DDB1* (GenBank^{TM} accession number NM_001923.5) was amplified by PCR with primer sets 1 and 2 (Table 1). Human *FOXO3* (NM_001455.4) was amplified by PCR with primer sets 3 and 4. The cDNA of human *Akt1* (NM_005163.2) was amplified using primers 5 and 6. Amplified *DDB1*, *FOXO3*, and *Akt1* were digested by the restriction enzymes *Not*I and *Xba*I, *BamH*I and *NotI*, and *BamH*I and *EcoR*I, respectively, and then ligated into the 3×FLAG-pcDNA4 vector (Invitrogen, Carlsbad, CA).

Preparation of antibodies

Antibodies against human Nrf2 and β-actin were prepared using a previously described method (1). Regarding the expression and purification of SKN-1 in *E.*

coli strain BL21(DE3) (Novagen, Madison, WI), the 1201–1872nd nucleotide of *C. elegans* SKN-1 (NM_171345.6) was amplified with primers 7 and 8 (Table 1). Amplified cDNA was digested by the restriction enzymes *BamH*I and *Hind*III and ligated into the pQE-80L vector (Qiagen, Hilden, Germany). The pQE-80L vector containing SKN-1 cDNA (1201–1872nd nucleotide, which is a common region to all SKN-1 isoforms), was transfected into *E. coli*, protein expression was induced by the addition of 1 mM isopropyl β-*d*-1-thiogalactopyranoside, and bacteria were harvested and lysed in lysis buffer (pH 7.5) containing 50 mM NaH2PO4 and 300 mM NaCl, sonicated for 5 min, and centrifuged at 25,000 × g for 30 min. The pellet was solubilized with lysis buffer containing 6 M guanidine hydrochloride (GdnHCl), centrifuged at 25,000 × g for 30 min, and the resulting supernatant was loaded onto a nickel-chelate-nitrilotriacetic acid agarose column (QIAGEN) in order to purify the 6xHis-tagged SKN-1 peptide (401-623rd amino acid of the SKN-1A isoform). The purified protein was injected into a rabbit as previously described (2). The cross-reactivity of the antibody was confirmed using the purified SKN-1 protein from *E. coli* and lysates obtained from the wild-type (N2), *skn-1* mutant (*skn-1(ok2315) IV/nT1 [qIs51](IV;V)*), and *skn-1* overexpressed (*ldIs7* [*skn-1B/C::GFP + pRF4(rol-6(su1006))*]) *C. elegans*. All experiments were conducted in accordance with guidelines on the welfare of experimental animals and with the approval of the Ethics Committee on the use of animals of Kwansei Gakuin University.

Table 1. Primers used for plasmid construction

No.	Sequences	Description
1	5'- ATAAGAATGCGGCCGCTCGTACAACTACGTGGTAAC -3'	Fw; 4–23 of human *DDB1* cDNA; underlined, *Not*I site
2	5'- GCTCTAGACTAATGGATCCGAGTTAGCT -3'	Rv; 3404–3423 of human *DDB1* cDNA; underlined, *Xba*I site; double underlined, stop codon
3	5'- TATGGATCCGCAGAGGCACCGGCTTCCCC -3'	Fw; 4–23 of human *FOXO3* cDNA; underlined, *BamH*I site
4	5'- ATAAGAATGCGGCCGCTCAGCCTGGCACCCAGCTCT -3'	Rv; 2003–2022 of human *FOXO3* cDNA; underlined, *Not*I site; double underlined, stop codon
5	5'- TATGGATCCAGCGACGTGGCTATTGTGA -3'	Fw; 4–22 of human *Akt1* cDNA; underlined, *BamH*I site
6	5'- CGGAATTCTCAGGCCGTGCCGCTGGCCG -3'	Rv; 1424–1443 of human *Akt1* cDNA; underlined, *EcoR*I site; double underlined, stop codon
7	5'- AAGGATCCATGCAAAACGACAGTCTTCA -3'	Fw; 1201–1220 of *C. elegans skn-1* cDNA; underlined, *BamH*I site
8	5'- TTTAAGCTTTCAGATGTAATGGGACATCT -3'	Rv; 1852–1872 of *C. elegans skn-1* cDNA; underlined, *Hind*III site; double underlined, stop codon

Knockdown experiment

The mRNA of human *Keap1*, *β-TrCP*, *FOXO3*, and *Akt1* were knocked down using shRNA with pBAsi-hU6 Neo Vector (Takara Bio Inc.) containing specific targets. siRNA against WDR23 (Cat. No. SI05029899) and AllStars Negative Control (SI03650318) for the knockdown of WDR23 were purchased from Qiagen (Hilden, Germany). si-DDB1 (Cat. No. 4427037) was purchased from Life Technologies (Tokyo, Japan). shRNA and siRNA targets are listed in Table 2 and transfected into cells using ScreenFect™ A according to the manufacturer's instructions. shRNA transfectants were selected using G418.

Table 2. shRNA and siRNA targets

Factor	Method	Target
Keap1	shRNA	5'- GCAGGCCTTTGGCATCATGAACG -3'
β-TrCP	shRNA	5'- AAGCGAATTCTCACAGGCCAT -3'
FOXO3	shRNA	5'- AACAGCACGGTGTTCGGACCT -3'
Akt	shRNA	5'- AAGATCCTCAAGAAGGAAGTC -3'
GFP	shRNA	5'- CTCGAGTACAACTATAACTCA -3'
WDR23	siRNA	5'- CUGGGUCUUUAGGGUAGGACA -3'
DDB1	siRNA	5'- CCAUCGAUGAGAUCCAGAA -3'

Immunoprecipitation and immunoblotting

Cells were washed with ice-cold PBS, collected, lysed in immunoprecipitation buffer (50 mM Tris-HCl, pH 7.5 and 150 mM NaCl, 0.5% NP40) with protease inhibitor cocktail, and centrifuged at 14,000 × *g* for 15 min. The protein-containing supernatant was incubated with the anti-FLAG antibody or unimmunized mouse serum at 4°C for 2 h. Protein G-Sepharose (50% w/v) was then added to the solution and incubated at 4°C for 1 h. Samples were washed with immunoprecipitation buffer containing 0.05% NP40 and analyzed by SDS-PAGE followed by immunoblotting. Anti-Nrf2, anti-DDB1, anti-IPO7, anti-SKN-1, anti-ubiquitin, anti-phosphoserine/threonine/tyrosine, anti-FLAG, or anti-β-actin was used for immunoblotting. Band intensities were quantified using NIH Image software ImageJ version 1.36b (National Institutes of Health, Bethesda, MD).

Immunofluorescence

Hep3B cells were cultured on 3.5-cm glass-bottomed dishes (Thermo Fisher Scientific, Waltham, MA). Cells were treated with CGA, Akt inhibitor XI, and/or LY294002, washed with PBS, fixed with 4% paraformaldehyde (Wako) for 20 min at 4°C, washed twice with TPBS (PBS containing 0.2% Tween20), and then

blocked with blocking buffer (0.1% bovine serum albumin in TPBS at 4°C for 1 h). Cells were subsequently incubated with the anti-Nrf2 or anti-FOXO3 antibody at 4°C for 1 h and washed twice with TPBS. Cells were then incubated with Alexa Fluor® 488- or Alexa Fluor® 594-conjugated goat anti-rabbit IgG with DAPI at 4°C for 1 h. Images were obtained by confocal microscopy (TCS SP8, Leica Microsystem, Wetzlar, Germany).

Luciferase reporter gene assay

Three copies of the antioxidant response element (ARE) from the NQO1 promoter (3×NQO1-ARE) with the sequence of 5'-ATCGCAGTCACAGTGACTCAGCAGAATCTGATCGCAGTCACAGTGACTCAGCAGAATCTGATCGCAGTCACAGTGACTCAGCAGAATCTG -3' were cloned into the pGL3-basic luciferase reporter plasmid with the *Bgl*II enzyme. The *DDB1* promoter was isolated from the genomic DNA of Hep3B cells with the forward primer of either:

5'- TTACGCGTCTGTCCTGCATCCAGCCA -3' (for the -3290/+50 construct),

5'- TTACGCGTATGAAGTTGTGAGTTGGCCT -3' (for the -2566 /+50 construct),

5'- TTACGCGTGTAACGATACAAGCTGCGGA -3' (for the -1502 /+50 construct), or

5'- GGGGTACCCTGGAGGCTGCAGGGCTGAC -3' (for the -813/+50 construct)

and the reverse primer of 5'- ATAGATCTCGTTCACGGCGGTGGGCT -3', digested with *Mlu*I and *Bgl*II, and inserted into the pGL3-basic luciferase reporter plasmid. Hep3B cells were transiently transfected with 0.25 μg pGL3-containing either 3×NQO1-ARE or *DDB1* promoter and the pRL-TK vector (12.5 ng) as an internal control with GenePORTER TM2 transfection reagent (Gene Therapy Systems). Cells were treated with or without CGA, or co-transfected with 0.25 μg of Mock or FLAG-FOXO3. Forty-eight hours post-transfection, luciferase activity was assessed with a luminometer (Lumat LB9507; Berthold) using the Dual-Luciferase Reporter Assay System (Promega) according to the manufacturer's protocol. Firefly luciferase activity was normalized to Renilla luciferase activity.

Isolation of RNA and RT-PCR

Total RNA was extracted from Hep3B cells and *Caenorhabditis elegans* using Isogen following the manufacturer's instructions and converted to cDNA by reverse transcription. PCR was performed with 10 pmol of each primer (Table 3), Go Taq polymerase, and cDNA (100 ng). PCR products were separated by electrophoresis on a 1% agarose gel, visualized with ethidium bromide staining, and quantified by scanning densitometry using NIH Image software ImageJ.

Table 3. Primers used in gene expression assessments

Organism	Primers	GenBank Accession No.		Sequences
Human	Keap1	NM_203500.2	Forward	5'- TCTTCAAGGCCATGTTCACC -3'
			Reverse	5'- GGCACGCTGGTGCAACTCCA -3'
	β-TrCP	NM_033637.4	Forward	5'- CGCACTCACAGCTTTCCAGA -3'
			Reverse	5'- GAGTTTCCGTTGCTTGGGCA -3'
	WDR23	NM_181357.2	Forward	5'- CACAGGATTGGAGAAGGAGG -3'
			Reverse	5'- TCGGCAGTCATAGAGTCGGA -3'
	CUL4A	NM_001008895.4	Forward	5'- CAGGCACAGATCCTTCCGTT -3'
			Reverse	5'- TGGTTTCTGTGTGCTGTGGT -3'
	CUL4B	NM_003588.4	Forward	5'- CGGGTGTTTCTGTGCAGTAT -3'
			Reverse	5'- TGTCCCAAATGGAGGGTAGC -3'
	DDB1	NM_001923.5	Forward	5'- CAGTGTTTCGGGGTCCTCTC -3'
			Reverse	5'- AAGTCGCCCTTGGTCTTCAG -3'
	RBX1	NM_014248.4	Forward	5'- ACTTCCACTGCATCTCTCGC -3'
			Reverse	5'- AAGTGATGCGCTCAGAGGAC -3'
	Nrf2	NM_006164.5	Forward	5'- GCCATTCACTCTCTGAACTT-3'
			Reverse	5'- GGTGACAAGGGTTGTACCAT-3'
	HO-1	BC001491.2	Forward	5'- CCAGCCATGCAGCACTATGT -3'
			Reverse	5'- AGCCCTACAGCAACTGTCGC -3'
	NQO1	NM_000903.3	Forward	5'- TGATCGTACTGGCTCACTCA -3'
			Reverse	5'- GTCAGTTGAGGTTCTAAGAC -3'
	$p21^{Cip1}$	NM_000389.5	Forward	5'- GCAGACCAGCATGACAGATT -3'
			Reverse	5'- AATGCCCAGCACTCTTAGGA -3'
	$p16^{Ink4a}$	NM_000077.5	Forward	5'- CTGGACACGCTGGTGGTGCT -3'
			Reverse	5'- GCATCTATGCGGGCATGGTT -3'
	Akt	NM_005163.2	Forward	5'- GAGCTGTTCTTCCACCTGTC -3'
			Reverse	5'- CCGGTACACCACGTTCTTCT -3'
	FOXO3	NM_001455.4	Forward	5'- ACGCAGCAGTGATGAGCTGG -3'
			Reverse	5'- CTGCCATATCAGTCAGCCGT -3'
	β-actin	NM_001101.5	Forward	5′- CAAGAGATGGCCACGGCTGCT -3′
			Reverse	5′- TCCTTCTGCATCCTGTCGGCA -3′
C. elegans	skn-1	NM_171345.6	Forward	5'- GTTCCAGTTA TGCCAATACT -3'
			Reverse	5'- TTGAACGACT CGAAGAATCC -3'
	gcs-1	NM_063526.9	Forward	5'- TCTCTTGGAG TACCTGGATT -3'
			Reverse	5'- CAACCATCTG GCTTCATCGA -3'
	gss-1	NM_063610.8	Forward	5'- GATCAATATT CAGCGGAATA -3'
			Reverse	5'- CATGTCATCG GTACTCCTAA -3'
	wdr-23	NM_059723.7	Forward	5'- CAATGTGGTTGGTCGATTCT -3'
			Reverse	5'- ATCATCCTCGTGAGCATTCA -3'
	cul-4	NM_063124.8	Forward	5'- GTGCTTGCACTTCTTGGTGG -3'
			Reverse	5'- TCTTGATATCGGCGGTGCTC -3'
	ddb-1	NM_069898.9	Forward	5'- GAACACGACCACCGAGTCTT -3'
			Reverse	5'- CGGGTGGATGCAACTTTTGG -3'
	rbx-1	NM_073095.8	Forward	5'- GTCGAGGAGGCCACAAATCA -3'
			Reverse	5'- CCAATGGGCATACCTGTCGT -3'
	sod-3	NM_078363.9	Forward	5'- AGCATCATGCCACCTACGTGA -3'
			Reverse	5'- CACCACCATTGAATTTCAGCG -3'
	act-1	NM_073418.9	Forward	5'- ATGAAGATCCTTACCGAGCG -3'
			Reverse	5'- TTGGCGTACAAGTCCTTACG -3'

ROS measurement

The amount of ROS was measured with 2',7'-dichlorodihydrofluorescein (H2-DCF-DA; Sigma, St. Louis, MO). Cells were treated with 100 nM for 30 min, followed by 2 washes with PBS. Reduced H_2DCFDA may be oxidized and converted into fluorescent 2', 7'-dichlorofluorescein (DCF) by intracellular ROS. The intensity of fluorescence was measured using the En Vision 2104 Multilabel Reader (PerkinElmer, MA) at an excitation wavelength of 485 nm and fluorescence wavelength of 538 nm. Background fluorescence intensity measured in PBS was subtracted. Fluorescence was normalized to the number of cells per sample.

Cell viability assay

Hep3B cells (5×10^4 cells/well) were cultured in 24-well plates, and after 24 h of growth, cells were treated with different concentrations of chlorogenic acid with or without 500 μM H_2O_2 for 48 h. The exposed cells were then treated with 100 μl of MTT solution (5 mg/ml in PBS) for 2 h. The culture medium was removed, and the resulting purple formazan was dissolved with 500 μl of isopropanol containing 0.04N HCl and 0.1% NP40, and the absorbance was measured at 590 nm using a microplate reader (PerkinElmer, Waltham, MA). The cell viability was calculated as a relative percentage to the control.

Preparation of CGA affinity resin and its binding assay

CGA-Sepharose resin was prepared as follows: CGA (0.1 mmol; 35.4 mg) was dissolved in 0.1 M citrate buffer (pH 5.5). N-Hydroxysuccinimide (NHS; 0.2 mmol; 23 mg) and 1-ethyl-3-(3-dimethylaminopropyl) carbodiimide hydrochloride (EDC; 0.2 mmol; 38.3) were added to the solution. The reaction was stirred at room temperature for 20 min and pH was raised above 7 using phosphate buffer (0.2 M, pH 7.4). Octylamine-Sepharose was added to the reaction and incubated at room temperature for 24 h. The resin was washed with wash buffer (50 mM Tris-HCl pH 8.0, 100 mM NaCl). Hep3B cells were transfected with either FLAG-Akt1 or FLAG-FOXO3, and after 48 h, cells were lysed in lysis buffer containing 50 mM Tris-HCl (pH 8.0), 100 mM NaCl, 0.5% NP40, and 0.05% PIC. The lysate was mixed with CGA affinity resin and incubated at 4°C for 1 hr. The resin was washed five times with wash buffer containing 0.05% NP40. Bound proteins were eluted with SDS-sample buffer at 95°C for 5 min and analyzed by immunoblotting.

C. elegans experiments

The following strains used in the present study were from the Caenorhabditis Genetic Center (CGC), Minneapolis, MN:

1. The wild-type reference strain N2 Bristol
2. VC1772 [*skn-1(ok2315)/nT1(qIs51)*]
3. LD1 [*skn-1b/c*::*gfp*]

4. LG357 [*skn-1(zu135)/nT1(qIs51); skn-1c::GFP*]
5. CF1038 [*daf-16(mu86)*]
6. GR1310 [*akt-1(mg144)*]
7. HT1888 [*daf-16(mgDf50); daf-16a::RFP*]
8. HT1889 [*daf-16(mgDf50); daf-16f::GFP*]

The following strains were provided by the National BioResource Project (Japan):

1. *wdr-23(tm1817)*
2. *ddb-1(tm1769/nT1)*

The following strain was generated in the present study:

1. *skn-1(ok2315); ldIs7*

All worms were maintained at 20˚C on standard nematode growth medium (NGM) plate seeded with OP50 bacteria using a standard technique (136). All experiments were performed on age-matched hermaphrodites synchronized by egg lay. A lifespan assay was performed at 20°C as described previously (137, 138), or 16°C when the *daf-16(mu86)* was included in the assay. In brief, all worms were synchronized using a hypochlorite treatment, and late L4 larvae or young-adult worms were transferred and defined as experimental day 0. Worms were transferred to a fresh plate and scored every two days for survival observations. Worms that did not respond to repeated prodding by a platinum wire were scored as dead, while missing worms were censored. For the chemical treatments including CGA, LY294002, and Akt inhibitor XI, the chemical solutions were added to autoclaved NGM at a desired final concentration before pouring the plates.

Statistical analysis

Statistical analyses for a single comparison between means were conducted using the Student's *t*-test. A one-way ANOVA followed by Tukey's *post-hoc* test was performed for multiple comparisons. The lifespan of *C. elegans* was plotted using a Kaplan-Meier survival analysis and compared among groups for significance using the Log-rank (Mantel-Cox) test. $P < 0.05$ was considered to be significant (*$p < 0.05$, **$p < 0.01$, ***$p < 0.001$).

III.3. Results

Effects of chlorogenic acid (CGA) on Nrf2

To examine the effects of CGA on Nrf2 activation, I treated several human cell lines with 50 and 100 μM CGA for 8 h and changes in total Nrf2 protein levels were investigated. Both concentrations increased Nrf2 protein levels in human hepatoma Hep3B cells (Fig. 1*A*), human cervical adenocarcinoma HeLa cells (Fig.

1*B*), human embryonic kidney HEK293 cells (Fig. 1*C*), and human lung adenocarcinoma A549 cells (Fig. 1*D*). Since Hep3B cells were more responsive to CGA, I used Hep3B cells in the subsequent experiments. CGA promoted Nrf2 transcriptional activity as shown in the ARE luciferase reporter assay (Fig. 1*E*). The increase in Nrf2 also increased the mRNA levels of its target genes *HO-1* and *NQO1* (Fig. 1*F* and *G*). The activation of the Nrf2 pathway by CGA reduced intracellular reactive oxygen species (ROS) levels (Fig. 1*H*). To further support the beneficial role of CGA in a cellular context, I investigated the effects of CGA in H_2O_2-induced senescence and toxicity. CGA prevented cell senescence induced by H_2O_2 (250 μM, 48 h) as shown by reductions in $p21^{Cip1}$ and $p16^{Ink4a}$ mRNA (Fig. 1*I*). In addition, H_2O_2 (500 μM, 48 h) significantly reduced cell viability, which was attenuated by CGA (Fig. 1*J*).

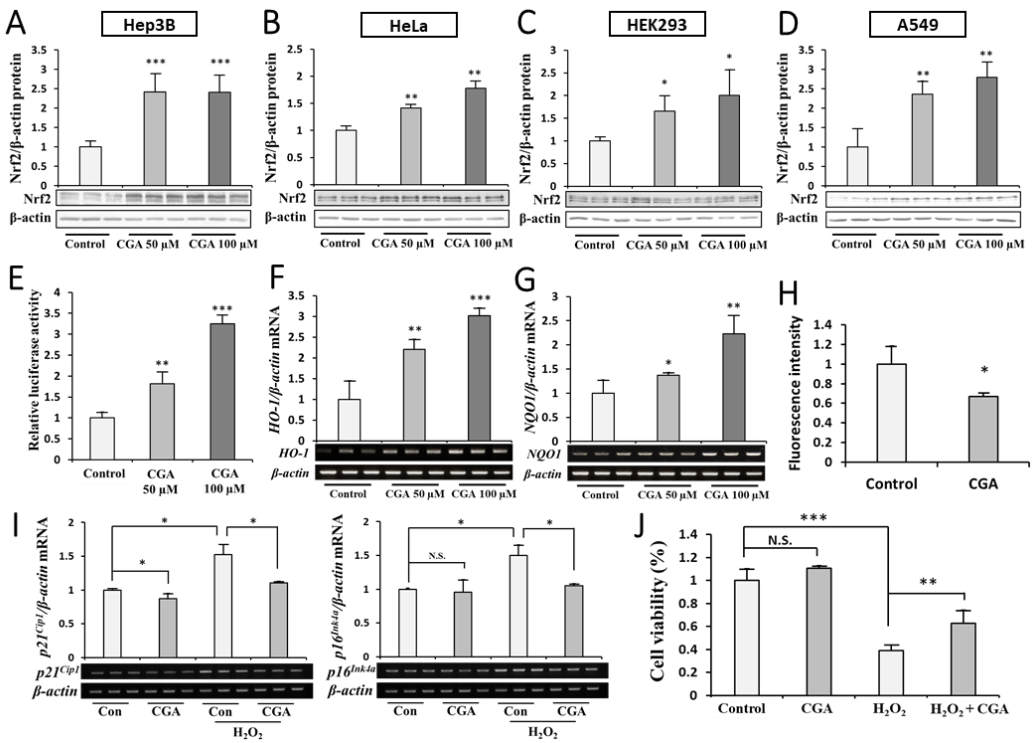

Figure 1. Effects of CGA on Nrf2 (A-D) Nrf2 protein levels in Hep3B (A), HeLa (B), HEK293 (C), and A549 (D) cells treated with CGA at final concentrations of 50 and 100 μM were detected by immunoblotting. (E) Nrf2 activity was measured in cells expressing a 3×NQO1-ARE luciferase reporter and pRL-TK treated with or without CGA (50 and 100 μM, 8 h). (F-G) *HO-1* (F) and *NQO1* (G) mRNA levels were assessed in cell lysates by RT-PCR. (H) ROS levels were measured by H_2DCFDA in cells treated with CGA (50 μM, 8 h). (I) $p21^{Cip1}$ and $p16^{Ink4a}$ mRNA levels in Hep3B cells treated with 50 μM CGA and 250 μM H_2O_2 for 48 h were detected by RT-PCR. (J) The viability of Hep3B cells treated with 50 μM CGA and 500 μM H_2O_2 for 48 h was measured using the MTT colorimetric assay. All values are means ± S.D. N.S. not significant, *p<0.05, **p<0.01, ***p<0.001 *versus* the group indicated.

The involvement of WDR23 for the effects of CGA on Nrf2

CGA treatment did not change *Nrf2* mRNA levels (Fig. 2*A*), suggesting that the activation of Nrf2 by CGA occurred at the post-transcriptional level. Nrf2 is widely known to be regulated post-transcriptionally by several ubiquitin-dependent proteasomal degradation pathways. β-TrCP, Keap1, and WDR23 are adaptors for CUL1, CUL3, and CUL4 E3 ligases, respectively, and have been identified as negative regulators of Nrf2 stability (2, 4, 42). To elucidate the mechanisms underlying CGA-induced Nrf2 activation, I treated β-TrCP, Keap1, and WDR23 knockdown cells with CGA. The efficiency of the knockdown of *Keap1* was approximately 40%, while that of *β-TrCP* and *WDR23* was approximately 60% (Fig. 2*B*). The results showed that the knockdown of WDR23, but not β-TrCP or Keap1, abolished the effects of CGA on Nrf2 protein levels (Fig. 2*C*) and transcriptional activity (Fig. 2*D*), suggesting the involvement of WDR23. These data are consistent with the finding that CGA induced Nrf2 in A549 cells which harbors loss-of-function mutation of *Keap1* (Fig. 1*D*).

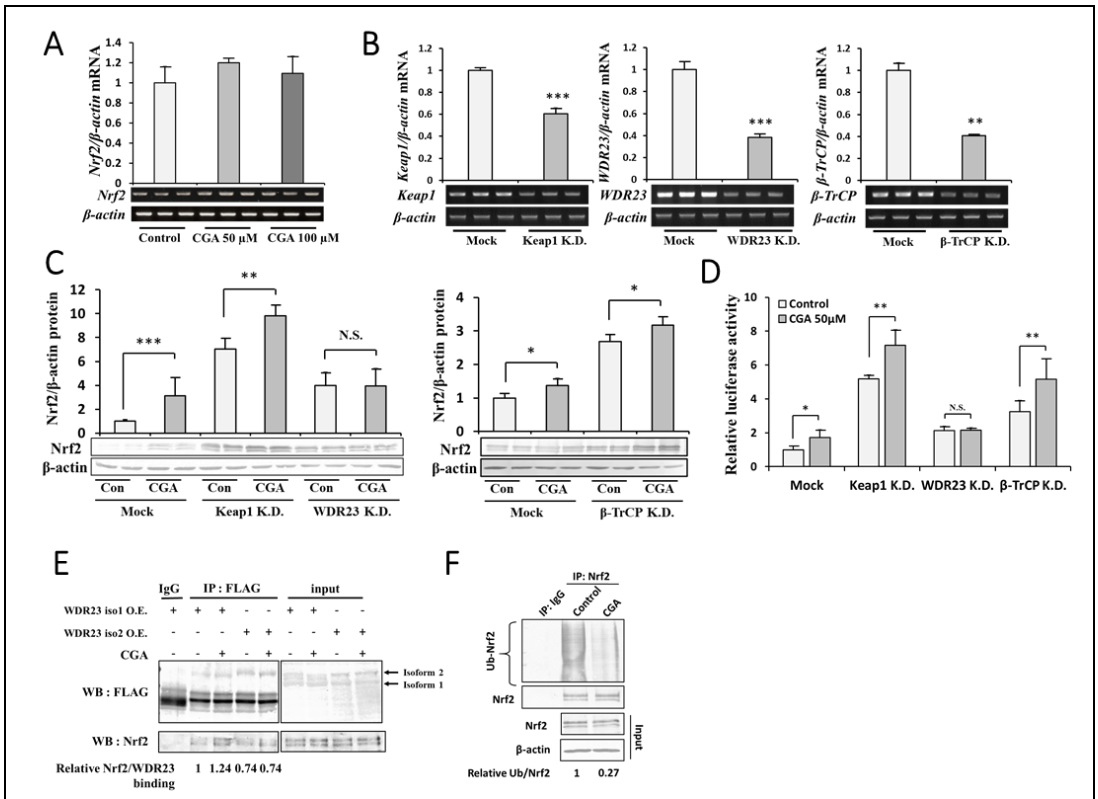

Figure 2. The role of WDR23 in the CGA-regulated Nrf2 levels. (A) *Nrf2* mRNA levels in Hep3B cells treated with CGA at final concentrations of 50 and 100 μM were detected by RT-PCR. (B) Keap1, WDR23, or β-TrCP knockdown cells were generated in Hep3B cells and efficiency was confirmed by RT-PCR. (C-D) Nrf2 protein levels (C) and 3×NQO1-ARE luciferase activity (D) in Keap1, WDR23, and β-TrCP knockdown Hep3B cells treated with control or CGA (50 μM, 8 h) were examined by immunoblotting and the Dual-Luciferase Reporter Assay system, respectively. (E) Hep3B cells were transfected with FLAG-WDR23 isoform 1 or 2, treated with control or CGA (50 μM, 8 h), immunoprecipitated with an anti-FLAG antibody, and analyzed with immunoblotting

against anti-FLAG and anti-Nrf2 antibodies. (F) Cells were treated with MG132 (5 μM, 8 h) and either control or CGA (50 μM, 8 h), cell lysates were immunoprecipitated with the anti-Nrf2 antibody, subjected to immunoblotting using anti-Nrf2, anti-ubiquitin, and anti-β-actin antibodies, and ubiquitinated Nrf2 relative to immunoprecipitated Nrf2 was assessed using ImageJ. All values are means ± S.D. N.S. not significant, *p<0.05, **p<0.01, ***p<0.001 *versus* the group indicated.

To clarify whether CGA increases Nrf2 protein levels by inducing the dissociation of WDR23-Nrf2 and preventing Nrf2 ubiquitination, I performed immunoprecipitation assays in the presence and absence of CGA. The CGA treatment enhanced Nrf2 binding to WDR23 isoform 1, but not WDR23 isoform 2 (Fig. 2*E*). In contrast, the ubiquitination of Nrf2 was decreased by CGA (Fig. 2*F*). These results suggested that CGA inhibited the activity of $CRL4^{WDR23}$ E3 ligase instead of inducing the dissociation of WDR23-Nrf2.

The role of DDB1 inhibition in Nrf2 activation by CGA

To elucidate the mechanisms underlying the CGA-induced inhibition of $CRL4^{WDR23}$ E3 ligase activity, I initially examined the effects of CGA on the mRNA expression of $CRL4^{WDR23}$ components, including *WDR23*, *CUL4A*, *CUL4B*, *DDB1*, and *RBX1*. *HO-1* mRNA was used as the control of Nrf2 activation by CGA (Fig. 3A). The expression of *DDB1* was down-regulated, while that of other genes was unchanged (Fig. 3B−F). The treatment of Hep3B cells with CGA also reduced the total protein levels of DDB1 (Fig. 3G). To further confirm that the inhibition of *DDB1* expression was responsible for the activation of Nrf2 by CGA, I overexpressed DDB1 in the CGA-treated Hep3B cells. As expected, by rescuing DDB1 in CGA-treated cells (Fig. 3G), the elevation in Nrf2 protein was also reversed (Fig. 3H) demonstrating the critical role of DDB1. These results are in agreement with the knockdown of DDB1 (Fig. 3I and J), further supporting the down-regulation of DDB1 stabilizing Nrf2 through the inhibition of $CRL4^{WDR23}$ ligase activity.

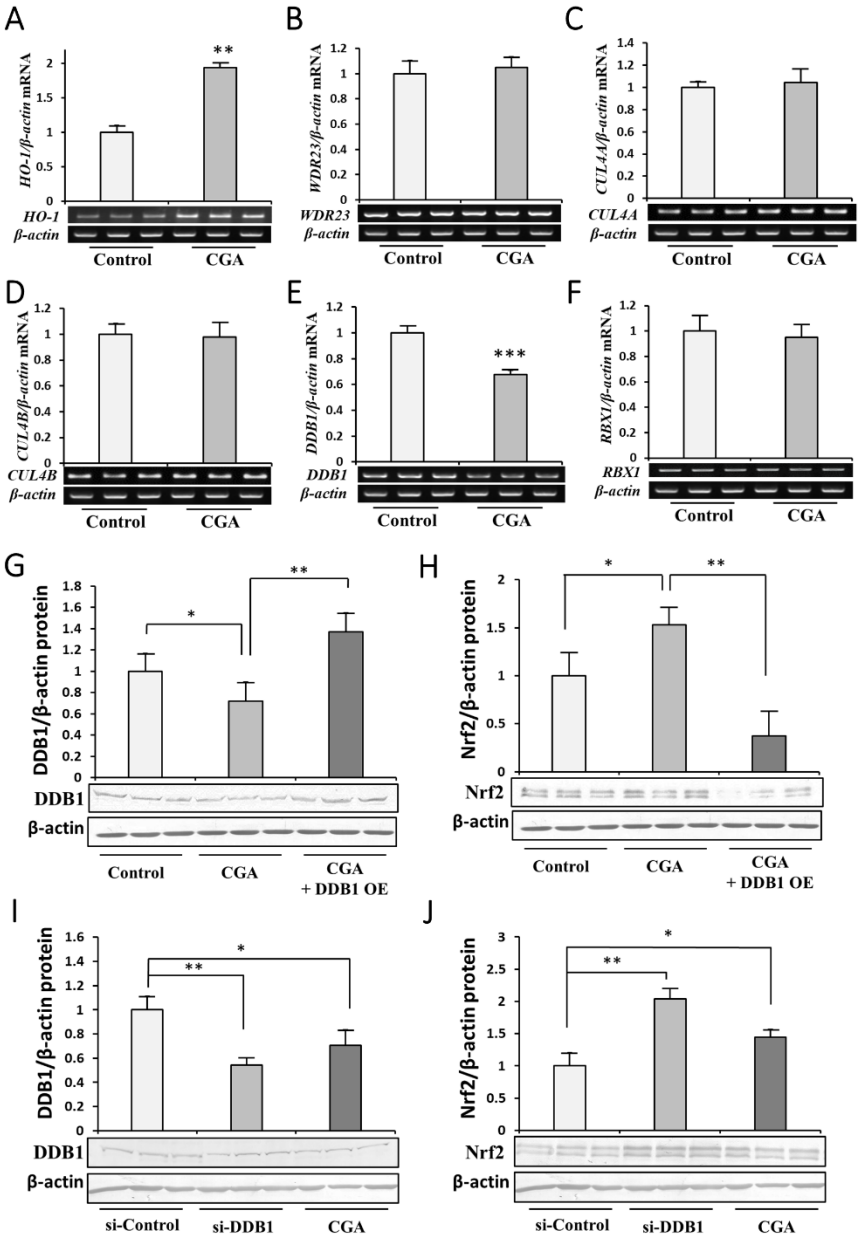

Figure 3. Effects of CGA on the expression of components of $CRL4^{WDR23}$. (A-F) Hep3B cells were treated with control or CGA (50 and 100 μM, 8 h) and the mRNA expression levels of *HO-1* (A), *WDR23* (B), *CUL4A* (C), *CUL4B* (D), *DDB1* (E), and *RBX1* (F) were examined using RT-PCR. (G-H) Hep3B cells transfected with pcDNA-Mock or pcDNA-DDB1 were treated with control or CGA (50 and 100 μM, 8 h) and protein levels of DDB1 (G) and Nrf2 (H) were assessed by immunoblotting. (I-J) Hep3B cells transfected with si-Control or si-DDB1 were treated with control or CGA (50 and 100 μM, 8 h) and protein levels of DDB1 (I) and Nrf2 (J) were assessed by immunoblotting. All graphs represent means ± S.D. *p<0.05, **p<0.01, ***p<0.001 *versus* the indicated group.

The role of FOXO3 in basal and inducible *DDB1* gene expression

To identify the mechanisms underlying the transcriptional regulation of *DDB1* by CGA, I investigated the transcription factor(s) responsible for the regulation of *DDB1* transcription. I predicted the active promoter and enhancer regions of *DDB1* using publicly available ChIP-Seq datasets of the human genome assembly–GRCh38/hg38 (http://chip-atlas.org). Active promoters are marked by H3K4me3 and RNA polymerase II (RNAPII), while the enrichment of H3K4me1 and H3K27Ac are hallmarks of active enhancers (139), and this ChIP-seq peak signature may be observed at approximately +50 to -3290 bp of *DDB1* visualized using the Integrative Genome Viewer (IGV) (Fig. 4).

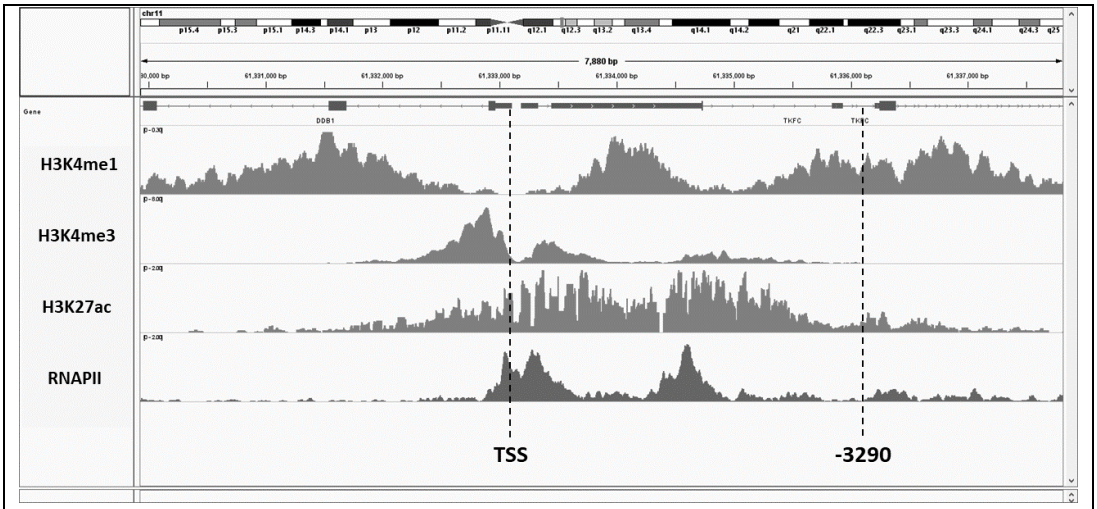

Figure 4. Prediction of active promoter and enhancer regions of *DDB1*. The prediction was performed by publicly available ChIP-Seq datasets of the human genome assembly–GRCh38/hg38 (http://chip-atlas.org) and visualized using Integrative Genome Viewer (IGV). The markers used were H3K4me1, H3K4me3, H3K27Ac, and RNAPII.

I then investigated the minimal *DDB1* upstream region for responding to the CGA treatment. Luciferase reporter plasmids (pGL3-basic) containing −3290/+50 bp or its consecutive 5′-end deletion of the *DDB1* genomic region were constructed and transfected into Hep3B cells. Basal promoter activity was similar with the 5′-end deletion up to −1502 bp and was significantly reduced in the −813/+50 construct (Fig. 5A). Similarly, the CGA treatment reduced the promoter activities of all constructs examined, except for the −813/+50 construct, suggesting that the regulatory region of *DDB1* by CGA is present between −813 and −1502 bp. Using Tfsitescan (140) to predict transcription factor binding sites within this region, I identified various transcription factor-binding sites.

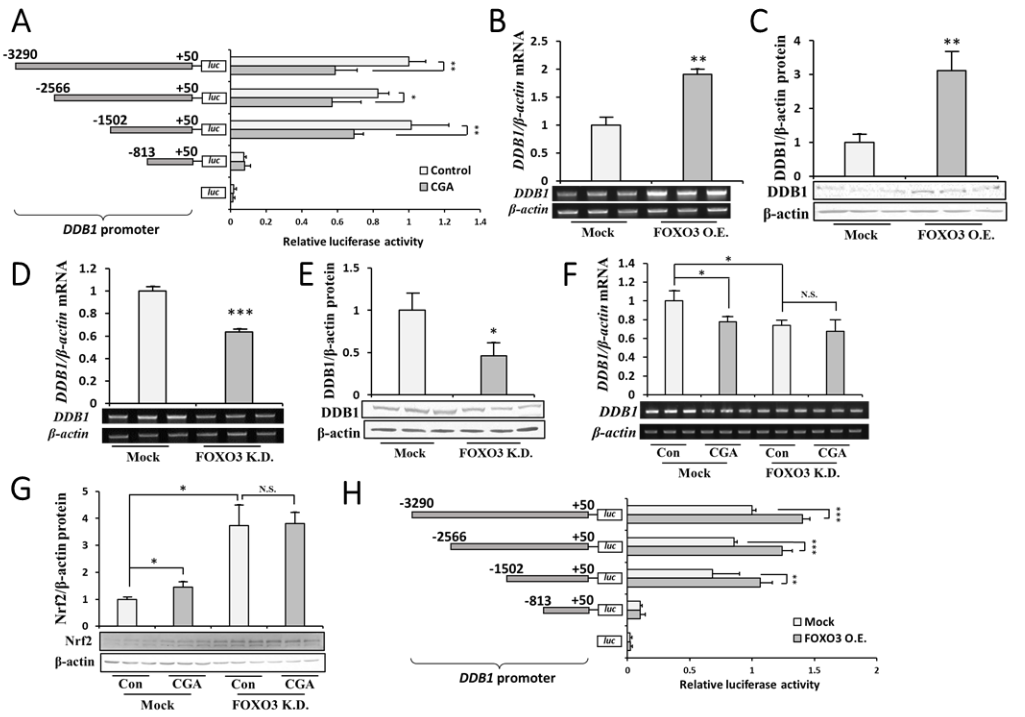

Figure 5. The role of FOXO3 in the regulation of *DDB1* gene expression. (A) The upstream region −3290/+50 of *DDB1* in pGL3 or its 5′-endo deletion construct was co-transfected with pRL-TK as an internal control plasmid into Hep3B cells. Luciferase activity was assessed 48 h after transfection using the Dual-Luciferase Reporter Assay system relative to the promoter-less construct pGL3-Basic. Cells were treated with CGA 8 h prior to assay. Results are shown as a ratio relative to the activity of *DDB1* promoter −3290/+50 in control cells. (B-C) Hep3B cells were transfected with either FLAG-Mock or FLAG-FOXO3. The mRNA levels (B) and protein abundance (C) of DDB1 were then examined by RT-PCR and immunoblotting, respectively. (D-E) The pBAsi-hU6 Neo vector containing sh-GFP or sh-FOXO3 was transfected into Hep3B cells. The mRNA levels (D) and protein abundance (E) of DDB1 were then examined by RT-PCR and immunoblotting, respectively. (F-G) CGA (50 μM, 8 h) was added to control and FOXO3 knockdown Hep3B cells, and the expression of *DDB1* (F) and protein level of Nrf2 (G) was measured with RT-PCR and immunoblotting, respectively. (H) The pGL3 vector containing the upstream region of *DDB1* was co-transfected with pRL-TK and FLAG-Mock or FLAG-DDB1, and luciferase activity was then assessed 48 h after transfection. All graphs are means ± S.D. *p<0.05, **p<0.01, ***p<0.001 *versus* the group indicated.

Among the transcription factors potentially regulating *DDB1* expression, I focused on FOXO3. FOXO3 has been implicated in cytoprotection against oxidative stress through its regulation of the expression of manganese-containing superoxide dismutase (MnSOD) and catalase (141, 142). However, limited information is currently available on the interactions between FOXO3 and Nrf2 pathways even though both regulate cellular oxidative stress responses.

To establish whether FOXO3 regulates the expression of *DDB1*, FLAG-FOXO3 was expressed in Hep3B cells. The mRNA abundance (Fig. 5*B*) and the total protein levels of DDB1 (Fig. 5*C*) were significantly higher in FOXO3-

overexpressed cells. In contrast, shRNA-mediated *FOXO3* knockdown significantly reduced the expression of *DDB1* (Fig. 5*D*) and its protein levels (Fig. 5*E*). These results suggest that FOXO3 is responsible for the basal transcription of *DDB1*. To clarify whether FOXO3 is responsible for CGA-suppressed *DDB1* expression, I treated FOXO3 knockdown cells with CGA. As expected, CGA did not reduce the expression of *DDB1* (Fig. 5*F*) and did not increase the protein level of Nrf2 (Fig. 5*G*) in FOXO3 knockdown cells. I then performed a luciferase reporter assay to confirm these results. The overexpression of FOXO3 significantly enhanced the luciferase activity of pGL3-containing −3290/+50, −2566/+50, and −1502/+50 bp, but not −813/+50 bp, of the *DDB1* genomic region (Fig. 5*H*).

Effects of FOXO3 in the protein abundance of Nrf2

Because FOXO3 regulates the expression and abundance of DDB1, next I examined the effects of FOXO3 on Nrf2 protein levels. The overexpression (Fig. 6*A*) and knockdown (Fig. 6*B*) of FOXO3 significantly reduced and increased the total protein levels of Nrf2, respectively, in Hep3B, HeLa, HEK293 and A549 cells (Fig. 6*C*). Nrf2 protein levels in FOXO3-overexpressing Hep3B, HeLa, HEK293 and A549 cells were not increased by the CGA treatment (Fig. 6*D*), demonstrating the critical role of FOXO3 inhibition as a mediator of CGA-induced Nrf2 activation.

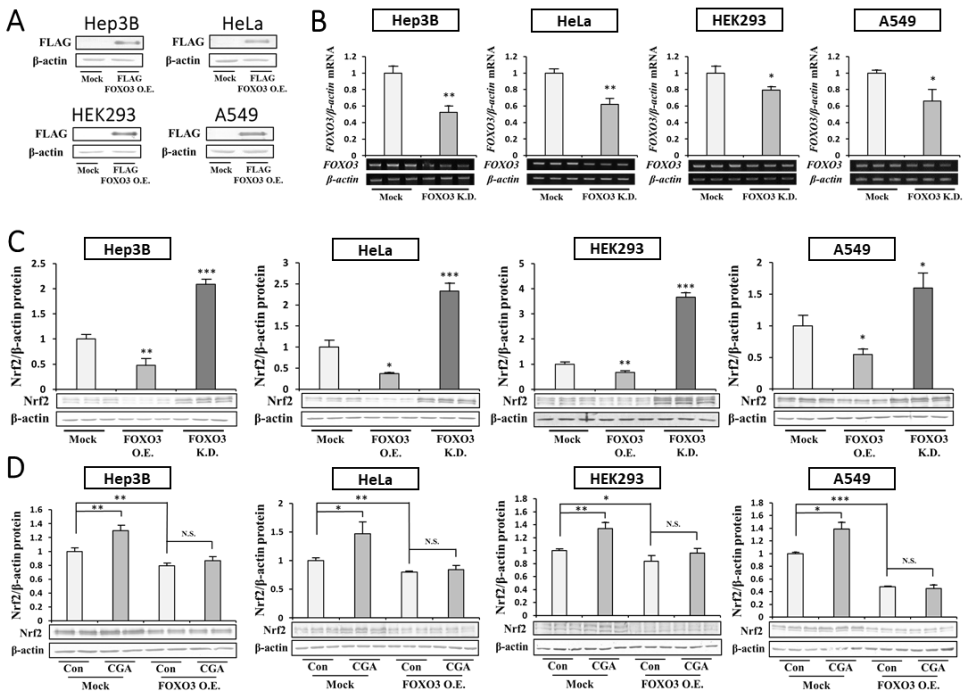

Figure 6. The role of FOXO3 in the regulation of Nrf2. Hep3B, HeLa, HEK293, and A549 cells were transfected with FLAG-Mock and sh-GFP (Mock), FLAG-FOXO3 and sh-GFP (FOXO3

O.E.), or FLAG-Mock and sh-FOXO3 (FOXO3 K.D.). (A) Overexpression was confirmed by immunoblotting. (B) Knockdown efficiency was examined by RT-PCR. (C) Total protein levels of Nrf2 were examined by immunoblotting. (D) The effects of CGA on Nrf2 levels in control cells or FOXO3-overexpressed Hep3B, HeLa, HEK293, and A549 cells were investigated by immunoblotting. All graphs are means ± S.D. *p<0.05, **p<0.01, ***p<0.001 *versus* the group indicated.

The role of Akt and IPO7 in CGA-regulated FOXO3 activity

The identification of a novel role for FOXO3 as a regulator of *DDB1* expression and as a mediator of Nrf2 activation by CGA prompted me to investigate the mechanisms by which CGA regulates FOXO3 activity. FOXO3 activity is mainly regulated by various stimuli through its nucleocytoplasmic localization (143). Therefore, I examined the effects of CGA on the subcellular localization of FOXO3. FOXO3 exclusively localized to the nucleus of Hep3B cells, while the CGA treatment induced the cytoplasmic accumulation of FOXO3 (Fig. 7*A*). FOXO3 phosphorylation by AKT was recognized by the 14-3-3 protein, leading to the nuclear exclusion of FOXO3 (144). To establish whether this mechanism drives the cytosolic accumulation of FOXO3 following CGA treatment, I treated cells with the nuclear export inhibitor leptomycin B. However, the cytosolic accumulation of FOXO3 by CGA was not inhibited by leptomycin B (Fig. 7*A*), suggesting that CGA retains FOXO3 in the cytosol rather than inducing nuclear export.

To gain mechanistic insights into the prevention of FOXO3 nuclear transport by CGA, I examined the effects of CGA on the interaction between FOXO3 and importin-7 (IPO7). IPO7 is a nuclear import receptor belonging to the β-karyopherin family that regulates the redox-sensitive nuclear import of FOXO3 (145). In the present study, the CGA treatment released the interaction between FOXO3 and IPO7 (Fig. 7*B*), which may be responsible for the cytoplasmic retention of FOXO3. IPO7 was recently found to utilize cation interactions in order to recognize and bind to the nuclear localization signal (NLS) in cargo proteins (146). Since Akt phosphorylates FOXO3 at Ser253 located in the NLS and disrupts NLS activity by introducing a negative charge to this basic NLS region (147), Akt appears to play a role in the CGA-induced cytosolic retention of FOXO3. I found that CGA induced the phosphorylation of Akt (Fig. 7*C*) and FOXO3 (Fig. 7*D*). I then demonstrated that the effects of CGA on FOXO3-IPO7 binding were attenuated by Akt inhibitor XI (Fig. 7*E*).

Akt is one of the major downstream targets of phosphatidylinositol 3-kinase (PI3K). To further support this role of Akt, I investigated the effect of Akt inhibitor XI and a PI3K inhibitor (LY294002) on DDB1. As expected, both inhibitors significantly increased *DDB1* mRNA (Fig. 7*F*) and DDB1 protein levels (Fig. 7*G*), and reduced Nrf2 protein levels (Fig. 7*H*). I then treated cells with CGA in the

presence of Akt inhibitor XI or LY294002. Under these conditions, CGA induced Nrf2 (Fig. 7*I*) and the nuclear retention of FOXO3 (Fig. 7*J*) in the presence of LY294002, but not Akt inhibitor XI, suggesting that CGA directly targets Akt to activate its downstream events. These results were supported using shRNA-mediated Akt knockdown cells (Fig. 7*K* and *M*), in which CGA did not induce Nrf2. The knockdown of FOXO3 in cells with the knockdown of Akt diminished the increased expression of *DDB1* (Fig. 7*L* and *N*), supporting Akt acting upstream of FOXO3 to regulate the expression of *DDB1*.

To gain mechanistic insights into the regulation of Nrf2 by CGA, I investigated the direct binding of CGA with Akt, IPO7, or FOXO3 using CGA-conjugated Sepharose. Hep3B cell lysates overexpressing Mock, FLAG-Akt1, or FLAG-FOXO3 were incubated with CGA-Sepharose, and bound proteins were detected by immunoblotting. I detected endogenous IPO7, but not FLAG-Akt1 or FLAG-FOXO3 in the lysates pulled-down with CGA-Sepharose (Fig. 7*O*). These results suggested that the direct binding of CGA to IPO7 prevented the FOXO3-IPO7 interaction and was responsible for the inhibition of FOXO3 nuclear localization.

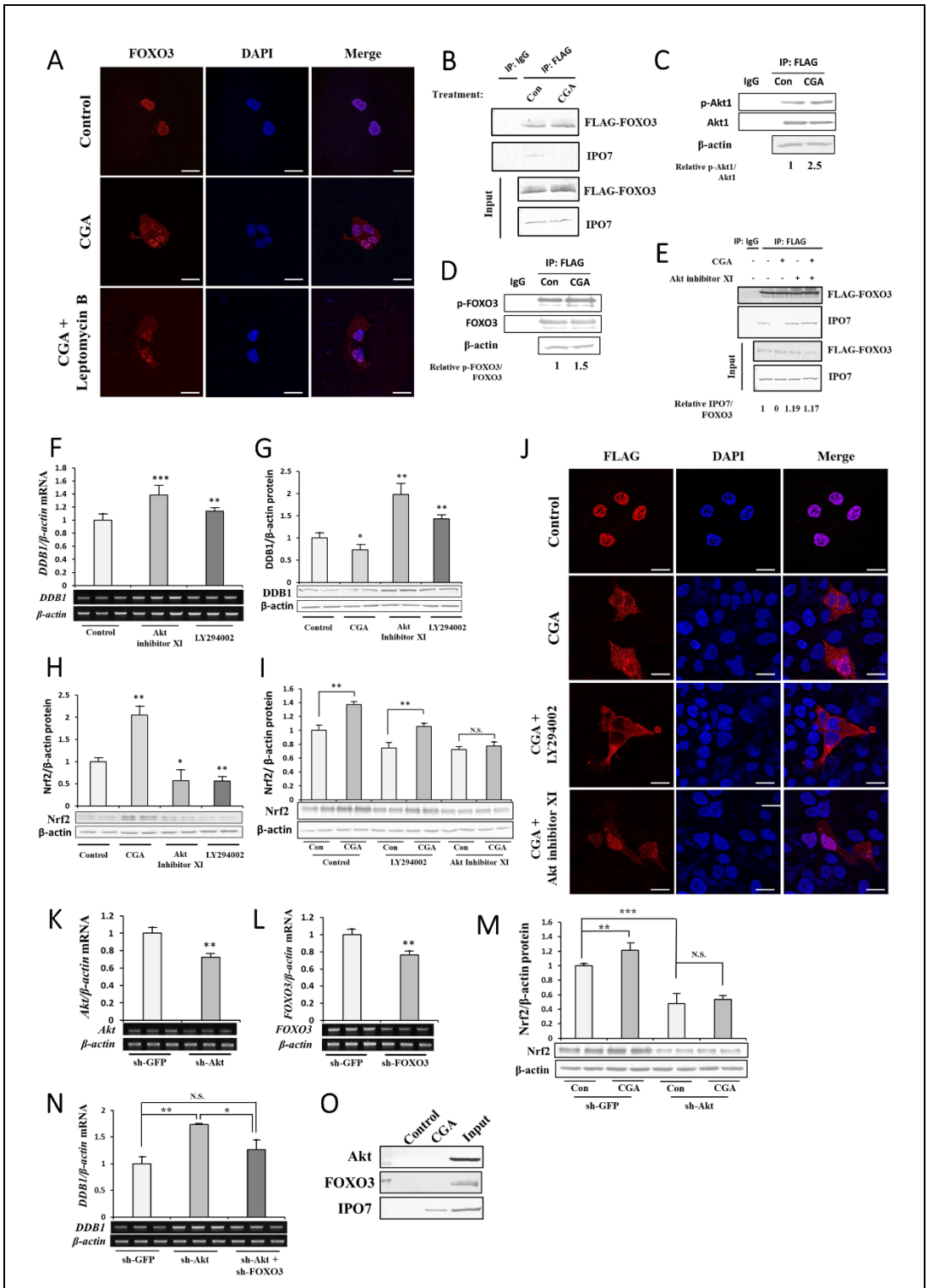

Figure 7. The involvement of Akt and IPO7 in the regulation of FOXO3 activity by CGA. (A) The cellular localization of FOXO3 (red) and DAPI (blue) was examined by immunofluorescence in control and CGA-treated Hep3B cells with or without leptomycin B, scale bar: 20 μm. (B) Hep3B cells were transfected with FLAG-FOXO3, treated with control or CGA (50 μM, 8 h), immunoprecipitated with the anti-FLAG antibody, and bound proteins were detected with immunoblotting against the anti-FLAG and anti-IPO7 antibodies. (C-D) Cells expressing FLAG-

Akt (C) or FLAG-FOXO3 (D) and treated with CGA were immunoprecipitated with the anti-FLAG antibody, and bound proteins were detected with immunoblotting against anti-FLAG and anti-phosphoserine/threonine/tyrosine antibodies. (E) Cells expressing FLAG-FOXO3 and treated with control or CGA (50 μM) with or without Akt inhibitor XI (1 μM) were immunoprecipitated with the anti-FLAG antibody and were then subjected to immunoblotting against the anti-FLAG and anti-IPO7 antibodies. (F-H) The mRNA (F) and protein (G) levels of DDB1 and Nrf2 protein levels (H) were measured with RT-PCR and immunoblotting, respectively, after an 8-h treatment with either Akt inhibitor XI (1 μM) or LY294002 (50 μM). (I) Nrf2 protein levels were assessed after the co-treatment of CGA with either Akt inhibitor XI (1 μM) or LY294002 (50 μM). (J) FLAG-FOXO3-expressing cells were treated with CGA and either LY294002 or Akt inhibitor XI, and the cellular localization of FOXO3 (red) and DAPI (blue) were examined by immunofluorescence, scale bar: 20 μm. (K-L) Hep3B cells were transfected with sh-Akt (K) or sh-FOXO3 (L) and knockdown efficiency was confirmed by RT-PCR. (M) CGA was added to either control or Akt knockdown cells, and Nrf2 protein abundance was measured by immunoblotting. (N) The effects of the single knockdown of Akt or double knockdown of Akt and FOXO3 on the abundance of *DDB1* mRNA were quantified by RT-PCR. (O) Cells were overexpressed with FLAG-Akt, FLAG-FOXO3, or FLAG-Mock and cell lysates were incubated with CGA-bound Sepharose. The proteins that bound to Sepharose were analyzed by immunoblotting with anti-FLAG or anti-IPO7 antibodies. Values are given as means ± S.D. N.S. not significant, *p<0.05, **p<0.01, ***p<0.001 *versus* the indicated group.

Effects of CGA on SKN-1 and the lifespan of *C. elegans*

The cellular responses to oxidative stress orchestrated by both FOXO3 and Nrf2 are highly conserved from humans to worms. The *C. elegans* homologs of FOXO3 and Nrf2 are DAF-16 and SKN-1, respectively, and have been widely reported to protect *C. elegans* from stress and promote longevity (148). Therefore, I investigated whether the observed role of the Akt-FOXO3-DDB1 axis in response to CGA was conserved in *C. elegans*. I initially confirmed whether SKN-1 regulated the lifespan of *C. elegans.* The reduction-of-function allele *skn-1*(*ok2315*) mutant and SKN-1 overexpressing (ldIs7 *skn-1b/c::gfp*) *C. elegans* had shorter and longer lifespans, respectively, than the N2 wild-type worm (Fig. 8*A*). I then found that 20 μM CGA increased SKN-1 protein levels (Fig. 8*B*), but not its mRNA levels (Fig. 8*C*), suggesting that CGA induced SKN-1 protein stability at the post-transcriptional level, similar to human cells. CGA also increased the mRNAs of downstream targets of SKN-1, γ-glutamine cysteine synthetase (*gcs-1*) and glutathione synthetase (*gss-1*) (Fig. 8*D* and *E*). *C. elegans* and other nematodes lack the Keap1 homolog, and WDR-23 is the only identified regulator of SKN-1 stability to date (14).

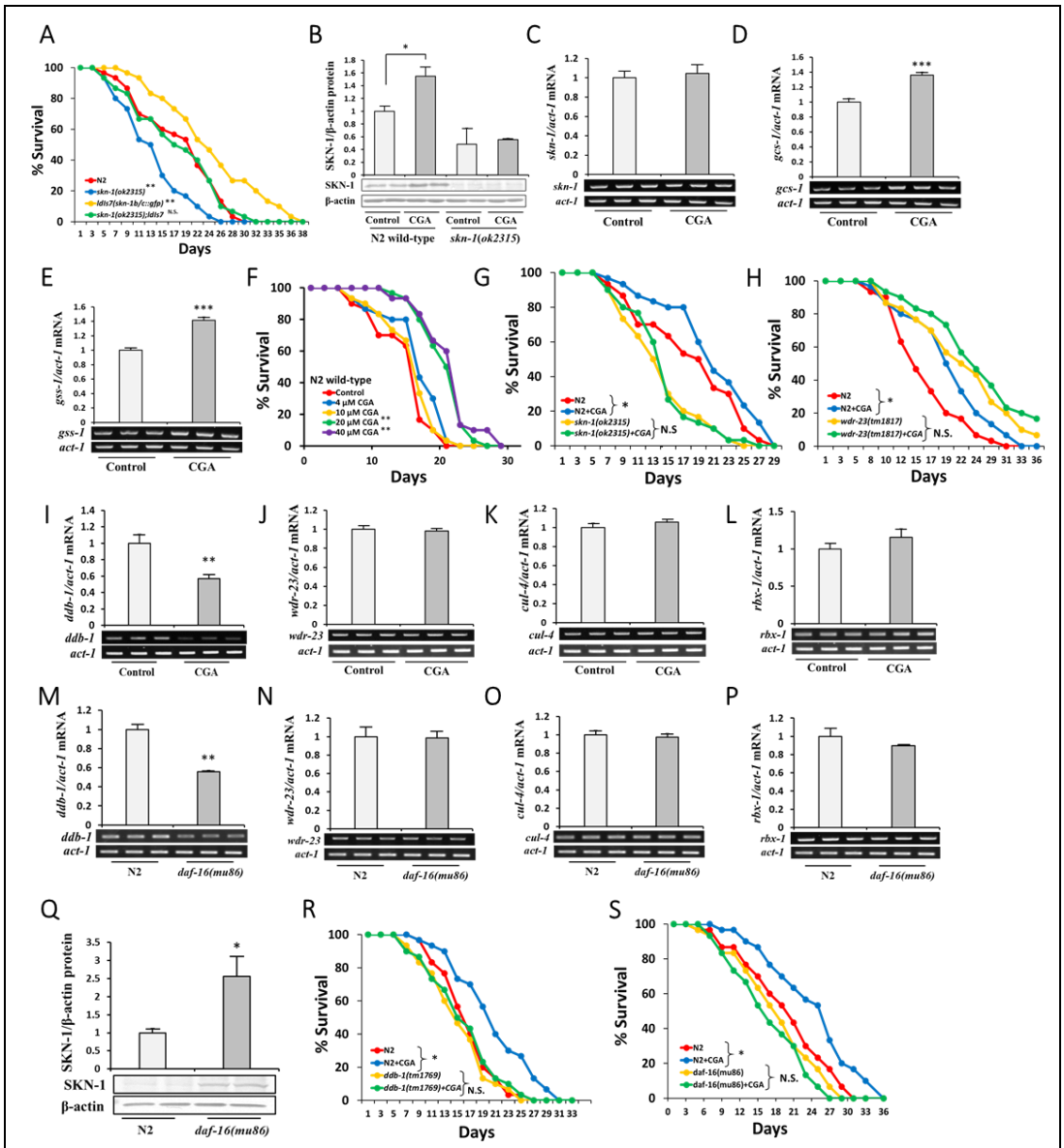

Figure 8. Effects of CGA on SKN-1 and the lifespan of *C. elegans.* (A) Kaplan-Meier survival curves of the *C. elegans* N2 wild-type worm, *skn-1* mutant strain *skn-1*(*ok2315*), *skn-1* overexpressed strain (ldIs7 *skn-1b/c::gfp*), and *skn-1*-rescued strain [*skn-1*(*ok2315*); ldIs7] maintained at 20°C. (B) Immunoblotting was used to analyze the effects of CGA (20 μM; 24 h) on SKN-1 protein levels in both N2 and *skn-1(ok2315)* worms. (C) The mRNA abundance of *skn-1* in N2 wild-type worms was measured after the CGA treatment. (D and E) The effects of CGA on the mRNA expression levels of the SKN-1 target genes, *gsc-1* (D) and *gss-1* (E) were examined by RT-PCR. (F) The effects of CGA at concentrations of 4, 10, 20, and 40 μM on the lifespan of N2 wild-type worms were plotted as Kaplan-Meier survival curves. (G and H) Kaplan-Meier survival curves of *C. elegans* N2 wild-type worms and *skn-1(ok2315)* (G) or *wdr-23(tm1817)* (H) cultured on NGM plates containing 20 μM CGA. (I-L) The effects of CGA (20 μM; 24 h) on the *ddb-1* (I), *wdr-23* (J), *cul-4* (K), and *rbx-1* (L) mRNA levels of N2 wild-type worms were examined by RT-PCR. (M-P) The expression levels of *ddb-1* (M), *wdr-23* (N), *cul-4* (O), and *rbx-1* (P) mRNA were compared between N2 wild-type and *daf-16(mu86)* worms by RT-PCR. (Q) The protein levels of SKN-1 were compared between N2 wild-type and *daf-16(mu86)* worms by immunoblotting. (R and S) The survival curves of *C. elegans* cultured on NGM plates containing 20 μM CGA of the N2 wild-type worm and *ddb-1(tm1769)* (R) or *daf-16(mu86)* (S). *P*-values of survival curves were obtained using by the Log-rank (Mantel-Cox) test. All graphs are the relative mean ± S.D, and significance was calculated by the *t*-test or Tukey's *post-hoc* test. N.S. not significant, *p<0.05, **p<0.01, ***p<0.001.

The induction of SKN-1 by CGA may increase lifespan. Treatment with 20 and 40 μM of CGA significantly increased the lifespan of N2 *C. elegans,* whereas lower doses of 4 and 10 μM did not (Fig. 8*F*). To confirm that these effects require SKN-1, I treated *skn-1*(*ok2315*) and *wdr-23*(*tm1817*) worms with CGA. As expected, the 20 μM CGA treatment increased the lifespan of N2, but not that of the *skn-1*(*ok2315*) or *wdr-23*(*tm1817*) strain (Fig. 8*G* and *H*), suggesting the critical roles of SKN-1 and WDR-23 in *C. elegans* responses to CGA. I then examined whether the molecular mechanisms underlying these effects were similar to those in human cells. The CGA treatment in N2 significantly decreased the mRNA levels of *ddb-1*, but not those of *wdr-23*, *cul-4*, or *rbx-1* (Fig. 8*I-L*). Similarly, the null mutation of *daf-16(mu86)* down-regulated *ddb-1* gene expression, but did not affect *wdr-23*, *cul-4*, or *rbx-1* (Fig. 8*M-P*). Additionally, the SKN-1 protein levels were elevated in *daf-16(mu86)* worms (Fig. 8*Q*). The down-regulated mRNA expression of *ddb-1* and increased protein levels of SKN-1 by both CGA and the mutation in *daf-16* led to a question whether the lifespan-extending effects of CGA also require DAF-16. The results obtained showed that CGA did not extend the lifespan of *ddb-1(tm1769)* or *daf-16(mu86)* worms, suggesting the requirement of DAF-16-regulated *ddb-1* in responses to CGA (Fig. 8*R* and *S*).

The role of distinct isoforms of *daf-16* on the expression of different target genes

Since *sod-3* is a well-known downstream of DAF-16, I measured the expression of *sod-3* as a control of DAF-16 activity. To my surprise, CGA significantly induced the expression of *sod-3,* while *daf-16(mu86)* expressed lower levels of *sod-3* than N2 worms (Fig. 9*A* and *B*). The distinct effects of CGA on *ddb-1* and *sod-3* suggested the more complex regulation of DAF-16 activity by CGA. Human FOXO contains four members encoded by distinctive genes (*FOXO1*, *FOXO3*, *FOXO4*, and *FOXO6*), while *C. elegans* DAF-16 is encoded by a single gene transcribed from three distinctive promoters (*daf-16a*, *daf-16b*, and *daf-16f*). A recent study suggested that the activity of DAF-16 isoforms is selectively regulated by different upstream signals and regulates either specific, overlapping, or cooperative target genes (149).

Since isoform B does not regulate lifespan (149), I examined the effects of DAF-16a and DAF-16f on the expression of *ddb-1.* The overexpression of both *daf-16a* and *daf-16f* in the *daf-16(mgDf50)* mutant background restored the expression of *sod-3* to wild-type levels (Fig. 9*C*), whereas only *daf-16a* overexpression rescued the expression of *ddb-1* (Fig. 9*D*), suggesting that *sod-3* is an overlapping target of both isoforms and *ddb-1* is a specific target of DAF-16a. CGA induced *sod-3* and reduced *ddb-1* expression levels. Therefore, I speculated that CGA distinctively affects the nuclear localization of DAF-16a and DAF-16f. The results obtained showed that CGA decreased nuclear DAF-16a content and induced the nuclear

accumulation of DAF-16f (Fig. 9*E*). To investigate whether CGA requires Akt to regulate the activity of DAF-16 and the expression of *ddb-1,* similar to human cells, I treated N2 with LY294002 or Akt inhibitor XI. The pretreatment with Akt inhibitor XI, but not LY294002, abrogated the effects of CGA on *ddb-1* (Fig. 9*F* and *G*), suggesting the conservation of this pathway. Additionally, I confirmed these results by using *akt-1(mg144),* in which the mutation of AKT-1 diminished the effects of CGA on the expression of *ddb-1* (Fig. 9*H*).

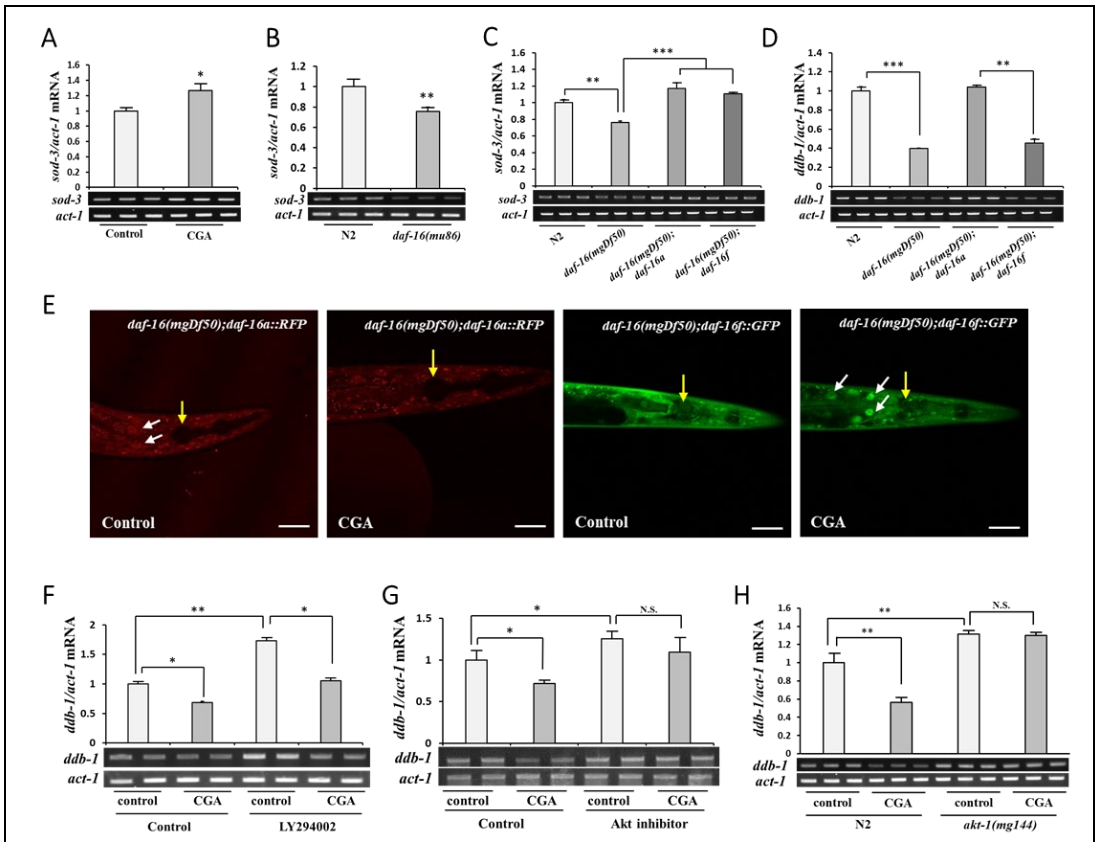

Figure 9. The role of distinct isoforms of *daf-16* on different target gene. (A) The effects of CGA (20 μM; 24 h) on the *sod-3* mRNA levels of N2 wild-type worms were examined by RT-PCR. (B) The expression levels of *sod-3* mRNA were compared between N2 wild-type and *daf-16(mu86)* worms by RT-PCR. (C and D) A comparison of *sod-3* (C) and *ddb-1* (D) mRNA expression in N2, *daf-16(mgDf50)*, *daf-16(mgDf50); daf-16a,* and *daf-16(mgDf50); daf-16f* worms by RT-PCR. (E) The cellular localization of either DAF-16a (*daf-16a::RFP*) or DAF-16f (*daf-16f::GFP*) following the treatment with CGA (20 μM; 24 h), white arrows indicate nuclear DAF-16, yellow arrows indicate lower bulb of pharynx, scale bar: 50 μm. (F) CGA was applied with either vehicle or the PI3K inhibitor (LY294002) for 24 h and the mRNA of *ddb-1* was measured by RT-PCR. (G) CGA was applied with either vehicle or Akt inhibitor XI for 24 h and the mRNA of *ddb-1* was measured by RT-PCR. (H) The effects of CGA on the expression levels of *ddb-1* mRNA were compared between N2 wild-type and *akt-1(mg144)* worms by RT-PCR. Band intensities were quantified using ImageJ and presented as relative values to β-actin. *P*-values of survival curves were obtained using by the Log-rank (Mantel-Cox) test. All graphs are the relative mean ± S.D, and significance was calculated by the *t*-test or Tukey's *post-hoc* test. *p<0.05, **p<0.01, ***p<0.001.

III.4. Discussion

Oxidative stress is the leading cause of many pathological conditions and aging. The recent use of naturally occurring compounds with antioxidant activities is becoming a global trend. The present and previous studies demonstrated that the antioxidant activity of CGA involved the activation of Nrf2. However, the underlying mechanisms have not yet been elucidated in detail. I herein clarified the mechanism underlying Nrf2 activation by the CGA treatment. Instead of relying on a canonical Keap1-dependent pathway, CGA activated Nrf2 and its downstream gene via a WDR23 pathway. Previous studies employed a computational analysis in which CGA interacts with Keap1 and, thus, stabilizes Nrf2 (19, 20). However, the present results suggested that CGA functions independently of Keap1. I revealed that CGA relied on the inhibition of $CRL4^{WDR23}$ activity by decreasing the expression and protein levels of DDB1, which were regulated by FOXO3. CGA apparently activates Akt and also directly binds to IPO7 in order to inhibit the nuclear transport and transcriptional activity of FOXO3 (Fig. 10). To the best of my knowledge, this is the first study to demonstrate that CGA activates Nrf2 through a pathway involving WDR23 and its regulation by the Akt-FOXO3-DDB1 axis.

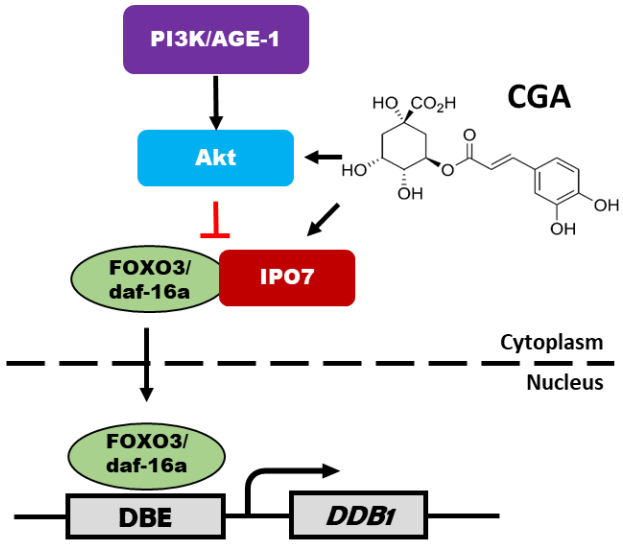

Figure 10. A working model describing the mechanism of action by which CGA activates Nrf2/SKN-1 via the modulation of the Akt-FOXO3/DAF16-DDB1 axis. CGA activates Akt independent of PI3K, as well as interacts with IPO7, which will lead to the cytosolic sequestration and inactivation of FOXO3. Since FOXO3 is a transcriptional regulator of *DDB1*, CGA decreases DDB1 and eventually leads to the inhibition of $CRL4^{WDR23}$ activity and causes stabilization of Nrf2. This mechanism of action seems to be conserved from human to nematode *C. elegans* and responsible for the lifespan extending effects of CGA.

WDR23, an E3 ligase substrate adaptor, has not yet been examined in detail. This study and others recently established a role for WDR23 in the regulation of Nrf2 stability (42, 43). However, the molecular mechanisms regulating the WDR23-Nrf2 pathway remain unclear. In the present study, the CGA treatment activated Nrf2 by inhibiting the activity of $CRL4A^{WDR23}$. The abundance and activities of E3 ligases are spatiotemporally controlled by various mechanisms, including tissue-specific expression, the cellular microenvironment, substrate protein levels, post-translational modifications, and the binding of adaptor molecules (150). In CHAPTER II, the expression of one component of $CRL4A^{WDR23}$, *CUL4A*, was induced by Sp1 in response to the knockdown of Keap1 and enhanced $CRL4A^{WDR23}$ E3 ligase activity towards Nrf2 (127). The CGA treatment in the present study appeared to regulate $CRL4A^{WDR23}$ activity via a similar mechanism, namely, by inhibiting the expression of another component of $CRL4A^{WDR23}$ called *DDB1*. The regulation of E3 ligase expression by small compounds has been reported. The green tea polyphenol (−)-epigallocatechin-3-gallate reduced the expression of E3 ligase *CUL5* (151). CGA was more recently shown to induce the expression of ring finger protein 146 (RNF146), which is involved in neuroprotection (152). I herein established the mechanistic regulation of $CRL4A^{WDR23}$ E3 ligase activity and are the first to demonstrate that CGA relies on this mechanism to induce Nrf2.

To elucidate the mechanisms by which CGA inhibits the expression of *DDB1*, I identified the transcription factor responsible for the regulation of *DDB1* gene. I demonstrated that FOXO3 regulated the basal and inducible expression of *DDB1*, thereby controlling the abundance and activity of Nrf2. A previous study reported that specificity protein 1 (Sp1) regulated the basal expression of both *DDB1* and *DDB2* (153). However, previous findings in CHAPTER II suggested that elevations in Sp1 levels did not up-regulate the expression of *DDB1* (127), indicating that Sp1 and FOXO3 co-function as regulators of the basal and inducible expression of *DDB1,* respectively. Although FOXO3 has been proposed as a major player in the oxidative stress response (141, 142), its interaction with the Nrf2 pathway was largely unknown. Guan *et al*. (154) found that FOXO3 deficiency down-regulated Keap1 and hyperactivated Nrf2 in cholangiocarcinoma. Collectively, these findings indicate that FOXO3 functions through Keap1 or WDR23 depending on the context and cell type. Of note, FOXO family proteins direct the transcription of genes in a highly cell type-specific manner (155). Previous studies demonstrated the double-edged effects of FOXO3 in the oxidative stress response in a highly context-dependent manner (156), and by acting as a suppressor of Nrf2, FOXO3 in this study functioned as a positive regulator of ROS. In addition to its role as an adaptor protein for CRL4, DDB1 is known for its involvement in the DNA damage response. A previous study suggested that FOXO3 induced the expression of genes involved in the DNA damage response, including *BTG1*, *GADD45*, and Cyclin G2

(157). Collectively, the present results and previous findings provide additional insights into the role of FOXO3 in a cellular context as well as the signaling pathways affected.

FOXO3 transcriptional activity is regulated by post-translational modifications, which affect interactions with other proteins and nucleocytoplasmic shuttling. A well-established mechanism is the phosphorylation of FOXO3 at T32 and S253 by Akt, which promotes the FOXO3 interaction with the 14-3-3 protein, resulting in the nuclear exclusion of FOXO3 and inhibition of its transcriptional activity (144). However, this study found that CGA treatment induced the cytoplasmic accumulation of FOXO3 possibly by inhibiting its nuclear localization instead of triggering its nuclear exclusion. The present results showed that this effect required Akt, suggesting a role for Akt in the regulation of the nuclear import of FOXO3, particularly during the induction by CGA. To date, the mechanisms underlying the nuclear relocation of FOXO3 and the karyopherin(s) responsible have not yet been examined in detail. A member of β-karyopherin family, IPO7, was recently found to bind and transport FOXO3 to the nucleus (145), and I herein demonstrated that CGA released this interaction. However, the underlying mechanisms remain unclear. The present results indicated that CGA directly binds to IPO7, which may contribute to the dissociation of FOXO3-IPO7. A previous study reported that CGA bound to the pleckstrin homology (PH) domain and directly phosphorylated Akt (158). However, I did not detect this interaction. Nevertheless, I observed that CGA induced the phosphorylation of Akt, but did not affect the FOXO3-IPO7 interaction under Akt inhibition, indicating the involvement, at least in part, of Akt in this context. FOXO3 phosphorylation by Akt occurs at Ser253 within the NLS and may disrupt NLS activity by introducing a negative charge to this basic NLS region (147). Further studies are needed to elucidate the exact mechanism of FOXO3 cytoplasmic retention by CGA, and the involvement of both Akt and IPO7.

FOXO3/DAF-16 is the key regulator of organismal lifespan due to its critical role in survival pathways, including oxidative stress, DNA repair, and stem cell maintenance (159). *FOXO3* is also one of only two genes with consistent associations with human longevity, with independent replication across all major ethnic groups (160), second only to *APOE* as a leading longevity-associated gene in humans (161). In the present study, I confirmed that SKN-1, the homolog of mammalian Nrf2, also played an important role in the lifespan determination. CGA treatment extended the lifespan of *C. elegans* by activating SKN-1, and these effects were achieved through the modulation of DAF-16. The present results are consistent with previous findings by Zheng and colleagues showing that CGA extended the lifespan of *C. elegans* in a manner that was dependent on DAF-16 (162). However, which isoform of DAF-16 is critical for these effects and their

biological role was not clear. In the present study, I added the necessity of SKN-1 activation by the inhibition of DAF-16a for CGA to achieve its beneficial effects on lifespan. A previous study on *C. elegans* found that insulin/IGF-1-like signaling (IIS) not only opposed DAF-16, it also directly inhibited SKN-1 by phosphorylating and preventing the nuclear accumulation of SKN-1 (148). The regulation of SKN-1 by DAF-16-activated *ddb-1*, as specifically demonstrated herein for the DAF-16a isoform, suggesting that IIS also functions as a positive regulator of SKN-1 and, thus, is involved in the oxidative stress response. The present results support the role of IIS as a regulator of the SKN-1 pathway.

The findings in both human cells and *C. elegans* in the present study support that CGA requires the inhibition of FOXO3/DAF-16a to activate Nrf2/SKN-1 and extend the lifespan. Indeed, the *in vitro* experiment using human cells unequivocally showed that CGA affects Nrf2 via inhibition of FOXO3. The inhibition of FOXO3 activity by CGA was essential as demonstrated by the results showing that genetic knockdown of FOXO3 diminished the effects of CGA on *DDB1* expression and Nrf2 protein levels. Similarly, in *C. elegans*, I showed that the genetic knockout of *daf-16* attenuated the lifespan-extending effect of CGA. Since CGA requires the inhibition of DAF-16, the complete absence of DAF-16 in *daf-16(mu86)* worms attenuated the effects of CGA, similar to the phenomena observed *in vitro*. I showed that the DAF-16a isoform was not accumulated in the nucleus following CGA treatment, similar to the *in vitro* findings using human cell lines, suggesting the possibility that DAF-16a activity was inhibited by CGA. Additionally, *in vitro* and *in vivo* studies suggested that FOXO3 and DAF-16a regulate the *DDB1* expression. To this end, I postulated that in regard to cellular response to CGA and Nrf2 regulation, DAF-16a is the functional homolog of FOXO3. There is plenty of evidence on the role of DAF-16 activation and lifespan elongation, however, little is known about the isoform(s) involved. In the present study, I demonstrated a distinct effect of CGA on DAF-16a and DAF-16f. CGA inhibited and activated DAF-16a and DAF-16f, respectively, and the inhibition of DAF-16a is critical to inhibit *ddb-1* expression, activate SKN-1, and extend lifespan of *C. elegans*.

Taken together, the present study has established a novel Akt-FOXO3/DAF16a-DDB1 pathway that links nutrient sensing and oxidative stress responses, and that this axis is conserved across species from *C. elegans* to humans. The present results provide insights into the molecular mechanisms underlying Nrf2/SKN-1 activation by CGA and the increase in *C. elegans* lifespan by CGA via this pathway.

CHAPTER IV

β-Glucan Reduces Nrf2 via WDR23 Pathway

[*] This chapter was adapted from the *Molecular Pharmacology*, in press, (2022), Ferbian Milas Siswanto, Akiyoshi Tamura, Rika Sakuma & Susumu Imaoka, Yeast β-glucan increases etoposide sensitivity in lung cancer cell line A549 by suppressing Nrf2 via the non-canonical NF-κB pathway.

IV.1. Introduction

Lung cancer is the second most common cancer, has the highest morbidity worldwide, and accounts for 25% of all cancer deaths (163). Since the majority of lung cancer patients are diagnosed at an advanced stage, chemotherapy is the primary treatment strategy. Etoposide is a commonly used chemotherapy agent for lung cancer that inhibits topoisomerase II, which induces double-stranded DNA breaks that are followed by antitumor effects (164). However, resistance to chemotherapeutic agents, including etoposide, frequently occurs in patients, which has a negative impact on clinical outcomes and contributes to a poor prognosis (165, 166). Therefore, the mechanisms underlying etoposide resistance in lung cancer need to be elucidated in more detail, and the discovery and development of novel strategies to overcome this resistance are urgently needed.

The mechanisms responsible for resistance to chemotherapeutics in lung cancer remain unclear. Previous studies indicated that a hypoxic tumor microenvironment (TME) contributed to drug resistance in non-small-cell lung carcinoma (NSCLC) in HIF1α- and HIF2α-dependent manners (167–169). The activation of the collagen receptor integrin α11β1 in NSCLC resulted in resistance to epidermal growth factor receptor tyrosine kinase inhibitors (EGFR-TKIs) (170). Furthermore, nuclear factor erythroid 2-related factor 2 (Nrf2) was shown to induce EGFR-TKI resistance in the lung adenocarcinoma cell line HCC827 by up-regulating GPX4 and SOD2 (171).

Nrf2 is a key factor in cellular redox homeostasis and defenses against potentially harmful insults, such as xenobiotics. It regulates cytoprotective responses against xenobiotic toxicity by orchestrating the expression of drug-metabolizing enzymes (DMEs) (43), including phase I and II DMEs, such as cytochromes P450 (CYPs) and UDP glucuronosyltransferases (UGTs) (29, 30), as well as phase III drug transporters, including multidrug resistance protein 1 (MDR1) (28, 31). The multidrug resistance phenotype in cancers is generally a result of cellular adaptation to chemotherapeutic agents, which include reduced drug uptake, enhanced intracellular drug metabolism, impairments in the apoptosis machinery, or increased drug efflux (172). Since Nrf2 regulates the expression of DMEs and the aberrant activation of Nrf2 is often observed in lung cancer (173), interventions that target the Nrf2 pathway may be useful for overcoming the drug resistance (109, 174).

Combinations of chemotherapeutic drugs for various cancer types are attracting increasing attention. The use of dietary supplements and natural products in combination with conventional chemotherapeutic drugs is considered to increase the efficacy of conventional chemotherapeutic drugs, and is associated with less harmful side effects and adverse reactions (175, 176). Furthermore, the use of

natural compounds, such as curcumin (177), sulforaphane (178), and epigallocatechin gallate (179), was shown to sensitize several types of cancer cells to drugs by regulating a number of resistance pathways (180). A major component of the fungal cell wall, called β-glucan, has been the focus of recent research due to its potential as a chemotherapeutic adjuvant. Sixteen clinical trials involving 1650 patients with a wide range of cancer types were conducted between 1992 and 2018 (181). β-glucan is mainly used as an adjuvant of conventional chemotherapy because it promotes the immune system (182, 183). The binding of β-glucan to its receptor was shown to induce the downstream innate immune system pathways and participate in orchestrating adaptive immune responses towards cancer cells (23, 24). However, it currently remains unclear whether β-glucan increases drug sensitivity.

In the present study, we examined the effects of β-glucan on etoposide sensitivity in the human NSCLC cell lines A549 and VMRC-LCD. We herein found that A549 cells were more resistant to etoposide than that of VMRC-LCD cells, due to the hyperactivation of Nrf2 in A549 cells. β-glucan improved etoposide sensitivity in A549 cells only. We then demonstrated that β-glucan sensitized A549 cells to etoposide by inhibiting the Nrf2 pathway and suppressing the expression of DMEs involved in the metabolism of etoposide. We found that the activation of the non-canonical nuclear factor kappa B (NF-κB) pathway was essential for the β-glucan-induced suppression of Nrf2. The present results revealed an advantageous property of β-glucan as a resistance-modifying agent in addition to its widely reported immunomodulatory effects for lung cancer therapy.

IV.2. Materials and methods

Chemicals

Yeast β-glucan, etoposide, and crystal violet were obtained from Tokyo Chemical Industry Co., Ltd. (Tokyo, Japan). Stattic was from Cayman Chemicals (Ann Arbor, MI, USA). SB203580 was purchased from Adipogen (San Diego, CA, USA). MG132 (Z-Leu-Leu-Leu-H) was purchased from the Peptide Institute (Osaka, Japan). Dulbecco's modified Eagle's medium (DMEM) low glucose, ScreenFect™ A, an anti-DYKDDDDK (FLAG) antibody, and anti-Myc tag monoclonal antibody were obtained from Wako Pure Chemical Industries, Ltd. (Osaka, Japan). Penicillin-streptomycin solution, fetal bovine serum (FBS), geneticin (G418), and 3-(4,5-dimethyl-2-thiazolyl)-2,5-diphenyl-2H-tetrazolium bromide (MTT) were purchased from Sigma Chemical Co. (St. Louis, MO, USA). Isogen was from Nippon Gene (Toyama, Japan), Revert Aid™ M-MuLV Reverse Transcriptase was from MBI Fermentas (Vilnius, Lithuania), and Go Taq polymerase was from Promega (Madison, WI). KOD Fx Neo was purchased from

Toyobo (Tokyo, Japan). The DNA Ligation Kit was from Takara Bio Inc. (Shiga, Japan). DAPI (4′,6-diamidino-2-phenylindole) was from Dojindo (Kumamoto, Japan). Anti-IKKalpha/beta antibody, Alexa Fluor® 488-conjugated goat anti-rabbit IgG, Alexa Fluor® 594-conjugated goat anti-mouse IgG were obtained from Abcam (Carlsbad, CA, USA). Anti-p65, anti-p-p65 (Ser536), anti-ephrin type-A receptor 2 (EphA2), anti-Cullin-4A (CUL4), and anti-DNA damage-binding protein 1 (DDB1) antibodies were from Santa Cruz Biotechnology, Inc. (Santa Cruz, CA); an anti-phosphoserine/threonine/tyrosine antibody was from GeneTex (Irvine, CA, USA); anti-RelB antibody was from Proteintech (Rosemont, IL, USA); and an anti-WD40 Repeat protein 23 (WDR23) antibody was obtained from Invitrogen (Carlsbad, CA, USA). Antibodies against Nrf2 and β-actin (5), HSP90α (184), and histone H3 (102) were prepared as previously described.

Cell culture, transfection, and treatment

The human non-small cell lung adenocarcinoma A549 and VMRC-LCD cell lines were obtained from the RIKEN BRC Cell Bank (Tsukuba, Japan) and the Japanese Collection of Research Bioresources Cell Bank (Tokyo, Japan), respectively. Cells were cultured in DMEM low glucose containing 10% FBS, penicillin (100 units/mL), and streptomycin (100 μg/mL) at 37°C in 5% CO_2. The transfection of the indicated constructs was performed using the calcium phosphate method. Cells were cultured in the presence or absence of β-glucan (2.5 μg/ml, 24 h unless otherwise indicated), SB203580 (10 μM, 24 h), stattic (5 μM; 24 h), etoposide (various concentrations, 72 h unless otherwise indicated), or MG132 (5 μM, 8 h).

Plasmid constructs

Human Keap1 (GenBank™ accession number NM_203500.2), WDR23 (NM_025230.4), and DDB1 (NM_001923.5) were amplified by PCR with primer sets 1 and 2, 3 and 4, and 5 and 6, respectively (Table 1). Amplified Keap1, WDR23, and DDB1 were then digested with *BamH*I and *Xho*I, *Not*I and *Xba*I, and *Not*I and *Xba*I, respectively, and inserted into the 3×FLAG-pcDNA4 vector (Invitrogen). The cDNA of human p65 (NM_021975.4) was isolated with primers 7 and 8, digested by *Xho*I and *Not*I, and then inserted into the pcDNA3.1(-) vector (Invitrogen). Human RelB cDNA (NM_006509.4) and CUL4A (NM_001008895.4) were amplified with primers 9 and 10, and 11 and 12, respectively, digested with *EcoR*I and *Bgl*II, and *Sal*I and *Not*I, respectively, and then ligated into the pCMV-Myc vector (Clontech Laboratories, Inc., CA, USA). The cDNA of human Nrf2 (NM_006164.5) was isolated with primers 13 and 14, digested by *BamH*I and *Xba*I, and then inserted into the pcDNA3.1(+) vector (Invitrogen).

Table 1. Primers used for plasmid constructs

No.	Sequences	Descriptions
1	5'- AATGGATCCATGCAGCCAGATCCCAGGCC -3'	Fw; 1–20 of human *Keap1* cDNA; underlined, *BamH*I site; double underlined, start codon
2	5'- CCGCTCGAGTCAACAGGTACAGTTCTGCT -3'	Rv; 1856–1875 of human *Keap1* cDNA; underlined, *Xho*I site; double underlined, stop codon
3	5'- ATAAGAATGCGGCCGCATGGGATCGCGGAACAGCAG -3'	Fw; 1–20 of human *WDR23* cDNA; underlined, *Not*I site; double underlined, start codon
4	5'- TATCTAGACTACTGGGGTGAGGAAAAGG -3'	Rv; 1621–1641 of human *WDR23* cDNA; underlined, *Xba*I site; double underlined, stop codon
5	5'- ATAAGAATGCGGCCGCTCGTACAACTACGTGGTAAC -3'	Fw; 4–23 of human *DDB1* cDNA; underlined, *Not*I site
6	5'- GCTCTAGACTAATGGATCCGAGTTAGCT -3'	Rv; 3404–3423 of human *DDB1* cDNA; underlined, *Xba*I site; double underlined, stop codon
7	5'- AAACTCGAGCCATGGACGAACTGTTCCCCCTCATCT -3'	Fw; 1–25 of human *p65* cDNA; underlined, *Xho*I site; double underlined, start codon
8	5'- ATTATATTGCGGCCGCTTAGGAGCTGATCTGACTCAGCAGG -3'	Rv; 1631–1656 of human *p65* cDNA; underlined, *Not*I site; double underlined, stop codon
9	5'- ATGAATTCATATGCTTCGGTCTGGGCCAGC -3'	Fw; 1–20 of human *RelB* cDNA; underlined, *EcoR*I site; double underlined, start codon
10	5'- ATAGATCTCTACGTGGCTTCAGGCCCCG -3'	Rv; 1721–1740 of human *RelB* cDNA; underlined, *Bgl*II site; double underlined, stop codon
11	5'- ATAAGTCGACCGCGGACGAGGCCCCGCGGAA -3'	Fw; 3–23 of human *CUL4A* cDNA; underlined, *Sal*I site
12	5'- TAGCATTTATGCGGCCGCTCAGGCCACGTAGTGGTACT -3'	Rv; 2261–2280 of human *CUL4A* cDNA; underlined, *Not*I site; double underlined, stop codon
13	5'- AAGGATCCATCATGATGGACTTGGAGCT -3'	Fw; 1–17 of human *Nrf2* cDNA; underlined, *BamH*I site; double underline, start codon
14	5'- TTTCTAGACTAGTTTTTCTTAACATC -3'	Rv; 1801–1818 of human *Nrf2* cDNA; underlined, *Xba*I site; double underlined, stop codon

Knockdown experiment

Regarding the knockdown of Nrf2 and WDR23, si-Nrf2 (Cat. No. SI03246950) and si-WDR23 (Cat. No. SI05029899) with the target sequences of 5'- CCCAUUGAUGUUUCUGAUCUA -3' and 5'- CUGGGUCUUUAGGGUAGGACA -3', respectively, and AllStars Negative Control (SI03650318) were purchased from Qiagen (Hilden, Germany). si-p65 (Cat. No. s11916) with the target sequence of 5'- GCCCUAUCCCUUUACGUC -3' was purchased from Thermo Fisher Scientific (Waltham, MA). Regarding the knockdown of CD11b, EphA2, and RelB using shRNA, the target sequences of 5'-AACCAGCTTCGGGAGAAGATC-3' (for CD11b), 5'-AAGCGCCTGTTCACCAAGATT-3' (for EphA2), and 5'-AAGGTGCAGAAAGAGGACATA-3' (for RelB) were inserted into the pBAsi-hU6 Neo Vector (Takara Bio Inc., Shiga, Japan) according to a previously described procedure (5, 97). The control for the shRNA experiment was the sequence of 5'-CTCGAGTACAACTATAACTCA-3' against GFP. siRNA was transfected into cells using ScreenFect™ A (Wako, Osaka, Japan) according to the manufacturer's

instructions, while shRNA was transfected with the calcium phosphate method. Transfectants of shRNA were selected using G418.

Immunocytochemistry and immunoblotting

A549 cells were grown on 3.5-cm glass-bottomed dishes and treated with β-glucan, fixed with 4% paraformaldehyde (Wako), blocked in 0.1% bovine serum albumin (BSA) in TPBS at 4°C for 1 h, incubated with the anti-EphA2, anti-p65 or anti-Myc antibody (1:1000 dilution in TPBS) at 4°C overnight, and then washed with TPBS. Cells were incubated with Alexa Fluor® 488-conjugated goat anti-rabbit IgG or Alexa Fluor® 594-conjugated goat anti-mouse IgG and counterstained with DAPI at 4°C for 1 h. Images were obtained by confocal microscopy (TCS SP8, Leica Microsystem, Wetzlar, Germany). Anti-Nrf2, anti-WDR23, anti-p65, anti-p-p65, anti-CUL4, anti-DDB1, anti-Myc, anti-FLAG, anti-HSP90α, anti-histone, and anti-β-actin antibodies were used for immunoblotting. Band intensities were quantified using the NIH Image software ImageJ.

Semi-quantitative reverse transcription PCR (RT-PCR)

cDNA was synthesized by reverse transcription using Revert Aid^{TM} M-MuLV Reverse Transcriptase from total RNA and extracted from A549 cells by Isogen according to the manufacturer's instructions. cDNA (100 ng) was then amplified with Go Taq polymerase and 10 pmol of each primer set (Table 2). PCR products were analyzed using 1% agarose gel electrophoresis, visualized with ethidium bromide staining, and quantified using the NIH Image software ImageJ.

Table 2. Primers used for gene expression assessments

Primers	GenBank Accession No.		Sequences
HO-1	NM_002133	Forward	5'- CCAGCCATGCAGCACTATGT -3'
		Reverse	5'- AGCCCTACAGCAACTGTCGC -3'
NQO1	NM_000903	Forward	5'- TGATCGTACTGGCTCACTCA -3'
		Reverse	5'- GTCAGTTGAGGTTCTAAGAC -3'
CYP3A5	NM_000777.5	Forward	5'- GCTCCTCTATCTATATGGGA -3'
		Reverse	5'- CTGCTTCCCGCCTCAAGTTT -3'
UGT1A1	NM_000463.2	Forward	5'- CTCATTCAGATCACATGACC -3'
		Reverse	5'- AGCATCAGCAATTGCCATAG -3'
MDR1	NM_000927	Forward	5'- GGAGGATTATGAAGCTAAAT -3'
		Reverse	5'- GTAATTACAGCAAGCCTGGA -3'
Dectin-1	NM_197947.3	Forward	5'- AAATAAAGAGAACCACAGTC -3'
		Reverse	5'- TACACAGTTGGTCATAAATG -3'
CD11b	NM_001145808.2	Forward	5'- GCTCGGTGGCAGTGTGATGC -3'
		Reverse	5'- CCGTGTGCTCTTCTGGACAT -3'
CD18	NM_000211.5	Forward	5'- CTCGGGTGCGTCCTCTCTCA -3'
		Reverse	5'- CGCCACCTAGCTTCTTGACA -3'
EphA2	NM_004431.5	Forward	5'- TCACACACCCGTATGGCAAA -3'
		Reverse	5'- CTGACGGTGATCTCATCGGG -3'

IL-1β	NM_000576.3	Forward	5’- AAGTGTCTGAAGCAGCCATG -3’
		Reverse	5’- GGCAGACTCAAATTCCAGCT -3’
iNOS	NM_000625.4	Forward	5’- TGAGCTTCTACCTCAAGCTATC -3’
		Reverse	5’- ACGTGTCTGCAGATGTGTTCAA -3’
COX-2	NM_000963.4	Forward	5’- TTCACGCATCAGTTTTTCAA -3’
		Reverse	5’- ATAGTCTCTCCTATCAGTAT -3’
IL-6	NM_000600.5	Forward	5’- CCCCTGACCCAACCACAAAT -3’
		Reverse	5’- AACTGCATAGCCACTTTCCA -3’
RelB	NM_006509.4	Forward	5’- AGTTTTAACAACCTGGGCAT -3’
		Reverse	5’- GCCCGCTTTCCTTGTTAATT -3’
WDR23	NM_181357.2	Forward	5'- CACAGGATTGGAGAAGGAGG -3'
		Reverse	5'- TCGGCAGTCATAGAGTCGGA -3'
CUL4A	NM_001008895.4	Forward	5'- CAGGCACAGATCCTTCCGTT -3'
		Reverse	5'- TGGTTTCTGTGTGCTGTGGT -3'
CUL4B	NM_003588.4	Forward	5'- CGGGTGTTTCTGTGCAGTAT -3'
		Reverse	5'- TGTCCCAAATGGAGGGTAGC -3'
DDB1	NM_001923.5	Forward	5'- CAGTGTTTCGGGGTCCTCTC -3'
		Reverse	5'- AAGTCGCCCTTGGTCTTCAG -3'
RBX1	NM_014248.4	Forward	5'- ACTTCCACTGCATCTCTCGC -3'
		Reverse	5'- AAGTGATGCGCTCAGAGGAC -3'
β-actin	NM_001101	Forward	5′- CAAGAGATGGCCACGGCTGCT -3′
		Reverse	5′- TCCTTCTGCATCCTGTCGGCA -3′

Cytotoxicity assay

A549 cells (5×10^4 cells/well) were cultured in 24-well plates, and after 24 h of growth, cells were treated with different concentrations of etoposide with or without β-glucan for 72 h. Exposed cells were then treated with 100 µl of MTT solution (5 mg/ml in PBS) for 2 h. The culture medium was removed, and the resulting purple formazan was dissolved with 500 µl of isopropanol containing 0.04 N HCl and 0.1% NP40. Absorbance was measured at 590 nm using a microplate reader (PerkinElmer, Waltham, MA). Cell viability was calculated as a relative percentage to the control. The concentration required to inhibit cell growth by 50% (IC50) was calculated using IBM SPSS Statistics for Windows, version 23.0 (IBM Corp., Armonk, NY, USA). The reversal efficacy of etoposide was calculated as the ratio of the IC50 of treated cells to that of control cells.

Colony formation assay

A549 cells (8×10^3 cells/well) were cultured in 24-well plates and allowed to attach (approximately 2 h). Cells were then exposed to various concentrations of etoposide with or without β-glucan for 48 h, washed with PBS, and cultured in a fresh medium at 37°C for another 7 days. Cells were then fixed with methanol for 30 min and stained with 0.5% (w/v) crystal violet for 30 min. After rinsing with distilled water, the colonies that had formed in each well were counted using ImageJ software according to a previously reported method (185). Each experiment was

performed in triplicate, and the number of colonies was shown as a percentage to that of control cells without etoposide.

Wound healing assay

A wound healing assay was used to assess the effects of β-glucan on the migration of etoposide-induced A549 cells. Cells were seeded on 24-well plates, and at approximately 80% confluency, an artificial wound/scratch was made across the well with a sterile 1-ml pipette tip, followed by washing with PBS to eliminate cell debris. A549 cells were exposed to various concentrations of etoposide with or without β-glucan for 48 h. Wound healing was examined and photographed with a digital camera (Moticam 2000, Shimadzu Rika Kikai, Tokyo, Japan) coupled to an inverted microscope (CK30-SLP; Olympus, Tokyo, Japan) under ×40 magnification 0, 8, 16, 24, 32, 36, and 48 h after scratching. The wound area was quantified in three random fields using ImageJ software. All experiments were performed in triplicate.

Luciferase assay

A549 cells were seeded on 24-well plates and co-transfected with 0.25 μg of the luciferase reporter gene of interest (pGL3-containing *CUL4A* promoter or 3×NQO1-ARE), 12.5 ng of pRL-null, and 0.25 μg of pCMV-Mock or pCMV-RelB with the GenePORTER TM2 transfection reagent (Gene Therapy Systems). Two days after transfection, cells were lysed in 65.2 μl of lysis buffer (Promega) and luciferase activity was assayed with a luminometer (Lumat LB9507; Berthold) using the Dual-Luciferase Reporter Assay System (Promega) according to the manufacturer's protocol. Firefly luciferase activity was normalized to Renilla luciferase activity.

Chromatin Immunoprecipitation (ChIP) assay

The ChIP assay was performed as previously described (127). The *CUL4A* promoter fragments were detected with the following primers: 5′-CAAGTACGTATCTTTACCCA-3′ (forward) and 5′-TGTGGTAACAGGGATAGGAA-3′ (reverse) to amplify the -1917/-1683 fragment, 5′-TGAGGGGGCCCGGGGTCTTT-3′ (forward) and 5′-GCGCGGAGGGTCCTCCGCGG-3′ (reverse) to amplify the -810/-610 fragment, and 5′-CGGGAGTCCCGGCGCGCGCC-3′ (forward) and 5′-CTCCGCCCGCCCCGGTCCGC-3′ (reverse) to amplify the -245/-42 fragment of the *CUL4A* promoter. For the amplification of The *NQO1* promoter fragments, the following primers were used: 5′-ATCACCTGAGGTCAGGAGTT-3′ (forward) and 5′-ACTGTGTCGCCCAGGCTGGA-3′ (reverse) to amplify the -1979/-1771 fragment, and 5′-CATTACCTGCCTTGAGGAGC-3′ (forward) and 5′-GAAGTCGTCCCAAGAGAGTC-3′ (reverse) to amplify the -621/-331 fragment of the *NQO1* promoter.

Statistical analysis

All data are shown as the mean ± standard deviation (SD) from three experimental replicates, each performed with at least three technical replicates, and analyzed with IBM SPSS Statistics for Windows, version 23.0. Statistical comparisons were performed with Student's *t*-test, one-way repeated measures analysis of variance (ANOVA), two-way repeated measures ANOVA, one-way repeated measures multivariate ANOVA, and respective post-hoc tests for multiple comparisons against specified groups as described in the figure legends. The family-wise error rate was controlled with Bonferroni correction. Differences were considered to be significant when $p < 0.05$ (*), < 0.01 (**), or < 0.001 (***).

IV.3. Results

Effects of β-glucan on the sensitivity of NSCLC to etoposide

The administration of β-glucan in combination with various chemotherapeutic drugs is attracting increasing attention. Since β-glucan is the most abundant component of the pathogenic fungal cell wall, it was initially identified as a pathogen-associated molecular pattern that triggers host immune responses by binding to cell surface receptors (PRRs). More biological activities of β-glucan were subsequently revealed, including anticancer activity, which has been attributed to its immunomodulatory and stimulatory activities, such as the activation of natural killer cells, macrophages, T cells, B cells, and the induction of host defense peptides, cytokines, and chemokines (183, 186). However, it has not yet been established whether β-glucan has the ability to reverse drug resistance.

I initially examined the dose-dependent effects of β-glucan on cell viability. A549 and VMRC-LCD cells were treated with various concentrations of β-glucan for 24 h. The results showed that β-glucan was not cytotoxic up to 5 and 10 μg/ml in VMRC-LCD and A549 cells, respectively (Fig. 1*A*). Non-cytotoxic concentrations for each cell were selected for subsequent experiments. Treatment of VMRC-LCD cells with various concentrations of β-glucan did not affect the cytotoxicity of etoposide. In contrast, a co-treatment of etoposide with 2.5 and 5 μg/ml β-glucan elicited a stronger cytotoxic response in A549 cells than that of etoposide alone (Fig. 1*B*).

Because β-glucan affected the etoposide sensitivity in A549 cells only, I then performed a colony formation assay in A549 cells and showed that the number of colonies formed by etoposide-treated cells in the presence of 2.5 μg/ml β-glucan was significantly reduced (Fig. 1*C*), indicating a decrease in cell proliferation. These results suggest that β-glucan enhanced the effects of etoposide on the proliferation and colony-forming ability of A549 cells. The 2.5 μg/ml β-glucan was

also found to enhance the inhibitory effects of 50, 100, and 200 μM etoposide on the migration of A549 cells using the wound healing assay (Fig. 1*D*). Collectively, these results support the resistance-modifying property of β-glucan, specifically in A549 cells and not VMRC-LCD cells.

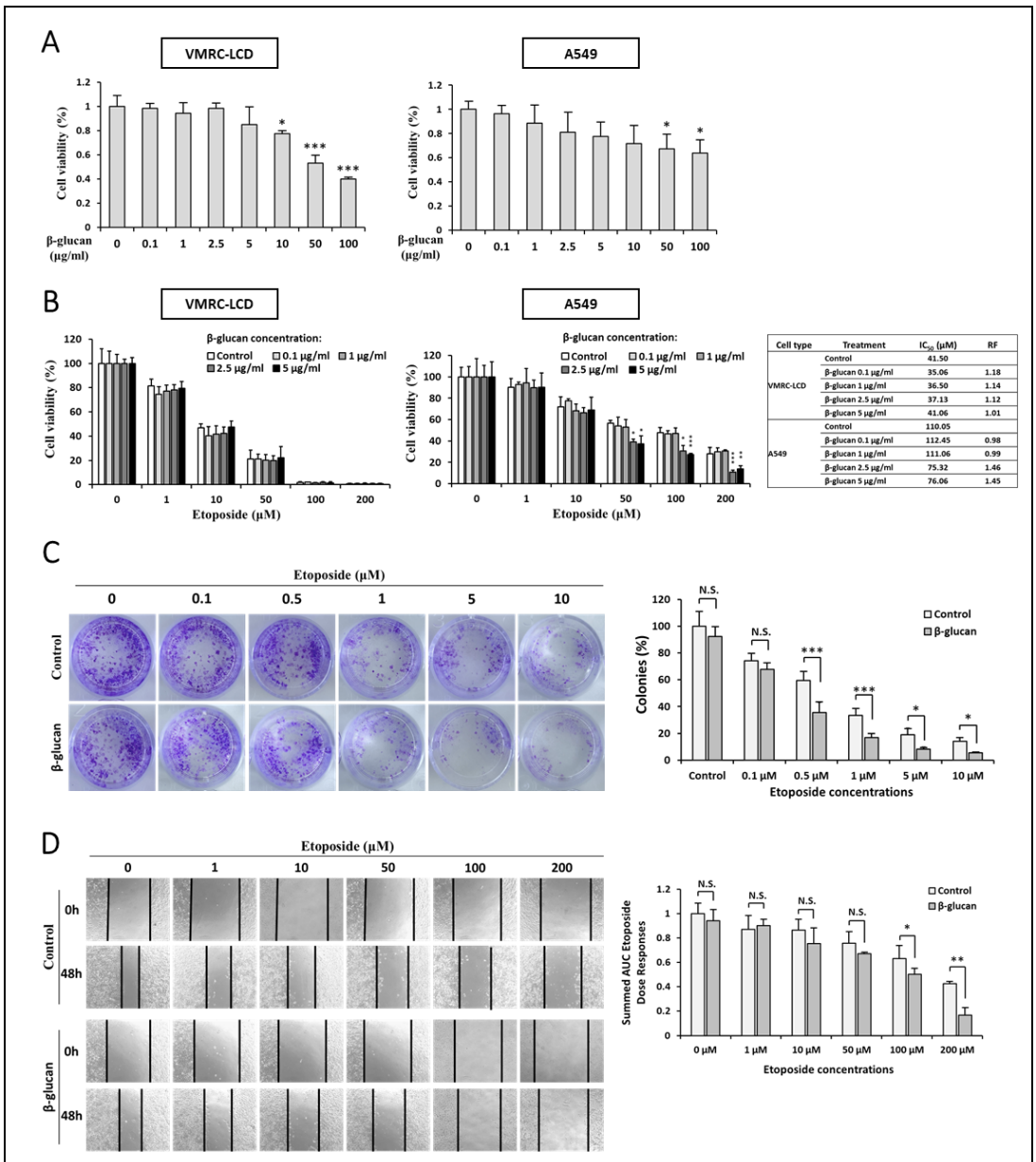

Figure 1. Effects of β-glucan on the sensitivity of NSCLC towards etoposide. (A) VMRC-LCD and A549 cells were treated with the indicated concentration of β-glucan for 24 h. The viability of cells was then assessed by the MTT colorimetric assay. Data are shown as mean ± S.D. from three independent experiments performed in triplicate relative to the corresponding treatments with vehicle (designated as 1). Differences to this value were analyzed by one-way repeated measures ANOVA with Dunnett's post-hoc test. (B) The viability of VMRC-LCD and A549 cells treated with the indicated doses of β-glucan and etoposide for 72 h was measured using the MTT colorimetric assay. Data are the mean ± S.D. from three independent experiments performed in triplicate,

analyzed by two-way repeated measures ANOVA and Fischer's LSD (least significant difference) post-hoc test. Half maximal inhibitory concentration (IC50) and reversal fold (RF) were calculated as described in *Materials and Methods*. (C) The proliferation of A549 cells was assessed by the colony formation assay. Cells were treated with 2.5 μg/ml β-glucan and the indicated doses of etoposide for 48 h, washed, and subsequently cultured in fresh medium for 5 days until colonies formed (left panel). The number of colonies that formed in each well was counted using ImageJ software (right panel). Data are the mean ± S.D. from three independent experiments performed in quadruplet, two-way repeated measures ANOVA and Fischer's LSD post-hoc test. (D) The migration rate of A549 cells treated with 2.5 μg/ml β-glucan and the indicated doses of etoposide for 48 h (left panel) was assessed by the wound healing assay. Migrated cells were quantified by ImageJ and presented as the area under the curve (AUC) relative to control cells without β-glucan and etoposide. Graphs represent means ± S.D. from three independent experiments performed in triplicate, two-way repeated measures ANOVA and Fischer's LSD post-hoc test. N.S. not significant, *p<0.05, **p<0.01, ***p<0.001 *versus* the indicated group.

The role of Nrf2 on etoposide resistance and β-glucan activities in A549 cells

The results showing that β-glucan affected etoposide sensitivity only in A549 cells is intriguing as it may lead to the understanding of the mechanism of action of β-glucan. Additionally, it is worth noticing that basal etoposide sensitivity of A549 cells was approximately 3-times less than that of VMRC-LCD cells (Fig. 1*D*). Therefore, β-glucan may regulate pathway responsible for etoposide resistance in A59 cells. Nrf2 is a key transcription factor that regulates the expression of a large number of DMEs and xenobiotic transporters. Since A549 cells harbor a homozygous mutation in the first Kelch domain of Keap1 that impairs the ubiquitination and degradation of Nrf2 (48, 187), while VMRC-LCD is a Keap1 wild-type cell line (188), I postulated that hyperactivated Nrf2 in A549 cells drives etoposide resistance.

To test this, I compared basal Nrf2 levels in VMRC-LCD and A549 cells and showed that endogenous Nrf2 levels were approximately 2.5-times higher in A549 than that of VMRC-LCD cells. Additionally, I depleted endogenous Nrf2 in A549 cells by siRNA-Nrf2, Keap1 overexpression, and WDR23 overexpression (Fig. 2*A*). Keap1 and WDR23 are adaptors for CUL3 and CUL4 E3 ligases, respectively, and have been identified as negative regulators of Nrf2 stability (42). The mRNA expression of the Nrf2-putative target genes, *HO-1* and *NQO1*, as well as the expression of several DMEs, including *UGT1A1* and *MDR1*, were all higher in A549 than that of VMRC-LCD cells. The knockdown of Nrf2 and overexpression of Keap1 and WDR23 in A549 cells resulted in decreasing mRNA levels of these genes. The expression of *CYP3A5* was also higher in A549 cells and decreased by knockdown of Nrf2 and overexpression of Keap1 and WDR23 in A549 cells, although it was not significant (Fig. 2*B*). The metabolism of etoposide is mediated by CYP3A4, CYP3A5, and UGT1A1 and excreted from cells by MDR1 (189). However, *CYP3A4* mRNA was not detected in A549 cells (data not shown). Since

the expression of etoposide-metabolizing enzymes was up-regulated in A549, I examined the cytotoxic potential of etoposide in control A49 cells or under the genetic inhibition of the Nrf2 pathway.

Consistently, A549 cells were approximately 3-times more resistant to etoposide than that of VMRC-LCD cells. As expected, the cell viabilities of Nrf2-knockdown, Keap1-overexpressing, and WDR23-overexpressing A549 cells were markedly lower than that of control cells (Fig. 2*C*). The calculated IC50 of etoposide was decreased by approximately 52, 45, and 45% in Nrf2-knockdown, Keap1-overexpressing, and WDR23-overexpressing A549 cells, respectively. These results validated the critical role of Nrf2 in etoposide resistance in A549 cells and that the response of A549 cells to etoposide may be enhanced by suppressing the Nrf2 pathway.

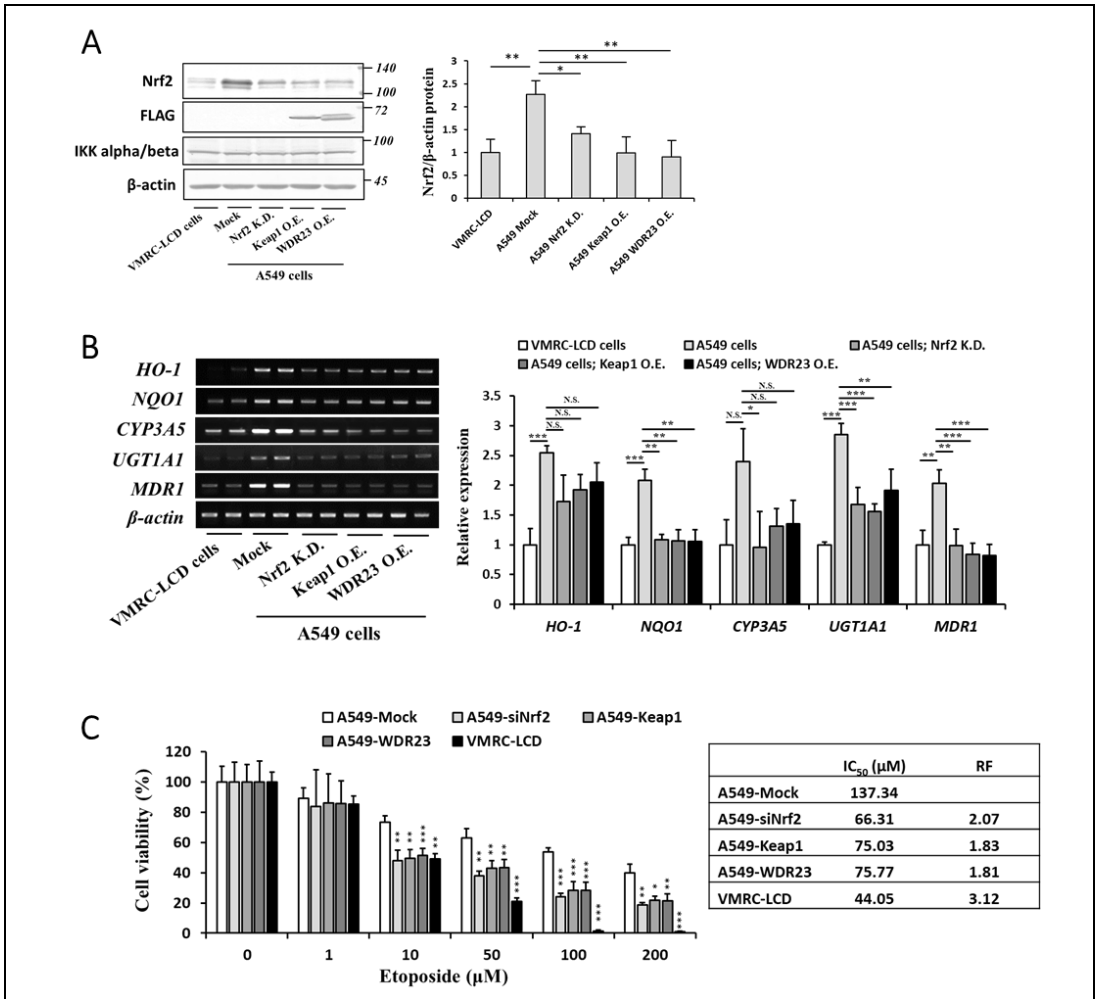

Figure 2. Involvement of Nrf2 in etoposide sensitivity in A549 cells. A549 cells were transfected with siRNA-Control and FLAG-Mock (Mock), siRNA-Nrf2 and FLAG-Mock (Nrf2 K.D.), siRNA-Control and FLAG-Keap1 (Keap1 O.E.), or siRNA-Control and FLAG-WDR23 isoform 1 (WDR23 O.E.). (A) The effects of Nrf2 knockdown, Keap1 overexpression, and WDR23 overexpression on Nrf2 and IKKs protein levels in A549 cells and the difference between A549 and VMRC-LCD cells were examined by immunoblotting against anti-Nrf2, anti-IKKalpha/beta, and anti-FLAG

antibodies and quantified with ImageJ relative to β-actin. Graph represents mean ± S.D. from three independent experiments, one-way repeated measures ANOVA with Tukey's post-hoc test. (B) The effects of Nrf2 knockdown, Keap1 overexpression, and WDR23 overexpression in A549 cells, as well as the difference between A549 and VMRC-LCD cells on the mRNA abundance of *HO-1*, *NQO1*, *CYP3A5*, *UGT1A1*, and *MDR1* were assessed by RT-PCR. Data are mean ± S.D. from three independent experiments performed in triplicate and the differences were analyzed by one-way repeated measures multivariate ANOVA with Tukey's post-hoc test. (C) The viability of VMRC-LCD and A549 cells (Mock, Nrf2 knockdown, Keap1 overexpression, and WDR23 overexpression) treated with etoposide for 72 h was measured using the MTT assay. Data are the mean ± S.D. from three independent experiments performed in triplicate, two-way repeated measures ANOVA and Fischer's LSD post-hoc test. The IC50 and RF were calculated as described in *Materials and Methods*. N.S. not significant, *p<0.05, **p<0.01, ***p<0.001 *versus* the indicated group.

The identified role of Nrf2 in etoposide resistance of A549 cells is intriguing as it suggests that β-glucan minimizes etoposide resistance via the Nrf2 pathway. To test this hypothesis, I treated A549 and VMRC-LCD cells with β-glucan and changes in total Nrf2 protein levels were quantified by immunoblotting. In A549 cells, β-glucan concentrations of 0.1 and 1 μg/ml did not affect Nrf2 levels, while 2.5 μg/ml and higher caused reductions. In contrast, any given concentration of β-glucan did not affect Nrf2 in VMRC-LCD cells (Fig. 3*A*). β-glucan concentration of 2.5 μg/ml and higher significantly reduced the transcriptional activity of Nrf2 in A549 cells, as shown by ARE luciferase activity (Fig. 3*B*), and down-regulated the mRNA expression of the bona fide Nrf2 target genes *HO-1* and *NQO1,* and the etoposide-metabolizing enzymes *CYP3A5*, *UGT1A1*, and *MDR1* (Fig. 3*C*). These results suggest a novel role for β-glucan as an inhibitor of the Nrf2, especially in a cell with a highly activated Nrf2 pathway. Importantly, the overexpression of Nrf2 abrogated the etoposide sensitization effects of β-glucan treatment (Fig. 3*D*), supporting the role of Nrf2 inhibition on the resistance-modifying property of β-glucan. Next, I examined the effects of etoposide on Nrf2 and tested whether β-glucan influences on Nrf2 also occur in the presence of etoposide. Interestingly, I found that etoposide concentration of 100 μM and higher decreased Nrf2 protein abundance; however, β-glucan were still able to decrease Nrf2 in the presence of etoposide (Fig. 3*E*).

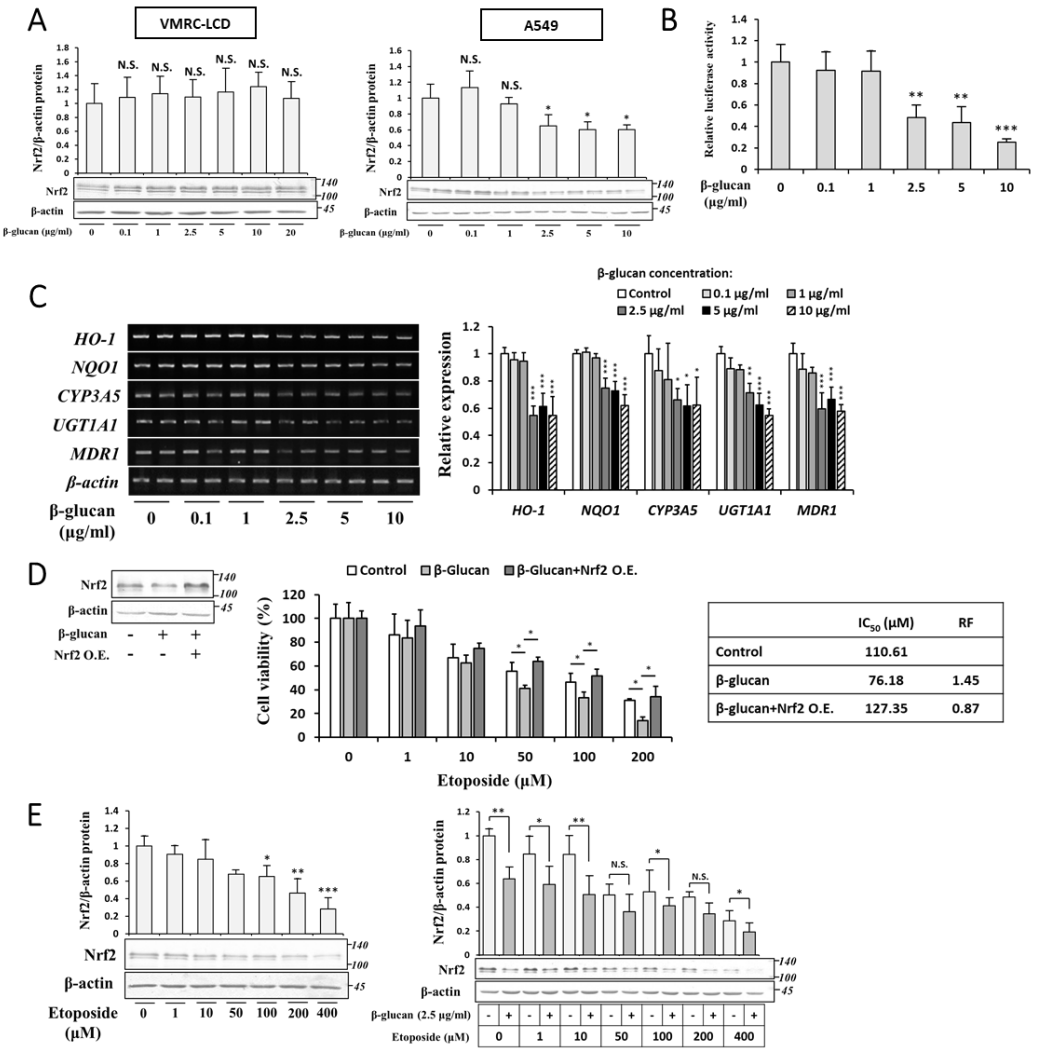

Figure 3. The effects of β-glucan on Nrf2 and its role on etoposide sensitivity. (A) VMRC-LCD and A549 cells were treated with the indicated concentration of β-glucan for 24 h and Nrf2 protein levels were assessed by immunoblotting. Data are mean ± S.D. from three independent experiments performed in triplicate and the differences were analyzed by one-way repeated measures ANOVA with Dunnett's post-hoc test. (B) Nrf2 transcriptional activity was measured in A549 cells expressing a 3×NQO1-ARE luciferase reporter and pRL-Null treated with the indicated concentration of β-glucan for 24 h. Data are mean ± S.D. from three independent experiments performed in triplicate, one-way repeated measures ANOVA with Dunnett's post-hoc test. (C) A549 cells were treated with the indicated concentration of β-glucan for 24 h and the mRNA abundance of *HO-1*, *NQO1*, *CYP3A5*, *UGT1A1*, and *MDR1* were assessed by RT-PCR. Data are mean ± S.D. from three independent experiments performed in triplicate and the differences were analyzed by one-way repeated measures multivariate ANOVA with Dunnett's post-hoc test. (D) The viability of control and Nrf2-overexpressed A549 cells treated with 2.5 μg/ml β-glucan and indicated doses of etoposide for 72 h was measured using the MTT assay. Data are the mean ± S.D. from three independent experiments performed in triplicate, two-way repeated measures ANOVA and Fischer's LSD post-hoc test. (E) A549 cells were treated with the indicated concentration of etoposide only (72 h, left panel) or co-treated with β-glucan (2.5 μg/ml, 24 h, right panel), and the total Nrf2 levels were assessed by immunoblotting. Data are mean ± S.D. from three independent experiments and the differences were analyzed by either one-way repeated measures ANOVA with Dunnett's post-hoc test (left panel) or two-way repeated measures ANOVA with Fischer's LSD post-hoc test (right panel). N.S. not significant, *p<0.05, **p<0.01, ***p<0.001 *versus* the indicated group.

The role of EphA2 in the β-glucan-induced suppression of Nrf2 in A549 cells

The recognition of β-glucan by innate immune cells and epithelial cells is mediated by the c-type lectin receptor dectin-1, an integrin dimer consisting of the $\alpha_M\beta_2$ (CD11b/CD18) receptor or complement receptor 3 (CR3), and the receptor tyrosine kinase EphA2 (23, 24). However, the qualitative RT-PCR showed that dectin-1 was not expressed in A549 cells, while the CR3 components (CD11b and CD18) and EphA2 were, with EphA2 being the most abundantly expressed receptor (Fig. 4*A*). To identify the critical receptor for the Nrf2-suppressing activity of β-glucan in A549 cells, I treated CD11b- and EphA2-knockdown cells with β-glucan. The efficiency of the knockdown of CD11b was ~45%, while that of EphA2 was ~55% (Fig. 4*B*). The knockdown of CD11b did not affect β-glucan-induced Nrf2 protein depletion (Fig. 4*C*). In contrast, the knockdown of EphA2 abolished the effects of β-glucan on Nrf2 (Fig. 4*D*), suggesting the involvement of the EphA2 receptor.

Based on these results, I confirmed the expression and localization of EphA2 in the plasma membrane of A549 cells using the immunofluorescence assay (Fig. 4*E*, upper panel). Since the activation of EphA2 is characterized by the formation of clusters and proceeds to endocytosis (190, 191), I investigated the localization of EphA2 after the treatment with β-glucan. EphA2 formed oligomers in β-glucan-treated cells, as shown by the accumulation of puncta, and was also internalized suggesting the activation of the EphA2 receptor (Fig. 4*E*, lower panel). The activation of EphA2 by β-glucan was also demonstrated by increases in phosphorylated EphA2 levels (Fig. 4*F*). The Ephrin-A1-induced phosphorylation of EphA2 was previously shown to be followed by its rapid degradation (192); however, my results revealed that the total protein levels of EphA2 were unchanged by β-glucan (Fig. 4*G*), indicating a difference in EphA2 signaling induced by Ephrin-A1 and β-glucan.

To validate the role of EphA2 to the resistance-modifying property of β-glucan, I assessed cell responses to etoposide in CD11b- and EphA2-knockdown A549 cells. The cytotoxicity of etoposide was increased by co-treatment with β-glucan to a similar extent of ~32% in control and CD11b-knockdown cells. However, etoposide toxicity was unaltered by β-glucan in EphA2-knockdown cells (Fig. 4*H*). These findings validate the critical involvement of EphA2 in Nrf2-dependent resistance-modifying property of β-glucan in A549 cells.

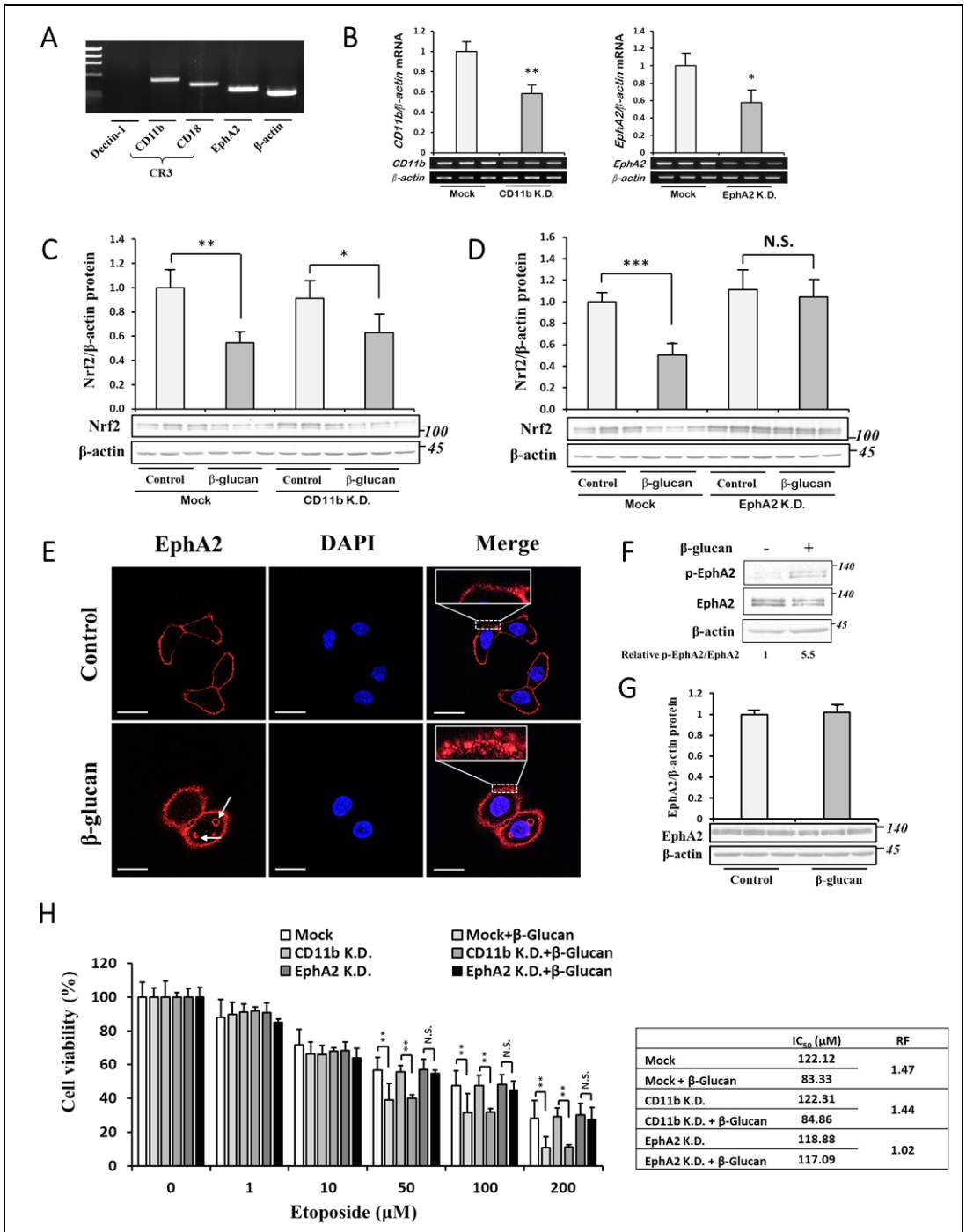

Figure 4. Involvement of EphA2 in A549 cell responses to β-glucan. (A) The qualitative expression of dectin-1, CR3 components (CD11b and CD18), and EphA2 receptors in A549 cells was evaluated by RT-PCR. (B-D) A549 cells were transfected with shRNA-GFP, shRNA-CD11b, or shRNA-EphA2 and transfectants were selected by G418. (B) The knockdown efficiency of CD11b and EphA2 was evaluated by RT-PCR (mean ± S.D., n= 3, one-sample t-test). (C and D) The effects of β-glucan (2.5 μg/ml, 24 h) on Nrf2 in control and CD11b-knockdown (C) or EphA2-knockdown (D) A549 cells were examined by immunoblotting. Data are shown as mean ± S.D. from three independent experiments performed in triplicates and the differences were analyzed by one-sample t-test with Bonferroni's correction for multiple testing. (E) The cellular localization of EphA2 (red) and DAPI (blue) was assessed by immunofluorescence in A549 cells treated with or without β-

glucan (2.5 μg/ml, 1 h), insets show images corresponding to the white dashed areas, white arrows indicate the localization of EphA2 in endosomes, scale bar: 20 μm. Images were representative of three independent experiments. (F) A549 cells were treated with or without β-glucan (2.5 μg/ml, 1 h), whole-cell lysates were immunoprecipitated with the anti-EphA2 antibody, and bound proteins were detected with immunoblotting against anti-EphA2 and anti-phosphoserine/threonine/tyrosine antibodies. (G) Total EphA2 protein levels in A549 cells were assessed after the treatment with 2.5 μg/ml β-glucan for 1 h (mean ± S.D., n= 3, one-sample t-test). (H) The viability of Mock, CD11b-knockdown, and EphA2-knockdown A549 cells treated with the indicated doses of β-glucan and etoposide for 72 h was measured using the MTT colorimetric assay. Data are the mean ± S.D. from three independent experiments performed in triplicate and analyzed with two-way repeated measures ANOVA and Fischer's LSD post-hoc test. The IC50 and RF were calculated as described in *Materials and Methods*. N.S. not significant, *p<0.05, **p<0.01, ***p<0.001 *versus* the indicated group.

The role of NF-κB in the suppression of Nrf2 and etoposide resistance by β-glucan

To provide insights into the molecular mechanisms underlying the inhibition of Nrf2 by β-glucan, I attempted to identify the β-glucan/EphA2 downstream pathway(s) involved. β-glucan activates downstream signaling pathways that are mainly involved in the innate immune system, including canonical (p65/p50) and non-canonical (RelB/p52) NF-κB pathways (193), and previous findings showed that NF-κB is activated by EphA2 (194, 195). In the present study, the treatment of A549 cells with β-glucan activated NF-κB pathways, as demonstrated by the nuclear accumulation of both p65 (Fig. 5*A*) and RelB (Fig. 5*B*), as well as the induction of NF-κB target genes, including interleukin-1β (IL-1β), inducible nitric oxide synthase (iNOS), and cyclooxygenase-2 (COX-2) (Fig. 5*C*). This activation was dependent on EphA2, as the increased expression of NF-κB target genes was impaired by the knockdown of EphA2 (Fig. 5*D*).

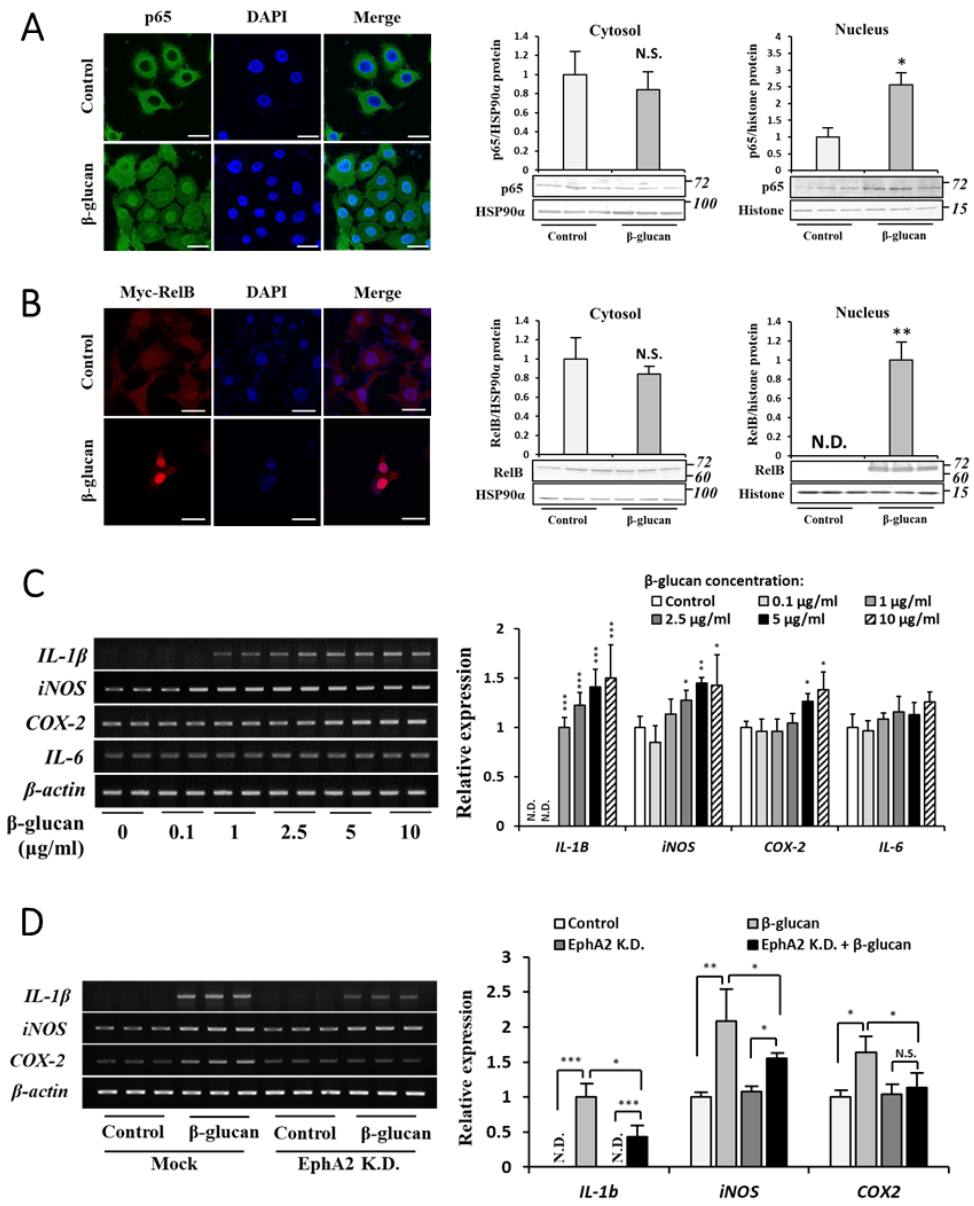

Figure 5. The activation of NF-κB pathway by β-glucan. (A) The cellular localization of p65 (green) and DAPI (blue) was examined by immunofluorescence in A549 cells treated with vehicle or 2.5 μg/ml β-glucan (left panel), scale bar: 25 μm, images were representative of three independent experiments. The abundance of cytosolic and nuclear p65 was examined by immunoblotting and quantified by ImageJ relative to the intensity of HSP90α (cytosol) and histone (nucleus). Data are presented as mean ± S.D. from three independent experiments performed in triplicates and analyzed by one-sample *t*-test. (B) A549 cells were transfected with pCMV-Myc containing RelB and the cellular localization of Myc-RelB (red) and DAPI (blue) was examined by immunofluorescence after treatment with or without 2.5 μg/ml β-glucan (left panel), scale bar: 25 μm. The abundance of cytosolic and nuclear RelB was examined by immunoblotting (mean ± S.D. from three independent experiments performed in triplicates and analyzed by one-sample *t*-test). (C) The effects of the indicated concentration of β-glucan on the mRNA abundance of *IL-1β, iNOS, COX-2,* and *IL-6* were measured with RT-PCR, presented as mean ± S.D. from three independent experiments performed in triplicate, and analyzed by one-way repeated measures multivariate ANOVA with Dunnett's post-hoc test. (D) The effects of β-glucan (2.5 μg/ml, 24 h) on the mRNA abundance of *IL-1β* and *iNOS* of control or EphA2-knockdown cells were measured with RT-PCR, presented as mean ± S.D. from three independent experiments performed in triplicate, and analyzed by one-sample *t*-test and corrected for multiple testing by Bonferroni's method. N.S. not significant, *p<0.05, **p<0.01, ***p<0.001.

I then investigated the importance of the activation of NF-κB in the β-glucan-induced suppression of Nrf2 and etoposide resistance. β-glucan decreased Nrf2 protein levels in p65-knockdown cells (Fig. 6*A*). On the other hand, the knockdown of RelB diminished the effects of β-glucan on Nrf2 (Fig. 6*B*), suggesting the involvement of the non-canonical NF-κB pathway. A previous study reported that in addition to the NF-κB pathway, β-glucan-stimulated EphA2 also activates signal transducer and activator of transcription 3 (STAT3) and p38 mitogen-activated protein kinase (MAPK) signaling (190). To test whether the effects of β-glucan on Nrf2 is solely mediated by NF-κB (RelB), I treated β-glucan in the presence of STAT3 inhibitor stattic and p38 MAPK inhibitor SB203580. I found that the effects of β-glucan on Nrf2 were not affected by both stattic (Fig. 6*C*) and SB203580 (Fig. 6*D*). Next, I assessed cell responses to etoposide in p65- and RelB-knockdown A549 cells, and in control cells in the presence of stattic or SB203580. The cytotoxicity of etoposide was increased by co-treatment with β-glucan in p65-knockdown cells, and in control cells in the presence of stattic and SB203580, but not in RelB-knockdown cells (Fig. 6*E*). In summary, these results support the involvement of RelB as a downstream of EphA2 signaling activated by β-glucan to suppress Nrf2 and enhance etoposide sensitivity in A549 cells.

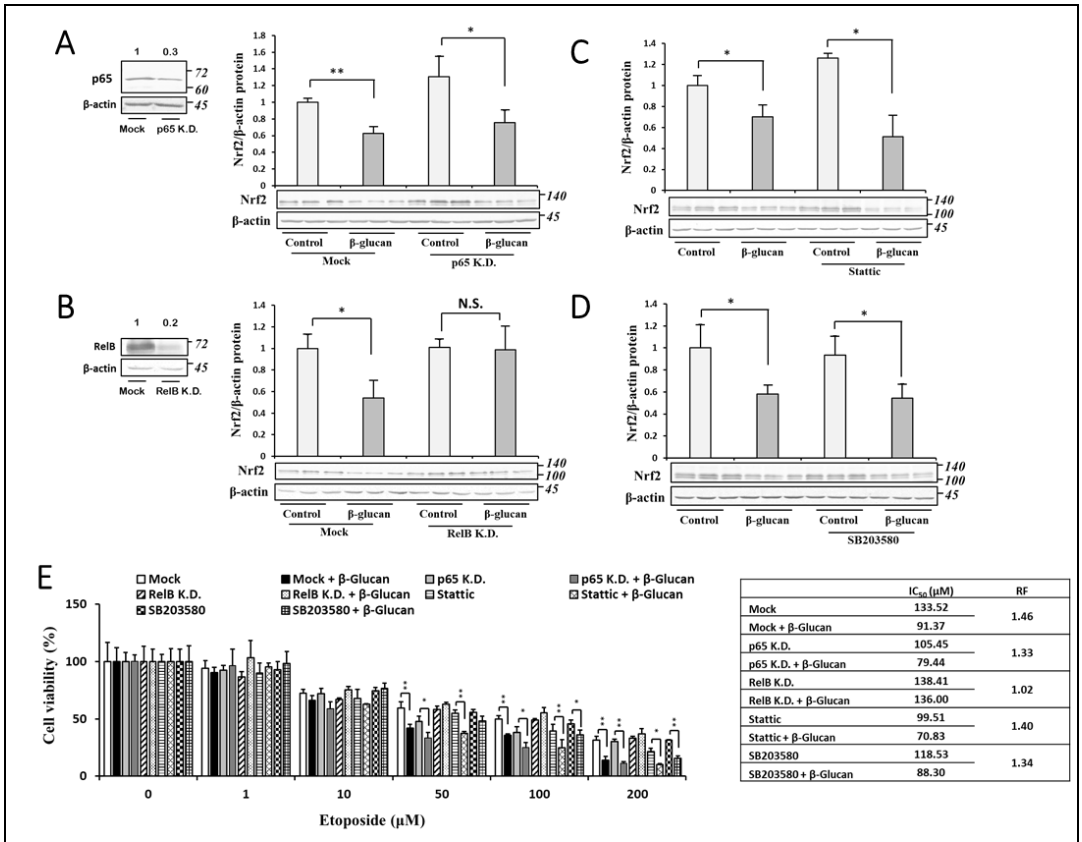

Figure 6. The role of non-canonical NF-κB in the biological activities of β-glucan on A549 cells. (A) A549 cells were transfected with si-Control or si-p65 and treated with vehicle or 2.5 μg/ml β-glucan. The protein abundance of p65 (left panel) and Nrf2 (right panel) were then quantified with

immunoblotting. (B) A549 cells were transfected with sh-GFP or sh-RelB and treated with vehicle or 2.5 μg/ml β-glucan. The protein abundance of RelB (left panel) and Nrf2 (right panel) were then measured by immunoblotting. (C) Nrf2 protein levels were assessed from A549 total cell lysates after the 24-h co-treatment of 2.5 μg/ml β-glucan and 5 μM stattic. (D) A549 were co-treated with 2.5 μg/ml β-glucan and 10 μM SB203580. For figure F-I, data are presented as mean ± S.D. from three independent experiments performed in triplicate and analyzed by one-sample *t*-test and corrected for multiple testing by Bonferroni's method. (E) The viability of control, p65-knockdown, RelB-knockdown, stattic-treated, or SB203580-treated A549 cells and co-treatment with 2.5 μg/ml β-glucan and indicated doses etoposide for 72 h was measured using the MTT colorimetric assay. Data are the mean ± S.D. from three independent experiments, two-way repeated measures ANOVA and Fischer's LSD post-hoc test. Half maximal inhibitory concentration (IC50) and reversal fold (RF) were calculated as described in *Materials and Methods*. N.S. not significant, *p<0.05, **p<0.01, ***p<0.001 *versus* the indicated group.

Effects of RelB on Nrf2 and etoposide sensitivity

The potential role of RelB on the regulation of Nrf2 and drug sensitivity was expected based on the proposed crosstalk between NF-κB and Nrf2. However, the interconnection between these two transcription factors is limited to the p65 complex at the transcriptional level, at which p65 and Nrf2 compete for transcriptional co-activator CBP-p300 binding (196). In the present study, I showed that the overexpression of RelB reduced Nrf2 protein levels (Fig. 7*A*), suggesting a new model of crosstalk between NF-κB and Nrf2. Reduced Nrf2 protein levels were then followed by decreases in the transcriptional activity of Nrf2, as shown by the ARE-reporter assay (Fig. 7*B*), and the expression of putative Nrf2 target genes, as well as the down-regulated expression of etoposide-metabolizing enzymes (Fig. 7*C*). Next, I asked whether RelB-regulated Nrf2 protein abundance is the sole reason for the decreasing Nrf2 activity. To explore this, I observed the effects of RelB overexpression on Nrf2 transcriptional activity under the presence of proteasome inhibitor MG132. Interestingly, the transcriptional activity of Nrf2 was also decreased by RelB overexpression under the presence of MG132 despite the comparable levels of Nrf2 (Fig.7*D*), which suggests an additional mechanism by which RelB regulates the Nrf2 pathway. Interestingly, by using ChIP assay, I found that Nrf2 binding to the ARE of the *NQO1* promoter was gradually reduced by increasing RelB expression (Fig.7*E*). I identified a potential RelB binding site close (134bp) to the ARE region, and I confirmed the *in vivo* binding of RelB to this site. These experiments indicate that RelB negatively regulates the Nrf2 pathway by inducing Nrf2 protein depletion and preventing DNA binding of Nrf2, at least in the *NQO1* promoter. The negative impact of RelB on the Nrf2 pathway affected etoposide sensitivity because the viability of cells following the etoposide treatment and the calculated IC50 of etoposide decreased by 28% in RelB-overexpressed A549 cells and increased by 30% in RelB-knockdown A549 cells (Fig. 7*F*).

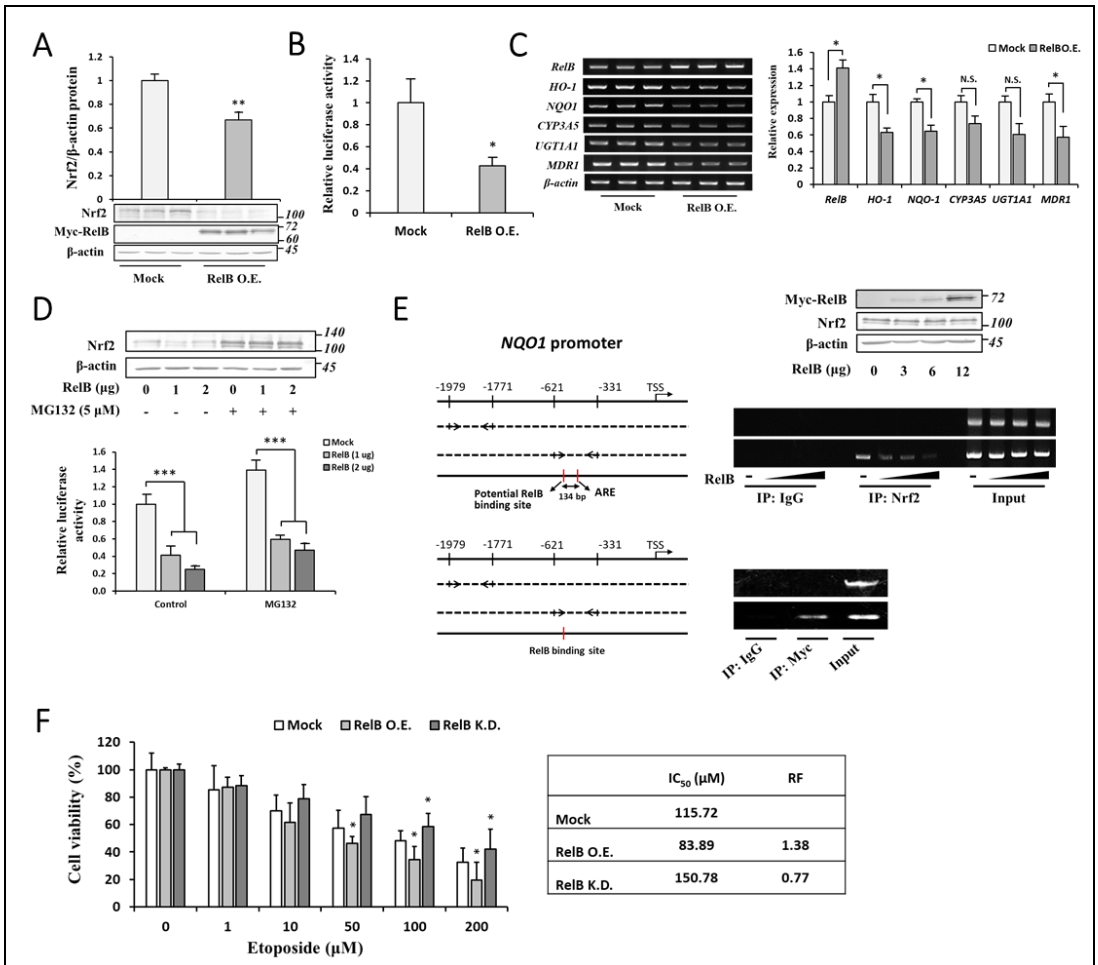

Figure 7. The role of RelB on the Nrf2 pathway and cellular responses to etoposide. The overexpression of RelB was achieved by the transfection of RelB in pCMV-Myc into A549 cells. (A) Immunoblotting was used to analyze the effects of the overexpression of RelB on Nrf2 protein abundance (data are mean ± S.D. from three independent experiments performed in triplicate, one-sample *t*-test). (B) A549 cells were transfected with the pGL3-containing 3×NQO1-ARE luciferase reporter, pRL-Null, and either pCMV-Mock or pCMV-RelB, followed by the measurement of luciferase activity 48-h post-transfection (data are shown as mean ± S.D. from three independent experiments performed in triplicate, one-sample *t*-test). (C) The mRNA abundance of *RelB, HO-1*, *NQO1*, *CYP3A5*, *UGT1A1*, and *MDR1* was assessed by RT-PCR from A549 cells transfected with pCMV-Mock and pCMV-RelB (data represents mean ± S.D. from three independent experiments performed in triplicate and the differences were analyzed by one-sample *t*-test with Bonferroni's correction for multiple testing). (D) A549 cells were transfected with the pGL3-containing 3×NQO1-ARE luciferase reporter, pRL-Null, and either pCMV-Mock or pCMV-RelB (1 or 2 μg), treated with or without 5 μM MG132 followed by the measurement of luciferase activity. Data are shown as mean ± S.D. from three independent experiments performed in triplicate. Differences to the respective pCMV-Mock-transfected cells were analyzed by one-way repeated measures ANOVA with Dunnett's multiple comparisons test. (E) Genomic positions of *NQO1* regions that were selected for the ChIP assay with a known Nrf2-binding site and potential RelB-binding (left panel). A549 cells were transfected with various dose of pCMV-RelB construct, treated with MG132 (5 μM, 8 h) and the ChIP assay was performed with either anti-Nrf2 or anti-Myc antibodies or control mouse IgG, with input chromatin as the positive control. After reverse crosslinking, DNA was amplified using the indicated primer sets (right panel). (F) The viability of RelB-knockdown cells generated using shRNA and RelB overexpression achieved by the transfection of pCMV-RelB treated with the indicated doses of etoposide for 72 h was measured by the MTT colorimetric assay. Graphs are the relative mean ± S.D. from three independent experiments performed in quadruplet, two-way repeated measures ANOVA and Fischer's LSD post-hoc test. N.S. not significant, *p<0.05, **p<0.01, ***p<0.001 *versus* the indicated group.

The role of the $CRL4^{WDR23}$ pathway on the β-glucan-induced suppression of Nrf2

I investigated the mechanisms by which β-glucan decreases Nrf2 protein levels. Since A549 cells harbor a mutation that renders Keap1 unable to mediate the ubiquitination of Nrf2 (48), I hypothesized that Nrf2 is mainly regulated by the newly identified $CRL4^{WDR23}$ pathway and that β-glucan relies on this pathway. I previously showed that the inactivation of Keap1 in hepatoma cell line Hep3B induced the activation of the WDR23 pathway (43). In the present study, I overexpressed each component of $CRL4^{WDR23}$, including WDR23 (Fig. 8*A*), CUL4A (Fig. 8*B*) and DDB1 (Fig. 8*C*), in A549 cells and found that Nrf2 protein levels were markedly reduced, confirming the regulation of Nrf2 by WDR23 in A549 cells. Based on these results, I examined the importance of WDR23 for the effects of β-glucan on Nrf2. The effects of β-glucan on Nrf2 were blunted by the knockdown of WDR23 (Fig. 8*D*), indicating that the depletion of the Nrf2 protein induced by β-glucan was dependent on WDR23. To verify the contribution of WDR23 to the resistance-modifying property of β-glucan, I assessed cell responses to etoposide in WDR23-knockdown A549 cells. WDR23-knockdown A549 cells (IC50= 150.39 μM) were more resistant to etoposide than control A549 cells (IC50= 107.85 μM), and the reversal efficacy of β-glucan was lower in WDR23-knockdown cells (8%) than in control cells (26%) (Fig. 8*E*).

To obtain a more detailed understanding of the mechanisms by which β-glucan regulates Nrf2 levels via WDR23, I examined the expression levels of components of $CRL4^{WDR23}$. The mRNA levels of *WDR23*, *CUL4B*, and *RBX1* were not affected by β-glucan, whereas the mRNA abundance of *CUL4A* and *DDB1* was significantly higher in β-glucan-treated cells (Fig. 8*F*). At the protein level, β-glucan did not affect WDR23 or DDB1 levels, but increased CUL4A protein levels (Fig. 8*G*), suggesting that the modulation of the intracellular abundance of CUL4A by β-glucan is responsible for decreases in Nrf2 levels.

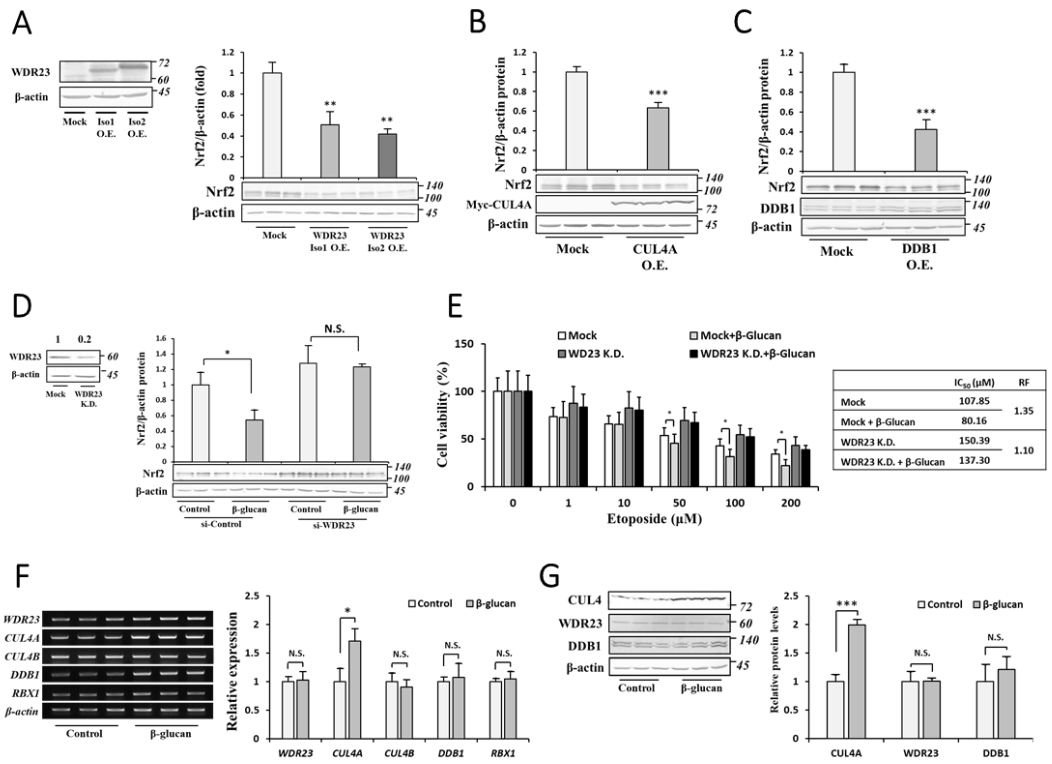

Figure 8. The role of the CRL4^{WDR23} pathway on the regulation of Nrf2 by β-glucan. (A) The effects of the overexpression of WDR23 isoforms 1 and 2 (left panel) on Nrf2 protein abundance (right panel) were measured by immunoblotting, data are presented as mean ± S.D. from three independent experiments performed in triplicate and were analyzed by one-way repeated measures ANOVA with Dunnett's post-hoc test. (B-C) A549 cells were transfected with pCMV-Mock or pCMV-CUL4A (B) and pCDNA-Mock or pCDNA-DDB1 (C), and the abundance of Nrf2 were measured by immunoblotting, data are presented as mean ± S.D. from three independent experiments performed in triplicate and were analyzed by one-sample *t*-test. (D) A549 cells were transfected with si-Control or si-WDR23 and knockdown efficiency was confirmed by immunoblotting (left panel). The effects of the WDR23 knockdown on Nrf2 protein levels in A549 cells treated with vehicle or β-glucan β-glucan (2.5 μg/ml, 24 h) were measured by immunoblotting (right panel). Data are shown as mean ± S.D. from three independent experiments performed in triplicates and the differences were analyzed by one-sample *t*-test with Bonferroni's correction for multiple testing. (E) The viability of control and WDR23-knockdown A549 cells treated with 2.5 μg/ml β-glucan and the indicated doses of etoposide for 48 h was measured by the MTT assay. Data represents mean ± S.D. from three independent experiments performed in triplicate, two-way repeated measures ANOVA and Fischer's LSD post-hoc test. The IC50 and RF were calculated as described in *Materials and Methods*. (F) The effects of β-glucan (2.5 μg/ml, 24 h) on the mRNA abundance of *WDR23*, *CUL4A*, *CUL4B*, *DDB1*, and *RBX1* were evaluated from A549 cell lysates by RT-PCR. Data are mean ± S.D. from three independent experiments performed in triplicate and the differences were analyzed by one-sample *t*-test with Bonferroni's correction for multiple testing. (G) The effects of β-glucan (2.5 μg/ml, 24 h) on the total protein levels of WDR23, CUL4A, and DDB1 were evaluated from A549 cell lysates by immunoblotting. Data are mean ± S.D. from three independent experiments performed in triplicate and the differences were analyzed by one-sample *t*-test with Bonferroni's correction for multiple testing. N.S. not significant, *p<0.05, **p<0.01, ***p<0.001 *versus* the indicated group.

The regulation of CUL4A expression by RelB

Based on the essential roles of RelB and CUL4A in the effects of β-glucan on the regulation of Nrf2, I attempted to elucidate the relationship between the activation of RelB and the up-regulated expression of CUL4A mRNA. Since RelB is a transcription factor, I speculated that it may directly regulate the expression of CUL4A. The overexpression of RelB significantly increased *CUL4A* mRNA levels (Fig. 9*A*), but not those of other components of $CRL4A^{WDR23}$ (data not shown). In addition, CUL4A protein levels were significantly higher in RelB-overexpressing cells than in control cells (Fig. 9*B*). To validate that the regulation CUL4A by β-glucan is mediated by EphA2 and RelB signaling, I examined the effects of β-glucan on mRNA and protein levels of CUL4A in EphA2- and RelB-knockdown cells. As expected, increasing levels of CUL4A mRNA and protein were diminished by the knockdown of EphA2 and RelB (Fig. 9*C* and *D*), highlighting the involvement of EphA2-RelB axis in the regulation of *CUL4A* expression by β-glucan.

To clarify the contribution of RelB to *CUL4A* transcription, I performed a luciferase assay on A549 cells co-transfected with the *CUL4A* reporter, and a control vector or plasmid containing RelB. The overexpression of RelB induced a 2.5-fold increase in the promoter activity of the reporter plasmid containing −1920/+50 bp of the *CUL4A* genomic region, which was maintained up to the construct containing −810/+50 bp of the *CUL4A* genomic region, but not −230/+50 bp (Fig. 9*E*), suggesting that the regulatory region of *CUL4A* by RelB is present within the −810/−230-bp segment. The online software AliBaba2.1 (197) identified two predicted RelB-binding sites within this segment. Finally, I confirmed the *in vivo* binding of RelB on both predicted binding sites using ChIP assays (Fig. 9*F*).

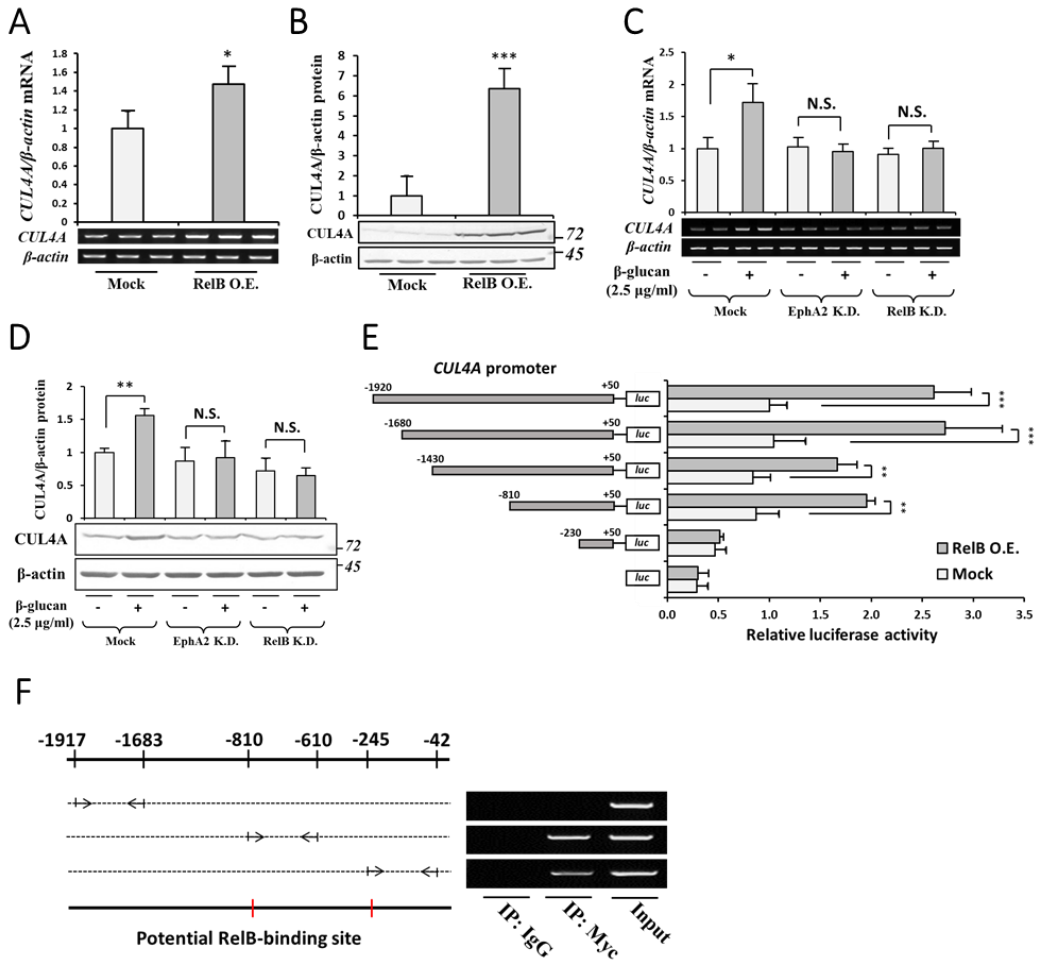

Figure 9. The regulation of *CUL4A* expression by RelB. (A-B) A549 cells were transfected with pCMV-Mock or pCMV-RelB. The mRNA levels (A) and protein abundance (B) of CUL4A were then examined by RT-PCR and immunoblotting, respectively. Data are presented as mean ± S.D. from three independent experiments performed in triplicate and were analyzed by one-sample t-test. (C-D) A549 cells were transfected with sh-GFP, sh-EphA2, or sh-RelB and treated with or without β-glucan (2.5 μg/ml, 24 h). The mRNA levels (C) and protein abundance (D) of CUL4A were then examined by RT-PCR and immunoblotting, respectively. Data are presented as mean ± S.D. from three independent experiments and were analyzed by one-sample t-test with Bonferroni's correction for multiple testing. (E) The pGL3-containing upstream regions −1920/+50, −1680/+50, −1430/+50, −810/+50, and −230/+50 of *CUL4A* or pGL3-basic were co-transfected with pRL-null and either pCMV-Mock or pCMV-RelB into A549 cells. Luciferase activity was assessed 48 h after transfection using the Dual-Luciferase Reporter Assay system. Results are shown as mean ± S.D. from three independent experiments performed in quadruplet relative to the activity of the *CUL4A* promoter −1920/+50 co-transfected with pCMV-Mock. Differences to this value were analyzed by one-sample t-test with Bonferroni's correction. (F) Genomic positions of *CUL4A* regions that were selected for the ChIP assay with potential RelB-binding sites as predicted by the online software AliBaba2.1 (left panel). A549 cells were transfected with pCMV-RelB, and the ChIP assay was performed with an anti-Myc antibody or control mouse IgG, with input chromatin as the positive control. After reverse crosslinking, DNA was amplified using the indicated primer sets (right panel). N.S. not significant, *p<0.05, **p<0.01, ***p<0.001 versus the indicated group.

IV.4. Discussion

Chemotherapeutic resistance in cancer remains one of the most challenging obstacles to overcome and is the first cause of cancer-associated death. Lung cancer patients treated with etoposide, one of the main chemotherapy agents, frequently develop resistance after long-term use (165). Therefore, efforts to elucidate the underlying mechanisms and discover methods to interfere with these processes are urgently needed. Since the up-regulation of Nrf2 is the major cause of chemoresistance in a broad spectrum of cancers, including lung cancer (173), targeting the Nrf2 pathway is a promising strategy. In the present study, I demonstrated that hyperactivated Nrf2 drove etoposide resistance in Keap1-mutant A549 cells and that treatment with β-glucan strongly sensitized A549 cells to etoposide by targeting Nrf2 pathway. I elucidated the molecular mechanisms by which β-glucan targeted Nrf2, which was mediated by the EphA2-RelB-CUL4A axis (Fig. 10).

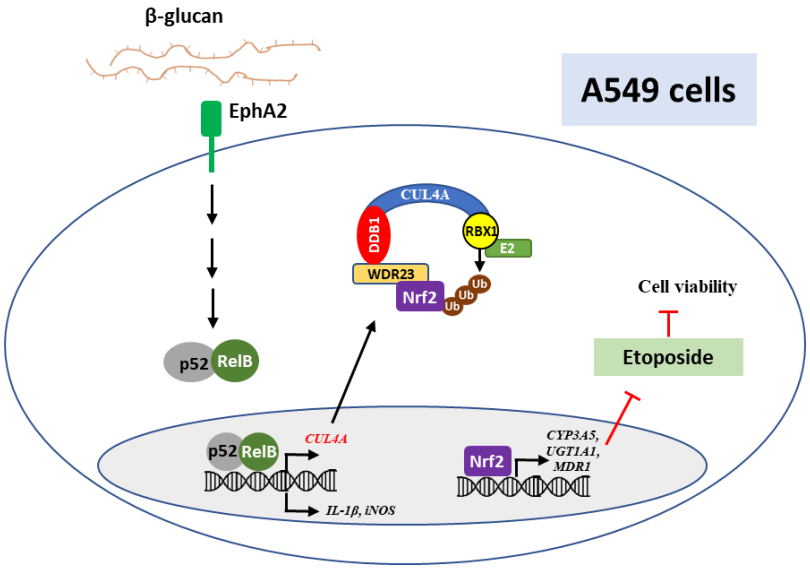

Figure 10. Proposed mechanism of action by which β-glucan enhances etoposide sensitivity in A549 cells by inhibiting Nrf2 pathway via the EphA2-RelB-CUL4A axis. β-glucan activates the non-canonical NF-κB (RelB) pathway via EphA2 receptor, which will lead to the nuclear accumulation and transcriptional activation of RelB. Since RelB is identified as a transcriptional regulator of *CUL4A*, β-glucan treatment induces RelB-dependent transcription of *CUL4A*, enhances $CRL4A^{WDR23}$ activity and eventually lead to the degradation of Nrf2. Reduced Nrf2 levels and transactivity lead to the suppression of etoposide-metabolizing enzymes; hence, enhancing the cytotoxicity of etoposide.

β-glucan is an important component of fungal and yeast cell walls and is recognized by host cells via PRRs. Due to its promotion of the immune system, β-glucan has been proposed as a potent chemotherapeutic adjuvant for a broad range of cancers (181). Tumor cells actively alter their TME to favor growth and progression, including the suppression of the immune system (198). The activity of β-glucan to change the TME from an immunosuppressive to pro-inflammatory state is considered to be the major reason for its beneficial effects as an adjuvant of conventional chemotherapy (182, 183). Another study proposed that the conversion of immunosuppressive tumor-associated macrophages into a classically activated phenotype by β-glucan may change resistant tumors into sensitive tumors (199). However, to the best of my knowledge, there is currently no direct evidence to support the resistance-modifying activity of β-glucan or the underlying mechanisms. In the present study, I unequivocally proved that β-glucan increased the sensitivity of A549 cells to etoposide.

The key players in A549 cell resistance to etoposide have been proposed by many studies and include caveolin-1 (200), Stat1 (201), c-Raf (202), and Nrf2 (11). In this study, I proved that β-glucan resistance-modifying activity is mediated by interventions against the Nrf2 pathway. I have previously demonstrated that Nrf2 regulated the expression of *CYP3A5*, *UGT1A1*, and *MDR1* (43), which are phase I, II, and III enzymes, respectively, that are involved in the metabolism of etoposide (189). Therefore, these results suggest that β-glucan functions as a potent inhibitor of the Nrf2 pathway and may be used to enhance the cytotoxicity of anticancer drugs against chemoresistant cells, particularly in cancers with a loss-of-function mutation in *Keap1* or a gain-of-function mutation in *Nrf2*. These findings are supported by Lo and colleague who found that Nrf2 inhibition by WDR23 overexpression enhanced etoposide sensitivity in A549 cells (42). Conversely, Zhang et al. reported that Nrf2 reduced etoposide efficacy in mononuclear cells (203). Singh and colleagues demonstrated that the suppression of overexpressed Nrf2 in A549 cells by siRNA increased the efficacy of chemotherapy (204). The cinnamomi cortex crude extract was also shown to enhance drug sensitivity by targeting the Nrf2 pathway (205). Collectively, this study and others established that targeting the Nrf2 pathway may overcome lung cancer chemoresistance.

In contrast to the present results, a previous study reported that β-glucan activated Nrf2 in RAW264.7 cells (206) and the oral keratinocyte cell line RT7 (207). This discrepancy is interesting because it suggests the dual activity of β-glucan, which may occur in a context-dependent manner. Yu and colleagues showed that β-glucan induced the activation of the dectin-1 receptor in lipopolysaccharide-treated RAW264.7 cells, which then increased Nrf2 levels. On the other hand, Ishida *et al.* reported that the effects of β-glucan on p38 mitogen-activated protein kinase-dependent Nrf2 activation did not require dectin-1. In the present study using

A549 cells consecutively expressing Nrf2, I showed the opposite effects of β-glucan on Nrf2. I demonstrated that dectin-1 was not expressed in A549 cells and also that the effects of β-glucan on Nrf2 were mediated by the EphA2 receptor. Therefore, this study and others confirmed the benefits of β-glucan to ameliorate the pathological Nrf2 pathway, suggesting its potential to either activate or inhibit Nrf2 in a context-dependent manner (i.e., the Nrf2 status and the receptor involved). However, further studies to elucidate the mechanisms underlying the diverse cellular responses to β-glucan are warranted.

A previous study reported the absence of the dectin-1 receptor in A549 cells (208), whereas Han *et al.* showed that dectin-1 was expressed in these cells (209). Another study by Lee and colleagues suggested that dectin-1 was not present in resting A549 cells, and that its expression was induced by *Mycobacterium tuberculosis* via the activation of toll-like receptor 2 (210). In the present study, I showed that the β-glucan treatment did not induce the expression of dectin-1 (data not shown), suggesting that the effects of β-glucan on the Nrf2 pathway and cell responses to etoposide were mediated by receptors other than dectin-1. By using the knockdown approach, I demonstrated that the effects of β-glucan on Nrf2 were mediated by EphA2, but not the CR3 receptor. The present results suggest that the non-canonical NF-κB pathway played a crucial role in the β-glucan-induced suppression of Nrf2, indicating that EphA2 activates the RelB-p52 complex. The activation of the NF-κB pathway by dectin-1 and CR3 has been widely reported (211–213); however, limited information is currently available on the axis involving EphA2 and NF-κB, particularly non-canonical subunits. A previous study suggested that the tyrosine phosphorylation of EphA2 by thrombin activates PI3K/Akt, resulting in the phosphorylation and activation of NF-κB (p65) (194). Another study showed that the activation of EphA2 by its ligand ephrin-A1 induced the nuclear accumulation of p65 (195). Despite evidence for the role of EphA2 as an upstream signal for the canonical (others study) and non-canonical (this study) NF-κB pathways, the relationship between EphA2 and NF-κB remains unclear.

The ability of β-glucan to reduce Nrf2 levels in A549 cells is of interest because it bears a defective Keap1-Nrf2 system. In the present study, I demonstrated that WDR23 regulated Nrf2 levels. The regulation and molecular functions of the WDR23-Nrf2 system remain largely unknown. I previously identified CUL4A as the rate-limiting component of $CRL4A^{WDR23}$ and also that the regulation of *CUL4A* gene expression by Sp1 in response to the knockdown of Keap1 drives $CRL4A^{WDR23}$ activity (127). In the present study, I identified a similar mechanism for β-glucan to trigger the activity of $CRL4A^{WDR23}$ towards Nrf2 in Keap1 mutant A549 cells. Instead of Sp1, I revealed a novel regulator of *CUL4A* expression. The NF-κB subunit RelB binds to the promoter of *CUL4A* and activates its transcription, leading to the activation of $CRL4A^{WDR23}$ and depletion of Nrf2. The regulation of

CUL4B, but not other *Cullins*, by NF-κB (p65, RelB, and c-Rel) and its implications on cell cycle progression were previously described (73). In the present study, I found that RelB specifically regulated the expression of *CUL4A*, but not *CUL4B.* This discrepancy may be attributed to the different stimuli and cells used in the present study. Of note, a previous study showed that NF-κB regulated overlapping and distinct gene clusters in stimulus- and cell type-specific manners, resulting in a broad spectrum of effects (214). Zhang *et al*. used an osteosarcoma cell line with the upstream stimuli of TNF-α/TNFR1, while I used a lung adenocarcinoma cell line with the upstream stimuli of β-glucan/EphA2.

The cell-autonomous roles of NF-κB on the expression of *Cullins* also suggest a novel mode of crosstalk between the NF-κB and Nrf2 pathways. It has long been proposed that these two pathways negatively and positively affect one another via several mechanisms (215). The negative relationship between these two factors has been demonstrated at the transcriptional level, at which NF-kB and Nrf2 compete for transcriptional co-activator CBP-p300 binding (196). In contrast, positive interplay was revealed by NF-κB-induced Nrf2 transcription, leading to the up-regulation of Nrf2 protein expression (216). In the present study, the result showing that RelB regulated the expression of *CUL4A* expands our knowledge on the negative crosstalk between NF-κB and Nrf2.

In conclusion, I herein established a novel role for β-glucan in cancer therapy through its potentiation of cellular sensitivity to drugs. I demonstrated that β-glucan increased drug sensitivity by suppressing Nrf2 via a new EphA2-RelB-CUL4A pathway. This axis also potentially links cellular responses to inflammation and oxidative stress, which may be useful for the development of effective strategies to treat not only cancer, but also a broad range of diseases.

General Conclusion and Perspective

Nrf2 is the key regulator of cellular stress response, and its dysregulation contributes to the development of many diseases. A more comprehensive elucidation on the precise regulation of Nrf2 may provide additional insight for the development of therapeutic strategy to overcome Nrf2-driven pathological conditions. In the present study, WDR23 was identified as a novel regulator of Nrf2, particularly in the condition when the function of canonical Keap1 pathway is impaired. These findings raise the possibility for WDR23 as a potential therapeutic target for the treatment of pathological conditions related to hyperactivated Nrf2 such as drug-resistance in cancer. The mechanism of crosstalk between Keap1 and WDR23 involving the transcription factor Sp1 has also been elucidated in the present study, which provides a more comprehensive insight for the development of therapeutic strategy. Furthermore, the WDR23 activity toward Nrf2 is affected by the treatment with coffee polyphenol CGA and fungal cell wall component β-glucan, resulting in the elevation and depletion of Nrf2, respectively. The modulation of Nrf2 via WDR23-dependent pathway by CGA and β-glucan provides a practical utilization of small compounds and the critical role of the newly identified WDR23 pathway in lifespan determination and pathological conditions.

References

1. Dodson, M., de la Vega, M. R., Cholanians, A. B., Schmidlin, C. J., Chapman, E., and Zhang, D. D. (2019) Modulating Nrf2 in disease: timing is everything. *Annu. Rev. Pharmacol. Toxicol.* **59**, 555–575

2. Rada, P., Rojo, A. I., Chowdhry, S., McMahon, M., Hayes, J. D., and Cuadrado, A. (2011) SCF/b-TrCP promotes glycogen synthase kinase 3-dependent degradation of the Nrf2 transcription factor in a Keap1-independent manner. *Mol. Cell. Biol.* **31**, 1121–1133

3. Wu, T., Zhao, F., Gao, B., Tan, C., Yagishita, N., Nakajima, T., Wong, P. K., Chapman, E., Fang, D., and Zhang, D. D. (2014) Hrd1 suppresses Nrf2-mediated cellular protection during liver cirrhosis. *Genes Dev.* **28**, 708–722

4. Itoh, K., Wakabayashi, N., Katoh, Y., Ishii, T., Igarashi, K., Engel, J. D., and Yamamoto, M. (1999) Keap1 represses nuclear activation of antioxidant responsive elements by Nrf2 through binding to the amino-terminal Neh2 domain. *Genes Dev.* **13**, 76–86

5. Baba, K., Morimoto, H., and Imaoka, S. (2013) Seven in absentia homolog 2 (Siah2) protein is a regulator of NF-E2-related factor 2 (Nrf2). *J. Biol. Chem.* **288**, 18393–18405

6. Tong, K. I., Katoh, Y., Kusunoki, H., Itoh, K., Tanaka, T., and Yamamoto, M. (2006) Keap1 recruits Neh2 through binding to ETGE and DLG motifs: characterization of the two-site molecular recognition model. *Mol. Cell. Biol.* **26**, 2887–900

7. Dalton, T. P., Shertzer, H. G., and Puga, A. (1999) Regulation of gene expression by reactive oxygen. *Annu. Rev. Pharmacol. Toxicol.* **39**, 67–101

8. Al-Sawaf, O., Clarner, T., Fragoulis, A., Kan, Y. W., Pufe, T., Streetz, K., and Wruck, C. J. (2015) Nrf2 in health and disease: current and future clinical implications. *Clin. Sci.* **129**, 989–999

9. Tissenbaum, H. A. (2015) Using C. elegans for aging research. *Invertebr. Reprod. Dev.* **59**, 59–63

10. Walker, A. K., See, R., Batchelder, C., Kophengnavong, T., Gronniger, J. T., Shi, Y., and Blackwell, T. K. (2000) A conserved transcription motif suggesting functional parallels between Caenorhabditis elegans SKN-1 and Cap'n'Collar-related basic leucine zipper proteins. *J. Biol. Chem.* **275**, 22166–22171

11. Wang, X.-J., Sun, Z., Villeneuve, N. F., Zhang, S., Zhao, F., Li, Y., Chen, W., Yi, X., Zheng, W., Wondrak, G. T., Wong, P. K., and Zhang, D. D. (2008) Nrf2 enhances resistance of cancer cells to chemotherapeutic drugs, the dark side of Nrf2. *Carcinogenesis*. **29**, 1235–1243

12. Bai, X., Chen, Y., Hou, X., Huang, M., and Jin, J. (2016) Emerging role of NRF2 in chemoresistance by regulating drug-metabolizing enzymes and efflux transporters. *Drug Metab. Rev.* **48**, 541–567

13. Kitamura, H., and Motohashi, H. (2018) NRF2 addiction in cancer cells. *Cancer Sci.* **109**, 900–911

14. Choe, K. P., Przybysz, A. J., and Strange, K. (2009) The WD40 repeat protein WDR-23 functions with the CUL4/DDB1 ubiquitin ligase to regulate nuclear abundance and activity of SKN-1 in Caenorhabditis elegans. *Mol. Cell. Biol.* **29**, 2704–2715

15. Lee, J., and Zhou, P. (2007) DCAFs, the missing link of the CUL4-DDB1 ubiquitin ligase. *Mol. Cell*. **26**, 775–80

16. Narita, Y., and Inouye, K. (2015) Chlorogenic acids from coffee. in *Coffee in Health and Disease Prevention*, pp. 189–199, Elsevier, 10.1016/B978-0-12-409517-5.00021-8

17. Liang, N., and Kitts, D. D. (2015) Role of chlorogenic acids in controlling oxidative and inflammatory stress conditions. *Nutrients*. 10.3390/nu8010016

18. Xiang, Z., and Ning, Z. (2008) Scavenging and antioxidant properties of compound derived from chlorogenic acid in South-China honeysuckle. *LWT - Food Sci. Technol.* **41**, 1189–1203

19. Wei, M., Zheng, Z., Shi, L., Jin, Y., and Ji, L. (2018) Natural polyphenol chlorogenic acid protects against acetaminophen-induced hepatotoxicity by activating ERK/Nrf2 antioxidative pathway. *Toxicol. Sci.* **162**, 99–112

20. Liang, N., Dupuis, J. H., Yada, R. Y., and Kitts, D. D. (2019) Chlorogenic acid isomers directly interact with Keap 1-Nrf2 signaling in Caco-2 cells. *Mol. Cell. Biochem.* **457**, 105–118

21. Han, D., Gu, X., Gao, J., Wang, Z., Liu, G., Barkema, H. W., and Han, B. (2019) Chlorogenic acid promotes the Nrf2/HO-1 anti-oxidative pathway by activating p21Waf1/Cip1 to resist dexamethasone-induced apoptosis in osteoblastic cells. *Free Radic. Biol. Med.* **137**, 1–12

22. Goodridge, H. S., Wolf, A. J., and Underhill, D. M. (2009) β-glucan recognition by the innate immune system. *Immunol. Rev.* **230**, 38–50

23. Desamero, M. J. M., Chung, S.-H., and Kakuta, S. (2021) Insights on the functional role of beta-glucans in fungal immunity using receptor-deficient mouse models. *Int. J. Mol. Sci.* **22**, 4778

24. Chan, G. C.-F., Chan, W. K., and Sze, D. M.-Y. (2009) The effects of β-glucan on human immune and cancer cells. *J. Hematol. Oncol.* **2**, 25

25. Sykiotis, G. P., and Bohmann, D. (2010) Stress-activated cap'n'collar transcription tactors in aging and human disease. *Sci. Signal.* **3**, re3–re3

26. Nguyen, T., Sherratt, P. J., and Pickett, C. B. (2003) Regulatory mechanisms controlling gene expression mediated by the antioxidant response element. *Annu. Rev. Pharmacol. Toxicol.* **43**, 233–60

27. Nakata, K., Tanaka, Y., Nakano, T., Adachi, T., Tanaka, H., Kaminuma, T., and Ishikawa, T. (2006) Nuclear receptor-mediated transcriptional regulation in Phase I, II, and III xenobiotic metabolizing systems. *Drug Metab. Pharmacokinet.* **21**, 437–457

28. Klaassen, C. D., and Slitt, A. L. (2005) Regulation of hepatic transporters by xenobiotic receptors. *Curr. Drug Metab.* **6**, 309–28

29. Kwak, M.-K., Wakabayashi, N., Itoh, K., Motohashi, H., Yamamoto, M., and Kensler, T. W. (2003) Modulation of gene expression by cancer chemopreventive dithiolethiones through the Keap1-Nrf2 pathway. *J. Biol. Chem.* **278**, 8135–8145

30. Shen, G., and Kong, A.-N. (2009) Nrf2 plays an important role in coordinated regulation of Phase II drug metabolism enzymes and Phase III drug transporters. *Biopharm. Drug Dispos.* **30**, 345–355

31. Nakamura, M., Yamanaka, H., Oguro, A., and Imaoka, S. (2018) Bisphenol A induces Nrf2-dependent drug-metabolizing enzymes through nitrosylation of Keap1. *Drug Metab. Pharmacokinet.* **33**, 194–202

32. Choe, K. P., Leung, C. K., and Miyamoto, M. M. (2012) Unique structure and regulation of the nematode detoxification gene regulator, SKN-1: implications to understanding and controlling drug resistance. *Drug Metab. Rev.* **44**, 209–223

33. Angers, S., Li, T., Yi, X., MacCoss, M. J., Moon, R. T., and Zheng, N. (2006) Molecular architecture and assembly of the DDB1–CUL4A ubiquitin ligase machinery. *Nature*. **443**, 590–593

34. Jin, J., Arias, E. E., Chen, J., Harper, J. W., and Walter, J. C. (2006) A family of diverse Cul4-Ddb1-interacting proteins includes Cdt2, which is required for S phase destruction of the replication factor Cdt1. *Mol. Cell*. **23**, 709–721

35. Chen, Z., Wang, K., Hou, C., Jiang, K., Chen, B., Chen, J., Lao, L., Qian, L., Zhong, G., Liu,

Z., Zhang, C., and Shen, H. (2017) CRL4BDCAF11 E3 ligase targets p21 for degradation to control cell cycle progression in human osteosarcoma cells. *Sci. Rep.* **7**, 1175

36. Djakbarova, U., Marzluff, W. F., and Köseoğlu, M. M. (2016) DDB1 and CUL4 associated factor 11 (DCAF11) mediates degradation of Stem-loop binding protein at the end of S phase. *Cell Cycle*. **15**, 1986–96

37. Ng, P.-S., Imaoka, S., Hiroi, T., Osada, M., Niwa, T., Kamataki, T., and Funae, Y. (2003) Production of inhibitory polyclonal antibodies against cytochrome P450s. *Drug Metab. Pharmacokinet.* **18**, 163–172

38. Ueda, K., Xu, J., Morimoto, H., Kawabe, A., and Imaoka, S. (2008) MafG controls the hypoxic response of cells by accumulating HIF-1a in the nuclei. *FEBS Lett.* **582**, 2357–2364

39. Fuse, Y., and Kobayashi, M. (2017) Conservation of the Keap1-Nrf2 system: an evolutionary journey through stressful space and time. *Molecules*. **22**, 436

40. Zhang, D. D., and Hannink, M. (2003) Distinct cysteine residues in Keap1 are required for Keap1-dependent ubiquitination of Nrf2 and for stabilization of Nrf2 by chemopreventive agents and oxidative stress. *Mol. Cell. Biol.* **23**, 8137–8151

41. Hur, W., Sun, Z., Jiang, T., Mason, D. E., Peters, E. C., Zhang, D. D., Luesch, H., Schultz, P. G., and Gray, N. S. (2010) A small-molecule inducer of the antioxidant response element. *Chem. Biol.* **17**, 537–547

42. Lo, J. Y., Spatola, B. N., and Curran, S. P. (2017) WDR23 regulates NRF2 independently of KEAP1. *PLOS Genet.* **13**, e1006762

43. Siswanto, F. M., Oguro, A., Arase, S., and Imaoka, S. (2020) WDR23 regulates the expression of Nrf2-driven drug-metabolizing enzymes. *Drug Metab. Pharmacokinet.* **35**, 441–455

44. Tong, K. I., Padmanabhan, B., Kobayashi, A., Shang, C., Hirotsu, Y., Yokoyama, S., and Yamamoto, M. (2007) Different electrostatic potentials define ETGE and DLG motifs as hinge and latch in oxidative stress response. *Mol. Cell. Biol.* **27**, 7511–7521

45. Suzuki, T., Muramatsu, A., Saito, R., Iso, T., Shibata, T., Kuwata, K., Kawaguchi, S.-I., Iwawaki, T., Adachi, S., Suda, H., Morita, M., Uchida, K., Baird, L., and Yamamoto, M. (2019) Molecular mechanism of cellular oxidative stress sensing by Keap1. *Cell Rep.* **28**, 746-758.e4

46. Kobayashi, M., Li, L., Iwamoto, N., Nakajima-Takagi, Y., Kaneko, H., Nakayama, Y., Eguchi, M., Wada, Y., Kumagai, Y., and Yamamoto, M. (2009) The Antioxidant Defense System Keap1-Nrf2 Comprises a Multiple Sensing Mechanism for Responding to a Wide Range of Chemical Compounds. *Mol. Cell. Biol.* **29**, 493–502

47. Feng, R., Lu, Y., Bowman, L. L., Qian, Y., Castranova, V., and Ding, M. (2005) Inhibition of activator protein-1, NF-kappaB, and MAPKs and induction of phase 2 detoxifying enzyme activity by chlorogenic acid. *J. Biol. Chem.* **280**, 27888–95

48. Singh, A., Misra, V., Thimmulappa, R. K., Lee, H., Ames, S., Hoque, M. O., Herman, J. G., Baylin, S. B., Sidransky, D., Gabrielson, E., Brock, M. V, and Biswal, S. (2006) Dysfunctional KEAP1-NRF2 interaction in non-small-cell lung cancer. *PLoS Med.* **3**, e420

49. Suzuki, A., Kawano, S., Mitsuyama, T., Suyama, M., Kanai, Y., Shirahige, K., Sasaki, H., Tokunaga, K., Tsuchihara, K., Sugano, S., Nakai, K., and Suzuki, Y. (2018) DBTSS/DBKERO for integrated analysis of transcriptional regulation. *Nucleic Acids Res.* **46**, D229–D238

50. Fiaschi, T., and Chiarugi, P. (2012) Oxidative stress, tumor microenvironment, and metabolic reprogramming: a diabolic liaison. *Int. J. Cell Biol.* **2012**, 1–8

51. Reuter, S., Gupta, S. C., Chaturvedi, M. M., and Aggarwal, B. B. (2010) Oxidative stress, inflammation, and cancer: How are they linked? *Free Radic. Biol. Med.* **49**, 1603–1616

52. Spatola, B. N., Lo, J. Y., Wang, B., and Curran, S. P. (2019) Nuclear and cytoplasmic WDR-23 isoforms mediate differential effects on GEN-1 and SKN-1 substrates. *Sci. Rep.* **9**, 11783

53. Kaspar, J. W., and Jaiswal, A. K. (2011) Tyrosine phosphorylation controls nuclear export of Fyn, allowing Nrf2 activation of cytoprotective gene expression. *FASEB J.* **25**, 1076–1087

54. Kosugi, S., Yanagawa, H., Terauchi, R., and Tabata, S. (2014) NESmapper: accurate prediction of leucine-rich nuclear export signals using activity-based profiles. *PLoS Comput. Biol.* **10**, e1003841

55. la Cour, T., Kiemer, L., Mølgaard, A., Gupta, R., Skriver, K., and Brunak, S. (2004) Analysis and prediction of leucine-rich nuclear export signals. *Protein Eng. Des. Sel.* **17**, 527–536

56. Guerrero-Santoro, J., Kapetanaki, M. G., Hsieh, C. L., Gorbachinsky, I., Levine, A. S., and Rapic-Otrin, V. (2008) The Cullin 4B-Based UV-Damaged DNA-Binding Protein Ligase Binds to UV-Damaged Chromatin and Ubiquitinates Histone H2A. *Cancer Res.* **68**, 5014–5022

57. Zou, Y., Mi, J., Cui, J., Lu, D., Zhang, X., Guo, C., Gao, G., Liu, Q., Chen, B., Shao, C., and Gong, Y. (2009) Characterization of nuclear localization signal in the N terminus of CUL4B and its essential role in cyclin E degradation and cell cycle progression. *J. Biol. Chem.* **284**, 33320–33332

58. Liu, W., Nichols, A. F., Graham, J. A., Dualan, R., Abbas, A., and Linn, S. (2000) Nuclear transport of human DDB protein induced by ultraviolet light. *J. Biol. Chem.* **275**, 21429–21434

59. Furukawa, M., Zhang, Y., McCarville, J., Ohta, T., and Xiong, Y. (2000) The CUL1 C-terminal sequence and ROC1 are required for efficient nuclear accumulation, NEDD8 modification, and ubiquitin ligase activity of CUL1. *Mol. Cell. Biol.* **20**, 8185–8197

60. Sarikas, A., Hartmann, T., and Pan, Z.-Q. (2011) The cullin protein family. *Genome Biol.* **12**, 220

61. Abu-Bakar, A., Lamsa, V., Arpiainen, S., Moore, M. R., Lang, M. A., and Hakkola, J. (2007) Regulation of CYP2A5 gene by the transcription factor nuclear factor (erythroid-derived 2)-like 2. *Drug Metab. Dispos.* **35**, 787–794

62. Wu, K. C., Cui, J. Y., and Klaassen, C. D. (2012) Effect of graded Nrf2 activation on phase-I and -II drug metabolizing enzymes and transporters in mouse liver. *PLoS One*. **7**, e39006

63. Su, S., Yang, X., and Omiecinski, C. J. (2014) Intronic DNA elements regulate Nrf2 chemical responsiveness of the human microsomal epoxide hydrolase gene (EPHX1) through a far upstream alternative promoter. *Biochim. Biophys. Acta*. **1839**, 493–505

64. Malhotra, D., Portales-Casamar, E., Singh, A., Srivastava, S., Arenillas, D., Happel, C., Shyr, C., Wakabayashi, N., Kensler, T. W., Wasserman, W. W., and Biswal, S. (2010) Global mapping of binding sites for Nrf2 identifies novel targets in cell survival response through ChIP-Seq profiling and network analysis. *Nucleic Acids Res.* **38**, 5718–34

65. Kaur, G., and Dufour, J. M. (2012) Cell lines: Valuable tools or useless artifacts. *Spermatogenesis*. **2**, 1–5

66. Yueh, M.-F., and Tukey, R. H. (2007) Nrf2-Keap1 signaling pathway regulates human UGT1A1 expression in vitro and in transgenic UGT1 mice. *J. Biol. Chem.* **282**, 8749–8758

67. Kalthoff, S., Ehmer, U., Freiberg, N., Manns, M. P., and Strassburg, C. P. (2010) Interaction between oxidative stress sensor Nrf2 and xenobiotic-activated aryl hydrocarbon receptor in the regulation of the human phase II detoxifying UDP-glucuronosyltransferase 1A10. *J. Biol. Chem.* **285**, 5993–6002

68. Penner, N., Woodward, C., and Prakash, C. (2012) Appendix: Drug metabolizing enzymes and biotransformation reactions. in *ADME-Enabling Technologies in Drug Design and*

Development, pp. 545–565, 10.1002/9781118180778.app1

69. Wang, Z., Wang, L., Xu, R., Zhan, Y., Huang, C., Dai, D., Cai, J., and Hu, G. (2016) Role of cytochrome P450 2D6 genetic polymorphism in carvedilol hydroxylation in vitro. *Drug Des. Devel. Ther.* 10.2147/DDDT.S106175

70. Cairns, W., Smith, C. A., McLaren, A. W., and Wolf, C. R. (1996) Characterization of the human cytochrome P4502D6 promoter. A potential role for antagonistic interactions between members of the nuclear receptor family. *J. Biol. Chem.* **271**, 25269–76

71. Jover, R., Bort, R., Gómez-Lechón, M. J., and Castell, J. V (1998) Re-expression of C/EBPα induces CYP2B6, CYP2C9 and CYP2D6 genes in HepG2 cells. *FEBS Lett.* **431**, 227–230

72. Sugatani, J., Osabe, M., Kurosawa, M., Kitamura, N., Ikari, A., and Miwa, M. (2010) Induction of UGT1A1 and CYP2B6 by an antimitogenic factor in HepG2 cells is mediated through suppression of cyclin-dependent kinase 2 activity: cell cycle-dependent expression. *Drug Metab. Dispos.* **38**, 177–186

73. Zhang, C., Chen, B., Jiang, K., Lao, L., Shen, H., and Chen, Z. (2018) Activation of TNF-α/NF-κB axis enhances CRL4BDCAF11 E3 ligase activity and regulates cell cycle progression in human osteosarcoma cells. *Mol. Oncol.* **12**, 476–494

74. Lawrence, M. S., Stojanov, P., Mermel, C. H., Robinson, J. T., Garraway, L. A., Golub, T. R., Meyerson, M., Gabriel, S. B., Lander, E. S., and Getz, G. (2014) Discovery and saturation analysis of cancer genes across 21 tumour types. *Nature*. **505**, 495–501

75. Jaramillo, M. C., and Zhang, D. D. (2013) The emerging role of the Nrf2-Keap1 signaling pathway in cancer. *Genes Dev.* **27**, 2179–2191

76. Frank, R., Scheffler, M., Merkelbach-Bruse, S., Ihle, M. A., Kron, A., Rauer, M., Ueckeroth, F., König, K., Michels, S., Fischer, R., Eisert, A., Fassunke, J., Heydt, C., Serke, M., Ko, Y.-D., Gerigk, U., Geist, T., Kaminsky, B., Heukamp, L. C., Clement-Ziza, M., Büttner, R., and Wolf, J. (2018) Clinical and Pathological Characteristics of KEAP1- and NFE2L2-Mutated Non–Small Cell Lung Carcinoma (NSCLC). *Clin. Cancer Res.* **24**, 3087–3096

77. Namani, A., Matiur Rahaman, M., Chen, M., and Tang, X. (2018) Gene-expression signature regulated by the KEAP1-NRF2-CUL3 axis is associated with a poor prognosis in head and neck squamous cell cancer. *BMC Cancer*. **18**, 46

78. Konstantinopoulos, P. A., Spentzos, D., Fountzilas, E., Francoeur, N., Sanisetty, S., Grammatikos, A. P., Hecht, J. L., and Cannistra, S. A. (2011) Keap1 mutations and Nrf2 pathway activation in epithelial ovarian cancer. *Cancer Res.* **71**, 5081–5089

79. Stewart, D., Killeen, E., Naquin, R., Alam, S., and Alam, J. (2003) Degradation of transcription factor Nrf2 via the ubiquitin-proteasome pathway and stabilization by cadmium. *J. Biol. Chem.* **278**, 2396–2402

80. Nguyen, T., Sherratt, P. J., Huang, H.-C., Yang, C. S., and Pickett, C. B. (2003) Increased protein stability as a mechanism that enhances Nrf2-mediated transcriptional activation of the antioxidant response element. *J. Biol. Chem.* **278**, 4536–4541

81. Dinkova-Kostova, A. T., Kostov, R. V., and Canning, P. (2017) Keap1, the cysteine-based mammalian intracellular sensor for electrophiles and oxidants. *Arch. Biochem. Biophys.* **617**, 84–93

82. Thimmulappa, R. K., Mai, K. H., Srisuma, S., Kensler, T. W., Yamamoto, M., and Biswal, S. (2002) Identification of Nrf2-regulated genes induced by the chemopreventive agent sulforaphane by oligonucleotide microarray. *Cancer Res.* **62**, 5196–203

83. Itoh, K., Chiba, T., Takahashi, S., Ishii, T., Igarashi, K., Katoh, Y., Oyake, T., Hayashi, N., Satoh, K., Hatayama, I., Yamamoto, M., and Nabeshima, Y. (1997) An Nrf2/small Maf heterodimer mediates the induction of phase II detoxifying enzyme genes through antioxidant response elements. *Biochem. Biophys. Res. Commun.* **236**, 313–322

84. Curran, S. P., and Lo, J. Y. (2016) WDR23 is an ancient regulator of NRF2-dependent cytoprotection in humans. *Gerontologist*. **56**, 650–650

85. Zhou, Z., Song, X., Wavelet, C. M., and Wan, Y. (2020) Cullin 4-DCAF proteins in tumorigenesis. in *Cullin-RING Ligases and Protein Neddylation*, pp. 241–259, 10.1007/978-981-15-1025-0_15

86. Le, R., Huang, Y., Zhang, Y., Wang, H., Lin, J., Dong, Y., Li, Z., Guo, M., Kou, X., Zhao, Y., Chen, M., Zhu, Q., Zhao, A., Yin, J., Sun, J., Su, Z., Shi, K., Gao, Y., Chen, J., Liu, W., Kang, L., Wang, Y., Li, C., Liu, X., Gao, R., Wang, H., Ju, Z., and Gao, S. (2021) Dcaf11 activates Zscan4-mediated alternative telomere lengthening in early embryos and embryonic stem cells. *Cell Stem Cell*. **28**, 732-747.e9

87. Wang, K., Liu, Y., Yu, Z., Gu, B., Hu, J., Huang, L., Ge, X., Xu, L., Zhang, M., Zhao, J., Hu, M., Le, R., Wu, Q., Ye, S., Gao, S., Zhang, X., Xu, R.-M., and Li, G. (2021) Phosphorylation at Ser68 facilitates DCAF11-mediated ubiquitination and degradation of CENP-A during the cell cycle. *Cell Rep.* **37**, 109987

88. Wu, S., Lu, H., and Bai, Y. (2019) Nrf2 in cancers: A double-edged sword. *Cancer Med.* **8**, 2252–2267

89. Kerins, M. J., and Ooi, A. (2018) A catalogue of somatic NRF2 gain-of-function mutations in cancer. *Sci. Rep.* **8**, 12846

90. Meissner, M., Stein, M., Urbich, C., Reisinger, K., Suske, G., Staels, B., Kaufmann, R., and Gille, J. (2004) PPARα activators inhibit vascular endothelial growth factor receptor-2 expression by repressing Sp1-dependent DNA binding and transactivation. *Circ. Res.* **94**, 324–332

91. Canaff, L., Zhou, X., and Hendy, G. N. (2008) The proinflammatory cytokine, interleukin-6, up-regulates calcium-sensing receptor gene transcription via Stat1/3 and Sp1/3. *J. Biol. Chem.* **283**, 13586–13600

92. Fridmacher, V., Kaltschmidt, B., Goudeau, B., Ndiaye, D., Rossi, F. M., Pfeiffer, J., Kaltschmidt, C., Israël, A., and Mémet, S. (2003) Forebrain-specific neuronal inhibition of nuclear factor-κB activity leads to loss of neuroprotection. *J. Neurosci.* **23**, 9403–9408

93. Khachigian, L. M., Lindner, V., Williams, A. J., and Collins, T. (1996) Egr-1-induced endothelial gene expression: a common theme in vascular injury. *Science (80-.).* **271**, 1427–1431

94. Nagaoka, M. (2001) Selected base sequence outside the target binding site of zinc finger protein Sp1. *Nucleic Acids Res.* **29**, 4920–4929

95. Wierstra, I. (2008) Sp1: Emerging roles—Beyond constitutive activation of TATA-less housekeeping genes. *Biochem. Biophys. Res. Commun.* **372**, 1–13

96. Samson, S., and Wong, N. (2002) Role of Sp1 in insulin regulation of gene expression. *J. Mol. Endocrinol.* 10.1677/jme.0.0290265

97. Oguro, A., Oida, S., and Imaoka, S. (2015) Down-regulation of EPHX2 gene transcription by Sp1 under high-glucose conditions. *Biochem. J.* **470**, 281–291

98. Ryu, H., Lee, J., Zaman, K., Kubilis, J., Ferrante, R. J., Ross, B. D., Neve, R., and Ratan, R. R. (2003) Sp1 and Sp3 are oxidative stress-inducible, antideath transcription factors in cortical neurons. *J. Neurosci.* **23**, 3597–3606

99. Schäfer, G., Cramer, T., Suske, G., Kemmner, W., Wiedenmann, B., and Höcker, M. (2003) Oxidative stress regulates vascular endothelial growth factor-A gene transcription through Sp1- and Sp3-dependent activation of two proximal GC-rich promoter elements. *J. Biol. Chem.* **278**, 8190–8198

100. Chhunchha, B., Fatma, N., Bhargavan, B., Kubo, E., Kumar, A., and Singh, D. P. (2011) Specificity protein, Sp1-mediated increased expression of Prdx6 as a curcumin-induced

antioxidant defense in lens epithelial cells against oxidative stress. *Cell Death Dis.* **2**, e234–e234

101. Tillu, H., and Bramhachari, P. V. (2017) Role of Sp1 in liver cancer. in *Role of Transcription Factors in Gastrointestinal Malignancies*, pp. 495–508, Springer Singapore, Singapore, 10.1007/978-981-10-6728-0_37

102. Kobayashi, Y., Oguro, A., and Imaoka, S. (2021) Feedback of hypoxia-inducible factor-1alpha (HIF-1alpha) transcriptional activity via redox factor-1 (Ref-1) induction by reactive oxygen species (ROS). *Free Radic. Res.* **55**, 154–164

103. Li, W.-C., Ralphs, K. L., and Tosh, D. (2010) Isolation and culture of adult mouse hepatocytes, pp. 185–196, 10.1007/978-1-59745-019-5_13

104. Fornes, O., Castro-Mondragon, J. A., Khan, A., van der Lee, R., Zhang, X., Richmond, P. A., Modi, B. P., Correard, S., Gheorghe, M., Baranašić, D., Santana-Garcia, W., Tan, G., Chèneby, J., Ballester, B., Parcy, F., Sandelin, A., Lenhard, B., Wasserman, W. W., and Mathelier, A. (2019) JASPAR 2020: update of the open-access database of transcription factor binding profiles. *Nucleic Acids Res.* 10.1093/nar/gkz1001

105. Kent, W. J. (2002) BLAT---The BLAST-Like Alignment Tool. *Genome Res.* **12**, 656–664

106. Lee, D.-F., Kuo, H.-P., Liu, M., Chou, C.-K., Xia, W., Du, Y., Shen, J., Chen, C.-T., Huo, L., Hsu, M.-C., Li, C.-W., Ding, Q., Liao, T.-L., Lai, C.-C., Lin, A.-C., Chang, Y.-H., Tsai, S.-F., Li, L.-Y., and Hung, M.-C. (2009) KEAP1 E3 ligase-mediated downregulation of NF-κB signaling by targeting IKKβ. *Mol. Cell*. **36**, 131–140

107. Kim, J.-E., You, D.-J., Lee, C., Ahn, C., Seong, J. Y., and Hwang, J.-I. (2010) Suppression of NF-κB signaling by KEAP1 regulation of IKKβ activity through autophagic degradation and inhibition of phosphorylation. *Cell. Signal.* **22**, 1645–1654

108. Kerppola, T. K. (2008) Bimolecular fluorescence complementation (BiFC) analysis as a probe of protein interactions in living cells. *Annu. Rev. Biophys.* **37**, 465–487

109. Panieri, E., and Saso, L. (2019) Potential applications of NRF2 inhibitors in cancer therapy. *Oxid. Med. Cell. Longev.* **2019**, 1–34

110. Taguchi, K., and Yamamoto, M. (2017) The KEAP1–NRF2 system in cancer. *Front. Oncol.* 10.3389/fonc.2017.00085

111. Hayes, J. D., and McMahon, M. (2009) NRF2 and KEAP1 mutations: permanent activation of an adaptive response in cancer. *Trends Biochem. Sci.* **34**, 176–188

112. Miranda-Carboni, G. A., Krum, S. A., Yee, K., Nava, M., Deng, Q. E., Pervin, S., Collado-Hidalgo, A., Galic, Z., Zack, J. A., Nakayama, K., Nakayama, K. I., and Lane, T. F. (2008) A functional link between Wnt signaling and SKP2-independent p27 turnover in mammary tumors. *Genes Dev.* **22**, 3121–3134

113. Ashok, C., Owais, S., Srijyothi, L., Selvam, M., Ponne, S., and Baluchamy, S. (2019) A feedback regulation of CREB activation through the CUL4A and ERK signaling. *Med. Oncol.* **36**, 20

114. Deniaud, E., Baguet, J., Chalard, R., Blanquier, B., Brinza, L., Meunier, J., Michallet, M.-C., Laugraud, A., Ah-Soon, C., Wierinckx, A., Castellazzi, M., Lachuer, J., Gautier, C., Marvel, J., and Leverrier, Y. (2009) Overexpression of Transcription Factor Sp1 Leads to Gene Expression Perturbations and Cell Cycle Inhibition. *PLoS One*. **4**, e7035

115. Burger, A. M., Kona, F., Amemiya, Y., Gao, Y., Bacopulos, S., and Seth, A. K. (2010) Role of the BCA2 ubiquitin E3 ligase in hormone responsive breast cancer. *Open Cancer J.* **3**, 116–123

116. Ge, W., Zhao, K., Wang, X., Li, H., Yu, M., He, M., Xue, X., Zhu, Y., Zhang, C., Cheng, Y., Jiang, S., and Hu, Y. (2017) iASPP is an antioxidative factor and drives cancer growth and drug resistance by competing with Nrf2 for Keap1 binding. *Cancer Cell*. **32**, 561-573.e6

117. Wei, S., Chuang, H.-C., Tsai, W.-C., Yang, H.-C., Ho, S.-R., Paterson, A. J., Kulp, S. K., and Chen, C.-S. (2009) Thiazolidinediones mimic glucose starvation in facilitating Sp1 degradation through the up-regulation of β-transducin repeat-containing protein. *Mol. Pharmacol.* **76**, 47–57

118. Wang, Y.-T., Chang, W.-C., and Hung, J.-J. (2009) RNF4 acted as an ubiquitin E3 ligase involved in ubiquitin-dependent degradation of Sumoylated-Sp1. *FASEB J.* **23**, 878.2-878.2

119. Wang, Y.-T., Yang, W.-B., Chang, W.-C., and Hung, J.-J. (2011) Interplay of posttranslational modifications in Sp1 mediates Sp1 stability during cell cycle progression. *J. Mol. Biol.* **414**, 1–14

120. Yeh, S. H., Yang, W. Bin, Gean, P. W., Hsu, C. Y., Tseng, J. T., Su, T. P., Chang, W. C., and Hung, J. J. (2011) Translational and transcriptional control of Sp1 against ischaemia through a hydrogen peroxide-activated internal ribosomal entry site pathway. *Nucleic Acids Res.* **39**, 5412–5423

121. Guo, D., Wu, B., Yan, J., Li, X., Sun, H., and Zhou, D. (2012) A possible gene silencing mechanism: Hypermethylation of the Keap1 promoter abrogates binding of the transcription factor Sp1 in lung cancer cells. *Biochem. Biophys. Res. Commun.* **428**, 80–85

122. Vizcaíno, C., Mansilla, S., and Portugal, J. (2015) Sp1 transcription factor: A long-standing target in cancer chemotherapy. *Pharmacol. Ther.* **152**, 111–124

123. Safe, S., Abbruzzese, J., Abdelrahim, M., and Hedrick, E. (2018) Specificity protein transcription factors and cancer: Opportunities for drug development. *Cancer Prev. Res.* **11**, 371–382

124. Li, C., Bu, J., Liao, Y., Zhang, J., Han, J., Zhang, H., Xing, H., Li, Z., Wu, H., Liang, L., Wang, M., Qin, W., and Yang, T. (2018) High expressions of CUL4A and TP53 in colorectal cancer predict poor survival. *Cell. Physiol. Biochem.* **51**, 2829–2842

125. Sharma, P., and Nag, A. (2014) CUL4A ubiquitin ligase: a promising drug target for cancer and other human diseases. *Open Biol.* **4**, 130217

126. Beishline, K., and Azizkhan-Clifford, J. (2015) Sp1 and the 'hallmarks of cancer.' *FEBS J.* **282**, 224–258

127. Siswanto, F. M., Oguro, A., and Imaoka, S. (2021) Sp1 is a substrate of Keap1 and regulates the activity of CRL4A(WDR23) ubiquitin ligase toward Nrf2. *J. Biol. Chem.* **296**, 100704

128. Brown-Borg, H. M., and Rakoczy, S. G. (2005) Glutathione metabolism in long-living Ames dwarf mice. *Exp. Gerontol.* **40**, 115–120

129. Lewis, K. N., Wason, E., Edrey, Y. H., Kristan, D. M., Nevo, E., and Buffenstein, R. (2015) Regulation of Nrf2 signaling and longevity in naturally long-lived rodents. *Proc. Natl. Acad. Sci.* **112**, 3722–3727

130. Davinelli, S., Willcox, D. C., and Scapagnini, G. (2012) Extending healthy ageing: nutrient sensitive pathway and centenarian population. *Immun. Ageing*. **9**, 9

131. Kanner, J. (2020) Polyphenols by generating H2O2, affect cell redox signaling, inhibit PTPs and activate Nrf2 axis for adaptation and cell surviving: in vitro, in vivo and human health. *Antioxidants*. **9**, 797

132. Wianowska, D., and Gil, M. (2019) Recent advances in extraction and analysis procedures of natural chlorogenic acids. *Phytochem. Rev.* **18**, 273–302

133. Duregon, E., Bernier, M., and de Cabo, R. (2020) A glance back at the Journal of Gerontology—Coffee, dietary interventions and life span. *Journals Gerontol. Ser. A*. **75**, 2029–2030

134. Hada, Y., Uchida, H. A., Otaka, N., Onishi, Y., Okamoto, S., Nishiwaki, M., Takemoto, R., Takeuchi, H., and Wada, J. (2020) The protective effect of chlorogenic acid on vascular senescence via the Nrf2/HO-1 pathway. *Int. J. Mol. Sci.* **21**, 4527

135. Liu, D., Wang, H., Zhang, Y., and Zhang, Z. (2020) Protective effects of chlorogenic acid on cerebral ischemia/reperfusion injury rats by regulating oxidative stress-related Nrf2 pathway. *Drug Des. Devel. Ther.* **14**, 51–60

136. Stiernagle, T. (2006) Maintenance of C. elegans. *WormBook*. 10.1895/wormbook.1.101.1

137. Sutphin, G. L., and Kaeberlein, M. (2009) Measuring Caenorhabditis elegans life span on solid media. *J. Vis. Exp.* 10.3791/1152

138. Park, H.-E. H., Jung, Y., and Lee, S.-J. V. (2017) Survival assays using Caenorhabditis elegans. *Mol. Cells*. **40**, 90–99

139. Heintzman, N. D., Stuart, R. K., Hon, G., Fu, Y., Ching, C. W., Hawkins, R. D., Barrera, L. O., Van Calcar, S., Qu, C., Ching, K. A., Wang, W., Weng, Z., Green, R. D., Crawford, G. E., and Ren, B. (2007) Distinct and predictive chromatin signatures of transcriptional promoters and enhancers in the human genome. *Nat. Genet.* **39**, 311–318

140. Ghosh, D. (2000) Object-oriented Transcription Factors Database (ooTFD). *Nucleic Acids Res.* **28**, 308–310

141. Kops, G. J. P. L., Dansen, T. B., Polderman, P. E., Saarloos, I., Wirtz, K. W. A., Coffer, P. J., Huang, T.-T., Bos, J. L., Medema, R. H., and Burgering, B. M. T. (2002) Forkhead transcription factor FOXO3a protects quiescent cells from oxidative stress. *Nature*. **419**, 316–321

142. Nemoto, S., and Finkel, T. (2002) Redox regulation of forkhead proteins through a p66shc-dependent signaling pathway. *Science*. **295**, 2450–2

143. Zanella, F., Rosado, A., García, B., Carnero, A., and Link, W. (2008) Chemical genetic analysis of FOXO nuclear-cytoplasmic shuttling by using image-based cell screening. *ChemBioChem*. **9**, 2229–2237

144. Brunet, A., Bonni, A., Zigmond, M. J., Lin, M. Z., Juo, P., Hu, L. S., Anderson, M. J., Arden, K. C., Blenis, J., and Greenberg, M. E. (1999) Akt promotes cell survival by phosphorylating and inhibiting a Forkhead transcription factor. *Cell*. **96**, 857–868

145. Putker, M., Vos, H. R., van Dorenmalen, K., de Ruiter, H., Duran, A. G., Snel, B., Burgering, B. M. T., Vermeulen, M., and Dansen, T. B. (2015) Evolutionary acquisition of cysteines determines FOXO paralog-specific redox signaling. *Antioxid. Redox Signal.* **22**, 15–28

146. Lacasse, V., Beaudoin, S., Jean, S., and Leyton, J. V. (2020) A novel proteomic method reveals NLS tagging of T-DM1 contravenes classical nuclear transport in a model of HER2-positive breast cancer. *Mol. Ther. - Methods Clin. Dev.* **19**, 99–119

147. Wang, X., Hu, S., and Liu, L. (2017) Phosphorylation and acetylation modifications of FOXO3a: independently or synergistically? *Oncol. Lett.* **13**, 2867–2872

148. Tullet, J. M. A., Hertweck, M., An, J. H., Baker, J., Hwang, J. Y., Liu, S., Oliveira, R. P., Baumeister, R., and Blackwell, T. K. (2008) Direct inhibition of the longevity-promoting factor SKN-1 by insulin-like signaling in C. elegans. *Cell*. **132**, 1025–38

149. Kwon, E.-S., Narasimhan, S. D., Yen, K., and Tissenbaum, H. A. (2010) A new DAF-16 isoform regulates longevity. *Nature*. **466**, 498–502

150. Balaji, V., and Hoppe, T. (2020) Regulation of E3 ubiquitin ligases by homotypic and heterotypic assembly. *F1000Research*. **9**, 88

151. Vittal, R., Selvanayagam, Z. E., Sun, Y., Hong, J., Liu, F., Chin, K.-V., and Yang, C. S. (2004) Gene expression changes induced by green tea polyphenol (-)-epigallocatechin-3-gallate in human bronchial epithelial 21BES cells analyzed by DNA microarray. *Mol. Cancer Ther.* **3**, 1091–9

152. Kim, H., Park, J., Kang, H., Yun, S. P., Lee, Y.-S., Lee, Y.-I., and Lee, Y. (2020) Activation of the Akt1-CREB pathway promotes RNF146 expression to inhibit PARP1-mediated neuronal death. *Sci. Signal.* 10.1126/scisignal.aax7119

153. Nichols, A. F. (2003) Basal transcriptional regulation of human damage-specific DNA-binding protein genes DDB1 and DDB2 by Sp1, E2F, N-myc and NF1 elements. *Nucleic Acids Res.* **31**, 562–569

154. Guan, L., Zhang, L., Gong, Z., Hou, X., Xu, Y., Feng, X., Wang, H., and You, H. (2016) FoxO3 inactivation promotes human cholangiocarcinoma tumorigenesis and chemoresistance through Keap1-Nrf2 signaling. *Hepatology*. **63**, 1914–1927

155. Webb, A. E., Kundaje, A., and Brunet, A. (2016) Characterization of the direct targets of FOXO transcription factors throughout evolution. *Aging Cell*. **15**, 673–685

156. Lu, M., Hartmann, D., Braren, R., Gupta, A., Wang, B., Wang, Y., Mogler, C., Cheng, Z., Wirth, T., Friess, H., Kleeff, J., Hüser, N., and Sunami, Y. (2019) Oncogenic Akt-FOXO3 loop favors tumor-promoting modes and enhances oxidative damage-associated hepatocellular carcinogenesis. *BMC Cancer*. **19**, 887

157. Ramaswamy, S., Nakamura, N., Sansal, I., Bergeron, L., and Sellers, W. R. (2002) A novel mechanism of gene regulation and tumor suppression by the transcription factor FKHR. *Cancer Cell*. **2**, 81–91

158. Gao, J., He, X., Ma, Y., Zhao, X., Hou, X., Hao, E., Deng, J., and Bai, G. (2018) Chlorogenic acid targeting of the AKT PH domain activates AKT/GSK3β/FOXO1 signaling and improves glucose metabolism. *Nutrients*. **10**, 1366

159. Davy, P. M. C., Allsopp, R. C., Donlon, T. A., Morris, B. J., Willcox, D. C., and Willcox, B. J. (2018) FOXO3 and exceptional longevity: insights from hydra to humans. *Curr. Top. Dev. Biol.* **127**, 193–212

160. Morris, B. J., Willcox, D. C., Donlon, T. A., and Willcox, B. J. (2015) FOXO3: a major gene for human longevity - a mini-review. *Gerontology*. **61**, 515–525

161. Raghavachari, N. (2020) The impact of apolipoprotein E genetic variability in health and life span. *Journals Gerontol. Ser. A*. **75**, 1855–1857

162. Zheng, S.-Q., Huang, X.-B., Xing, T.-K., Ding, A.-J., Wu, G.-S., and Luo, H.-R. (2017) Chlorogenic Acid Extends the Lifespan of Caenorhabditis elegans via Insulin/IGF-1 Signaling Pathway. *J. Gerontol. A. Biol. Sci. Med. Sci.* **72**, 464–472

163. Siegel, R. L., Miller, K. D., Fuchs, H. E., and Jemal, A. (2021) Cancer statistics, 2021. *CA. Cancer J. Clin.* **71**, 7–33

164. Montecucco, A., Zanetta, F., and Biamonti, G. (2015) Molecular mechanisms of etoposide. *EXCLI J.* **14**, 95–108

165. Boolell, V., Alamgeer, M., Watkins, D., and Ganju, V. (2015) The evolution of therapies in non-small cell lung cancer. *Cancers (Basel).* **7**, 1815–1846

166. Lardinois, D., Suter, H., Hakki, H., Rousson, V., Betticher, D., and Ris, H.-B. (2005) Morbidity, survival, and site of recurrence after mediastinal lymph-node dissection versus systematic sampling after complete resection for non-small cell lung cancer. *Ann. Thorac. Surg.* **80**, 268–275

167. Salem, A., Asselin, M.-C., Reymen, B., Jackson, A., Lambin, P., West, C. M. L., O'Connor, J. P. B., and Faivre-Finn, C. (2018) Targeting hypoxia to improve non–small cell lung cancer outcome. *JNCI J. Natl. Cancer Inst.* **110**, 14–30

168. Fischer, C., Leithner, K., Wohlkoenig, C., Quehenberger, F., Bertsch, A., Olschewski, A., Olschewski, H., and Hrzenjak, A. (2015) Panobinostat reduces hypoxia-induced cisplatin resistance of non-small cell lung carcinoma cells via HIF-1α destabilization. *Mol. Cancer*. **14**, 4

169. Wu, H.-M., Jiang, Z.-F., Ding, P.-S., Shao, L.-J., and Liu, R.-Y. (2015) Hypoxia-induced autophagy mediates cisplatin resistance in lung cancer cells. *Sci. Rep.* **5**, 12291

170. Yamazaki, S., Higuchi, Y., Ishibashi, M., Hashimoto, H., Yasunaga, M., Matsumura, Y.,

Tsuchihara, K., Tsuboi, M., Goto, K., Ochiai, A., and Ishii, G. (2018) Collagen type I induces EGFR-TKI resistance in EGFR-mutated cancer cells by mTOR activation through Akt-independent pathway. *Cancer Sci.* **109**, 2063–2073

171. Ma, C., Lv, Q., Zhang, K., Tang, Y., Zhang, Y., Shen, Y., Lei, H., and Zhu, L. (2021) NRF2-GPX4/SOD2 axis imparts resistance to EGFR-tyrosine kinase inhibitors in non-small-cell lung cancer cells. *Acta Pharmacol. Sin.* **42**, 613–623

172. Gottesman, M. M. (2002) Mechanisms of cancer drug resistance. *Annu. Rev. Med.* **53**, 615–627

173. Bauer, A. K., Hill, T., and Alexander, C.-M. (2013) The involvement of NRF2 in lung cancer. *Oxid. Med. Cell. Longev.* **2013**, 1–10

174. Tsuchida, K., Tsujita, T., Hayashi, M., Ojima, A., Keleku-Lukwete, N., Katsuoka, F., Otsuki, A., Kikuchi, H., Oshima, Y., Suzuki, M., and Yamamoto, M. (2017) Halofuginone enhances the chemo-sensitivity of cancer cells by suppressing NRF2 accumulation. *Free Radic. Biol. Med.* **103**, 236–247

175. Lin, S.-R., Fu, Y.-S., Tsai, M.-J., Cheng, H., and Weng, C.-F. (2017) Natural compounds from herbs that can potentially execute as autophagy inducers for cancer therapy. *Int. J. Mol. Sci.* **18**, 1412

176. Surien, O., Rohi Ghazali, A., and Fathiah Masre, S. (2019) Lung cancers and the roles of natural compounds as potential chemotherapeutic and chemopreventive agents. *Biomed. Pharmacol. J.* **12**, 85–98

177. Tang, X., BI, H., Feng, J., and Cao, J. (2005) Effect of curcumin on multidrug resistance in resistant human gastric carcinoma cell line SGC7901/VCR. *Acta Pharmacol. Sin.* **26**, 1009–1016

178. Wang, Y., Zhou, Y., Zheng, Z., Li, J., Yan, Y., and Wu, W. (2018) Sulforaphane metabolites reduce resistance to paclitaxel via microtubule disruption. *Cell Death Dis.* **9**, 1134

179. Datta, S., and Sinha, D. (2019) EGCG maintained Nrf2-mediated redox homeostasis and minimized etoposide resistance in lung cancer cells. *J. Funct. Foods*. **62**, 103553

180. Turrini, E., Ferruzzi, L., and Fimognari, C. (2014) Natural compounds to overcome cancer chemoresistance: toxicological and clinical issues. *Expert Opin. Drug Metab. Toxicol.* **10**, 1677–1690

181. Steimbach, L., Borgmann, A. V., Gomar, G. G., Hoffmann, L. V., Rutckeviski, R., de Andrade, D. P., and Smiderle, F. R. (2021) Fungal beta-glucans as adjuvants for treating cancer patients – A systematic review of clinical trials. *Clin. Nutr.* **40**, 3104–3113

182. Cognigni, V., Ranallo, N., Tronconi, F., Morgese, F., and Berardi, R. (2021) Potential benefit of β-glucans as adjuvant therapy in immuno-oncology: a review. *Explor. Target. Anti-tumor Ther.* **2**, 122–138

183. Roudi, R., Mohammadi, S. R., Roudbary, M., and Mohsenzadegan, M. (2017) Lung cancer and β-glucans: review of potential therapeutic applications. *Invest. New Drugs*. **35**, 509–517

184. Kobayashi, Y., Oguro, A., and Imaoka, S. (2018) Bisphenol A and its derivatives induce degradation of HIF-1alpha via the lysosomal pathway in human hepatocarcinoma cell line, Hep3B. *Biol. Pharm. Bull.* **41**, 374–382

185. Guzmán, C., Bagga, M., Kaur, A., Westermarck, J., and Abankwa, D. (2014) ColonyArea: an ImageJ plugin to automatically quantify colony formation in clonogenic assays. *PLoS One*. **9**, e92444

186. Geller, A., Shrestha, R., and Yan, J. (2019) Yeast-derived β-glucan in cancer: novel uses of a traditional therapeutic. *Int. J. Mol. Sci.* **20**, 3618

187. Tian, Y., Wu, K., Liu, Q., Han, N., Zhang, L., Chu, Q., and Chen, Y. (2016) Modification of platinum sensitivity by KEAP1/NRF2 signals in non-small cell lung cancer. *J. Hematol.*

Oncol. **9**, 83

188. Goldstein, L. D., Lee, J., Gnad, F., Klijn, C., Schaub, A., Reeder, J., Daemen, A., Bakalarski, C. E., Holcomb, T., Shames, D. S., Hartmaier, R. J., Chmielecki, J., Seshagiri, S., Gentleman, R., and Stokoe, D. (2016) Recurrent loss of NFE2L2 exon 2 is a mechanism for Nrf2 pathway activation in human cancers. *Cell Rep.* **16**, 2605–2617

189. Yang, J., Bogni, A., Schuetz, E. G., Ratain, M., Eileen Dolan, M., McLeod, H., Gong, L., Thorn, C., Relling, M. V., Klein, T. E., and Altman, R. B. (2009) Etoposide pathway. *Pharmacogenet. Genomics*. **19**, 552–553

190. Swidergall, M., Solis, N. V., Lionakis, M. S., and Filler, S. G. (2018) EphA2 is an epithelial cell pattern recognition receptor for fungal β-glucans. *Nat. Microbiol.* **3**, 53–61

191. Singh, D. R., Kanvinde, P., King, C., Pasquale, E. B., and Hristova, K. (2018) The EphA2 receptor is activated through induction of distinct, ligand-dependent oligomeric structures. *Commun. Biol.* **1**, 15

192. Xu, Q., Lin, W.-C., Petit, R. S., and Groves, J. T. (2011) EphA2 receptor activation by monomeric Ephrin-A1 on supported membranes. *Biophys. J.* **101**, 2731–2739

193. Xu, J., Liu, D., Yin, Q., and Guo, L. (2016) Tetrandrine suppresses β-glucan-induced macrophage activation via inhibiting NF-κB, ERK and STAT3 signaling pathways. *Mol. Med. Rep.* **13**, 5177–5184

194. Chan, B., and Sukhatme, V. P. (2009) Receptor tyrosine kinase EphA2 mediates thrombin-induced upregulation of ICAM-1 in endothelial cells in vitro. *Thromb. Res.* **123**, 745–752

195. Carpenter, T. C., Schroeder, W., Stenmark, K. R., and Schmidt, E. P. (2012) Eph-A2 promotes permeability and inflammatory responses to bleomycin-induced lung injury. *Am. J. Respir. Cell Mol. Biol.* **46**, 40–47

196. Liu, G.-H., Qu, J., and Shen, X. (2008) NF-κB/p65 antagonizes Nrf2-ARE pathway by depriving CBP from Nrf2 and facilitating recruitment of HDAC3 to MafK. *Biochim. Biophys. Acta - Mol. Cell Res.* **1783**, 713–727

197. Grabe, N. (2002) AliBaba2: context specific identification of transcription factor binding sites. *In Silico Biol.* **2**, S1-15

198. Baghban, R., Roshangar, L., Jahanban-Esfahlan, R., Seidi, K., Ebrahimi-Kalan, A., Jaymand, M., Kolahian, S., Javaheri, T., and Zare, P. (2020) Tumor microenvironment complexity and therapeutic implications at a glance. *Cell Commun. Signal.* **18**, 59

199. Liu, M., Luo, F., Ding, C., Albeituni, S., Hu, X., Ma, Y., Cai, Y., McNally, L., Sanders, M. A., Jain, D., Kloecker, G., Bousamra, M., Zhang, H., Higashi, R. M., Lane, A. N., Fan, T. W.-M., and Yan, J. (2015) Dectin-1 activation by a natural product β-glucan converts immunosuppressive macrophages into an M1-like phenotype. *J. Immunol.* **195**, 5055–5065

200. Bélanger, M. M., Gaudreau, M., Roussel, É., and Couet, J. (2004) Role of caveolin-1 in etoposide resistance development in A549 lung cancer cells. *Cancer Biol. Ther.* **3**, 954–959

201. Kaewpiboon, C., Srisuttee, R., Malilas, W., Moon, J., Oh, S., Jeong, H. G., Johnston, R. N., Assavalapsakul, W., and Chung, Y.-H. (2015) Upregulation of Stat1-HDAC4 confers resistance to etoposide through enhanced multidrug resistance 1 expression in human A549 lung cancer cells. *Mol. Med. Rep.* **11**, 2315–2321

202. Sypniewski, D., Bednarek, I., Gałka, S., Loch, T., Błaszczyk, D., and Sołtysik, D. (2013) Cytotoxicity of etoposide in cancer cell lines in vitro after BCL-2 and C-RAF gene silencing with antisense oligonucleotides. *Acta Pol. Pharm.* **70**, 87–97

203. Zhang, B., Zhao, J., Li, S., Zeng, L., Chen, Y., and Fang, J. (2015) Mangiferin activates the Nrf2-ARE pathway and reduces etoposide-induced DNA damage in human umbilical cord mononuclear blood cells. *Pharm. Biol.* **53**, 503–511

204. Singh, A., Boldin-Adamsky, S., Thimmulappa, R. K., Rath, S. K., Ashush, H., Coulter, J.,

Blackford, A., Goodman, S. N., Bunz, F., Watson, W. H., Gabrielson, E., Feinstein, E., and Biswal, S. (2008) RNAi-mediated silencing of nuclear factor erythroid-2-related factor 2 gene expression in non-small cell lung cancer inhibits tumor growth and increases efficacy of chemotherapy. *Cancer Res.* **68**, 7975–7984

205. Ohnuma, T., Matsumoto, T., Itoi, A., Kawana, A., Nishiyama, T., Ogura, K., and Hiratsuka, A. (2011) Enhanced sensitivity of A549 cells to the cytotoxic action of anticancer drugs via suppression of Nrf2 by procyanidins from Cinnamomi Cortex extract. *Biochem. Biophys. Res. Commun.* **413**, 623–629

206. Yu, C., Chen, H., Du, D., Lv, W., Li, S., Li, D., Xu, Z., Gao, M., Hu, H., and Liu, D. (2021) β-Glucan from Saccharomyces cerevisiae alleviates oxidative stress in LPS-stimulated RAW264.7 cells via Dectin-1/Nrf2/HO-1 signaling pathway. *Cell Stress Chaperones*. **26**, 629–637

207. Ishida, Y., Ohta, K., Naruse, T., Kato, H., Fukui, A., Shigeishi, H., Nishi, H., Tobiume, K., and Takechi, M. (2018) Candida albicans β-glucan-containing particles increase HO-1 expression in oral keratinocytes via a reactive oxygen species/p38 Mitogen-Activated Protein Kinase/Nrf2 pathway. *Infect. Immun.* **86**, e00575-17

208. Heyl, K. A., Klassert, T. E., Heinrich, A., Müller, M. M., Klaile, E., Dienemann, H., Grünewald, C., Bals, R., Singer, B. B., and Slevogt, H. (2014) Dectin-1 is expressed in human lung and mediates the proinflammatory immune response to nontypeable Haemophilus influenzae. *MBio*. **5**, e01492-14

209. Han, X., Yu, R., Zhen, D., Tao, S., Schmidt, M., and Han, L. (2011) β-1,3-Glucan-induced host phospholipase D activation is involved in Aspergillus fumigatus internalization into type II human pneumocyte A549 cells. *PLoS One*. **6**, e21468

210. Lee, H.-M., Yuk, J.-M., Shin, D.-M., and Jo, E.-K. (2009) Dectin-1 is inducible and plays an essential role for mycobacteria-induced innate immune responses in airway epithelial cells. *J. Clin. Immunol.* **29**, 795–805

211. Reid, D. M., Gow, N. A., and Brown, G. D. (2009) Pattern recognition: recent insights from Dectin-1. *Curr. Opin. Immunol.* **21**, 30–37

212. Doz-Deblauwe, É., Carreras, F., Arbues, A., Remot, A., Epardaud, M., Malaga, W., Mayau, V., Prandi, J., Astarie-Dequeker, C., Guilhot, C., Demangel, C., and Winter, N. (2019) CR3 engaged by PGL-I triggers Syk-calcineurin-NFATc to rewire the innate immune response in leprosy. *Front. Immunol.* **10**, 2913

213. Sun, X., Wang, X., Chen, T., Li, T., Cao, K., Lu, A., Chen, Y., Sun, D., Luo, J., Fan, J., Young, W., and Ren, Y. (2010) Myelin activates FAK/Akt/NF-kappaB pathways and provokes CR3-dependent inflammatory response in murine system. *PLoS One*. **5**, e9380

214. Martin, E. W., Pacholewska, A., Patel, H., Dashora, H., and Sung, M.-H. (2020) Integrative analysis suggests cell type–specific decoding of NF-κB dynamics. *Sci. Signal.* **13**, eaax7195

215. Wardyn, J. D., Ponsford, A. H., and Sanderson, C. M. (2015) Dissecting molecular cross-talk between Nrf2 and NF-κB response pathways. *Biochem. Soc. Trans.* **43**, 621–626

216. Rushworth, S. A., Zaitseva, L., Murray, M. Y., Shah, N. M., Bowles, K. M., and MacEwan, D. J. (2012) The high Nrf2 expression in human acute myeloid leukemia is driven by NF-κB and underlies its chemo-resistance. *Blood*. **120**, 5188–5198

Abbreviations

ARE, antioxidant response element

CGA, Chlorogenic acid

CR3, complement receptor 3

CRL4, Cullin 4-RING ligase

CUL4A, Cullin4A

CYP, cytochromes P450

DDB1, DNA damage-binding protein 1

DMEs, drug-metabolizing enzymes

EphA2, ephrin type-A receptor 2

EpRE, electrophile responsive element

HO-1, heme oxygenase-1

Keap1, Kelch-like ECH-associated protein 1

MDR1, multidrug resistance protein 1

NF-κB, nuclear factor kappa B

NQO1, NAD(P)H quinone dehydrogenase 1

Nrf2, Nuclear factor erythroid 2-related factor 2

NSCLC, non-small-cell lung carcinoma

RBX1, RING box protein 1

shRNA, short hairpin RNA

siRNA, small interference RNA

SKN-1, Skinhead protein-1

Sp1, Specificity protein 1

UGTs, UDP glucuronosyltransferases

WDR23, WD40 Repeat protein 23

Bibliography

Research articles

1. **Siswanto FM**, Oguro A, Arase S, and Imaoka S. "WDR23 regulates the expression of Nrf2-driven drug-metabolizing enzymes". *Drug Metab Pharmacokinet.* 2020 Oct;35(5): 441-455.

2. Oguro A, Ishihara Y, **Siswanto FM**, Yamazaki T, Ishida A, Imaishi H, Imaoka S. "Contribution of DHA diols (19,20-DHDP) produced by cytochrome P450s and soluble epoxide hydrolase to the beneficial effects of DHA supplementation in the brains of rotenone-induced rat models of Parkinson's disease". *Biochim Biophys Acta Mol Cell Biol Lipids.* 2021 Feb;1866(2): 158858.

3. **Siswanto FM**, Oguro A, and Imaoka S. "Sp1 is a substrate of Keap1 and regulates the activity of $CRL4A^{WDR23}$ ubiquitin ligase toward Nrf2". *J Biol Chem.* 2021 April; 296: 100704.

4. **Siswanto FM**, Tamura A, Sakuma R, and Imaoka S. "Yeast β-glucan increases etoposide sensitivity in lung cancer cell line A549 by suppressing Nrf2 via the non-canonical NF-κB pathway". *Mol Pharmacol.,* in press.

Conference presentations

1. **Siswanto FM**, and Imaoka S. The 93rd Annual Meeting of the Japanese Biochemical Society, September 14th-16th 2020.

2. **Siswanto FM**, and Imaoka S. The 48th Annual Meeting of the Japanese Society of Toxicology, July 7th-9th 2021.

3. **Siswanto FM**, and Imaoka S. The 94th Annual Meeting of the Japanese Biochemical Society, November 3rd-5th 2021.

4. Tamura A, **Siswanto FM**, Imaoka S, and Oka M. The 94th Annual Meeting of the Japanese Biochemical Society, November 3rd-5th 2021.

Acknowledgments

First and foremost, I would like to express many courteous thanks to my supervisor, Prof. Susumu Imaoka, for his patient guidance, valuable suggestions, encouragement, and advice throughout this study.

I wish to express my gratitude to the thesis committee member, Prof. Yohei Hirai, for providing valuable insights and recommendations to complete this thesis. My sincere thanks also go to Prof. Kiyoji Nishiwaki as a thesis committee member and for his helpful technical support and guidance in experiments involving *C. elegans*.

I especially thank the Yoshida Scholarship Foundation for the financial support and given the opportunity to pursue my Doctoral Degree.

My sincere thanks also go to all members of Imaoka Laboratory.

In addition, I would like to thank my family who always supporting my dream. Without you, it is all meaningless.

Last but not least, I would like to praise and thank God, who has granted countless blessing, knowledge, and opportunity so that I have been finally able to accomplish this thesis.

I can do all this through Him who gives me strength. (Philippians 4:13)

Ferbian Milas Siswanto

February 2022